STRINGQFT

String-Theoretic Construction
of Quantum Field Theory

VOLUME V

Topological String Preliminaries

Xingyang Yu

StringQFT v1.0 / Source build candidate

Drafted with AI assistance under the supervision of the author.
Manuscript free to read. All rights reserved.

How to read this volume

Topological string theory provides a way to organize selected quantities that recur in geometric constructions of quantum field theory. This volume builds the language needed to calculate and interpret those quantities, starting with the twist and the two-dimensional sigma model.

Chapters 1–2 establish the fields and observables of the twisted theory. Chapters 3–5 develop periods, mirror calculations and the holomorphic anomaly. Chapters 6–9 introduce open-string sectors and several concrete computational descriptions. Chapter 10 returns to the spacetime quantities for which these methods are used. The worldsheet foundations are in Volume II, the brane interfaces in Volume III, and the geometric prerequisites in Volume IV.

Follow one worked quantity through its definitions before comparing two methods of computing it. The expansion parameter, choice of background, boundary data and normalization belong to the question being asked. Agreement of two formal expressions does not by itself establish that they compute the same physical observable. Each application therefore states the identification on which the calculation depends.

The volume is a foundation for the later geometric-engineering and protected quantity chapters. It does not attempt a proof of every mathematical structure used by topological string theory. The worked examples derive the tools needed here, while the source discussion states the scope of the broader results being invoked. Exercises test both the calculation and that scope.

Contents

How to read this volume **i**

V.1 N=(2,2) worldsheet theories and the A/B twists **1**

V.1.1 A supercharge on a curved surface 1

V.1.2 R currents and spin 2

V.1.3 Scalar supercharges . . . 4
V.1.4 Local observables . . . 6
V.1.5 Localization equations . . . 8
V.1.6 The protected boundary . . . 11
V.1.7 Exercises . . . 13
V.1.8 Take-home message . . . 14
Status and sources . . . 14

V.2 Topological sigma models and Gromov–Witten theory 16
V.2.1 Three points and one sphere map . . . 16
V.2.2 Holomorphic maps and observables . . . 16
V.2.3 Virtual dimension . . . 18
V.2.4 Compactification of map space . . . 21
V.2.5 Quantum product . . . 24
V.2.6 Local Calabi–Yau curve counting . . . 25
V.2.7 Exercises . . . 28
V.2.8 Take-home message . . . 28
Status and sources . . . 29

V.3 The B-model, special geometry, and Picard–Fuchs equations 30
V.3.1 A cycle that remembers complex structure . . . 30
V.3.2 Periods and cycles . . . 30
V.3.3 Special coordinates . . . 32
V.3.4 Picard–Fuchs from geometry . . . 34
V.3.5 Singular points and monodromy . . . 37
V.3.6 From CY periods to an engine . . . 38
V.3.7 Exercises . . . 40
V.3.8 Take-home message . . . 41
Status and sources . . . 41

V.4 Mirror symmetry as a computational tool 44
V.4.1 A number hidden in a period . . . 44
V.4.2 Choose a mirror pair and a chamber . . . 45
V.4.3 The mirror map . . . 47
V.4.4 Yukawa data . . . 49
V.4.5 Instanton extraction . . . 52
V.4.6 A local toric curve . . . 56
V.4.7 Exercises . . . 58
V.4.8 Take-home message . . . 59

V.5 Holomorphic anomaly equations 61
V.5.1 Why a topological amplitude remembers both moduli . . . 61
V.5.2 Contact terms and the two nodal boundaries . . . 62
V.5.3 Frames and covariant derivatives . . . 64
V.5.4 The separate genus-one equation . . . 66
V.5.5 The first two higher-genus sources . . . 67

V.5.6 Integrating the genus-two equation . . . 69
V.5.7 Local sections and compatible choices . . . 72
V.5.8 A protected conifold singularity . . . 74
V.5.9 Fixing a finite ambiguity with boundary data . . . 76
V.5.10 Exercises . . . 77
V.5.11 Take-home message . . . 78

V.6 Open topological strings and branes 81
V.6.1 What an open string remembers . . . 81
V.6.2 A and B boundary conditions . . . 82
V.6.3 Open observables . . . 84
V.6.4 Ext groups as arrows . . . 86
V.6.5 Products and interactions . . . 89
V.6.6 The fractional brane interface . . . 92
V.6.7 From open fields to actions . . . 95
V.6.8 From categorical data to a physical spectrum . . . 98
V.6.9 Exercises . . . 99
V.6.10 Take-home message . . . 100
Status and sources . . . 100

V.7 The topological vertex 104
V.7.1 A curve from two local patches . . . 104
V.7.2 Toric vertices and boundary partitions . . . 105
V.7.3 Schur functions and specializations . . . 107
V.7.4 Gluing the conifold . . . 110
V.7.5 Relative and closed curve invariants . . . 113
V.7.6 Framing and orientation . . . 116
V.7.7 Connected curves and degree zero . . . 118
V.7.8 Exercises . . . 121
V.7.9 Take-home message . . . 122

V.8 Gopakumar–Vafa invariants and BPS state counting 125
V.8.1 One curve and many rational numbers . . . 125
V.8.2 The M-theory particle interpretation . . . 126
V.8.3 The multicover organization . . . 129
V.8.4 Recovering integer data . . . 133
V.8.5 Spin and genus . . . 137
V.8.6 Scope of integrality . . . 140
V.8.7 Exercises . . . 144
V.8.8 Take-home message . . . 145
Status and sources . . . 145

V.9 Matrix models and topological recursion 148
V.9.1 A matrix integral as an expansion . . . 148
V.9.2 Loop equations . . . 152
V.9.3 Branch points and local data . . . 154

V.9.4 Topological recursion . . . 157
V.9.5 Which partition function? . . . 163
V.9.6 Exercises . . . 167
V.9.7 Take-home message . . . 168
Status and sources . . . 169

V.10 Topological amplitudes as physical F-terms 171
V.10.1 A physical use for a topological amplitude . . . 171
V.10.2 The selected amplitude and its zero modes . . . 172
V.10.3 Tensor contractions and chiral couplings . . . 175
V.10.4 Canonical fields and gravitational limits . . . 177
V.10.5 A local gauge theory from a shrinking fibre . . . 180
V.10.6 Boundaries and a flux superpotential . . . 182
V.10.7 Local coefficients and missing dynamics . . . 186
V.10.8 Exercises . . . 188
V.10.9 Take-home message . . . 189
Status and sources . . . 190

Chapter V.1

N=(2,2) worldsheet theories and the A/B twists

V.1.1 A supercharge on a curved surface

A flat worldsheet lets a supersymmetry parameter look constant. On a curved Riemann surface, a spinor is a section of a spin bundle, so there is generally no global constant parameter of that kind. The topological twist changes the way worldsheet rotations act on fields. If an appropriate quantum R symmetry exists, the changed rotation law makes certain supercharges scalars. Those charges select a cohomology of operators, whose correlators retain geometric information that the full untwisted theory does not isolate so simply.

There are two choices of R current in a two-dimensional $N = (2, 2)$ theory. They lead to the A and B twists, and ultimately to different questions about a Kähler target X. In the A model the fixed maps can be holomorphic; in the B model the fixed maps are constant under the conditions used below. This chapter constructs the scalar charges first, then explains the operator dictionary, the fixed equations, and the boundary between a protected correlator and a physical string coupling. Chapter 2 will study the A-model map sectors and their enumerative consequences; Chapter 3 will develop the B-model period side. The untwisted multiplets are treated in Volume I, Chapter 4, and the worldsheet CFT currents in Volume II, Chapter 2.

The needed qualifications are part of the construction. A classical R current may fail in the quantum theory, an interacting superpotential may break it, and a scalar supercharge need not square to zero in a sector with central charge. We will work in the ordinary geometric sector with both central charges zero and use a smooth Kähler sigma model for the target examples. For the B example, a smooth compact Kähler target with holomorphically trivial canonical bundle is a sufficient geometric class, provided the continuous axial symmetry and the stated quantum measure conditions survive. Real $c_1(TX) = 0$ alone is not substituted for that holomorphic condition.

V.1.2 R currents and spin

How can a spinorial charge act globally on a curved worldsheet? Let M_E generate Euclidean rotations in the convention $M_E = 2s$, so s is the ordinary spin. Write F_V and F_A for vector and axial R charges. If the selected $U(1)_R$ is conserved and integrally charged in this normalization, we can couple its background connection to the worldsheet spin connection. The new rotation generator and the spin of a field with charges (m, q_R) are

$$M'_E = M_E + F_R, \qquad s' = \frac{m + q_R}{2}, \qquad m = 2s. \tag{V.1.1}$$

This formula describes a change of bundles on a curved Riemann surface. It does not merely relabel a flat-space field. A field of spin zero becomes a section of the trivial spin bundle, while spin $+1$ is a one-form of one chirality in the source convention. The integral-charge assumption makes the new bundle assignment meaningful in the stated spin/R frame.

One can see the geometric operation without invoking a particular target. If the untwisted covariant derivative on a field of spin s and R charge q_R contains $s\,\omega_\mu + q_R A^R_\mu$, then choosing the background R connection proportional to the spin connection gives the new coefficient $s + q_R/2$ in the convention above. On a flat patch the connection can be gauged away, so the local equations may look unchanged. On a curved Σ, the transition functions of the line bundle change. This is why the same local fermion can become a globally defined scalar in one twist and a one-form in the other. It is also why a globally nonconserved R current cannot be used as a harmless change of variables.

$$D^{\mathrm{tw}}_\mu \sim \partial_\mu + (s + q_R/2)\omega_\mu, \qquad s + q_R/2 = 0 \implies \text{scalar bundle.} \tag{V.1.2}$$

The actual four supercharge rows, in the order used throughout this chapter, carry the following charges:

	m	q_V	q_A
Q_-	1	-1	1
$\bar{Q}_+$	-1	1	1
$\bar{Q}_-$	1	1	-1
Q_+	-1	-1	-1

. (V.1.3)

The bars and subscripts in this table matter. In particular, the second row is $\bar{Q}_+$, not Q_+. Applying (V.1.1) separately to each row produces the vector-twisted spins

$$s_A(Q_-, \bar{Q}_+, \bar{Q}_-, Q_+) = \tfrac{1}{2}(1-1, -1+1, 1+1, -1-1) = (0, 0, 1, -1), \tag{V.1.4}$$

and the axial-twisted spins

$$s_B(Q_-, \bar{Q}_+, \bar{Q}_-, Q_+) = \tfrac{1}{2}(1+1, -1+1, 1-1, -1-1) = (1, 0, 0, -1). \tag{V.1.5}$$

Only after this calculation may we name the scalar pairs. They are $(Q_-, \bar{Q}_+)$ for A and $(\bar{Q}_-, \bar{Q}_+)$ for B. Figure V.1.1 records the four rows and the change in their bundle character. It is a picture of the sourced charge calculation, not a criterion for anomaly cancellation.

charge	(m, q_V, q_A)	**before** s	**A spin**	**B spin**
Q_-	$(1,-1,1)$	$+1/2$	$\bigcirc\ 0$	$\rightarrow\ +1$
$\bar{Q}_+$	$(-1,1,1)$	$-1/2$	$\bigcirc\ 0$	$\bigcirc\ 0$
$\bar{Q}_-$	$(1,1,-1)$	$+1/2$	$\rightarrow\ +1$	$\bigcirc\ 0$
Q_+	$(-1,-1,-1)$	$-1/2$	$\rightarrow\ -1$	$\rightarrow\ -1$

Figure V.1.1: The same four charges under the original, vector-twisted, and axial-twisted rotations. A circle marks spin zero and a one-form symbol marks spin ± 1; the signs remain in the table. The supercharge rows are not interchanged between the two twists.

A matter fermion gives a second check of the bundle change. For a chiral superfield whose lowest scalar has $q_V = q_A = 0$, the source assigns ψ_- the same triple $(m, q_V, q_A) = (1,-1,1)$ as Q_-. Thus

$$s(\psi_-) = \tfrac{1}{2}, \qquad s_A(\psi_-) = 0, \qquad s_B(\psi_-) = 1. \tag{V.1.6}$$

Locally the A-twisted ψ_- is a scalar, while the B-twisted one is a one-form. On a curved Σ, this changes the line bundle from a square root of the canonical bundle to the trivial bundle or the relevant one-form bundle. The coordinate scalar ϕ retains spin zero. The geometry of a sigma model needs these assignments globally, which is why an R symmetry available only classically does not suffice.

For instance, changing the sign of the vector R current while keeping the same charge table would give

$$s_{A,-} = (\tfrac{m-q_V}{2})_{\text{rows}} = (1,-1,0,0). \tag{V.1.7}$$

The scalar pair would then be $(\bar{Q}_-, Q_+)$, not the A pair above. A convention sign is therefore part of the calculation, not an innocuous typographical choice. In the rest of this chapter the plus sign in (V.1.1) is fixed.

Whether either R current survives must be checked in the given theory. In an abelian gauged linear sigma model, Hori et al. derive the axial gauge anomaly coefficient and theta shift

$$b_{1,a} = \sum_i Q_{ia}, \qquad \theta_a \longmapsto \theta_a - 2\alpha b_{1,a} \tag{V.1.8}$$

for an axial rotation by α. In a one-factor example with charges $(1,1,-2)$, the sum is zero; with charges $(1,1)$, it is two and $\Delta\theta = -4\alpha$. Thus the latter does not have the continuous axial symmetry required for this B twist, as far as this gauge anomaly is concerned. Vanishing of this one coefficient alone does not certify all global, interaction, or measure conditions. For an ordinary chiral superpotential W, vector R invariance requires W to have vector charge 2; with a compatible Kähler potential, this is the quasi-homogeneity condition. Axial invariance instead requires W to have axial charge

0, which is possible with zero axial charges for the chiral fields in this setting. That classical interaction test is separate from the axial gauge anomaly in (V.1.8) and does not settle other quantum or global conditions.

For a geometric B sigma model, Witten identifies a fermion-determinant obstruction tied to $c_1(TX)$. We use a smooth compact Kähler target with a holomorphically trivial canonical bundle K_X and a surviving quantum axial R symmetry as the sufficient worked setting. A holomorphic trivialization is a global nowhere-vanishing holomorphic top form. The distinction between such a form and real Chern-class vanishing was developed in Volume IV, Chapter 2. The GLSM charge sum and the geometric determinant obstruction belong to their respective descriptions; equating them across every phase would require an additional argument. The A twist likewise requires a compatible continuous vector R symmetry and absence of relevant anomalies. The next section adds a logically different test: the scalar combination must also be a differential.

The two charge-list examples are deliberately different from the compact B target just named. They test the coefficient of one axial gauge anomaly in a GLSM. They do not produce a holomorphic top form on a target, and a vanishing coefficient does not identify a particular smooth geometric phase. Conversely, $c_1(TX)$ is an obstruction in the geometric fermion determinant, not a substitute for checking every gauge and interaction condition in a chosen ultraviolet model. Keeping those claims separate will matter when Chapter 2 changes the instanton sector and when Chapter 3 uses global complex geometry.

V.1.3 Scalar supercharges

What algebra turns a scalar charge into the protected-sector differential? The two scalar sums selected by the spin table are

$$Q_A = Q_- + \bar{Q}_+, \qquad Q_B = \bar{Q}_- + \bar{Q}_+, \tag{V.1.9}$$

up to nonzero overall normalization. The $(2,2)$ algebra quoted by Hori et al. includes central terms. In the source normalization its implication for these sums is

$$Q_A^2 = \widetilde{Z}, \qquad Q_B^2 = Z. \tag{V.1.10}$$

The right-hand sides are not spin charges. Making Q_A or Q_B scalar therefore says nothing by itself about their squares.

Here and below we restrict the ordinary geometric complex to

$$Z = \widetilde{Z} = 0 \quad \Longrightarrow \quad Q_A^2 = Q_B^2 = 0. \tag{V.1.11}$$

Hori et al. impose this zero-center condition in their topological-sector setup. It is a condition on the sector under discussion. A central charge can commute with all local operators while acting nontrivially on a state; trivial adjoint action on local operators is not the statement that the charge vanishes in every soliton sector. Massive solitons and equivariant extensions with nonzero center are outside this construction. Witten's component transformations supply a separate qualifier: without retained auxiliary

fields, their square closes modulo field equations. The algebraic zero-center premise and off-shell closure are distinct issues.

In the declared sector, define an operator $\mathcal{O}$ to be Q-closed when its graded commutator with Q vanishes, and Q-exact when $\mathcal{O} = [Q, \Lambda\}$ for another operator Λ. Since $Q^2 = 0$, every exact operator is closed, and the classes are

$$H^k_Q(\mathcal{O}) = \frac{\ker(Q : \mathcal{O}^k \to \mathcal{O}^{k+1})}{\mathrm{im}(Q : \mathcal{O}^{k-1} \to \mathcal{O}^k)}. \tag{V.1.12}$$

Multiplying Q by a nonzero constant leaves both kernel and image unchanged. Cohomology retains closed operators up to changes by exact ones; the latter are alternate representatives, not additional observables. This is the precise reason the protected sector contains less information than the full operator algebra.

There is an elementary consistency check behind the quotient. If Λ has degree $k-1$, then $Q\Lambda$ has degree k, and $Q(Q\Lambda) = Q^2\Lambda = 0$. Thus $\mathrm{im}\, Q$ really lies inside $\ker Q$ in the same degree. If Q^2 were a nonzero central operator on the selected states, this inclusion need not hold for their state complex, even though the supercharge remains a scalar under rotations. The order of operations is fixed: select a sector satisfying (V.1.11), then take the quotient.

$$Q^2 = 0 \quad \Longrightarrow \quad \mathrm{im}(Q|_{\mathcal{O}^{k-1}}) \subseteq \ker(Q|_{\mathcal{O}^k}). \tag{V.1.13}$$

The grading k here is the *topological* ghost degree, normalized by

$$\mathrm{gh}_{\mathrm{top}}(Q) = 1, \qquad \mathrm{gh}_{\mathrm{top}}(\phi) = 0. \tag{V.1.14}$$

In Witten's A fields the scalar χ has degree $+1$ and its one-form partner ψ degree -1. In the B fields, η and θ have degree $+1$, and the one-form ρ degree -1. These assignments organize local operators. Their quantum selection rules can have an index anomaly and depend on genus and insertions; the degree is not a universal all-genus conservation law. It is also distinct from the reparametrization bc-ghost number introduced for the worldsheet gauge fixing in Volume II, Chapter 2. The two systems serve different purposes even if both use the word "ghost."

A small finite complex makes the quotient operation fully visible. Let $C^0 = \langle u, v\rangle$, $C^1 = \langle x, y, z\rangle$, and $C^2 = \langle w\rangle$ over $\mathbb{C}$, with maps

$$\begin{aligned} &d_0 u = 2x + 3y, \quad d_0 v = 0, \\ &d_1 x = 3w, \qquad\quad d_1 y = -2w, \quad d_1 z = 0. \end{aligned} \tag{V.1.15}$$

The only possibly nonzero composition on the displayed basis is

$$d_1 d_0 u = 2(3w) + 3(-2w) = 0, \qquad d_1 d_0 v = 0. \tag{V.1.16}$$

Thus it is genuinely a complex. At degree zero, $d_0(au + bv) = a(2x + 3y)$, so $\ker d_0 = \langle v\rangle$. At degree one, write $\xi = Ax + By + Cz$. Then

$$d_1\xi = (3A - 2B)w = 0 \quad \Longleftrightarrow \quad (A, B, C) = (2t, 3t, c). \tag{V.1.17}$$

Hence $\ker d_1 = \langle 2x + 3y, z\rangle$, while $\operatorname{im} d_0 = \langle 2x + 3y\rangle$. Finally d_1 is onto, because $d_1 x = 3w$. The three quotients are

$$\begin{aligned} H^0 = \langle [v]\rangle, \qquad H^1 = \langle [z]\rangle, \qquad H^2 = 0, \\ (\dim H^0, \dim H^1, \dim H^2) = (1, 1, 0). \end{aligned} \tag{V.1.18}$$

The closed vector $2x + 3y$ disappears because it is $d_0 u$. One can also check the result with ranks. The two matrices in the ordered bases displayed above each have rank one. Rank-nullity gives nullities one and two. The first is $\dim H^0$; subtracting the rank of d_0 from the second gives $\dim H^1 = 1$; and surjectivity of d_1 gives $H^2 = 0$. The explicit kernel basis tells us which class survives, information that dimensions alone cannot supply.

$$\dim H^0 = 2 - 1 = 1, \qquad \dim H^1 = (3 - 1) - 1 = 1, \qquad \dim H^2 = 1 - 1 = 0. \tag{V.1.19}$$

Figure V.1.2 places that image inside the degree-one kernel. The example tests the algebraic meaning of "closed modulo exact"; it does not prove the quantum-field-theory identification of A or B operators. The next section states that identification from the sourced sigma-model construction.

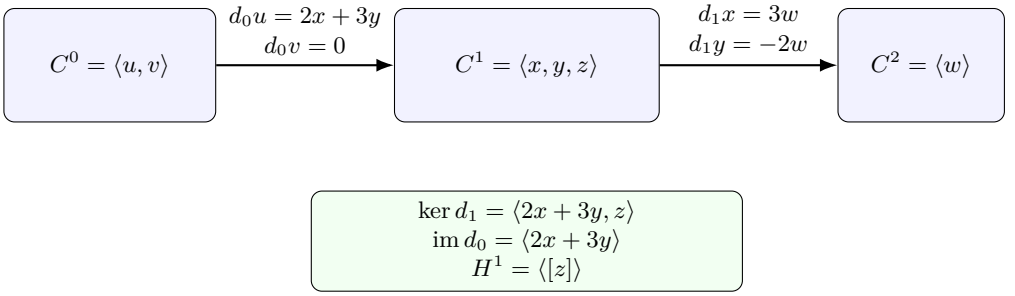


Figure V.1.2: The finite complex has a two-dimensional kernel in C^1. The image $\langle 2x + 3y\rangle$ is a line inside it, leaving the class $[z]$. The arrow labels are the actual coefficients in (V.1.15); this finite calculation is distinct from the sigma-model operator theorem.

V.1.4 Local observables

Which geometrical classes survive Q? First retain the target conventions of Volume IV, Chapter 1. For local holomorphic coordinates z^a on a Kähler target X,

$$ds^2 = 2g_{a\bar{b}} dz^a d\bar{z}^{\bar{b}}, \qquad J = i g_{a\bar{b}} dz^a \wedge d\bar{z}^{\bar{b}}, \qquad dJ = 0. \tag{V.1.20}$$

The target complex structure lets us split forms into (p, q) types. The A and B twists use different fermion zero-form combinations and so turn different target tensors into local observables.

In the A model, Witten associates a differential r-form $\omega = \omega_{I_1\cdots I_r}(\phi)d\phi^{I_1}\wedge\cdots\wedge d\phi^{I_r}$ to a local field constructed from the degree-one scalars χ^I:

$$\mathcal{O}_\omega(P) = \omega_{I_1\cdots I_r}(\phi(P))\chi^{I_1}(P)\cdots\chi^{I_r}(P). \tag{V.1.21}$$

Anticommutativity of the χ fields mirrors the antisymmetry of a differential form. In Witten's component convention the Q variation is $-\mathcal{O}_{d\omega}$. Its overall minus sign depends on the field convention, while the closed/exact criterion does not:

$$\begin{aligned} d\omega = 0 \;&\Rightarrow\; [Q,\mathcal{O}_\omega\} = 0,\\ \omega = d\lambda \;&\Rightarrow\; \mathcal{O}_\omega \text{ is } Q\text{-exact},\\ H_Q(\mathcal{O}_A) &\simeq H^*_{\mathrm{dR}}(X). \end{aligned} \tag{V.1.22}$$

The last is the sourced local-operator identification under the A-model assumptions. The two implications alone show how representatives behave; the assertion that all local classes are obtained this way is an additional result of that construction. It is not deduced from the finite complex.

The classical cohomology of $\mathbb{CP}^1$ supplies an explicit product before any worldsheet instanton sum. Let $H \in H^2(\mathbb{CP}^1)$ be the normalized positive generator with $\int_{\mathbb{CP}^1} H = 1$. Since the real target dimension is two, there is no degree-four cohomology:

$$H^0(\mathbb{CP}^1) = \mathbb{C}\langle 1\rangle, \quad H^2(\mathbb{CP}^1) = \mathbb{C}\langle H\rangle, \quad H^4(\mathbb{CP}^1) = 0. \tag{V.1.23}$$

Cup product adds degree, so $H \smile 1 = H$ and

$$H \smile H \in H^4(\mathbb{CP}^1) = 0, \qquad H^*(\mathbb{CP}^1,\mathbb{C}) \simeq \mathbb{C}[H]/(H^2). \tag{V.1.24}$$

For two actual classes $a + bH$ and $c + dH$, multiplication is

$$(a + bH) \smile (c + dH) = ac + (ad + bc)H. \tag{V.1.25}$$

For example, $(2 + 3H) \smile (5 - 4H) = 10 + 7H$: the discarded term is $-12H^2$, which vanishes by degree. This calculation is the ordinary classical cup ring. The A-model quantum product can receive nonconstant map contributions, and Hori et al. explicitly separate the classical relation from its instanton-deformed counterpart. The classical intersection pairing makes the same point from an integral. Only the degree-two part contributes over the real two-dimensional target. Thus $\int 1 \smile 1 = 0$, $\int 1 \smile H = 1$, and $\int H \smile H = 0$. The pairing is nondegenerate on the two-dimensional vector space even though $H^2 = 0$, because 1 pairs with H. The distinction between an intersection pairing and a product coefficient becomes useful when three-point functions define a quantum product in Chapter 2.

$$\eta_{\mathrm{cl}} = \begin{pmatrix} 0 & 1 \\ 1 & 0 \end{pmatrix}_{(1,H)}, \qquad \det \eta_{\mathrm{cl}} = -1. \tag{V.1.26}$$

Chapter 2 will set that product's parameter convention. We do not import one here or infer it from the classical degree argument.

The B operators begin with a $(0,p)$ form valued in a holomorphic q-polyvector bundle. In a coordinate patch, write

$$V = \frac{1}{p!q!} V^{j_1\cdots j_q}_{\bar{i}_1\cdots\bar{i}_p} d\bar{z}^{\bar{i}_1} \wedge \cdots \wedge d\bar{z}^{\bar{i}_p} \otimes \partial_{j_1} \wedge \cdots \wedge \partial_{j_q}. \tag{V.1.27}$$

Here $\eta^{\bar{i}}$ is a scalar valued in $\phi^* T^{0,1}X$, whereas θ_j is a scalar valued in $\phi^*(T^{1,0}X)^*$. Contracting their indices with those of V gives the local operator at $P \in \Sigma$:

$$\mathcal{O}_V(P) = \frac{1}{p!q!} V^{j_1\cdots j_q}_{\bar{i}_1\cdots\bar{i}_p}(\phi(P)) \eta^{\bar{i}_1}(P)\cdots\eta^{\bar{i}_p}(P)\theta_{j_1}(P)\cdots\theta_{j_q}(P), \qquad \mathrm{gh}_{\mathrm{top}}(\mathcal{O}_V) = p+q. \tag{V.1.28}$$

The fermions' anticommutation implements the two tensor antisymmetries. The B transformations make $Q\phi^{\bar{i}}$ proportional to $\eta^{\bar{i}}$ and leave η and θ closed. Thus acting on the coefficient of (V.1.28) differentiates it in an antiholomorphic direction: $[Q, \mathcal{O}_V\}$ is proportional to $\mathcal{O}_{\bar{\partial}V}$, with the overall sign set by the component convention. Witten's displayed operator uses a lower-index ψ_j in this final contraction; the lower-index scalar defined in his B-field list is θ_j, which we use throughout, rather than the one-form ρ or the A-model antighost. Hence closed and exact representatives obey the Dolbeault rules. The full local-operator isomorphism remains a sourced statement:

$$H_Q(\mathcal{O}_B) \simeq \bigoplus_{p,q} H^p(X, \wedge^q T^{1,0}X), \qquad \bar{\partial}V = 0 \pmod{V \sim V + \bar{\partial}S}. \tag{V.1.29}$$

This is a local-operator statement, not a statement that every local coordinate tensor extends globally. The target complex structure is essential to the $\bar{\partial}$ problem; the source also requires an anomaly-free B model.

For a concrete patch $U \subset \mathbb{C}$ with coordinate z, take $V = f(z)\partial_z$ for $f(z) = z^2 + 1$. Direct differentiation gives

$$\bar{\partial}\big((z^2+1)\partial_z\big) = (\partial_{\bar{z}} z^2 + \partial_{\bar{z}} 1) d\bar{z} \otimes \partial_z = 0. \tag{V.1.30}$$

Its actual local field is $\mathcal{O}_V(P) = (\phi^z(P)^2 + 1)\theta_z(P)$, of degree one; the coefficient's vanishing $\bar{\partial}$ makes it Q-closed under the stated local B transformations. By contrast $V = \bar{z}\partial_z$ gives $\bar{\partial}V = d\bar{z} \otimes \partial_z \neq 0$. A $(0,1)$-valued tensor of the form $\bar{\partial}S$ is closed because $\bar{\partial}^2 = 0$ but is removed in the quotient. These local statements do not compute a global $H^p(X, \wedge^q T^{1,0}X)$ on a compact target. Figure V.1.3 places the two sourced operator dictionaries on different target-complex branches. It also shows why neither geometric branch is the bc-ghost complex of worldsheet diffeomorphism gauge fixing.

For another local B example, take $S = \bar{z}^2\partial_z$ on the same flat patch. Its $\bar{\partial}$ is a closed $(0,1)$-valued polyvector, but its class vanishes because it is visibly exact. This parallels the finite complex, where $2x + 3y$ is closed and exact. The comparison explains the quotient; the field-theory identification remains the sourced B statement.

$$\bar{\partial}S = 2\bar{z}\, d\bar{z} \otimes \partial_z, \qquad \bar{\partial}(\bar{\partial}S) = 0, \qquad [\bar{\partial}S] = 0. \tag{V.1.31}$$

V.1.5 Localization equations

Why do A and B retain different maps? A twist changes the spin of fields, but the statement about path-integral fixed loci needs more. In a sector of fixed map degree,

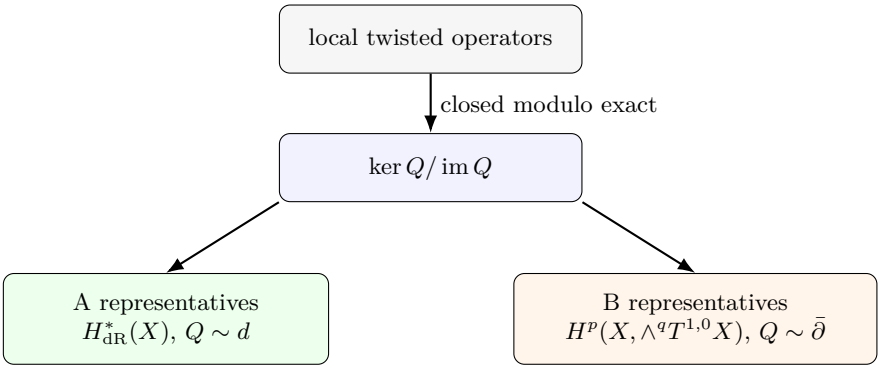


Figure V.1.3: A local twisted operator first enters $\ker Q/\operatorname{im} Q$. In the A construction its representatives are target differential forms; in the B construction they are Dolbeault polyvectors. The arrows summarize the sourced operator identifications under their model hypotheses, while the *bc* system has a different worldsheet gauge-fixing role.

Witten writes the A action as a Q-exact term plus a topological term depending on the Kähler class. Schematically, without importing his opposite-sign Kähler-form symbol or coupling normalization, its dependence has the form

$$S_A(t) = t\{Q, V_A\} + S_{\mathrm{top}}([\phi]), \qquad [\phi] \text{ fixed in the variation of } t. \tag{V.1.32}$$

In the actual source, the degree contribution is pulled outside the Q-exact integral before changing the coupling. For Q-closed insertions and a Q-invariant measure, a Ward identity then makes the remaining fixed-degree integral independent of t, provided convergence and boundary/contact terms permit the deformation. At large positive coupling, the positive bosonic term selects the source's holomorphic-map equation

$$\bar\partial\phi = 0 \quad \text{or locally} \quad \partial_{\bar z}\phi^a = 0, \qquad \partial_z\bar\phi^{\bar a} = 0. \tag{V.1.33}$$

Its solutions can be nonconstant. Their degrees distinguish the worldsheet instanton sectors that Chapter 2 studies. The fixed equation is not, by itself, the theorem that the quantum measure localizes with its determinants and zero modes correctly included.

On a flat target chart, the positive quadratic term controlling the local A equation can be read as the squared norm of the antiholomorphic derivative. With the common positive area form suppressed, the two local fixed-equation residuals compare as

$$E_A^{\mathrm{loc}} = \int_\Sigma |\bar\partial\phi|^2, \qquad E_B^{\mathrm{loc}} = \int_\Sigma \big(|\partial\phi|^2 + |\bar\partial\phi|^2\big). \tag{V.1.34}$$

Both are nonnegative in this Euclidean illustration. The A zero set allows a nonzero $\partial\phi$; the B zero set does not. This positivity argument explains why the local solution

spaces differ. It does not replace the source's path-integral argument on a compact target, where determinants and map-space geometry must be retained.

For the B model, Witten's action has a Q-exact part and another term whose relevant metric variation has the stated topological behavior. Under the source's anomaly, convergence and Ward assumptions, its weak-coupling argument reduces to constant maps. The local bosonic condition may be recorded as

$$d\phi = 0 \quad \Longleftrightarrow \quad \partial_z \phi^a = \partial_{\bar{z}} \phi^a = 0 \quad \text{in a flat target chart.} \tag{V.1.35}$$

Its remaining target zero mode can vary over X in the path integral; "constant" means constant as a function on the worldsheet, not a single distinguished point of X. The target complex structure still enters the B operator dictionary even though the worldsheet map is constant.

An affine local calculation makes the two equations unambiguous. In a target chart modeled on $\mathbb{C}$, let

$$\phi(z, \bar{z}) = az + b\bar{z} + c, \qquad \partial_z \phi = a, \quad \partial_{\bar{z}} \phi = b. \tag{V.1.36}$$

The A residual is $|b|^2$ and the B constant-map residual is $|a|^2 + |b|^2$. For four real coefficient pairs, the full arithmetic is

(a, b)	$\lvert b\rvert^2$	$\lvert a\rvert^2 + \lvert b\rvert^2$	A fixed	B fixed
$(2, 0)$	0	4	yes	no
$(0, 3)$	9	9	no	no
$(0, 0)$	0	0	yes	yes
$(2, -3)$	9	13	no	no

. (V.1.37)

The first row is the decisive counterexample to identifying the two loci: $\phi = 2z + c$ is nonconstant and holomorphic. The last row checks that neither condition can be rescued by a cancellation between the two derivatives. Figure V.1.4 displays the inclusion of the constant locus in the holomorphic one for this local chart. The inclusion can be stated directly in terms of the coefficients:

$$\{(a, b) : a = b = 0\} \subsetneq \{(a, b) : b = 0\} \subset \mathbb{C}^2. \tag{V.1.38}$$

The strictness comes from $(a, b) = (2, 0)$. The real squares in (V.1.37) diagnose zero sets. Their precise action normalization can vary with the metric and coupling convention; only the zero sets are used here.

There are two limits to the example. A holomorphic map from a compact Riemann surface to the whole affine line can be constant by a separate global holomorphic-function theorem. This does not change the local equation or erase nonconstant holomorphic maps to compact targets such as $\mathbb{CP}^1$. Conversely, allowing a noncompact affine target can make the full path integral divergent because its zero modes are not confined. The four-row derivative calculation establishes no quantum correlator. When the A instanton sum is well defined, it is the input for Chapter 2; the B zero-mode integral and its complex-structure dependence feed Chapter 3.

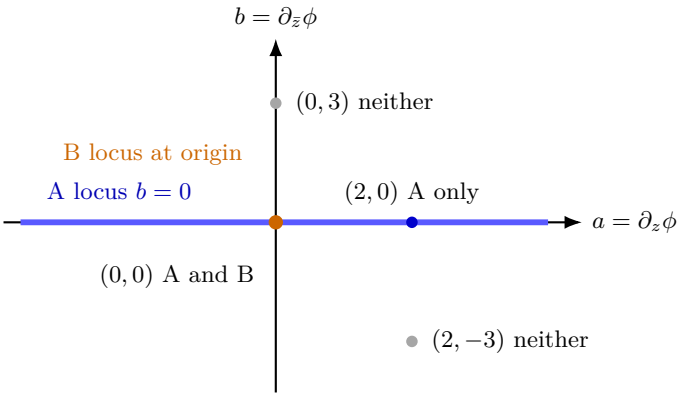


Figure V.1.4: The affine local map family is parameterized by (a, b). The A equation is the $b = 0$ axis; the B equation is its origin $a = b = 0$. The marked $(2, 0)$ map belongs only to the A locus; the positions of the nonzero marked pairs are schematic. These derivative conditions illustrate the sourced fixed equations; quantum localization requires the measure, convergence and zero-mode premises stated in the text.

V.1.6 The protected boundary

What can a twisted correlator determine about the untwisted physical theory? In this section $\langle A\rangle_B$ denotes the unnormalized topological integral $\int D\Phi\, A e^{-S_B}$, with its specified insertions; it is not divided by the empty amplitude. Suppose a particular twisted theory has a Q-exact stress tensor, with the schematic graded relation

$$T^{\mathrm{tw}}_{\mu\nu} = \{Q, G_{\mu\nu}\}. \tag{V.1.39}$$

Take Q-closed insertions $\mathcal{O}_i$ at separated points. A variation of worldsheet metric inserts the stress tensor, with normalization fixed by the action convention. If the integral converges, the measure is Q-invariant, and boundary, contact and insertion variations cause no extra term, the unnormalized Ward identity gives

$$\begin{aligned}\delta_h \left\langle \prod_i \mathcal{O}_i \right\rangle &\propto \int_\Sigma \delta h^{\mu\nu} \left\langle \{Q, G_{\mu\nu}\} \prod_i \mathcal{O}_i \right\rangle \\ &= 0.\end{aligned} \tag{V.1.40}$$

The second line uses those hypotheses; Q-closedness alone controls neither integration boundaries nor contact terms. Hori et al. derive the stress-tensor relation for this topological setup.

One may instead form a normalized quotient only when both integrals are finite and $Z = \int D\Phi\, e^{-S}$ is nonzero. Set $\langle A\rangle_{\mathrm{norm}} = N_A/Z$ with $N_A = \int D\Phi\, A e^{-S}$. With the insertion and measure fixed in λ, and differentiation under the integral justified, a parameter with $\partial_\lambda S = \{Q, V\}$ differentiates both numerator and denominator. Its connected response is

$$\partial_\lambda \langle A\rangle_{\mathrm{norm}} = -\langle A\{Q, V\}\rangle_{\mathrm{norm}} + \langle A\rangle_{\mathrm{norm}} \langle \{Q, V\}\rangle_{\mathrm{norm}}. \tag{V.1.41}$$

For $[Q, A\} = 0$, both terms vanish by the valid Ward identity. Measure, boundary and contact control remain conditions on the integral, not consequences of $Q^2 = 0$.

The source argument below uses the unnormalized correlators defined above, so it requires no division by Z. It holds for fixed insertions and measure, or when their extra variations vanish by a separately controlled Ward argument, and with the convergence, contact and boundary hypotheses of the Ward step. In Hori's B-twisted setting, a D-term deformation inserts a Q-exact integrated density. Under those conditions its derivative vanishes:

$$\partial_{\lambda_D} \langle \mathcal{O}_1 \cdots \mathcal{O}_n \rangle_B = - \left\langle \int_\Sigma \{Q, V_D\} \mathcal{O}_1 \cdots \mathcal{O}_n \right\rangle_B = 0. \tag{V.1.42}$$

The source shows this for the B D term by writing the inserted superspace expression as a Q commutator. By contrast, a chiral-parameter deformation yields an integrated two-form descendant $\mathcal{O}^{(2)}_{\mathrm{ch}}$, the deformation density on Σ. It is Q-invariant in the relevant integrated sense and need not be Q-exact, so the derivative need not vanish:

$$\partial_{\lambda_{\mathrm{ch}}} \langle \mathcal{O}_1 \cdots \mathcal{O}_n \rangle_B \propto \left\langle \int_\Sigma \mathcal{O}^{(2)}_{\mathrm{ch}} \mathcal{O}_1 \cdots \mathcal{O}_n \right\rangle_B . \tag{V.1.43}$$

This is the source's chiral descendant; the A model exchanges the type of retained protected parameter in the same setting. Topological correlators can therefore depend on specified couplings.

For a more concrete protected observable, consider a B-twisted genus-zero unnormalized three-point function of Q-closed operators, with the requisite zero-mode and insertion conditions. Its D-term response is zero by (V.1.42); a chiral deformation can change it by (V.1.43). For a positive-dimensional Calabi–Yau B target, the cited genus-zero ghost-number selection rule requires insertions of total degree $2 \dim_{\mathbb{C}} X$; an empty amplitude of degree zero can therefore vanish. We do not normalize this example by that amplitude. An ordinary untwisted excitation energy $E_n(h, \lambda_D)$ is a different quantity. No equation above identifies E_n with this three-point function, so the Ward argument imposes no corresponding D-term independence on that energy. The same applies to a generic untwisted scattering amplitude. One must identify a particular physical coupling with specified twisted insertions and establish its protection and zero-mode conditions before transferring a topological calculation.

Here a twisted physical local operator is a Q-cohomology class; untwisted string vertices also obey worldsheet constraints and their own ghost rules. A proposed physical-coupling transfer must specify its untwisted coupling and insertion map and justify the zero-mode and measure identification.

Witten discusses special physical Yukawa couplings related to the A/B constructions. That further physical argument is taken up in Chapter 10. Figure V.1.5 draws this as a separate arrow. It prevents a common overextension: a protected twisted correlator does not by itself define an arbitrary physical string amplitude. Worldsheet *bc* ghosts, spacetime on-shell conditions, integrated vertices and other physical-string ingredients still have their own roles when a string amplitude is claimed.

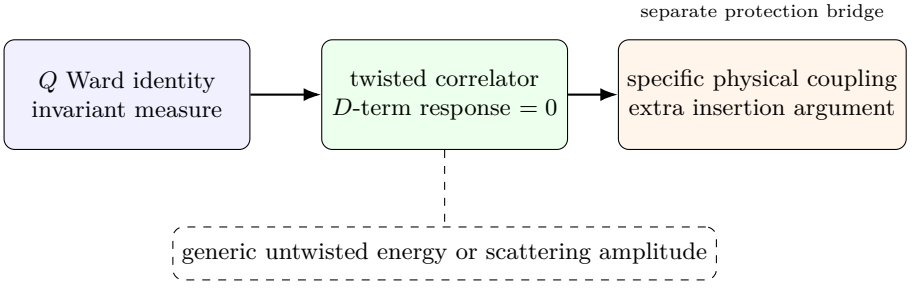


Figure V.1.5: The Ward identity protects specified twisted correlators against Q-exact variations. A further, source-specific insertion and protection argument is needed to identify a physical Yukawa coupling. A generic untwisted energy or scattering amplitude sits outside that implication.

V.1.7 Exercises

The reader companion specifies the exact submitted JSON fields for Exercises 1–4 under task identifiers `FI-IV-1-E1` through `FI-IV-1-E4`. The short-answer checker evaluates those fields; the requested explanations are written work. Exercise 5 is written only.

1. Use the row order and charge triples in (V.1.3). Compute all four A and B spins from $m' = m + q_R$ and list each scalar pair in that row order. Explain why a classically conserved but anomalous R current does not define the same twist on an arbitrary curved worldsheet.

2. For the complex (V.1.15), compute the three cohomology dimensions, check $d_1 d_0 = 0$, and decide whether $2x + 3y$ is exact and whether $[z]$ is nontrivial. Show the degree-one kernel and image, rather than inferring the answer from dimensions alone.

3. Consider two separate one-factor abelian GLSMs without superpotentials, with chiral charge lists $(1, 1, -2)$ and $(1, 1)$. Use (V.1.8) to calculate their sums, decide whether the continuous axial symmetry passes this gauge-anomaly test for the B twist, and give the coefficient of α in the second theta shift. Identify the interaction and global conditions that the sum does not test.

4. For the local flat maps $\phi = az + b\bar{z} + c$, test $(a, b) = (2, 0), (0, 3), (0, 0), (2, -3)$ in that order. Submit $|\bar{\partial}\phi|^2$, $|\partial\phi|^2 + |\bar{\partial}\phi|^2$, and the A and B fixed-locus flags. Explain why this local calculation does not establish convergence of a noncompact-target path integral.

5. In a B-twisted setting satisfying the Q Ward identity, explain the response of a Q-closed correlator to a Q-exact D-term deformation. Contrast an ordinary untwisted excitation energy and state what extra physical argument is needed before using a twisted result for a Yukawa coupling. This is a written interpretation task.

V.1.8 Take-home message

Take-home message

An anomaly-free integral R current changes the rotation generator and can make two supercharges scalar. In the stated zero-central-charge sector, their sums define Q-cohomology. The A and B local operators then probe de Rham and Dolbeault-polyvector geometry, respectively, under the sourced sigma-model identifications. Conditional localization retains holomorphic maps for A and constant maps for B. A Q-exact stress tensor protects specified correlators when the quantum Ward premises hold; a physical coupling needs its own insertion and protection bridge.

The reader should now be able to compute twisted spins from the source charges, distinguish scalar spin from nilpotence, calculate a finite cohomology quotient, test the abelian axial anomaly, and classify the local A/B fixed equations. These operations prepare the enumerative A-model construction of Chapter 2, the B-model geometry of Chapter 3, the open sectors of Chapter 6, and the protected-coupling discussion of Chapter 10. The quantum operator identifications, localization argument and Ward identity are cited with their conditions; the finite and affine examples do not prove them.

Status and sources

R currents and spin. The Euclidean charge and twist convention is the stated $M_E + F_R$ frame. Hori et al.'s actual component and supercharge tables are at Hori et al. 2003, physical PDF pp. 420–423, Sec. 16.2. Equations (V.1.4)–(V.1.7) are direct arithmetic in that table [MATH]. The abelian theta shift is the cited GLSM anomaly result Hori et al. 2003, physical PDF pp. 374–376, eqs. (15.50)–(15.58) [ANOM]; the two integer sums are direct examples [MATH]. Witten's B determinant obstruction is at Witten 1991, physical PDF p. 16, Sec. 4.1 [ANOM]. The distinct vector-charge-2 and axial-charge-0 superpotential conditions, including vector quasi-homogeneity, are at Hori et al. 2003, physical PDF p. 315, Sec. 13.2.1, eq. (13.27). The holomorphically trivial compact Kähler target is a sufficient worked class subject to the stated quantum symmetry and measure conditions, not a classification of all globally valid twists.
Scalar supercharges. The central-charge algebra is at Hori et al. 2003, physical PDF p. 303, eqs. (12.78)–(12.79), and the zero-center topological setup at Hori et al. 2003, physical PDF p. 417, eqs. (16.1)–(16.2) [WS-T]. Witten's component closure qualifier is at Witten 1991, physical PDF p. 8, eq. (3.1), p. 14, eq. (4.2) [WS-T]. The topological field degrees are from Witten 1991, physical PDF pp. 10, 16–17; they are distinct from the reparametrization ghost convention of Volume II, Chapter 2. The three-term complex is calculated explicitly here [MATH]; it certifies no field-theory nilpotence or operator theorem.
Local observables. The A form-to-operator map and its Q differential are at Witten 1991, physical PDF pp. 10–11, eqs. (3.9)–(3.10); the B Dolbeault-polyvector map is at Witten 1991, physical PDF pp. 16–17, eqs. (4.8)–(4.10) [WS-T]. The $\mathbb{CP}^1$ ordinary cup product and patchwise $\bar{\partial}$ examples are direct mathematical calculations [MATH]. The

classical versus instanton-product distinction is explicit at Hori et al. 2003, physical PDF p. 436, eqs. (16.79)–(16.82); no quantum product relation is claimed here. Witten defines $\eta^{\bar{i}}$ and θ_i at Witten 1991, physical PDF p. 14, eqs. (4.1)–(4.2); his displayed lower-index ψ in the local-operator contraction is at Witten 1991, physical PDF p. 17, eqs. (4.8)–(4.10).

Localization equations. The fixed-degree A argument and its holomorphic locus are cited from Witten 1991, physical PDF pp. 8–10, eqs. (3.3)–(3.8); the B weak-coupling constant-map locus is cited from Witten 1991, physical PDF pp. 14–15, eqs. (4.4)–(4.6) [WS-T]. Both use the source's quantum, convergence and zero-mode assumptions. The four affine residuals are local derivative calculations [MATH], with no noncompact-target path-integral conclusion.

The protected boundary. The conditional twisted stress-tensor relation is in Hori et al. 2003, physical PDF pp. 424–425, eqs. (16.27)–(16.28); B D-term exactness and potential chiral dependence are in Hori et al. 2003, physical PDF pp. 425–426, eqs. (16.29)–(16.35) [WS-T]. The Ward manipulation shown here assumes an invariant measure and controlled insertions, contacts, boundaries and convergent integrals; its normalized illustration additionally assumes nonzero Z. The genus-zero B selection rule used to delimit the unnormalized example is at Witten 1991, physical PDF p. 17, eq. (4.7). The special physical Yukawa discussion is sourced at Witten 1991, physical PDF pp. 2–3; no general physical-coupling transfer is proved here. The graded fields of E1–E4 check the four displayed finite tasks; their written parts and E5 are reasoning exercises, not numerical certifications.

References

Hori, K. et al. (2003). *Mirror Symmetry*. Vol. 1. Clay Mathematics Monographs. American Mathematical Society and Clay Mathematics Institute.

Witten, E. (1991). *Mirror Manifolds and Topological Field Theory*. arXiv: `hep-th/9112056`.

Chapter V.2

Topological sigma models and Gromov–Witten theory

V.2.1 Three points and one sphere map

Place three marked points on a worldsheet sphere and ask an A-model map to send them to three chosen points of a target sphere. A degree-one holomorphic map can meet those conditions exactly once. This simple observation is the beginning of curve counting in the A model. It is also a useful warning: a count made on smooth maps must still be related to the compact space of maps used to define a Gromov–Witten invariant.

Chapter 1 supplied the scalar A charge in the ordinary sector with vanishing central charges. Here we first keep the worldsheet complex structure and insertion positions fixed. We then allow marked domains to move and acquire nodes. The distinction matters even for an elementary sphere example: fixed-domain localization motivates an incidence count, while stable maps and a virtual class define its mathematical extension. The resulting three-point invariant changes the product of cohomology classes. A rigid curve in a Calabi–Yau threefold gives a second lesson: degree-two maps can cover an existing curve, so a rational coefficient need not count new embedded curves.

The target will be a smooth projective variety over $\mathbb{C}$ when a stable-map theorem is used. Our running compact target is $X = \mathbb{CP}^1$. We write $H \in H^2(X, \mathbb{Z})$ for the point class, normalized by $\int_X H = 1$. The local-curve example uses only positive-degree maps to a rigid embedded $\mathbb{P}^1$ and a specified obstruction integral. These two examples will supply the inputs for the mirror computations of Chapter 4 and the curve-counting organization of Chapter 8.

V.2.2 Holomorphic maps and observables

What does an A-model insertion at a marked point actually constrain? Let Σ be a fixed Riemann surface with complex coordinate z, let X be Kähler, and let $\phi : \Sigma \to X$ be

the bosonic map. In the ordinary zero-center A twist, the scalar-charge fixed equation on the map is the holomorphic-map equation. In target holomorphic coordinates u^i it reads

$$\bar\partial\phi^i = 0, \qquad \partial\phi^{\bar\imath} = 0. \tag{V.2.1}$$

We use the target form and metric $J = ig_{i\bar\jmath}\, du^i \wedge d\bar u^{\bar\jmath}$ and $ds^2 = 2g_{i\bar\jmath}\, du^i d\bar u^{\bar\jmath}$. Thus $\int_C J > 0$ for an effective holomorphic curve C. The fixed equation selects a locus; the path-integral reduction also requires a compatible measure and the zero-mode conditions stated below.

A closed A-model local observable associated with a cohomology class $\gamma \in H^*(X)$ is inserted at a chosen $x \in \Sigma$. On a smooth fixed-domain map space $\mathcal{M}_\Sigma(X,\beta)$, the marked point determines an evaluation map. Pulling back γ turns the observable into a cohomology class on maps:

$$\mathrm{ev}_x : \mathcal{M}_\Sigma(X,\beta) \longrightarrow X, \qquad f \longmapsto f(x), \qquad \mathcal{O}_\gamma(x) \longleftrightarrow \mathrm{ev}_x^*\,\gamma. \tag{V.2.2}$$

Here $\beta = f_*[\Sigma]$ is the homology class. If γ is Poincaré dual to a subvariety D, the insertion asks that $f(x)$ lie on D. For $X = \mathbb{CP}^1$, H is dual to a point, so $\mathrm{ev}_x^* H$ imposes one target-point condition. In the source's action convention, ω_{Hori} is its Kähler form and B_{Hori} its real B field. Relative to the book forms J and B, they are $\omega_{\mathrm{Hori}} = J/(2\pi\alpha')$ and $B_{\mathrm{Hori}} = B/(2\pi\alpha')$. Define the fixed-class action weight $q_\beta = \exp[-\int_\beta(\omega_{\mathrm{Hori}} - iB_{\mathrm{Hori}})]$; its relation to the book parameter q_C is given in (V.2.26). For the evaluation-only formula below, the fixed-worldsheet index must be nonnegative and the one-form fermion ρ must have no zero modes. Geometrically, the latter is the unobstructed condition $H^1(\Sigma, f^*TX) = 0$ for the fixed-source map deformation problem, whose obstruction space appears again in the next section. Assume also a smooth map space and transverse insertions. Under these restrictions, a product of observables reduces to an intersection of evaluation pullbacks:

$$\left\langle \prod_{i=1}^n \mathcal{O}_{\gamma_i}(x_i) \right\rangle_{\beta,\Sigma} \;\sim\; q_\beta \int_{\mathcal{M}_\Sigma(X,\beta)} \bigwedge_{i=1}^n \mathrm{ev}_{x_i}^*\,\gamma_i. \tag{V.2.3}$$

For a holomorphic map, the bosonic action in the source normalization is bounded below by its Kähler area. The excess is a nonnegative norm of the antiholomorphic derivative. Including the B coupling gives the schematic fixed-locus decomposition

$$S_{\mathrm{bos}}(\phi) = \|\bar\partial\phi\|^2 + \int_\beta(\omega_{\mathrm{Hori}} - iB_{\mathrm{Hori}}), \qquad S_{\mathrm{bos}}\big|_{\bar\partial\phi=0} = \int_\beta(\omega_{\mathrm{Hori}} - iB_{\mathrm{Hori}}). \tag{V.2.4}$$

The norm depends on the metrics, while the last term depends only on the curve class. Holomorphic maps minimize the action. Cancellation of other fluctuations is a separate localization premise.

The symbol $\sim$ keeps these premises visible. When ρ has zero modes, an obstruction contribution requires further treatment; the bare evaluation integral does not supply it, even on a smooth map space. For the genus-zero $\mathbb{CP}^1$ maps below, $f^*TX \simeq \mathcal{O}(2d)$ has vanishing H^1. The stable-map invariant defined later uses varying domains and a virtual class; this fixed-domain expression is not its definition.

To see the incidence mechanism directly, take the domain and target to be $\mathbb{CP}^1$. Use the affine coordinate z on the domain and w on the target. Choose ordered domain marks $(x_1, x_2, x_3) = (0, 1, \infty)$ and distinct target points $(y_1, y_2, y_3) = (1, \infty, 0)$. A degree-one map has the Möbius form $w = (az + b)/(cz + d)$ with $ad - bc \neq 0$. The first and third incidences give $b/d = 1$ and $a/c = 0$; the second forces $c + d = 0$. Projective rescaling leaves one map:

$$(a : b : c : d) = (0 : 1 : -1 : 1), \qquad f(z) = \frac{1}{1 - z}, \qquad \big(f(0), f(1), f(\infty)\big) = (1, \infty, 0). \tag{V.2.5}$$

The matrix determinant is 1, so this is genuinely degree one. More generally, each condition $f(x_i) = y_i$ is linear in the homogeneous coefficients (a, b, c, d) once x_i and y_i are written as pairs of homogeneous coordinates. Three distinct source and target points give three independent rows. Their nullspace is one-dimensional, and its nonzero determinant selects a projective automorphism. Thus the special numerical choice is not a coincidence of the affine chart. Any two ordered triples of distinct points are related by unique coordinate changes on their spheres. Hence the special coordinates prove the same statement for generic distinct triples. Figure V.2.1 shows the two triples and their orientation as complex spheres.

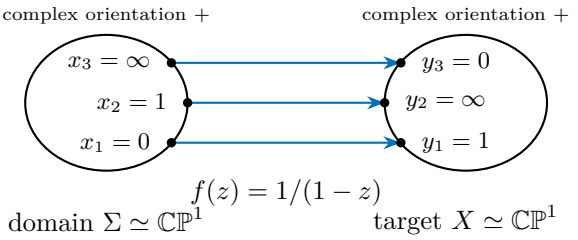


Figure V.2.1: Three ordered smooth marks on the complex-oriented domain sphere and three distinct target points. The arrows encode the degree-one holomorphic map $f(z) = 1/(1 - z)$ in the displayed affine charts. The point at infinity is a chart point, not a fourth marked insertion.

This calculation has a useful limit. A smooth degree-d map can exist without meeting the number of generic point conditions needed by a correlator. The fixed-domain argument also says nothing by itself about nodal limits. The next section supplies the dimension test; the third supplies the compactified object. These distinctions prevent a literal smooth-map count from being mistaken for a general definition of the A-model invariant.

V.2.3 Virtual dimension

Why can an insertion correlator vanish when maps of the required degree exist? The first filter compares the complex dimension expected of the map space with the total complex codimension of the insertions. Let D be a smooth connected genus-g source

with n ordered markings, $f : D \to X$ a map of class β, and $m = \dim_{\mathbb{C}} X$. Infinitesimal deformations of f with the source fixed lie in $H^0(D, f^*TX)$; obstructions lie in $H^1(D, f^*TX)$. Their difference is the map index

$$\chi(D, f^*TX) = h^0(D, f^*TX) - h^1(D, f^*TX) = m(1-g) + \int_\beta c_1(TX). \tag{V.2.6}$$

This is Riemann–Roch for the rank-m bundle f^*TX. It is an index even when the actual deformation space is larger than expected. For a smooth pointed source, infinitesimal automorphisms are sections of $TD(-p_1 - \cdots - p_n)$, the tangent sheaf whose vector fields vanish at the marks; first-order deformations are measured by its H^1. Riemann–Roch gives $\chi\big(TD(-p_1 - \cdots - p_n)\big) = \deg TD - n + 1 - g = 3 - 3g - n$. Therefore the difference between deformations and infinitesimal automorphisms of the marked curve is the pointed-curve index

$$\dim \mathrm{Def}(D, p_1, \ldots, p_n) - \dim \mathrm{Aut}(D, p_1, \ldots, p_n) = 3g - 3 + n. \tag{V.2.7}$$

For an unstable underlying marked curve, the two terms separately need not have the familiar moduli interpretation, but their difference still enters the stable-map deformation complex. Adding the two indices gives the expected complex dimension that will govern stable-map intersections. Denote this index by $v_{g,n}(X, \beta)$:

$$v_{g,n}(X, \beta) = (m-3)(1-g) + \int_\beta c_1(TX) + n. \tag{V.2.8}$$

Figure V.2.2 keeps the map and domain contributions separate. The virtual class defined below will be assigned this dimension. It is not an assertion that every component of the ordinary moduli space has that dimension.

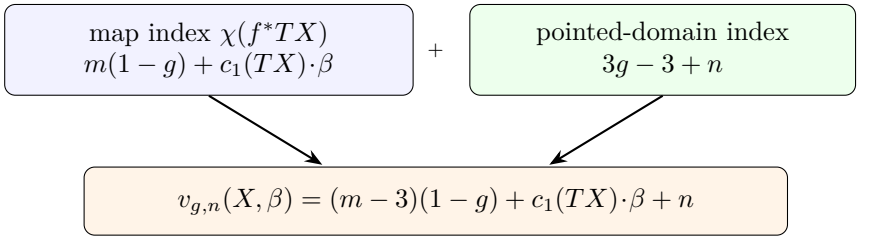


Figure V.2.2: The two complex deformation indices. The $H^0 - H^1$ term varies the map with the domain fixed; the $3g - 3 + n$ term varies marked domains modulo infinitesimal automorphisms. Their sum is the virtual dimension, even when an obstruction space makes the actual moduli space singular.

Each insertion $\gamma_i \in H^{2c_i}(X)$ has complex codimension c_i. For the primary invariant defined below, its total complex codimension must fill $v_{g,n}(X, \beta)$:

$$\sum_{i=1}^{n} c_i = (m-3)(1-g) + \int_\beta c_1(TX) + n. \tag{V.2.9}$$

This is a necessary condition. Even at matching degree, geometry or symmetry can make the invariant zero. There is a related physical selection rule on a fixed worldsheet. If an A observable comes from a Hodge class of bidegree (p_i, q_i), the vector and axial charge balances in the fixed-domain treatment require equal holomorphic and antiholomorphic sums. Each sum equals the fixed-map index $k = m(1-g) + c_1(TX) \cdot \beta$ under that treatment's zero-mode assumptions:

$$\sum_i p_i = \sum_i q_i = k, \qquad k = m(1-g) + c_1(TX) \cdot \beta. \tag{V.2.10}$$

This is a selection rule for fixed source complex structure and fixed insertion positions. The stable-map dimension additionally includes the pointed-domain index $3g - 3 + n$. At genus zero with three marks, that extra index is zero. This is why the H, H, H example can be read in both languages with the same number $k = 3$. For general g or n, simply copying the fixed-worldsheet selection rule into a stable-map integral would omit domain-moduli data. The virtual class used below has this top degree; its existence is a mathematical theorem.

For $X = \mathbb{CP}^1$, $m = 1$, $c_1(TX) = 2H$, and $\beta = d[\mathbb{CP}^1]$. At genus zero with three marks, the two indices and their sum are especially transparent:

$$\chi(f^*T\mathbb{CP}^1) = 2d + 1, \qquad 3g - 3 + n = 0, \qquad v_{0,3}(\mathbb{CP}^1, d) = 2d + 1. \tag{V.2.11}$$

At $d = 1$, three H insertions have total codimension $1 + 1 + 1 = 3$, equal to $2d + 1 = 3$. The Möbius calculation then gives a nonzero example, once the compactification and multiplicity are checked. Replace one H by the identity $1 \in H^0(X)$ and the insertion codimension falls to 2, while the virtual dimension stays 3. Thus $\langle H, H, 1\rangle_{0,1} = 0$ by dimension. Keep three H insertions but set $d = 2$ and the dimension rises to 5; hence $\langle H, H, H\rangle_{0,2} = 0$ by dimension. These zeros do not say that degree-two maps are absent.

For comparison, $d = 0$ gives virtual dimension 1. The invariant $\langle H, 1, 1\rangle_{0,0}$ fills that dimension and reduces to $\int_X H = 1$ because a three-marked degree-zero map is a constant map with its image in X. This is the unit's classical three-point pairing. These four cases are precisely the data used in the first two exercises.

One can also see why $\mathbb{CP}^1$ is unusually friendly. For a smooth degree-d sphere map, $f^*T\mathbb{CP}^1 \simeq \mathcal{O}(2d)$, so $h^0 = 2d + 1$ and $h^1 = 0$. The projective target is convex in genus zero. After the stable-map space is defined, this will identify its virtual class with its ordinary class. A general target can have nonzero H^1 and extra-dimensional or singular components. Replacing vdim by the actual dimension there would undo the reason virtual intersection theory is needed.

A second count checks the genus-zero $\mathbb{CP}^1$ result without invoking Riemann–Roch anew. A degree-d rational map is a pair of degree-d homogeneous polynomials (P_d, Q_d) without a common zero, modulo a common nonzero scalar. The coefficients give $2(d + 1) - 1 = 2d + 1$ parameters for a fixed parameterized source. Quotienting by the three complex parameters of PGL_2 and adding n marked source points gives

$$[2(d + 1) - 1] - 3 + n = 2d - 2 + n. \tag{V.2.12}$$

This agrees with $v_{0,n}(\mathbb{CP}^1, d) = 2d - 2 + n$. At $n = 3$ and $d = 1$, the result is 3: exactly the three free target images of the ordered marks. The quotient count is valid on the

smooth-map locus and uses the absence of a continuous stabilizer for a nonconstant map. It is a check of the index, not a replacement for virtual theory at the nodal boundary. The next section makes that boundary explicit.

For primary insertions on $\mathbb{CP}^1$, let r of the $n = r + s$ insertions be H and the other s be 1. The degree rule simplifies to

$$r = 2d - 2 + n = 2d - 2 + r + s, \qquad 2d - 2 + s = 0. \tag{V.2.13}$$

This exposes the two cases seen above: at positive degree with no identity insertions, $d = 1$ is the only possibility; at degree zero, two identities are needed for the three-point pairing with one H. A compatible degree is still no guarantee of nonvanishing, because an actual incidence or virtual-intersection calculation remains necessary.

V.2.4 Compactification of map space

What remains of a map when its domain develops a node? A stable map records more than a limiting rational function. It consists of a connected nodal curve D of arithmetic genus g, ordered distinct smooth marks $p_1, \ldots, p_n$, and a map $f : D \to X$ with $f_*[D] = \beta$. Two such data sets are identified only by a marked-domain isomorphism τ satisfying $f' = f \circ \tau^{-1}$. A component of D may be contracted. Stability requires a contracted genus-zero component to have at least three special points and a contracted genus-one component to have at least one; special points are marks or node branches. Equivalently, the automorphism group of the map must be finite.

At a node, both branches must have the same image in X. If $D = D_1 \cup D_2$ is a rational tree with one node, and $f_i = f|_{D_i}$ has degree d_i into $\mathbb{CP}^1$, then the class and matching conditions are

$$d = d_1 + d_2, \qquad f_1(q_1) = f_2(q_2), \qquad q_1 \sim q_2 \text{ is the domain node.} \tag{V.2.14}$$

The equality of images is geometric gluing data. It is not an equality of the two local coordinates on the normalization. Both components can have positive degree and hence be stable with only one node. If a degree-zero sphere is inserted between them, it must carry enough marks or further nodes to reach three special points.

Here is an explicit degeneration rather than only a picture. For $t \neq 0$ and $t \neq 1$, consider the degree-two rational map

$$f_t(z) = z + \frac{t}{z} = \frac{z^2 + t}{z}, \qquad (p_1, p_2, p_3) = (1, \infty, t). \tag{V.2.15}$$

The numerator and denominator have no common root for $t \neq 0$, so the map has degree two. As $t \to 0$, the marks p_1, p_2 stay at $1, \infty$, while p_3 approaches $z = 0$. On the main chart, away from $z = 0$, the map tends to $f_{mmain}(z) = z$. To retain what concentrates near $z = 0$, introduce a second chart $w = z/t$. Then

$$z = tw, \qquad f_t(tw) = tw + \frac{1}{w} \xrightarrow[t \to 0]{} f_{\text{bubble}}(w) = \frac{1}{w}, \qquad p_3 : w = 1. \tag{V.2.16}$$

The overlap between these charts has another useful coordinate $v = 1/w = t/z$. The smoothing relation is $zv = t$, and the family map becomes $f_t = z + v$. At $t = 0$, the

equation $zv = 0$ has two branches. The branch $v = 0$ carries $f = z$; the branch $z = 0$ carries $f = v = 1/w$:

$$zv = t, \qquad f_t = z + v, \qquad t = 0 : \ \{v = 0\} \cup \{z = 0\}, \qquad f|_{v=0} = z, \quad f|_{z=0} = v. \tag{V.2.17}$$

The two branches meet at $(z, v) = (0, 0)$, which maps to target 0. This equation specifies the coordinate transformation and the gluing point instead of relying on a suggestive drawing. Both limiting maps have degree one. The main component attaches at $z = 0$; the bubble attaches at $w = \infty$. Their node images agree, since $f_{\text{main}}(0) = 0$ and $f_{\text{bubble}}(\infty) = 0$. The total degree remains $1 + 1 = 2$. The first two marks are smooth points on the main component and the third is a smooth point on the bubble. No mark coincides with the node. Figure V.2.3 shows both charts and the common target point. This construction is the model for written Exercise E5. It also shows why simply cancelling the common factor z in $f_0 = (z^2 + 0)/z$ loses information: the resulting rational function z remembers only the main component. The rescaled chart retains the missing degree. The family of stable maps retains total degree two while the naive cancelled expression has degree one.

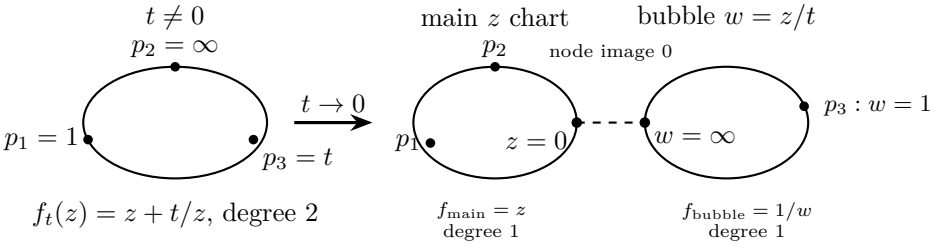


Figure V.2.3: A concrete degree-two limit of $f_t(z) = z + t/z$. For $t \neq 0$ the domain is one sphere. In the limit, the z chart carries $f_{\text{main}} = z$ and the $w = z/t$ chart carries $f_{\text{bubble}} = 1/w$. The node identifies $z = 0$ with $w = \infty$, both mapping to target 0. The ordered marks distribute as (p_1, p_2) and p_3; both components have degree one.

A contracted bubble gives a different stability test. Imagine moving two marked points onto a degree-zero sphere attached by one node to a positive-degree component. That bubble has two marks plus the node, hence three special points and finite automorphisms. With just one mark and the node it would have only two special points; a continuous Möbius subgroup would remain, so that component is not stable. This rule is local to contracted components. The degree-one bubble in our explicit family is already stable because a nonconstant finite-degree map has finite automorphisms.

For the displayed $\mathbb{CP}^1$ split, the boundary has the expected codimension one. If component i carries n_i ordinary marks and one node mark, its genus-zero virtual dimension is $2d_i - 2 + (n_i + 1) = 2d_i - 1 + n_i$. Add the two component dimensions, then impose equality of the two node evaluations in the one-complex-dimensional target:

$$(2d_1 - 1 + n_1) + (2d_2 - 1 + n_2) - 1 = 2d - 3 + n. \tag{V.2.18}$$

The smooth-map space has dimension $2d - 2 + n$, one higher. The missing dimension

is the smoothing parameter t in $zv = t$. This is a local dimension explanation of the boundary, not a proof of the general gluing theorem.

The stable-map stack $\overline{\mathcal{M}}_{g,n}(X,\beta)$ allows such nodal domains and varying marks. Its complex virtual dimension is the previously computed $v_{g,n}(X,\beta)$. For smooth projective X, properness and the existence of a virtual fundamental class are established mathematical results. We use those theorems in the definition below. For $\gamma_i \in H^*(X)$, the primary Gromov–Witten invariant is defined by

$$\langle \gamma_1, \ldots, \gamma_n \rangle_{g,\beta}^X := \int_{[\overline{\mathcal{M}}_{g,n}(X,\beta)]^{\mathrm{vir}}} \prod_{i=1}^{n} \mathrm{ev}_i^* \, \gamma_i, \qquad \mathrm{ev}_i([D,\mathbf{p},f]) = f(p_i). \tag{V.2.19}$$

The virtual class has complex dimension given by (V.2.8). It weights obstructed families in their expected dimension. The formula neither identifies the virtual number with a count of isolated maps nor constructs the virtual class. Compactness, virtual-class construction and gluing are cited theorems; the chart limit above only teaches what one boundary point records.

The physical and mathematical routes now meet in a controlled special case. Fixed-worldsheet A localization keeps the complex structure and insertion positions fixed. The stable-map invariant integrates over varying marked domains and includes nodal boundary strata. Coupling a worldsheet theory to the needed topological-gravity or domain-moduli measure is an additional physical step. For genus-zero three-point primary functions, $\overline{\mathcal{M}}_{0,3}$ has no continuous domain moduli, so the smooth incidence problem is particularly close to the stable-map one. That observation alone does not erase the boundary or prove a general path-integral equality.

We can now justify the value of the degree-one three-H invariant. A degree-one stable map has one positive-degree component. Any attached tree of contracted rational components would need at least two marks. Indeed, if such a tree has k vertices and m marks, the total number of special-point incidences is $2(k-1)+1+m$; stability demands at least $3k$, hence $m \geq k+1 \geq 2$. But two distinct target-point insertions cannot lie on the same contracted tree, because all its marks have the same image. Thus the three distinct incidences exclude contracted boundary trees. The combinatorics can be kept in one line:

$$2(k-1)+1+m \geq 3k \quad \Longrightarrow \quad m \geq k+1 \geq 2. \tag{V.2.20}$$

The 1 counts the attachment to the positive-degree component. If the contracted tree carried two marks, both would evaluate to its one image, contradicting their distinct target conditions. The remaining map is the unique Möbius map of (V.2.5). Its automorphism is trivial: $f \circ \tau = f$ and invertibility of f imply $\tau = 1$. The evaluation map from the smooth degree-one three-mark locus to triples of distinct target points is locally an isomorphism, so the incidence has multiplicity one. Consequently,

$$\langle H, H, H \rangle_{0,1}^{\mathbb{CP}^1} = 1. \tag{V.2.21}$$

This argument uses the convexity of $\mathbb{CP}^1$ to identify its virtual and ordinary classes. Distinct incidence is essential to the boundary exclusion. The result is the nontrivial coefficient needed by the next section.

V.2.5 Quantum product

How can one map change a classical ring relation? Ordinary cohomology of $\mathbb{CP}^1$ has basis $(1, H)$ with $H \smile H = 0$ for degree reasons. The A-model small quantum product uses genus-zero three-point invariants instead. To turn a three-point number into a product coefficient, first compute the Poincaré pairing $\eta_{ab} = \int_X T_a \smile T_b$ for $(T_0, T_1) = (1, H)$. The only nonzero entries are $\eta_{01} = \eta_{10} = 1$, and the inverse matrix has the same off-diagonal form:

$$(\eta_{ab}) = (\eta^{ab}) = \begin{pmatrix} 0 & 1 \\ 1 & 0 \end{pmatrix}, \qquad \int_X 1 \smile H = 1, \qquad \int_X H \smile H = 0. \tag{V.2.22}$$

Let $C_{abc}(q_C) = \sum_{d \geq 0} q_C^d \langle T_a, T_b, T_c \rangle_{0,d}$. With the third index raised by the inverse pairing, the product is

$$T_a * T_b = \sum_{c,e} C_{abe}(q_C)\, \eta^{ec} T_c. \tag{V.2.23}$$

For $H * H$, the coefficient along 1 pairs the two H factors with H, because $\eta^{H,1} = 1$. At degree zero this is $\int_X H^3 = 0$. At degree one it is (V.2.21); higher degrees fail (V.2.9). The coefficient along H instead tests $\langle H, H, 1 \rangle_{0,d}$ and vanishes by dimension in every nonnegative degree. Thus the complete relation is

$$H * H = q_C\, 1, \qquad QH^*(\mathbb{CP}^1) \simeq \mathbb{Q}[H, q_C]/(H^2 - q_C). \tag{V.2.24}$$

The same index raising determines every basis entry, which is useful before using the quotient-ring presentation. At degree zero, $\langle 1, 1, H \rangle_{0,0} = \int_X H = 1$ supplies the unit coefficient of $1 * 1$, and $\langle 1, H, 1 \rangle_{0,0} = 1$ supplies the H coefficient of $1 * H$. The other possible primary three-point degrees have mismatched codimension. We can summarize the nonzero data actually used as

$$\langle 1, 1, H \rangle_{0,0} = \langle 1, H, 1 \rangle_{0,0} = \langle H, H, H \rangle_{0,1} = 1. \tag{V.2.25}$$

The unit property follows from the degree-zero pairing and the standard genus-zero primary axioms. For this ring, it can be checked directly on the basis: $1 * 1 = 1$ and $1 * H = H$. The relation is a deformation of $H \smile H = 0$, not a change of the underlying additive cohomology.

The parameter q_C has a physical normalization. For a curve class C the book uses the complexified Kähler period

$$t_C = \frac{1}{4\pi^2 \alpha'} \int_C (B + iJ), \qquad q_C = e^{2\pi i t_C} = \exp\left[-\frac{1}{2\pi\alpha'} \int_C (J - iB) \right]. \tag{V.2.26}$$

A shift of the normalized B period by an integer changes t_C by an integer, so it leaves q_C invariant. For an effective class $d[C]$, the action is additive and the weight is q_C^d. Thus the degree-one incidence found above enters the product with exactly one power of q_C, while the classical constant maps enter with $q_C^0 = 1$. The B period is unit-periodic in this convention. The source expression $e^{-t_{\mathrm{Hori}}}$ uses $t_{\mathrm{Hori}} = \int_C (\omega_{\mathrm{Hori}} - iB_{\mathrm{Hori}})$. Its action weight matches (V.2.26) when $\omega_{\mathrm{Hori}} = J/(2\pi\alpha')$ and $B_{\mathrm{Hori}} = B/(2\pi\alpha')$. We

therefore identify $e^{-t_{\mathrm{Hori}}} = q_C$ at the level of weights. The two symbols t_{Hori} and t_C have different definitions and are not equated. Figure V.2.4 displays the pairing step and the resulting product.

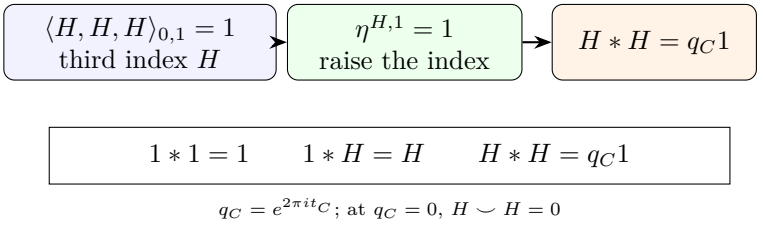


Figure V.2.4: Raising the last index of a three-point invariant with the off-diagonal pairing. The H, H, H coefficient at degree one contributes to the unit channel of $H * H$. The small multiplication table uses the book weight $q_C = e^{2\pi i t_C}$; its classical limit is $q_C \to 0$.

A nonunit example tests more than the single relation. For $a, b, c, d \in \mathbb{Q}$ the product is

$$(a + bH) * (c + dH) = (ac + bdq_C) + (ad + bc)H. \tag{V.2.27}$$

Set $q_C = 2/3$. Multiplying $(1 + 2H)$ and $(3 - H)$ gives the intermediate terms $3 - H + 6H - 2H^2$, hence

$$(1 + 2H) * (3 - H) = 3 + 5H - 2q_C = \frac{5}{3} + 5H. \tag{V.2.28}$$

At $q_C = 0$ the constant coefficient returns to 3. Associativity is also visible in a small nontrivial check: $(H * H) * H = q_C H = H * (H * H)$. This calculation tests the presented ring, while the general associativity of quantum cohomology is a theorem about genus-zero invariants and gluing. The next chapter will use the B-model side; Chapter 4 will compare its periods with this A-model product.

V.2.6 Local Calabi–Yau curve counting

Why can a genus-zero Gromov–Witten coefficient be rational when the geometric input consists of curves? A map of degree $d > 1$ can cover a curve already present in the target. Such maps form families and are weighted by virtual intersection theory. Consider an embedded infinitesimally rigid $C \simeq \mathbb{P}^1$ in a smooth compact Calabi–Yau threefold Y, with normal bundle

$$N_{C/Y} \simeq \mathcal{O}_{\mathbb{P}^1}(-1) \oplus \mathcal{O}_{\mathbb{P}^1}(-1), \qquad H^0(C, N_{C/Y}) = 0. \tag{V.2.29}$$

The vanishing of normal sections explains the word rigid. It does not remove the families of degree-d maps that cover C. The proper base for their genus-zero local contribution is the stable-map stack $\overline{\mathcal{M}}_{0,0}(C, d)$, not an unrestricted integral over the noncompact total space of $N_{C/Y}$.

Let $\pi : \mathcal{U} \to \overline{\mathcal{M}}_{0,0}(C,d)$ be the universal domain curve and $F : \mathcal{U} \to C$ the universal map. For positive d, the concavity of $\mathcal{O}(-1)$ on every nonconstant component, together with stability of contracted trees, gives $R^0\pi_* F^* N_{C/Y} = 0$ in the local construction. Thus the normal obstruction spaces form the bundle $E_d = R^1\pi_* F^* N_{C/Y}$. For a smooth degree-$d$ cover, Riemann–Roch gives $\chi(f^*\mathcal{O}(-1)) = 1-d$ and $h^0 = 0$, hence $h^1 = d-1$ for each summand. The rank is therefore $2d-2$:

$$\operatorname{rk}_{\mathbb{C}} E_d = 2(d-1) = 2d-2 = \operatorname{vdim}_{\mathbb{C}} \overline{\mathcal{M}}_{0,0}(\mathbb{P}^1, d). \tag{V.2.30}$$

The last equality follows by substituting $m=1$, $g=n=0$ and $c_1(T\mathbb{P}^1)\cdot d = 2d$ into (V.2.8). Rank matching makes a top Euler-class integral possible. It does not determine its value.

The vanishing of R^0 can be understood component by component. On a positive-degree rational component, a section of $f^*\mathcal{O}(-1)$ vanishes because its degree is negative. A contracted component has constant sections, but a node attached to a component where the section vanishes forces that constant to be zero. Since the domain is a connected tree and at least one component has positive degree, this condition propagates through all contracted components. This argument explains concavity for the stated positive-degree genus-zero family. It does not define a degree-zero local target invariant.

The local contribution is defined by the proper-base obstruction integral

$$C_{0,d} := \int_{[\overline{\mathcal{M}}_{0,0}(\mathbb{P}^1,d)]^{\mathrm{vir}}} c_{2d-2}\big(R^1\pi_* F^*[\mathcal{O}(-1)\oplus\mathcal{O}(-1)]\big), \qquad d>0. \tag{V.2.31}$$

Here the stable-map stack is proper and has a projective coarse moduli space; the integral over its virtual class is well-defined in the cited local-curve setup. Finite cover automorphisms remain part of the stack calculation. One may instead use an explicitly specified equivariant integral on the noncompact total space, with proper fixed loci and localized coefficients. An unrestricted noncompact degree-zero integral has not been defined by (V.2.31).

The localization theorem for this precise genus-zero rigid $(-1,-1)$ case is

$$C_{0,d} = \frac{1}{d^3}, \qquad d = 1,2,\ldots. \tag{V.2.32}$$

The first values are $1, 1/8, 1/27$. For $d=1$, the base has virtual dimension zero and the obstruction bundle has rank zero; its contribution is 1. For $d=2$, an explicit cover is $f([Z_0:Z_1]) = [Z_0^2 : Z_1^2]$. On its smooth domain, $f^*\mathcal{O}(-1) \simeq \mathcal{O}(-2)$, so each negative normal summand has $h^1 = 1$ and the two summands give rank two. The base has complex virtual dimension two and the obstruction bundle has rank two. Its Euler class is a top-degree class on that base, and the localization integral evaluates to $1/8$. The rank check tells us why this integral has the correct degree, while the localization calculation supplies the nontrivial fraction. We have defined the bundle and checked its rank; we have not replaced the virtual-localization proof with this arithmetic. Figure V.2.5 separates the embedded curve from maps that cover it twice. Their target image can be the same even though their map degrees and virtual weights differ.

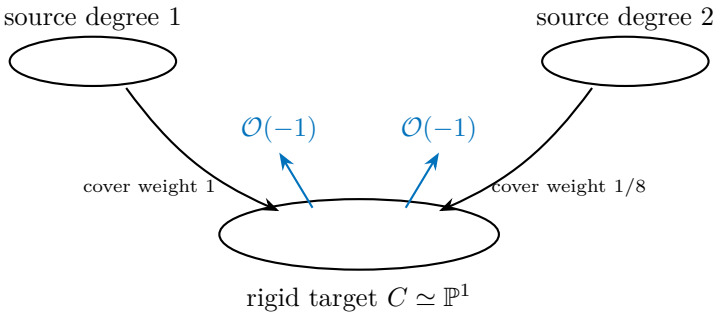


Figure V.2.5: One infinitesimally rigid target curve $C \simeq \mathbb{P}^1$ with two negative normal directions. A degree-one map and a degree-two cover have the same image C but enter different class coefficients. The double cover contributes $1/8$ under the proper-base obstruction integral; the diagram does not evaluate that integral.

Under a stated inventory of isolated rigid curves in distinct primitive classes, let N_d be the rational genus-zero Gromov–Witten coefficient at total degree d, and let n_r denote the primitive contribution at degree r in that inventory. Degree-d maps include k-fold covers of primitive degree-r curves when $d = kr$. In this restricted setting, summing their cover weights gives

$$N_d = \sum_{r|d} \frac{n_r}{(d/r)^3} = \sum_{k|d} \frac{n_{d/k}}{k^3}. \tag{V.2.33}$$

This divisor sum applies only to the stated rigid-curve inventory. It does not assert that every Calabi–Yau has such an inventory or that every n_r is a proven integer. The local normal-bundle and rigidity assumptions are the reason the same $1/k^3$ weight can be used for each term.

For a numerical example, suppose the inventory has $n_1 = 2$ and $n_2 = 3$. At total degree two the divisors are $r = 1, 2$. The two degree-one primitive curves contribute two double covers, each of weight $1/8$, while the three degree-two primitive curves contribute weight one:

$$N_2 = \frac{n_1}{2^3} + n_2 = \frac{2}{8} + 3 = \frac{13}{4}. \tag{V.2.34}$$

Conversely, if $N_2 = 13/4$ and $n_1 = 2$ are supplied under the same hypotheses, cover subtraction gives $n_2 = 13/4 - 1/4 = 3$. At total degree three the same conditional inventory would give $N_3 = n_3 + n_1/27$. This comparison shows that the denominator tracks cover degree, while the primitive degree labels which target curve is being covered. The fraction $13/4$ is a virtual amplitude made from distinct maps; it is not a literal count of new degree-two embedded curves. Chapter 8 will develop the broader integer and BPS organization. That later physics does not follow from the finite subtraction in this section.

V.2.7 Exercises

For E1–E4, use the exact JSON fields and types in the public `questions.json` companion. Show the reasoning in written work as requested. E5 is a written interpretation task.

E1. For a genus-zero degree-one map to $\mathbb{CP}^1$ with three marks and three H insertions, compute $c_1(TX) \cdot \beta$, $\chi(f^*TX)$, the pointed-curve index, the complex virtual dimension and insertion codimension. Decide whether they match. Explain why the first two indices have different geometric roles.

E2. Compute the four primary invariants $\langle H, H, H\rangle_{0,1}$, $\langle H, H, 1\rangle_{0,1}$, $\langle H, H, H\rangle_{0,2}$ and $\langle H, 1, 1\rangle_{0,0}$ in that order. For the nonzero degree-one case, use three distinct ordered domain marks and target points. Distinguish the unique-map argument from the dimension-forced zeros.

E3. In $QH(\mathbb{CP}^1) = \mathbb{Q}[H, q_C]/(H^2 - q_C)$, set $q_C = 2/3$. Compute the unit coefficient of $H * H$, both coefficients of $(1+2H)*(3-H)$, and the constant coefficient in the classical $q_C = 0$ limit. Submit exact rational strings and show the multiplication.

E4. Assume two primitive degree-one rigid $(-1,-1)$ curves and the genus-zero $1/k^3$ cover rule. Given $N_2 = 13/4$, compute the degree-two cover contribution from n_1, recover n_2, and reconstruct N_2. Submit exact rational strings. Explain why the rational total is not a literal count of new curves.

E5. Draw a degree-two stable-map degeneration with two degree-one rational components. Use $f_t(z) = z + t/z$ as one possible family. Label both charts, node branches, node images, three ordered markings and component degrees. Work out the two chart limits, then explain when a degree-zero rational bubble is stable. State which additional definition is needed before using a noncompact local target in a curve-counting integral.

V.2.8 Take-home message

Take-home message

The A-model fixed equation selects holomorphic maps under the stated quantum localization conditions. Evaluation classes turn marked insertions into incidence conditions. Stable maps preserve nodal limits, and the virtual class makes their intersections meaningful at the expected dimension. For $\mathbb{CP}^1$, the one degree-one map through three distinct incidences gives $H * H = q_C 1$ after raising an index with the Poincaré pairing. For a rigid $(-1,-1)$ curve, the defined positive-degree local obstruction integral assigns a degree-d cover weight $1/d^3$.

The reader should be able to distinguish fixed-domain localization from a stable-map invariant, calculate a virtual dimension and insertion test, resolve a nodal map into component charts, compute a quantum product from three-point data, and subtract a rigid-curve cover contribution. Properness, virtual-class existence, general gluing

and the local localization value are cited mathematical results. The displayed finite examples do not prove them.

Status and sources

Holomorphic maps and observables. The zero-center A frame and Kähler form are defined above. Fixed-worldsheet localization, its explicit no-ρ-zero-mode premise and evaluation pullbacks are at Hori et al. 2003, physical PDF pp. 429–433, especially p. 432 before eq. (16.61) and Witten 1991, physical PDF pp. 9–11 [WS-T]. The source action uses the translation to the stated curve weight. The Möbius incidence is calculated here [MATH].
Virtual dimension. The deformation sequence, pointed tangent sheaf and two indices are at Hori et al. 2003, physical PDF pp. 526–527, eqs. (24.2)–(24.3) [MATH]. The distinct fixed-worldsheet zero-mode rule is at Hori et al. 2003, physical PDF pp. 430–432, eqs. (16.55)–(16.62) [WS-T]. CP1 arithmetic is direct; convexity of projective space is cited on physical PDF p. 527.
Compactification of map space. Stable-map definitions are at Hori et al. 2003, physical PDF p. 521, Definitions 24.0.3–24.0.5. Properness and gluing use its Chapter 24; the virtual class uses Hori et al. 2003, physical PDF pp. 539–540, Sec. 26.1 [MATH]. The two-chart limit and contracted-tree inequality are direct [MATH].
Quantum product. The CP1 three-point result is at Hori et al. 2003, physical PDF pp. 435–436, eqs. (16.77)–(16.82); index raising is at Hori et al. 2003, physical PDF pp. 553–554, eqs. (26.13)–(26.15) [MATH]. The action weights use the specified curve period. The pairing and nonunit product are calculated here [MATH].
Local Calabi–Yau curve counting. Rigid-curve premises, obstruction fiber and rank are at Hori et al. 2003, physical PDF pp. 566–567, Sec. 27.5. The proper-base integral and genus-zero value are at Faber and Pandharipande 2000, physical PDF p. 3, eq. (7) [MATH]. Rank and N_2 arithmetic are direct. No all-genus equality, noncompact degree-zero integral or universal integrality is inferred. E1–E4 grade finite answers; E5 is written reasoning.

References

Faber, C. and R. Pandharipande (2000). "Hodge Integrals and Gromov–Witten Theory". In: *Inventiones Mathematicae* 139, pp. 173–199. arXiv: `math/9810173`.

Hori, K. et al. (2003). *Mirror Symmetry*. Vol. 1. Clay Mathematics Monographs. American Mathematical Society and Clay Mathematics Institute.

Witten, E. (1991). *Mirror Manifolds and Topological Field Theory*. arXiv: `hep-th/9112056`.

Chapter V.3

The B-model, special geometry, and Picard–Fuchs equations

V.3.1 A cycle that remembers complex structure

On a torus, an oriented closed path can be carried as its complex structure varies. Integrating a holomorphic one-form along that path produces a number that varies with the torus. The analogous construction on a Calabi–Yau threefold integrates its holomorphic three-form over a three-cycle. These integrals, called periods, turn a family of geometries into functions of parameters. Their differential equations make complex-structure variation calculable.

The B model of Chapter 1 singles out a protected sector in which complex-structure variation has this geometric description. This chapter follows one concrete route from cycles to equations. We first separate an intrinsic ratio of periods from the arbitrary scale of the form. We then derive the differential operator for the invariant periods of the mirror quintic, solve it near one boundary point, and examine what a loop around that point does to the solutions. The final section asks which further information is required before a local limit can describe gauge-theory masses. Chapter 4 will use the local coordinate obtained here in the mirror comparison.

V.3.2 Periods and cycles

What remains fixed when a complex structure changes? Let $\pi : \mathcal{X} \to U$ be a smooth proper family of compact Kähler Calabi–Yau threefolds over a regular, simply connected patch U. On the free lattice $H_3(X_u, \mathbb{Z})/\text{torsion}$, the intersection form is integral, perfect and antisymmetric. Transport in the family identifies these lattices locally. The Hodge decomposition of their complexification varies with u. These are results of the standard compact Hodge and smooth-family package; we use them under the stated hypotheses. Choose oriented cycles A^I, B_I with

$$A^I \cdot A^J = 0, \qquad B_I \cdot B_J = 0, \qquad A^I \cdot B_J = \delta^I_J. \tag{V.3.1}$$

The index runs from 0 to $h^{2,1}$. If Ω_u is a locally chosen nonzero holomorphic three-form, its period column is

$$X^I(u) = \int_{A^I} \Omega_u, \qquad F_I(u) = \int_{B_I} \Omega_u, \qquad \Pi(u) = \begin{pmatrix} X^I(u) \\ F_I(u) \end{pmatrix}. \tag{V.3.2}$$

The column depends on the chosen cycle basis and on the scale of Ω. The family and the form must both be specified before the numbers are defined. For a Calabi–Yau threefold the compact Hodge decomposition has four types,

$$H^3(X_u, \mathbb{C}) = H_u^{3,0} \oplus H_u^{2,1} \oplus H_u^{1,2} \oplus H_u^{0,3}, \qquad b_3 = 2h^{2,1} + 2. \tag{V.3.3}$$

The holomorphic form spans $H_u^{3,0}$. Its derivative with respect to a complex-structure coordinate can acquire an $H_u^{2,1}$ component. This is why periods vary even though the transported integral cycles and their intersection numbers stay fixed locally. The decomposition and derivative statement require the compact Hodge package just specified. For the simply connected Calabi–Yau threefold setting of the cited B-model description, selected chiral primaries are represented by components of H^3. Variation of the holomorphic form and its periods supplies protected geometric information in that sector. This does not identify every state of the full conformal field theory with a cohomology class.

The torus makes both choices visible. Put $E_\tau = \mathbb{C}/(\mathbb{Z} + \tau\mathbb{Z})$, with $\operatorname{Im}\tau > 0$. Orient A from 0 to 1, B from 0 to τ, and choose their intersection as $A \cdot B = +1$. For $\Omega = \lambda\, du$, $\lambda \neq 0$, direct integration on the covering plane gives

$$\Pi_A = \int_0^1 \lambda\, du = \lambda, \qquad \Pi_B = \int_0^\tau \lambda\, du = \lambda\tau, \qquad \frac{\Pi_B}{\Pi_A} = \tau. \tag{V.3.4}$$

At $\lambda = 7/3$ and $\tau = 2i$, the individual periods are $7/3$ and $14i/3$. Their ratio is $2i$. Replacing λ by 2λ doubles both integrals but leaves the complex structure and their ratio unchanged. Figure V.3.1 fixes the orientation used in this calculation. Its edge labels are identifications, so a path crossing an edge continues on the opposite edge.

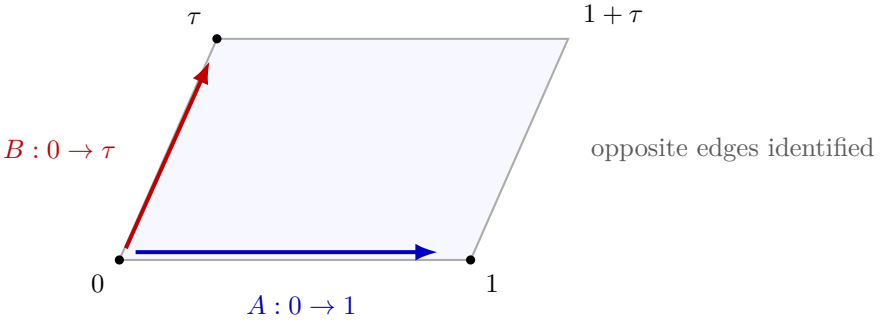


Figure V.3.1: A fundamental parallelogram for E_τ, with opposite edges identified. The blue A path runs from 0 to 1 and the red B path from 0 to τ. Their ordered intersection at the origin is chosen positive. The diagram fixes the period and active-transport conventions used below.

The torus also displays the pairing numerically. In the ordered basis (A, B), its matrix and two possible shears are

$$J = \begin{pmatrix} 0 & 1 \\ -1 & 0 \end{pmatrix}, \qquad A \cdot (B + A) = 1, \qquad A \cdot (B + 2A) = 1. \tag{V.3.5}$$

Both combinations have the same intersection with A, but they record different transported cycles. The distinction cannot be read from the pairing alone. A path in parameter space must decide which combination occurs.

The cycle basis carries more information than an arbitrary basis of solutions of a differential equation. An integral change of cycles preserves integer intersection numbers. A local differential equation, in contrast, is linear over $\mathbb{C}$ and allows any complex linear combination of its solutions. Identifying a solution with an integral period therefore requires the cycle and continuation data, not only a power series. This distinction will matter when logarithms appear near $z = 0$.

The compact hypotheses also matter. The affine quadric $Q = \{\sum_{i=1}^{4} w_i^2 = 1\} \subset \mathbb{C}^4$ is noncompact. Writing $w = x + iy$ shows that $|x|^2 - |y|^2 = 1$ and $x \cdot y = 0$. The complex quadric retracts onto its real S^3, and $H_3(Q, \mathbb{Z})$ has rank one. A nondegenerate antisymmetric pairing cannot live on a rank-one free lattice. Thus a local threefold can possess a meaningful vanishing three-cycle without admitting the compact symplectic-basis statement of (V.3.1). Chapter IV.2 supplies the compact holomorphic-top-form setting; the local models used in later construction chapters require their own boundary and charge conditions.

V.3.3 Special coordinates

Which period quantities describe a complex structure without remembering how we scaled Ω? Under $\Omega \mapsto \lambda\Omega$, every entry of (V.3.2) transforms by the same λ. On a chart with $X^0 \neq 0$, define the affine coordinate $t^i = X^i/X^0$. It is unchanged by that transformation. The full vector still matters, since it contains the dual periods and their pairing. Figure V.3.2 distinguishes the ray of homogeneous vectors from its representative on the $X^0 = 1$ chart.

$$\Omega \longmapsto \lambda\Omega \quad \Longrightarrow \quad (X^I, F_I) \longmapsto \lambda(X^I, F_I), \qquad t^i = \frac{X^i}{X^0} \longmapsto t^i. \tag{V.3.6}$$

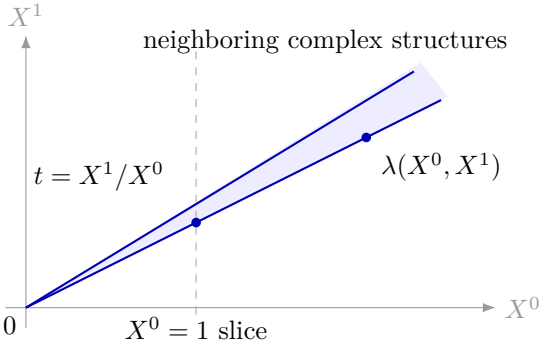


Figure V.3.2: A schematic slice of the homogeneous period cone. Scaling the holomorphic form moves along a ray. Where $X^0 \neq 0$, that ray meets the affine $X^0 = 1$ slice once. The displayed $t = X^1/X^0$ is a coordinate on this local slice, not an additional period.

The local special-geometry premise says that the dual periods can be obtained as derivatives of a homogeneous function of degree two. In the source notation this function is $G = z^a w_a$, with $\partial_a G = 2w_a$. Translating $z^a = X^I$ and $w_a = F_I$, we set $F = G/2$. Euler's identity then reads

$$F_I = \frac{\partial F}{\partial X^I}, \qquad 2F = X^I F_I, \qquad F = \frac{1}{2} X^I F_I = \frac{1}{2} G. \tag{V.3.7}$$

The existence of such an F is a local special-geometry statement in an appropriate period chart. The algebra here checks its normalization once that premise is in place. It does not construct a global single-valued prepotential across arbitrary monodromy patches.

For one modulus, write $t = X^1/X^0$ and $F(X^0, X^1) = (X^0)^2 f(t)$. The chain rule must account for the change of t when X^0 changes. Holding X^1 fixed gives $\partial t/\partial X^0 = -t/X^0$, while holding X^0 fixed gives $\partial t/\partial X^1 = 1/X^0$. Therefore

$$\frac{\partial t}{\partial X^0} = -\frac{t}{X^0}, \qquad \frac{\partial t}{\partial X^1} = \frac{1}{X^0}, \qquad \frac{F_0}{X^0} = 2f - tf', \qquad \frac{F_1}{X^0} = f'. \tag{V.3.8}$$

One can check the chain rule independently against homogeneity. Substitute the two expressions for F_I into $X^0 F_0 + X^1 F_1$. The terms proportional to tf' cancel:

$$X^0 F_0 + X^1 F_1 = (X^0)^2 (2f - tf') + X^0 X^1 f' = 2(X^0)^2 f. \tag{V.3.9}$$

This reproduces Euler's identity in (V.3.7). It is an algebraic consistency check of the local chart, independent of the numerical example.

This calculation explains why F_0 is not simply $2X^0 f$. The dependence of t on X^0 supplies the second term. It also separates the homogeneous dual periods F_I from affine derivatives of f.

For a numerical algebraic example, take

$$f(t) = \frac{7}{6} t^3 + 3t^2 - 5t + 2, \qquad f'(t) = \frac{7}{2} t^2 + 6t - 5, \qquad f'''(t) = 7. \tag{V.3.10}$$

At $t = 2$, $f = \frac{28}{3} + 12 - 10 + 2 = \frac{40}{3}$ and $f' = 14 + 12 - 5 = 21$. Choosing $X^0 = 3$, $X^1 = 6$ gives $F_1 = 3(21) = 63$ and $F_0 = 3(80/3 - 42) = -46$. The homogeneous identity checks this arithmetic:

$$2F = 2(3)^2\frac{40}{3} = 240, \qquad X^0F_0 + X^1F_1 = 3(-46) + 6(63) = 240. \tag{V.3.11}$$

If we scale the period vector by 2, the affine value $t = 2$ and $f''' = 7$ remain fixed, while F, F_0 and F_1 scale by 4, 2 and 2 respectively. The number 7 is the third derivative of this declared local function. A physical Yukawa coupling needs the source's field normalization and the appropriate covariant relation; the polynomial exercise alone does not fix one. This is the same reason that Hori's third derivatives of G differ by a factor of two from derivatives of our F.

The next task is to determine actual period functions rather than manipulate a chosen polynomial. For the mirror quintic, a defining equation supplies differential relations among period integrals. Solving those relations produces a local projective coordinate, but the choice of an integral basis remains a further geometric question.

V.3.4 Picard–Fuchs from geometry

How can a polynomial equation constrain its periods? Consider the degree-five hypersurface $P = 0$ in $\mathbb{P}^4$, with $P = \sum_{i=1}^5 a_i X_i^5 + a_0 \prod_{i=1}^5 X_i$. On the invariant chart set $a_i = 1$ and $a_0 = -5\psi$. The mirror construction quotients by diagonal fifth-root phases $X_i \mapsto \lambda_i X_i$ with $\prod_i \lambda_i = 1$, modulo the common projective phase. This is $(\mathbb{Z}_5)^3$; resolving its fixed loci gives the one-parameter invariant sector used here. We do not need the resolution construction to compute these periods. Near large complex structure,

$$P = \sum_{i=1}^5 X_i^5 - 5\psi \prod_{i=1}^5 X_i, \qquad x = \frac{a_1a_2a_3a_4a_5}{a_0^5} = -z, \qquad z = (5\psi)^{-5}. \tag{V.3.12}$$

Define $\theta_x = x\,d/dx$ and $\theta = z\,d/dz$. Because $x = -z$, these operators agree on functions of x or z. A residue representation of a period contains $1/P$. Repeated differentiation with respect to polynomial coefficients inserts monomials into that denominator. This is the source of the toric relation

$$\left(\prod_{i=1}^5 \frac{\partial}{\partial a_i} - \frac{\partial^5}{\partial a_0^5}\right)\Pi = 0, \qquad \Pi = a_0^{-1}v(x). \tag{V.3.13}$$

Here Π is the raw period in the displayed source gauge, while v is a rescaled function. The residue signs can be checked directly. Set $M = \prod_i X_i$. Differentiating P^{-1} once with respect to each a_i gives $-5!M^5/P^6$; five a_0 derivatives give the same expression. In the ψ chart, $\partial_\psi/5 = -\partial_{a_0}$, so five such derivatives instead give $+5!M^5/P^6$. Thus the ψ-frame relation has a plus sign between these two derivative terms. This sign is fixed before rescaling the period.

The rescaling in (V.3.13) has real algebraic consequences. Since x is linear in each a_i, $\partial_{a_i} = (1/a_i)\theta_x$ on v. Since $a_0\partial_{a_0}x = -5x$, differentiation of $a_0^{-1}v$ gives $\partial_{a_0}(a_0^{-1}v) = -a_0^{-2}(1+5\theta_x)v$. Repeating it five times gives

$$\prod_{i=1}^{5}\partial_{a_i}\Pi = a_0^{-6}x^{-1}\theta_x^5 v, \qquad \partial_{a_0}^5\Pi = -a_0^{-6}\prod_{j=1}^{5}(5\theta_x+j)v. \tag{V.3.14}$$

For example, the first two a_0 derivatives are

$$\partial_{a_0}\Pi = -a_0^{-2}(5\theta_x+1)v, \qquad \partial_{a_0}^2\Pi = a_0^{-3}(5\theta_x+2)(5\theta_x+1)v. \tag{V.3.15}$$

Each additional derivative increases the integer in the new left factor and reverses the sign. The second product in (V.3.14) therefore has $j = 1,2,3,4,5$; omitting its last factor changes the operator. Multiplying (V.3.13) by $a_0^6 x$ yields a fifth-order relation

$$\left[\theta_x^5 + x\prod_{j=1}^{5}(5\theta_x+j)\right]v = 0. \tag{V.3.16}$$

One cannot move x through θ_x as if they commute. The identity $\theta_x x = x(\theta_x+1)$ implies

$$\theta_x\left[\theta_x^4 + 5x\prod_{j=1}^{4}(5\theta_x+j)\right]v = 0, \qquad \theta_x x = x(\theta_x+1). \tag{V.3.17}$$

The factor 5 comes from $5\theta_x + 5 = 5(\theta_x+1)$. Replacing x by $-z$ changes the sign of the second term.

Define the fourth-order operator

$$L = \theta^4 - 5z(5\theta+1)(5\theta+2)(5\theta+3)(5\theta+4). \tag{V.3.18}$$

Equation (V.3.17) says $\theta Lv = 0$, hence only $Lv = C$ on a connected punctured chart. The geometric input is that these periods obey the fourth-order equation: Hori gives this result from the weight-three Hodge variation, while HKTY invokes period asymptotics as $a_0 \to \infty$ to set $C = 0$. Neither claim follows by cancelling θ. To see what an asymptotic exclusion must do, suppose a period has a local expansion whose leading part is a polynomial in $\log z$ of degree at most three, with analytic coefficient functions. Then θ^4 kills its leading logarithmic polynomial; the remaining terms in Lv vanish as $z \to 0$ (also when multiplied by finite powers of $\log z$). Since Lv is constant, it is zero. A fourth-log leading term could instead leave a nonzero constant. This conditional calculation explains the boundary test; the geometric choice of period space is the cited input. For a holomorphic v, the zero constant term of Lv gives the same conclusion directly. The raw source period is $\Pi = -(5\psi)^{-1}v$. A separate source convention writes $\Omega_i = (5\psi)^{-1}\omega_i$. Their signs and chosen forms differ; neither raw period is asserted to have leading coefficient one. We choose $v(0) = 1$ only for the rescaled holomorphic solution.

The operator now produces coefficients without further integration. Write $v(z) = \sum_{n\geq 0} c_n z^n$, with $c_{-1} = 0$. Since $\theta z^n = nz^n$, the coefficient of z^n in Lv is

$$n^4 c_n - 5(5n-4)(5n-3)(5n-2)(5n-1)c_{n-1} = 0 \qquad (n \geq 1). \tag{V.3.19}$$

At $n = 1$, $c_1 = 5(1)(2)(3)(4)c_0 = 120c_0$. At $n = 2$, $16c_2 = 5(6)(7)(8)(9)c_1 = 15120c_1$, so $c_2 = 945c_1 = 113400c_0$. At $n = 3$, the recurrence becomes $81c_3 = 5(11)(12)(13)(14)c_2$. Its right-hand multiplier is 120120, so $c_3 = (120120/81)c_2 = 168168000c_0$. This third step checks both the n^4 denominator and the shift of the four numerator factors. The general ratio telescopes:

$$\frac{c_n}{c_{n-1}} = \frac{(5n)(5n-1)(5n-2)(5n-3)(5n-4)}{n^5}, \qquad c_n = c_0 \frac{(5n)!}{(n!)^5}. \tag{V.3.20}$$

For unit c_0, the coefficients through $n = 5$ are

$$\begin{aligned}(c_0, c_1, c_2, c_3, c_4, c_5) = (1, 120, 113400, 168168000,\\ 305540235000, 623360743125120).\end{aligned} \tag{V.3.21}$$

The nonunit choice $c_0 = 7/3$ instead begins $7/3, 280, 264600, 392392000$. The last three entries are the coefficients requested in E1. Substitution into (V.3.19) checks each displayed value and shows that changing the initial scale changes all coefficients together.

The location of a singular point is also visible in L. Expanding the product, its highest-derivative term is $(1 - 3125z)\theta^4$. Thus the finite discriminant point in this chart is $z = 1/3125$, corresponding to $\psi^5 = 1$; it is not $z = 1$. The displayed equation locates a singular coordinate value. It does not calculate continuation around it. Figure V.3.3 shows the punctures and the separate loop around $z = 0$ used in the next section.

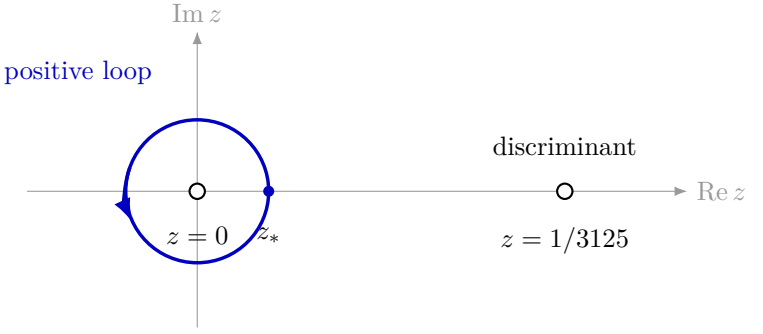


Figure V.3.3: The local z plane with the large-complex-structure point at 0 and the finite discriminant point at 1/3125. The blue path is a counterclockwise loop around 0 from the marked base point z_*, avoiding the second puncture. No monodromy around the discriminant or at infinity is inferred from this drawing.

The construction has produced a local equation for the rescaled invariant periods. It has not chosen which four solutions arise from a particular integral basis of H_3. That distinction sets the scope of the monodromy calculation.

V.3.5 Singular points and monodromy

What can the differential equation say about going around $z = 0$? The indicial polynomial of L there is ρ^4. A repeated root allows solutions with logarithms. A convenient way to obtain the first one is to vary the exponent in a Frobenius family. Define

$$c_n(\rho) = \frac{\Gamma(5n + 5\rho + 1)}{\Gamma(n + \rho + 1)^5}, \qquad \Phi(\rho, z) = \sum_{n\geq 0} c_n(\rho) z^{n+\rho}. \tag{V.3.22}$$

For $n \geq 1$, the ratio $c_n(\rho)/c_{n-1}(\rho)$ cancels the coefficient of $z^{n+\rho}$ in $L\Phi$. To verify the cancellation, the coefficient of $z^{n+\rho}$ for $n \geq 1$ is

$$(n + \rho)^4 c_n(\rho) - 5 \prod_{j=1}^{4} (5n + 5\rho - 5 + j) c_{n-1}(\rho) = 0. \tag{V.3.23}$$

The gamma quotient supplies exactly this ratio. The $n = 0$ term remains, so

$$L\Phi(\rho, z) = \rho^4 c_0(\rho) z^\rho. \tag{V.3.24}$$

The zeroth through third ρ derivatives at $\rho = 0$ therefore solve the homogeneous equation as local formal series. The fourth derivative instead has $L\partial_\rho^4 \Phi|_{\rho=0} = 24$, a diagnostic for the extra fifth-order branch, not a proof that geometry selects the first four. The first derivative is $f_{\log} = f_0 \log z + g$, where $f_0 = \Phi(0, z)$ and $g(0) = 0$. The derivative of the gamma ratio can be written using harmonic numbers $H_m = \sum_{k=1}^{m} 1/k$:

$$g_n = c_n(0)\, 5(H_{5n} - H_n), \qquad f_{\log} = f_0 \log z + \sum_{n\geq 1} g_n z^n. \tag{V.3.25}$$

Indeed, the digamma recurrence $\Psi(m + 1) = H_m - \gamma$ at nonnegative integers gives

$$\partial_\rho \log c_n(\rho)|_{\rho=0} = 5\Psi(5n + 1) - 5\Psi(n + 1) = 5(H_{5n} - H_n).$$

The two Euler constants cancel, including at $n = 0$.

At $n = 1$, $H_5 - H_1 = 77/60$, so $g_1 = 120 \cdot 5 \cdot 77/60 = 770$. At $n = 2$, $H_{10} - H_2 = 3601/2520$, hence $g_2 = 113400 \cdot 5 \cdot 3601/2520 = 810225$. Continuing gives

$$g(z) = 770z + 810225z^2 + \frac{3745679000}{3} z^3 + \frac{4627120640625}{2} z^4 + O(z^5). \tag{V.3.26}$$

There is also a direct operator check. Since $\theta \log z = \log z\, \theta + 1$ and $Lf_0 = 0$, writing $P(s) = \prod_{j=1}^{4}(5s + j)$ gives

$$\begin{aligned} Lg &= -[L, \log z] f_0, \\ P'(0) &= 250, \\ [z][L, \log z] f_0 &= 4(120) - 5P'(0) \\ &= 480 - 1250 = -770. \end{aligned}$$

The z coefficient of Lg is g_1, hence $g_1 = 770$. Substitution of the four displayed g_n through z^4 tests this same inhomogeneous equation; changing the sign of g_2 leaves the

first coefficient intact but gives a nonzero z^2 residual. These are finite formal-series checks, not a proof that the series equals a chosen integral period.

Choose a branch of $\log z$ near a base point z_* and the positive loop in Figure V.3.3. Analytic coefficients return to themselves, while $\log z$ gains $2\pi i$. Thus the local Frobenius pair transforms as

$$f_0 \longmapsto f_0, \qquad f_{\log} \longmapsto f_{\log} + 2\pi i f_0. \tag{V.3.27}$$

Define $t_B = f_{\log}/(2\pi i f_0)$ and $q_B = \exp(2\pi i t_B)$ on this branch. The logarithm cancels in the exponential:

$$t_B = \frac{\log z}{2\pi i} + \frac{g}{2\pi i f_0}, \qquad q_B = z\exp(g/f_0) = z + 770z^2 + O(z^3). \tag{V.3.28}$$

Under simultaneous multiplication of f_0 and $f_{\log}$ by $7/3$, the function g also multiplies by $7/3$. Both t_B and q_B remain the same. Scaling only one member of the pair changes the ratio and is a different choice of functions. The coordinate q_B is local B-side data; identifying it with an A-model Kähler coordinate requires the mirror statement of Chapter 4.

An actual cycle transformation can be shown in the separate elliptic nodal example. Keep $A \cdot B = +1$ and choose an active positive primitive continuation with $A \mapsto A$ and $B \mapsto B + A$. On the ordered period column $(\Pi_A, \Pi_B)^T$, this gives

$$T = \begin{pmatrix} 1 & 0 \\ 1 & 1 \end{pmatrix}, \qquad J = \begin{pmatrix} 0 & 1 \\ -1 & 0 \end{pmatrix}, \qquad T^T J T = J. \tag{V.3.29}$$

The last equality follows by multiplication, or from $\det T = 1$ in this rank-two case. Acting on the earlier numerical periods produces $(7/3, 14i/3 + 7/3)^T$. A two-shear also preserves J, but it represents $B \mapsto B + 2A$, not the specified primitive path. Reversing the loop or using a passive basis changes the matrix convention. The genus-one picture does not determine a four-by-four integral monodromy matrix for the mirror quintic. To obtain that matrix, one must match local solutions to transported integral three-cycles and continue them along declared paths around the other singular points.

The lesson is precise. The differential equation supplies analytic continuation in its local solution space. Integral monodromy asks how actual cycles continue. Their identification is additional global information, even when the local logarithmic shift looks familiar.

V.3.6 From CY periods to an engine

A compact period equation is useful in later field-theory constructions only after the relevant limit is identified. Consider first a sourced local example, the noncompact bundle $\mathcal{O}(-1) \oplus \mathcal{O}(-1) \to \mathbb{P}^1$. In the local mirror description its Kähler parameter is t, with $Q = e^{-t}$. Its prepotential has a trilogarithm term and a polynomial ambiguity,

$$F_{\rm loc}(t) = P_3(t) + \sum_{n\geq 1} \frac{Q^n}{n^3}, \qquad Q = e^{-t}, \qquad \Pi_2 = t, \quad \Pi_4 = \frac{\partial F_{\rm loc}}{\partial t}. \tag{V.3.30}$$

The series and its termwise derivatives initially converge for $|Q| < 1$, equivalently $\operatorname{Re} t > 0$, or can be read as formal series near $Q = 0$. Analytic continuation is a separate step. The source interprets Π_2 as a compact curve period and Π_4 as a dual noncompact-brane period. The coefficients of P_3 are not all fixed because the dual brane has infinite volume. This is a different setting from the compact free-H_3 symplectic basis used earlier.

The local example has its own differential-operator route. In the mirror Landau–Ginzburg contour representation, take periodic variables Y_i, nonzero coefficients μ_i, a chosen local branch of their logarithms, and an integer Calabi–Yau charge row Q_i with $\sum_i Q_i = 0$. On a contour where differentiation under the integral is valid, the relevant integrand is $\exp(-\sum_i \mu_i e^{-Y_i})$ subject to $\sum_i Q_i Y_i = t$. Each ∂_{μ_i} inserts $-e^{-Y_i}$. The Calabi–Yau sum condition makes the two derivative orders, and hence their minus signs, equal. The constraint then gives the source's relation

$$\prod_{Q_i>0} \left(\frac{\partial}{\partial \mu_i}\right)^{Q_i} \Pi = e^{-t} \prod_{Q_i<0} \left(\frac{\partial}{\partial \mu_i}\right)^{-Q_i} \Pi. \tag{V.3.31}$$

For the bundle $\mathcal{O}(-1) \oplus \mathcal{O}(-1) \to \mathbb{P}^1$, order the charge row as $(1, 1, -1, -1)$. Then $Y_1 + Y_2 - Y_3 - Y_4 = t$ implies $e^{-Y_1 - Y_2} = e^{-t} e^{-Y_3 - Y_4}$. Each side has two coefficient derivatives, so its two minus signs cancel. The resulting relation and invariant parameter are

$$\partial_{\mu_1}\partial_{\mu_2}\Pi = e^{-t}\partial_{\mu_3}\partial_{\mu_4}\Pi, \qquad t_{\text{eff}} = t - \log\frac{\mu_1\mu_2}{\mu_3\mu_4}. \tag{V.3.32}$$

Explicitly set $Y_i' = Y_i - \log \mu_i$, so $\mu_i e^{-Y_i} = e^{-Y_i'}$. The constraint becomes $\sum_i Q_i Y_i' = t - \sum_i Q_i \log \mu_i = t_{\text{eff}}$, giving the displayed ratio on the chosen branch. This change assumes the chosen contour can be shifted consistently; it acts on specified noncompact contours with boundary conditions different from those of the compact mirror quintic.

There is a short calculation behind the nonpolynomial term. Since $dQ/dt = -Q$, each derivative of $\sum_{n\geq 1} Q^n/n^3$ removes one power of n and changes sign. Three derivatives yield a geometric series:

$$\frac{d^3}{dt^3} \sum_{n\geq 1} \frac{Q^n}{n^3} = -\sum_{n\geq 1} Q^n = -\frac{Q}{1-Q}. \tag{V.3.33}$$

If P_3 has a cubic term, its third derivative adds a constant; lower-degree terms disappear. The local contour calculation quoted in the source obtains the displayed $-Q/(1-Q)$ contribution after differentiating the dual period twice. The contour endpoints and regularization control its polynomial part. Thus even when a differential equation determines the varying part, it need not fix a noncompact period's complete polynomial normalization.

For a concrete comparison, take $t = \log 2$, so $Q = 1/2$. The nonpolynomial third derivative in (V.3.33) is -1. Adding $P_3(t) = \alpha t^3 + \beta t^2 + \gamma t + \delta$ changes it to

$$F_{\text{loc}}'''(t)|_{t=\log 2} = 6\alpha - 1, \qquad \left.\frac{d^3}{dt^3} \sum_{n\geq 1} \frac{e^{-nt}}{n^3}\right|_{t=\log 2} = -1. \tag{V.3.34}$$

In contrast, the compact affine polynomial of (V.3.10) has the declared derivative $f''' = 7$ in its own coordinate and normalization. Equating these numbers would mix different geometry, coordinates and source conventions. The example makes the ambiguity tangible without assigning either number a gauge-theory interpretation.

A proposed passage to four-dimensional Seiberg–Witten variables must specify more than an ODE. It needs a local scaling parameter and a limit of the family, cycles that survive with finite periods, an electric-magnetic charge lattice, and a conversion from geometric period units to physical mass units. Only then can periods be assigned to the variables a and a_D in $Z = n_e a + n_m a_D$ and $M = \sqrt{2}|Z|$. Figure V.3.4 places these missing maps next to the two period settings. It does not assert that the displayed local bundle is itself a Seiberg–Witten limit.

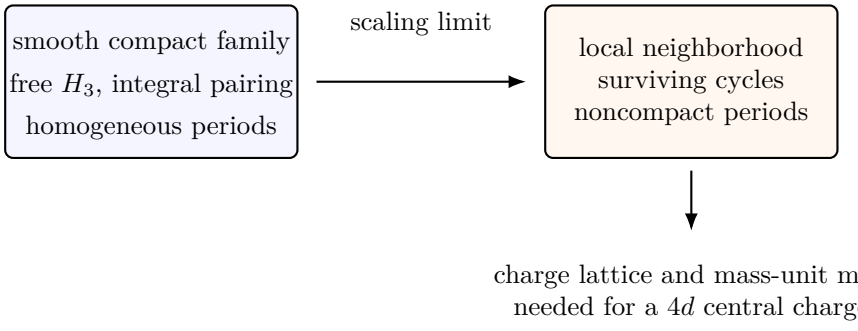


Figure V.3.4: Two distinct period problems. The left box represents a smooth compact family with its free integral H_3 pairing; the right box represents a chosen local neighborhood and noncompact cycles. The lower arrow names the extra scaling, cycle, charge and unit maps needed before a four-dimensional mass formula can be used. The arrow is a required construction, not an established identification in this chapter.

The compact-to-noncompact relation in the source uses boundary-state and deformation premises to compare selected periods. It is not a general theorem that every compact differential equation fixes a gauge-theory mass dictionary. Chapter 4 can use q_B to compare mirror coordinates. Future engineering chapters must make the scaling and charge identifications separately. The reader can now calculate a local period series, state its geometric limits, and recognize precisely where an additional physical construction enters.

V.3.7 Exercises

For E1–E4, submit the exact fields and types specified in the public `questions.json` companion. Give the intermediate reasoning in written work. E5 is a written interpretation task.

E1. Set $c_0 = 7/3$ in (V.3.19). Compute c_1, c_2, c_3 as exact rational strings. Show the recurrence at $n = 1, 2, 3$ and check one value against the factorial expression.

E2. Use $f_0 = 1 + 120z + \cdots$ and the first ρ derivative in (V.3.25). Find the coefficient of z^2 in $q_B = \exp(f_{\log}/f_0)$. Explain why this local logarithmic solution is not, by itself, an integral B-cycle period.

E3. For $f(t) = 7t^3/6+3t^2-5t+2$, compute f''' as an exact rational string. Reconstruct F_0/X^0 and F_1/X^0 at $t = 2$, and explain why the derivative does not yet have a physical Yukawa normalization.

E4. In the ordered elliptic basis with $A \cdot B = +1$, a chosen active continuation sends $A \mapsto A$, $B \mapsto B + A$. Submit its integer matrix and whether it preserves J. Multiply out $T^T JT$ and explain why this calculation does not give the full mirror-quintic integral monodromy.

E5. Suppose one proposes to read a Seiberg–Witten central charge directly from a compact Calabi–Yau period equation. State the scaling parameter, surviving cycles, charge lattice, dimensions and conversion to the declared mass units that would have to be supplied. Say which of these is absent from the compact differential equation, and distinguish the noncompact dual-period polynomial ambiguity from a numerical scaling limit.

V.3.8 Take-home message

Take-home message

An oriented cycle and a holomorphic form produce a period. Compact smooth-family hypotheses supply a free integral symplectic lattice, while a local differential equation supplies analytic solutions. For the mirror quintic, the toric relation, source rescaling and geometric period asymptotics lead to $L = \theta^4 - 5z\prod_{j=1}^{4}(5\theta + j)$ and the holomorphic series $\sum_n (5n)!z^n/(n!)^5$. Its logarithmic companion gives the local coordinate $q_B = z+770z^2+\cdots$. Integral monodromy and any gauge-theory mass interpretation require additional cycle and physical normalization data.

The reader should be able to orient and integrate an elliptic cycle pair, distinguish homogeneous periods from affine ratios, derive the invariant quintic recurrence, calculate the leading logarithmic coordinate and an elliptic shear, and list the data needed for a local gauge-theory limit. Compact Hodge variation, the special-geometry prepotential, geometric period asymptotics and the local contour interpretation are source premises. The finite algebra above does not prove those general statements.

Status and sources

Periods and cycles. The selected B-model chiral-sector premise and moving weight-three Hodge summands are in Bershadsky et al. 1994, physical PDF pp. 26–28, eqs. (2.25)–(2.30) [WS-T]. The compact smooth-family and free-lattice hypotheses delimit the cited Hodge and intersection package [MATH]; the elliptic periods and affine-quadric rank

calculation are direct [MATH]. The oriented torus convention is also in Hori, Katz, et al. 2003, physical PDF p. 110.

Special coordinates. The local period chart and the source $G = z^a w_a$, $\partial_a G = 2w_a$ are in Hori, Katz, et al. 2003, physical PDF pp. 105–107 [MATH]. Our $F = G/2$ and the one-modulus chain rule are explicit algebra, not a global-prepotential theorem. The declared polynomial derivative is not a physically normalized Yukawa.

Picard–Fuchs from geometry. The projective quintic, diagonal phase quotient, resolution and invariant one-parameter sector are in Hori, Katz, et al. 2003, physical PDF pp. 109–110. The residue period and fourth-order geometric-period statement are in Hori, Katz, et al. 2003, physical PDF pp. 111–113, especially p. 113; the toric relation, raw $a_0^{-1}v$ rescaling and asymptotic appeal are in Hosono et al. 1993, physical PDF pp. 20–21, eqs. (3.16), (3.19), (3.20) [GEO-E]. HKTY p. 21 says the period asymptotics set the fifth-order integration constant to zero and points to section 4, without giving a separate local three-log expansion theorem there; the body's logarithmic boundary test is conditional algebra. The literal HKTY (3.20) lacks the factor 5 forced by its (3.16)/(3.19). The literal Hori p. 112 five-derivative relation has a minus sign in the ψ frame; residue differentiation gives plus, while p. 113 has the resulting fourth-order operator. Hori p. 115 labels the conifold $z = 1$; in the chapter's fixed $z = (5\psi)^{-5}$ chart, the leading θ^4 coefficient is $1 - 3125z$, so the finite discriminant is $z = 1/3125$. These are source-printing qualifications, not changes to the derived algebra. The recurrence and finite coefficients are direct [MATH]. No claim is anchored to the unread Candelas original.

Singular points and monodromy. Local Frobenius and period discussion is in Hori, Katz, et al. 2003, physical PDF pp. 113–114 [MATH]. Hori p. 114 calls its fourth ρ-derivative solution a linear combination of the first four; for the displayed gamma family, however, $L\partial_\rho^4\Phi|_0 = 24$ while derivatives of orders zero through three have zero residual. For the source-normalized fourth derivative $f_4 = \partial_\rho^4\Phi|_0/[4!(2\pi i)^4]$, the residual is $1/(2\pi i)^4$. That literal statement cannot hold for this family and normalization. The orientation-dependent nodal continuation and elliptic example are in Hori, Katz, et al. 2003, physical PDF pp. 460–461. The displayed finite logarithmic coefficients and pairing multiplication are direct; no full quintic integral monodromy is asserted.

From CY periods to an engine. The local charge operator, dual noncompact period and polynomial ambiguity are in Hori and Vafa 2000, physical PDF pp. 59–61, eqs. (6.4)–(6.20) [GEO-E]. Its compact/noncompact comparison retains the boundary-state premises. The Seiberg–Witten central charge uses the normalization of Volume I, Chapter 5; the scaling, charge and unit map is not derived here. E1–E4 test bounded answers; E5 asks for written physical premises.

References

Bershadsky, M. et al. (1994). "Kodaira-Spencer theory of gravity and exact results for quantum string amplitudes". In: *Communications in Mathematical Physics* 165, pp. 311–428. arXiv: `hep-th/9309140`.

Hori, K., S. Katz, et al. (2003). *Mirror Symmetry*. Vol. 1. Clay Mathematics Monographs. American Mathematical Society and Clay Mathematics Institute.

Hori, K. and C. Vafa (2000). *Mirror Symmetry*. v3 source edition used. arXiv: `hep-th/0002222`.

Hosono, S. et al. (1993). *Mirror Symmetry, Mirror Map and Applications to Calabi-Yau Hypersurfaces*. v2 source edition used. arXiv: `hep-th/9308122`.

Chapter V.4

Mirror symmetry as a computational tool

V.4.1 A number hidden in a period

A smooth quintic threefold contains rational curves, but counting their contributions by finding curves directly becomes difficult even at low degree. Its mirror turns one protected genus-zero question into a calculation with periods of a holomorphic three-form. Near a chosen boundary of the mirror's complex-structure space, a period ratio supplies an instanton coordinate. A second piece of period geometry gives a three-point coupling. Their power series can be calculated one coefficient at a time.

This chapter follows that route for the quintic. The first three positive-degree coefficients of the normalized coupling are 2875, 4876875 and 8564575000. They are *not* three primitive numbers: a degree-one curve can contribute at higher degree through a multiple cover. Removing those contributions gives 2875, 609250 and 317206375 in the stated genus-zero organization. We will compute every transformation leading to these values, then state the mathematical and physical premises that let the resulting formal series describe the smooth quintic's protected A-model data.

A separate local resolved-conifold example ends the chapter. Its Laurent polynomial has a square Newton support and a calculable critical value. This local curve is an interface to the toric geometry of later brane constructions; it does not inherit the compact quintic's classical intersection number. Chapter 3 established the period equation and local special coordinate. Here the ratio becomes an actual computational input. Chapter 5 studies a different, higher-genus question through the holomorphic anomaly.

V.4.2 Choose a mirror pair and a chamber

Where does a local power series have geometric meaning? Let $X \subset \mathbb{P}^4_{\mathbb{C}}$ be a *smooth* degree-five hypersurface. Its hyperplane class H satisfies

$$\int_X H^3 = 5, \qquad K_X \simeq \mathcal{O}_X. \tag{V.4.1}$$

The first equality is the degree of X; the second follows from adjunction, since $K_{\mathbb{P}^4} = \mathcal{O}(-5)$. Smoothness matters when the stable-map virtual class is introduced later. On the mirror side, take the one-parameter Dwork family and then the Greene–Plesser diagonal phase quotient with its fixed loci resolved. The period statements below concern its invariant one-parameter sector; the raw quotient has fixed points and is not silently treated as a smooth mirror.

The intersection can be checked directly in the ambient space. A degree-five hypersurface represents the cohomology class $5H$ in $\mathbb{P}^4$, and $\int_{\mathbb{P}^4} H^4 = 1$. Pushing the integral from X into the ambient space gives

$$\int_X H^3 = \int_{\mathbb{P}^4} (5H)H^3 = 5. \tag{V.4.2}$$

This geometric computation distinguishes the degree-zero cubic coefficient from quantities fitted to the instanton series. It is also why the smooth-target condition cannot be dropped casually: the protected stable-map invariant of a smooth target and a singular Dwork member are different objects, even though both are described by degree-five equations.

$$P_\psi(X_1, \dots, X_5) = \sum_{i=1}^{5} X_i^5 - 5\psi \prod_{i=1}^{5} X_i = 0, \qquad z = (5\psi)^{-5}, \qquad \theta = z\frac{d}{dz}. \tag{V.4.3}$$

A large value of ψ gives $z \to 0$. This is the large-complex-structure point used in the mirror comparison with the A-model large-radius coordinate. The statement that these two limits correspond is the mirror identification, not a consequence of changing variables in (V.4.3). Once a local branch has been selected, the rescaled invariant geometric periods obey the fourth-order Picard–Fuchs operator derived in Chapter 3:

$$L = \theta^4 - 5z(5\theta + 1)(5\theta + 2)(5\theta + 3)(5\theta + 4), \qquad Lf = 0. \tag{V.4.4}$$

This geometric-period equation is an input from the mirror family. In particular, it cannot be obtained merely by cancelling θ from a factored fifth-order relation: $\theta Lf = 0$ would only say Lf is constant. The geometric period and asymptotic input selects the four-solution sector. We now use that input to do algebra the reader can check.

Put $f_0(z) = \sum_{n\geq 0} a_n z^n$ and normalize $a_0 = 1$. The z^n coefficient of (V.4.4) gives

$$n^4 a_n = 5(5n - 4)(5n - 3)(5n - 2)(5n - 1)a_{n-1}, \qquad n \geq 1. \tag{V.4.5}$$

At the first two steps this is $a_1 = 5(1)(2)(3)(4) = 120$ and $16a_2 = 5(6)(7)(8)(9)120$, hence $a_2 = 113400$. Multiplying the ratio at every step produces a factorial rather than

a new independent assumption:

$$\begin{aligned}\frac{a_n}{a_{n-1}} &= \frac{(5n)!}{(5n-5)!}\frac{(n-1)!^5}{n!^5},\\ f_0(z) &= \sum_{n\geq 0}\frac{(5n)!}{(n!)^5}z^n \\ &= 1 + 120z + 113400z^2 + 168168000z^3 + \cdots .\end{aligned} \tag{V.4.6}$$

For example, the $n = 3$ recurrence says $81a_3 = 5(11)(12)(13)(14)(113400)$, which indeed yields 168168000. The coefficient sequence is a local holomorphic solution. Its chosen scale $f_0(0) = 1$ is a computational normalization; matching it to an oriented geometric period requires the source gauge described in Section V.4.4.

The recurrence gives a useful local analytic check. Its ratio tends to 3125:

$$\lim_{n\to\infty}\frac{a_n}{a_{n-1}} = 5\lim_{n\to\infty}\frac{(5n-4)(5n-3)(5n-2)(5n-1)}{n^4} = 3125. \tag{V.4.7}$$

Consequently the holomorphic series has radius of convergence $1/3125$ by the ratio test. This analytic statement applies to f_0 around $z = 0$; it is narrower than a claim about all periods or global mirror symmetry. The finite singular point $z = 1/3125$ limits this Taylor disk. It is not a natural boundary, since the differential equation has ordinary points elsewhere on the circle $|z| = 1/3125$, across which a local solution can be continued. The ratio test does not determine continuation around the singular point or the behavior of another period there.

The operator also identifies a limit of the chart. The coefficient of its highest θ power is

$$1 - 5z\,(5^4) = 1 - 3125z, \qquad z_{\mathrm{disc}} = \frac{1}{3125}. \tag{V.4.8}$$

The calculation locates a finite singular value in this coordinate. It does not determine every global branch or all analytic continuations. In Figure V.4.1, the small blue circle denotes a local series neighborhood; its radius is schematic and does not assert a convergence theorem. The orange point is the finite discriminant. Treating the two marks as the same point would erase the chamber choice that makes the subsequent series meaningful.

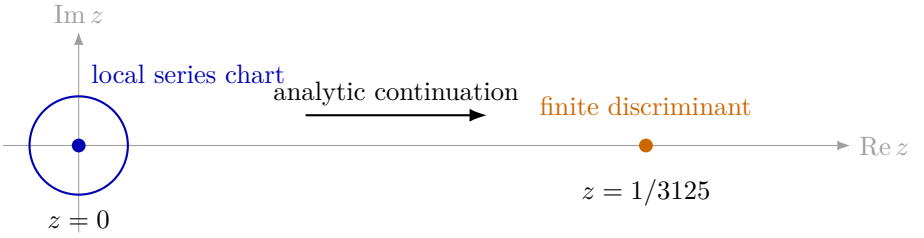


Figure V.4.1: The chosen large-complex-structure chart has $z = 0$ and a distinct finite discriminant at $z = 1/3125$. The blue circle marks a schematic local expansion neighborhood; the continuation arrow represents a further task, not a result of the coefficient computation.

Chapter 3 explains why periods solve the differential equation and why a local solution is not automatically an integral-cycle period. Here the recurrence fixes the holomorphic member needed for a ratio. The next question is how its logarithmic partner changes the coordinate in which positive powers can be read as worldsheet instantons.

V.4.3 The mirror map

How can a period ratio become a degree-counting parameter? Let $f_{\log}$ be the logarithmic local solution paired with f_0 in the chosen branch. The Frobenius derivative of the period family gives a regular part g; define harmonic numbers by $H_m = \sum_{j=1}^{m} 1/j$, with $H_0 = 0$. Then

$$f_{\log} = f_0 \log z + g(z), \qquad g(z) = \sum_{n\geq 1} 5a_n(H_{5n} - H_n)z^n. \tag{V.4.9}$$

The formula follows by differentiating the gamma quotient for a_n with respect to its Frobenius exponent: the two Euler constants cancel and leave $5(H_{5n} - H_n)$. This is the same local logarithmic construction as Chapter 3; here we need four orders because the inverse coordinate will be used in a cubic coupling.

For clarity, the exponent method is an actual differential-equation calculation. Set $c_n(\rho) = \Gamma(5n + 5\rho + 1)/\Gamma(n + \rho + 1)^5$ and $\Phi(\rho, z) = \sum_{n\geq 0} c_n(\rho)z^{n+\rho}$. The recurrence cancels each coefficient with $n \geq 1$ in $L\Phi$, leaving only the leading term

$$L\Phi(\rho, z) = \rho^4 c_0(\rho)z^\rho. \tag{V.4.10}$$

At $\rho = 0$, both Φ and its first ρ derivative solve $Lf = 0$. The first derivative differentiates z^ρ into $\log z$ and differentiates c_n into $5c_n(H_{5n} - H_n)$. This is a formal local solution under the geometric fourth-order period premise; it does not identify an integral cycle. Set $u = f_{\log}/f_0$, $t = u/(2\pi i)$ and $q = e^u$. On a positive loop around $z = 0$, $\log z$ gains $2\pi i$ while g and f_0 return to their Taylor branches. Thus $f_{\log} \mapsto f_{\log} + 2\pi i f_0$ and $t \mapsto t + 1$, so $q = e^{2\pi i t}$ is single-valued around that loop. A different loop or a global integral basis requires separate continuation data.

At $n = 1$, $H_5 - H_1 = 77/60$, so $g_1 = 120 \cdot 5 \cdot 77/60 = 770$. At $n = 2$, $H_{10} - H_2 = 3601/2520$, so $g_2 = 113400 \cdot 5 \cdot 3601/2520 = 810225$. Continuing the same finite harmonic sum yields

$$g = 770z + 810225z^2 + \frac{3745679000}{3}z^3 + \frac{4627120640625}{2}z^4 + O(z^5). \tag{V.4.11}$$

The large integers are useful checks, but they are not the mirror-map coefficients: the logarithmic period must be divided by f_0 first. Set $A = 2\pi i$ and define

$$u = \frac{f_{\log}}{f_0} = \log z + \frac{g}{f_0}, \qquad t = \frac{u}{A}, \qquad q = e^u = z\exp(g/f_0), \qquad \lim_{z\to 0}\frac{q}{z} = 1. \tag{V.4.12}$$

The coordinate t is the source's period-ratio variable; under the mirror identification it is the book's complexified Kähler coordinate with $q = e^{2\pi i t}$. Its unit B-field period follows the convention of Chapter IV.1. The relation to the A model is a geometric and protected-sector input. The formal equality $q = z\exp(g/f_0)$ is algebra once that input and branch have been chosen.

To see exactly where the q coefficients arise, series division gives

$$\frac{g}{f_0} = 770z + 717825z^2 + \frac{3225308000}{3}z^3 + O(z^4). \tag{V.4.13}$$

For instance, the z^2 coefficient is $810225 - 120(770) = 717825$. Exponentiation uses $e^h = 1 + h + h^2/2 + h^3/6 + \cdots$; its first nontrivial combination is $717825 + 770^2/2 = 1014275$. The full needed expansion is

$$\exp(g/f_0) = 1 + 770z + 1014275z^2 + 1703916750z^3 + O(z^4), \tag{V.4.14}$$

so multiplication by the leading z gives

$$q(z) = z + 770z^2 + 1014275z^3 + 1703916750z^4 + O(z^5). \tag{V.4.15}$$

The first correction $770z^2$ measures the difference between the polynomial coordinate of the mirror family and the flat instanton coordinate. Reading instanton degrees directly from powers of z would be a coordinate error.

The Yukawa function is initially known as a function of z, so we must invert (V.4.15). Write $z(q) = q + b_2q^2 + b_3q^3 + b_4q^4 + O(q^5)$. Comparing $q(z(q))$ with q order by order gives a triangular calculation:

$$\begin{aligned} b_2 + 770 &= 0, \\ b_3 + 1540b_2 + 1014275 &= 0, \\ b_4 + 770(b_2^2 + 2b_3) + 3042825b_2 + 1703916750 &= 0. \end{aligned} \tag{V.4.16}$$

The second equation, for example, uses the $2b_2q^3$ term in $z(q)^2$. The solution is

$$z(q) = q - 770q^2 + 171525q^3 - 81623000q^4 + O(q^5). \tag{V.4.17}$$

The coefficient comparison already establishes $q(z(q)) = q + O(q^5)$. Since $q(z)$ has unit linear coefficient, its formal inverse is unique; the reverse composition is a useful additional arithmetic check. Powers of $q(z)$ give

$$\begin{aligned} z(q(z)) &= z + (770 + b_2)z^2 \\ &\quad + (1014275 + 1540b_2 + b_3)z^3 \\ &\quad + (1703916750 + b_2(770^2 + 2028550) + 2310b_3 + b_4)z^4 \\ &= z + O(z^5). \end{aligned} \tag{V.4.18}$$

The numerical z^4 expression uses $[z^4]q(z)^2 = 770^2 + 2(1014275)$ and $[z^4]q(z)^3 = 3(770)$. This reverse check tests the coefficient -81623000 through a different collection of terms.

There is one remaining scale choice. A permitted replacement of the logarithmic period by $f_{\log} + cf_0$ shifts u to $u + c$ and multiplies q by e^c. The leading condition $q/z \to 1$ fixes this scale, apart from exponent-trivial integral monodromy. Adding a bare constant c to $f_{\log}$ instead changes q by $\exp(c/f_0)$, generally not by a constant factor and generally not by an allowed period. The difference matters already in the z^2 coefficient. Figure V.4.2 summarizes the operations, with the dashed arrow reserved for the mirror identification that the algebra does not prove.

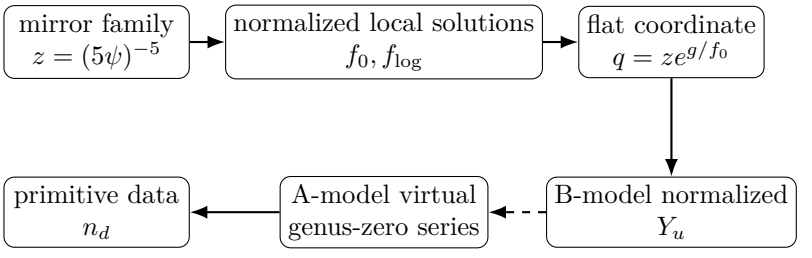


Figure V.4.2: The compact calculation from the chosen mirror family to primitive genus-zero coefficients. Top solid arrows give normalized local solutions and their ratio; their oriented geometric scale is fixed separately by (V.4.19). The vertical solid arrow includes the inverse-square period gauge and flat-coordinate Jacobian. The dashed arrow is the scoped A/B genus-zero identification; the final solid arrow is divisor subtraction.

The inverse series now supplies z in the coordinate used by the A-model expansion. Before using it, we must transform a three-index coupling with its holomorphic-form gauge and with the source's $2\pi i$ convention intact.

V.4.4 Yukawa data

Which factors turn a simple B-model rational function into the flat-coordinate A-model three-point series? The holomorphic three-form itself has a variable scale. In the Candelas–de la Ossa–Green–Parkes source gauge, the form is the residue form specified by its equation (2.9), and the orientation of its second A cycle is chosen consistently

with $A^2 \cdot B_2 = +1$. With $A = 2\pi i$ as above, the oriented period called G_2 and the source's ψ-component of the holomorphic Yukawa are

$$G_2 = \left(\frac{A}{5}\right)^3 f_0(z), \qquad \kappa_{\psi\psi\psi} = \left(\frac{A}{5}\right)^3 \frac{5\psi^2}{1-\psi^5}. \tag{V.4.19}$$

These formulas belong to the same source frame. In particular $f_0(0) = 1$ does not make $G_2 = 1$. If Ω changes by a holomorphic factor h, periods change by h and this Yukawa changes by h^2. Dividing by G_2^2 therefore removes that gauge weight.

The gauge statement can be checked on a concrete rescaling before coordinate derivatives are taken. If the same holomorphic form is multiplied by 2, G_2 doubles and $\kappa_{\psi\psi\psi}$ becomes four times its former value. Their quotient is unchanged. Rescaling only the period while keeping the source coupling fixed would divide the final answer by four; it would mix two gauges. A nonconstant holomorphic factor obeys the same local weight rule, provided the coupling is evaluated in the transformed frame. The source uses the normalized gauge $w^2 = 1$ and its coordinate t from Section V.4.3; in that frame the coupling is

$$\kappa_{ttt}^{(w^2=1)} = \frac{\kappa_{\psi\psi\psi}}{G_2^2}\left(\frac{d\psi}{dt}\right)^3. \tag{V.4.20}$$

The three Jacobian factors are required because all three coordinate indices change. The square period factor is required for a different reason, the scale of Ω. Dropping either gives a series with an incorrect classical normalization or instanton coefficients.

We can perform the coordinate change without treating the ψ-coupling as an unqualified z-tensor. From (V.4.3), $\psi^5 = (3125z)^{-1}$ and $d\psi/dz = -\psi/(5z)$. Since $u = At$, the chain rule gives

$$\frac{d\psi}{dt} = A\frac{d\psi}{dz}\frac{dz}{du} = -\frac{A\psi}{5z}\frac{dz}{du}, \qquad \frac{\psi^5}{1-\psi^5} = -\frac{1}{1-3125z}. \tag{V.4.21}$$

The two minus signs are easy to miss: one comes from differentiating $\psi(z)$, and the other from the denominator $1-\psi^5$. Cubing the first and using the second makes the final answer positive. Define the *computational normalized function* Y_u to be the source's ttt coupling, expressed as a function of u:

$$Y_u := \kappa_{ttt}^{(w^2=1)} = \frac{5}{z^3(1-3125z)f_0(z)^2}\left(\frac{dz}{du}\right)^3, \qquad u = \log q. \tag{V.4.22}$$

The notation records which coordinate is used for the series, rather than changing the tensor index silently. In the *same* fixed holomorphic gauge, an actual uuu component obeys

$$\kappa_{uuu}^{(w^2=1)} = A^{-3}Y_u, \qquad A = 2\pi i. \tag{V.4.23}$$

It would be wrong to label the numerical series below an unqualified κ_{uuu}, since $u = At$ supplies precisely that factor. Similarly, the rational numerator $Y_z^{\text{num}} = 5/[z^3(1-3125z)]$ is merely a convenient part of (V.4.22), not the complete source tensor component.

For a quick component check at the large-radius point, the constant term of the normalized ttt function is 5, whereas the same fixed-gauge uuu tensor component has constant $5/A^3$. These are components on different tangent vectors: $\partial_t = A\partial_u$, and a trilinear tensor acts on three such vectors. Calling Y_z^{num} a z component would make a second, independent mistake by omitting its period-gauge factor. The superscript "num" says that a rational expression can be a computational numerator without being the fully normalized observable.

The formal derivative $dq/du = q$ now simplifies the calculation. Because $du/dz = q'(z)/q(z)$, we have $dz/du = q/q'$. After cancelling z^3 in (V.4.22), the three separate correction factors are

$$Y_u(z) = 5\,(1-3125z)^{-1} f_0(z)^{-2} \left(\frac{q(z)}{zq'(z)}\right)^3. \tag{V.4.24}$$

For a reproducible expansion, (V.4.15) first gives

$$\begin{aligned} \frac{q}{zq'} &= 1 - 770z - 842750z^2 - 1470940000z^3 + O(z^4), \\ f_0^{-2} &= 1 - 240z - 183600z^2 - 261600000z^3 + O(z^4). \end{aligned} \tag{V.4.25}$$

The remaining geometric factor starts as $(1-3125z)^{-1} = 1 + 3125z + 9765625z^2 + \cdots$. Its cubic coefficient is $3125^3 = 30517578125$. In particular, the linear coefficient of the product is $5(3125 - 240 - 3\cdot 770) = 2875$. Multiplication through cubic order gives the complete series in the original coordinate:

$$Y_u(z) = 5 + 2875z + 7090625z^2 + 18991003125z^3 + O(z^4). \tag{V.4.26}$$

To obtain instanton coefficients, substitute the inverse map, rather than simply renaming z as q. The first two positive-degree terms illustrate the correction explicitly:

$$[q]Y_u = 2875, \qquad [q^2]Y_u = 7090625 - 770(2875) = 4876875. \tag{V.4.27}$$

At degree three, $z^2 = q^2 - 1540q^3 + O(q^4)$ and $z^3 = q^3 + O(q^4)$, so

$$[q^3]Y_u = 18991003125 - 1540(7090625) + 171525(2875) = 8564575000. \tag{V.4.28}$$

The normalized answer is therefore

$$\boxed{Y_u(q) = 5 + 2875q + 4876875q^2 + 8564575000q^3 + O(q^4).} \tag{V.4.29}$$

The constant 5 agrees with the independently known triple intersection (V.4.1). This is a meaningful normalization control: fitting it to the positive-degree coefficients alone would not establish the scale of the source period.

The vertical arrow in Figure V.4.2 represents both operations in (V.4.24): the flat-coordinate Jacobian and the inverse square of the oriented period. The caption identifies them separately because they answer different normalization questions. The figure's normalized local solutions acquire their geometric scale and orientation only through the sourced relation (V.4.19).

A prepotential convention also needs translation. The source's affine prepotential begins $F_{\mathrm{CDGP}}(t) = -5t^3/6 + \cdots$, and in that convention $\kappa_{ttt} = -\partial_t^3 F_{\mathrm{CDGP}}$. A mathematical generating function whose u third derivative equals our Y_u can be defined by

$$F_{\mathrm{math}}(u) = -A^3 F_{\mathrm{CDGP}}(u/A) + P_2(u), \qquad \partial_u^3 F_{\mathrm{math}} = Y_u, \tag{V.4.30}$$

where P_2 is an arbitrary polynomial of degree at most two. The chain rule supplies three factors of A^{-1} and cancels $-A^3$. A cubic shift would alter the displayed classical coupling, so it is not part of this harmless integration ambiguity. Chapter 2 develops the A-model quantum product; (V.4.29) is the one-parameter genus-zero three-point datum it will receive under the smooth-quintic mirror premise. The next step is to distinguish its coefficients from connected virtual and primitive contributions.

V.4.5 Instanton extraction

Why is the q^2 coefficient not the number assigned to primitive degree-two curves? A worldsheet map of degree two can have a degree-two image, but it can also wrap a line twice. The protected genus-zero formalism organizes both contributions. Before doing divisor arithmetic, we must say what the A-model numbers mean and what theorem connects them to the mirror series.

For $d > 0$, let $\overline{M}_{0,0}(X, d)$ be the proper moduli stack of connected genus-zero stable maps of hyperplane degree d into our smooth quintic. Its virtual dimension is zero. We write the degree of its virtual fundamental class as

$$N_d := \int_{[\overline{M}_{0,0}(X,d)]^{\mathrm{vir}}} 1. \tag{V.4.31}$$

This is a virtual Gromov–Witten invariant. It need not equal a literal count of embedded smooth rational curves. Maps may be multiple covers, their domains may be nodal, and the virtual class records obstruction multiplicities. In particular the connected stable-map problem is the appropriate mathematical object, rather than a set of projective equations with each visible image counted once.

The smooth-hypersurface theorem used here has concrete geometry. For genus zero, the map $i : \overline{M}_{0,n}(X, d) \to \overline{M}_{0,n}(\mathbb{P}^4, d)$ is induced by the inclusion of X. With π the universal curve and f the universal map over the ambient stable-map space, define

$$E_d = \pi_* f^* \mathcal{O}_{\mathbb{P}^4}(5), \qquad \operatorname{rank} E_d = 5d + 1, \tag{V.4.32}$$

because a degree-$5d$ line bundle on a genus-zero domain has $5d + 1$ global sections in this setting. The hypersurface equation gives a section of E_d whose zero locus is the stable-map locus of X. For a smooth degree-five hypersurface in $\mathbb{P}^4$ and the stated genus-zero virtual-class setting, the theorem identifies the pushed-forward virtual class with its Euler class:

$$i_*[\overline{M}_{0,n}(X, d)]^{\mathrm{vir}} = e(E_d) \cap [\overline{M}_{0,n}(\mathbb{P}^4, d)]. \tag{V.4.33}$$

The rank matches the dimension difference: $\dim \overline{M}_{0,n}(\mathbb{P}^4, d) = 5d + 1 + n$, while $\operatorname{vdim} \overline{M}_{0,n}(X, d) = n$. This dimension check explains why the Euler class can produce

a zero-dimensional invariant at $n = 0$; it is not a proof of (V.4.33). Properness and the virtual-class construction are part of the cited theorem.

The further mirror theorem is an ambient, one-parameter *formal* statement. Its A-model side is a genus-zero descendant correlator, and its B-model side is a hypergeometric series. Define the A-model formal coordinate T and its degree variable $Q = e^T$ independently of the mirror coordinate z. Let $\hbar$ denote the formal descendant parameter. On the two-marked ambient stable-map space, ev_2 evaluates a map at its second marking into $\mathbb{P}^4$, and ψ_2 is the first Chern class of the cotangent line there. The section-evaluation map $E_d \to \mathrm{ev}_2^* \mathcal{O}_{\mathbb{P}^4}(5)$ has kernel E'_d of rank $5d$. With the usual degree-zero unit term, the source's ambient correlator is

$$S_X(T,\hbar) = e^{HT/\hbar}\left[1 + \sum_{d>0} Q^d\,(\mathrm{ev}_2)_*\left(\frac{e(E'_d)}{\hbar - \psi_2}\right)\right], \qquad Q = e^T. \tag{V.4.34}$$

Here the evaluation map in the positive-degree term targets $\mathbb{P}^4$, rather than X, because the virtual hypersurface class has been pushed into the ambient space. The Euler insertion is the same hypersurface mechanism as (V.4.33), now with two marked points; the descendant denominator records the cotangent class. This definition makes the mathematical comparison object explicit. It is not a physical partition function or a claim that all worldsheet observables agree.

On the hypergeometric side H is the ambient hyperplane generator. The quintic I series in our z chart is

$$I(z,\hbar) = e^{H\log z/\hbar} \sum_{d\geq 0} z^d\, \frac{\prod_{m=1}^{5d}(5H + m\hbar)}{\prod_{m=1}^{d}(H + m\hbar)^5}. \tag{V.4.35}$$

The empty products at $d = 0$ equal one. Expanding the product first at $H = 0$ gives $f_0(z)$; differentiating it to first order in $H/\hbar$ gives $f_0 \log z + g$. One can check the first nontrivial degree without invoking the full theorem. At $d = 1$, the scalar part of the product ratio is $5! = 120$. The logarithmic derivative of the five numerator factors contributes $5H_5$, while the denominator contributes $5H_1$. Its coefficient of $H/\hbar$ is therefore $120 \cdot 5(H_5 - H_1) = 770$. The outside exponential supplies the separate $120 \log z$ term at degree one. Thus the same two series that made q are the first scalar and linear pieces of the theorem's I object:

$$I(z,\hbar) = f_0(z) + \frac{H}{\hbar}\big(f_0(z)\log z + g(z)\big) + O(H^2), \qquad T = \frac{f_{\log}}{f_0} = u. \tag{V.4.36}$$

Here T is the formal flat coordinate in this chosen normalization. For the smooth quintic and its genus-zero virtual theory, the cited ambient mirror theorem states at $\hbar = 1$, after restriction to the ambient classes $\mathbb{Q}[H]/(H^4)$,

$$S_X(T(z),1) = \frac{I(z,1)}{f_0(z)}, \qquad T(z) = \log z + \frac{g(z)}{f_0(z)} = u, \qquad Q = e^{T(z)} = q(z). \tag{V.4.37}$$

The scalar unit in S_X forces the division by f_0: the unnormalized I has scalar part $f_0 = 1 + 120z + \cdots$, whereas S_X has scalar part 1. The theorem uses localization, a

class-P uniqueness statement and transformations that preserve that class. The finite scalar and linear calculations above determine the coordinate change, but do not prove the identity or identify complete physical conformal field theories.

The source's string, dilaton and divisor relations give the part of this descendant correlator that carries the connected virtual invariants. At $\hbar = 1$ and modulo H^4 they reduce the smooth-quintic expression to

$$S_X(T,1) = e^{HT}\left[1 + \frac{H^2}{5}\sum_{d>0} dN_d Q^d - \frac{2H^3}{5}\sum_{d>0} N_d Q^d\right]. \tag{V.4.38}$$

Write J_2 and J_3 for the H^2 and H^3 coefficients of this normalized $S_X(T,1)$. Expanding the exponential shows $J_2 = T^2/2 + \sum dN_d Q^d/5$ and $J_3 = T^3/6 + T\sum dN_d Q^d/5 - 2\sum N_d Q^d/5$. The terms involving $T\sum dN_d Q^d$ cancel in

$$\frac{5}{2}(TJ_2 - J_3) = \frac{5}{6}T^3 + \sum_{d>0} N_d Q^d. \tag{V.4.39}$$

This is the mathematical prepotential up to a polynomial of degree at most two. It explains why the descendant theorem, rather than the scalar period alone, supplies the virtual numbers.

There is a finite check of the normalization at degree one. At $\hbar = 1$, the z coefficient of the product in (V.4.35) is $120 + 770H + 575H^2 - 1150H^3$ modulo H^4. Dividing by f_0 and removing the factor e^{HT} leaves the degree-one correction

$$[z]\big(e^{-HT(z)}I(z,1)/f_0(z) - 1\big) = 575H^2 - 1150H^3 = \frac{N_1}{5}H^2 - \frac{2N_1}{5}H^3. \tag{V.4.40}$$

Thus this coefficient matches $N_1 = 2875$. This finite identity checks the normalization and the sourced reduction; it does not establish the all-degree mirror theorem.

In the resulting one-parameter generating convention, F_{math} has classical term $5u^3/6$ and positive-degree terms $N_d q^d$. Three u derivatives, using $dq^d/du = dq^d$, give

$$F_{\mathrm{math}}(u) = \frac{5}{6}u^3 + \sum_{d\geq 1} N_d q^d + P_2(u), \qquad Y_u = 5 + \sum_{d\geq 1} d^3 N_d q^d. \tag{V.4.41}$$

In particular the first two connected virtual values encoded by (V.4.29) are $N_1 = 2875$ and $N_2 = 4876875/8$. The fraction in N_2 is not an arithmetic failure. A virtual stable-map invariant includes automorphism and cover contributions, so a literal integer curve count is not its definition.

A different organization writes the positive-degree prepotential as a sum of trilogarithms. Define $\mathrm{Li}_3(x) = \sum_{k\geq 1} x^k/k^3$ as a formal series, and introduce primitive genus-zero coefficients n_d by

$$F_{\mathrm{math}}(u) = \frac{5}{6}u^3 + \sum_{d\geq 1} n_d \,\mathrm{Li}_3(q^d) + P_2(u), \qquad N_m = \sum_{d|m} \frac{n_d}{(m/d)^3}. \tag{V.4.42}$$

The second relation follows simply by taking the coefficient of q^m: only degrees d dividing m can contribute, with cover number $k = m/d$. Three derivatives remove the

k^{-3} factor but supply d^3, giving

$$Y_u = 5 + \sum_{d\geq 1} n_d d^3 \frac{q^d}{1-q^d}, \qquad a_m := [q^m]Y_u = \sum_{d|m} n_d d^3. \tag{V.4.43}$$

This divisor sum is the computational reason a coefficient a_m cannot be read as n_m. The genus-zero multicover organization is an input; the divisor relation is its formal coefficient consequence.

The degree-two fraction now has a useful decomposition. The primitive degree-two contribution is 609250, while a double cover of each degree-one contribution carries weight $1/2^3$ in the prepotential. Thus $N_2 = 609250 + 2875/8 = 4876875/8$. This is a bridge between two definitions of coefficients, not two competing counts of the same set. The factor $1/8$ comes from the stated genus-zero multicover organization; its appearance in algebra does not derive the physical zero-mode calculation assumed in the original 1991 argument.

Use the coupling coefficients in (V.4.29). At degree one there is only one divisor. At degree two, the degree-one line contributes again; at degree three it contributes a third time. The complete subtraction is

$$\begin{aligned} n_1 &= a_1 = 2875, \\ n_2 &= \frac{a_2 - n_1}{2^3} = \frac{4876875 - 2875}{8} = 609250, \\ n_3 &= \frac{a_3 - n_1}{3^3} = \frac{8564575000 - 2875}{27} = 317206375. \end{aligned} \tag{V.4.44}$$

For a degree-four coefficient, the divisors would be $1, 2, 4$, so both line fourfold covers and conic double covers would have to be removed. Reconstructing the known coefficients is a useful independent check:

$$\begin{aligned} a_2 &= n_1 + 8n_2 = 2875 + 4874000 = 4876875, \\ a_3 &= n_1 + 27n_3 = 2875 + 8564572125 = 8564575000. \end{aligned} \tag{V.4.45}$$

These low-degree numbers agree with the classic mirror-quintic result. At these degrees the values have a familiar rational-curve interpretation under the relevant genericity and enumerativity conditions. The general virtual-to-literal passage requires more than the finite arithmetic just performed. In particular nodal images and multiple maps complicate an arbitrary-degree claim. The original physical calculation assumes a cover zero-mode factor in organizing instantons; its finite agreement is not a stand-alone proof of that factor. The smooth-quintic virtual mirror theorem supplies the stated protected mathematical bridge, not an all-genus or full-SCFT equivalence.

The final solid arrow in Figure V.4.2 is exactly the divisor subtraction in (V.4.44). It does not stand for the dashed A/B mirror identification. Separating these arrows prevents a correct integer subtraction from being mistaken for evidence that the mirror theorem's hypotheses hold for a different target.

A concrete reasoning check makes the boundary useful rather than ceremonial. If one saw only the q^2 term 4876875, calling it 609250 would require both the factor 2^3 and subtraction of the 2875 line covers. If one integrated only the positive-degree

terms of Y_u three times, one could add αu^3 and change the classical coupling by 6α. The known intersection value 5 fixes that compact cubic; the positive-degree fit does not. These are separate mistakes with separate repairs. Chapter 8 will meet a broader protected-amplitude organization, while later engineering chapters must supply their own geometric and physical dictionaries before using these numbers.

V.4.6 A local toric curve

What geometric datum of a local mirror can later appear in a brane-tiling construction? Consider a *different* Calabi–Yau threefold, the noncompact resolved conifold $\mathrm{Tot}(\mathcal{O}(-1)\oplus\mathcal{O}(-1)\to\mathbb{P}^1)$. Hori and Vafa describe it with four charged fields ordered as $(-1,-1,+1,+1)$. Their dual variables X_i obey a constraint and enter a potential

$$\begin{aligned}(Q_1,Q_2,Q_3,Q_4)&=(-1,-1,+1,+1),\\ X_1X_2=e^{t_{\mathrm{HV}}}X_3X_4,&\qquad W=X_1+X_2+X_3+X_4.\end{aligned}\tag{V.4.46}$$

The symbol t_{HV} keeps the source coordinate visible. The instanton variable used for this local geometry is $q_{\mathrm{book}}=e^{-t_{\mathrm{HV}}}$; it is not the compact quintic's t or its q. In this source frame $\lambda=e^{t_{\mathrm{HV}}}=q_{\mathrm{book}}^{-1}$.

On a torus chart with $X_2\neq 0$, eliminate X_1 using the middle equation of (V.4.46), then define $x=X_3/X_2$ and $y=X_4/X_2$. Every step is visible:

$$X_1=\lambda\frac{X_3X_4}{X_2},\qquad W=X_2+X_3+X_4+\lambda\frac{X_3X_4}{X_2}=X_2\big(1+x+y+\lambda xy\big).\tag{V.4.47}$$

Because X_2 is nonzero on this chart, the Laurent curve relevant here is

$$H(x,y)=1+x+y+\lambda xy=0,\qquad (x,y)\in(\mathbb{C}^*)^2,\quad \lambda\in\mathbb{C}^*.\tag{V.4.48}$$

The four monomials have exponent vectors $(0,0),(1,0),(0,1),(1,1)$. Their convex hull is a unit square. Multiplication of H by a Laurent monomial translates all four exponents; a torus-coordinate change can change their lattice basis. Thus the square is understood in the declared (x,y) coordinates, while its toric support is the geometric comparison datum. Figure V.4.3 keeps the monomials at their vertices and states the inverse relation between λ and the local instanton variable.

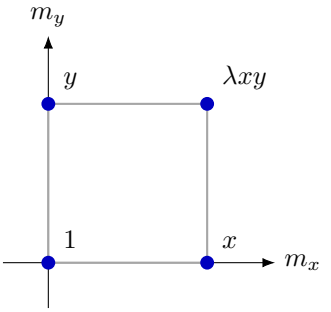
The coefficient λ actually changes the curve. To find when it is singular *inside the algebraic torus*, impose $H=H_x=H_y=0$. The two derivative equations fix a candidate point:

$$H_x=1+\lambda y=0,\qquad H_y=1+\lambda x=0\quad\Longrightarrow\quad x=y=-\lambda^{-1}.\tag{V.4.49}$$

Substitution into H gives a single scalar condition,

$$H(-\lambda^{-1},-\lambda^{-1})=1-\frac{1}{\lambda}-\frac{1}{\lambda}+\frac{1}{\lambda}=\frac{\lambda-1}{\lambda}=0\quad\Longleftrightarrow\quad\lambda=1.\tag{V.4.50}$$

At that value the point is $(x,y)=(-1,-1)$; indeed $H=(1+x)(1+y)$ in this chart. At $\lambda=2$, by contrast, the derivative equations give $(-1/2,-1/2)$ but $H=1/2$, so there is



$$H = 1 + x + y + \lambda xy$$

$$q_{\text{book}} = \lambda^{-1}$$

$$H = H_x = H_y = 0 : \ \lambda = 1$$

critical point $(x, y) = (-1, -1)$

Figure V.4.3: Newton support of $H = 1 + x + y + \lambda xy$ in the specified (x, y) torus coordinates. The labels $1, x, y, \lambda xy$ name the four monomials. For finite nonzero λ, the displayed algebraic-torus critical point occurs at $\lambda = 1$; the drawing does not classify boundary degenerations of a compactification.

no torus critical point. This numerical counterexample helps prevent the unsupported claim that every coefficient produces a singular curve. The calculation addresses only finite nonzero λ in $(\mathbb{C}^*)^2$. Degenerations at the boundary of a toric compactification, including loss of Newton support at limiting parameter values, require separate analysis. Also $q_{\text{book}} \to 0$ corresponds to $\lambda \to \infty$, not to the finite critical value.

The local form of the degeneration is calculable. Center the coordinates at the candidate critical point by $\xi = x + \lambda^{-1}$ and $\eta = y + \lambda^{-1}$. Substitution into (V.4.48) cancels the linear terms and gives

$$H = \lambda\xi\eta + \frac{\lambda - 1}{\lambda}. \tag{V.4.51}$$

At $\lambda = 1$, this is $\xi\eta = 0$, a transverse pair of branches in the local algebraic-torus chart. Nearby finite values give a smoothing $\xi\eta = -(\lambda - 1)/\lambda^2$. This identifies the local singularity more precisely than the critical value alone, while remaining silent about boundary points and worldvolume dynamics. The square Newton support stays the same for every finite nonzero λ; fixed support does not imply fixed smoothness.

The local curve does not determine a compact classical triple intersection. In the same local source, the prepotential is given with a degree-three polynomial ambiguity:

$$F_{\text{local}}(t_{\text{HV}}) = P_3(t_{\text{HV}}) + \text{Li}_3(e^{-t_{\text{HV}}}), \qquad P_3(t_{\text{HV}}) = \alpha t_{\text{HV}}^3 + \beta t_{\text{HV}}^2 + \gamma t_{\text{HV}} + \delta. \tag{V.4.52}$$

The source ties the ambiguity of part of P_3 to the noncompact dual-brane period and its infinite-volume regularization. The instanton series is unambiguous as a formal expansion near $q_{\text{book}} = 0$. Since $dq_{\text{book}}/dt_{\text{HV}} = -q_{\text{book}}$, three derivatives give

$$\frac{d^3}{dt_{\text{HV}}^3}\,\text{Li}_3(q_{\text{book}}) = -\sum_{n\geq 1} q_{\text{book}}^n = -\frac{q_{\text{book}}}{1 - q_{\text{book}}}, \qquad \frac{d^3 F_{\text{local}}}{dt_{\text{HV}}^3} = 6\alpha - \frac{q_{\text{book}}}{1 - q_{\text{book}}}. \tag{V.4.53}$$

If instead $v = \log q_{\text{book}} = -t_{\text{HV}}$, the instanton third derivative is $+q_{\text{book}}/(1 - q_{\text{book}})$. The sign change is a coordinate derivative, not an argument about the compact source's

negative prepotential. A cubic addition changes the full third derivative by a constant; only terms of degree at most two disappear. The compact quintic's classical 5 in (V.4.29) follows from (V.4.1) and has no automatic local analogue.

Here is a numerical written-reasoning example. Set $q_{\text{book}} = 1/2$, so $t_{\text{HV}} = \log 2$ and $\lambda = 2$. The local curve is smooth in the algebraic torus by (V.4.50); the instanton part of its t_{HV} third derivative is $-(1/2)/(1-1/2) = -1$. If $P_3 = \alpha t_{\text{HV}}^3$ is changed from $\alpha = 0$ to $\alpha = 1/6$, the full derivative changes from -1 to 0, while the curve and every positive-degree coefficient of the trilogarithm stay the same. This example shows exactly which degree-zero datum the local calculation leaves open. It also shows why a finite local curve condition is not a proof of a universal physical duality: neither a state-by-state map nor the dynamics of an NS5/D5 worldvolume has been constructed by taking a Newton polygon. Chapter VII.4 uses the conifold square as toric support for a chosen tiling; its physical NS5 curve and a Kasteleyn representative are not identified as polynomials by this calculation.

The two worked geometries now have distinct outputs. The compact smooth quintic supplies a protected genus-zero coupling and virtual invariants under a mirror theorem. The local resolved conifold supplies a Laurent curve, its torus critical value and a separate instanton prepotential with a cubic ambiguity. Chapter 5 follows the compact B-model to higher genus by different equations, and later toric construction chapters use the local support only with their own brane premises.

V.4.7 Exercises

For E1–E4, use the JSON fields in the public companion. The file is `questions.json`. Show the intermediate work on paper. E5 is a written interpretation task.

E1. Starting from (V.4.9), compute g/f_0, exponentiate to obtain $q(z)$ through z^4, and invert it. Submit the coefficients of q^2, q^3, q^4 in $z(q)$. Check both compositions through fourth order, including the cubic cross-term in $q(z)^2$.

E2. Keep $f_0(0) = 1$, $u = \log q = 2\pi i t$ and the fixed source holomorphic gauge. Expand (V.4.24), substitute $z(q)$ and submit the coefficients of q, q^2, q^3 in normalized Y_u. State separately how its value relates to the uuu tensor component.

E3. Given (V.4.29) and the divisor organization (V.4.43), submit (n_1, n_2, n_3). Show how line covers enter degrees two and three; distinguish these numbers from the connected virtual invariants N_d.

E4. Starting from (V.4.46), eliminate X_1, give the four exponent pairs of H in any order, and submit the finite λ where $H = H_x = H_y = 0$ in $(\mathbb{C}^*)^2$. Include the candidate critical point and test it in H.

E5. Explain where the smooth-quintic virtual-class and mirror-theorem premises enter the protected-data comparison. Separate N_d, n_d and literal embedded-curve counts. Use the degree-two subtraction and the $P_3 = \alpha t_{\mathrm{HV}}^3$ example to explain what positive-degree coefficients cannot determine, including the compact classical 5 versus the local cubic ambiguity. Explain why the torus critical value alone establishes no universal string or brane duality.

V.4.8 Take-home message

Take-home message

For the smooth quintic near its large-radius mirror chamber, the period ratio gives $q = z + 770z^2 + \cdots$ and its inverse. The source's oriented period, holomorphic-form gauge and coordinate Jacobian then give the normalized ttt coupling $Y_u = 5 + 2875q + 4876875q^2 + 8564575000q^3 + \cdots$. The compact classical 5 comes from $\int_X H^3$. Divisor subtraction removes covers and yields $n_1 = 2875$, $n_2 = 609250$, $n_3 = 317206375$. The smooth-quintic virtual-class and mirror theorem supply the protected A/B bridge; the finite algebra does not supply it. The local resolved-conifold curve has square Newton support and a torus critical value $\lambda = 1$, with a separate cubic prepotential ambiguity.

A reader should now be able to construct and invert a local mirror map, carry the source Yukawa through both gauge and coordinate changes, subtract covers from a coefficient, and identify which part of a local Laurent curve can enter a later toric construction. These are useful inputs to Chapter 5's next protected sector and to the toric geometry of Chapter VII.4. Neither continuation beyond the chosen chamber nor physical dynamics of the later branes follows from these series.

Status and sources

Mirror family and periods. The smooth quintic, the Greene–Plesser quotient and its resolution, and the local invariant-period equation are treated in Hori, Katz, et al. 2003, physical PDF pp. 109–115 [GEO-E]; the period recurrence and displayed coefficients are formal consequences [MATH]. The fourth-order geometric-period premise is distinct from formal cancellation of a fifth-order factor. The printed intermediate five-derivative relation on physical PDF p. 112 has a sign inconsistent with its following derivative rule; the operator and recurrence used here follow the consistent fourth-order relation on p. 113 and direct differentiation. The finite discriminant follows in our declared z coordinate. The scale and logarithmic-period shift use the stated period conventions.
Yukawa normalization. The source gauge for Ω is Candelas et al. 1991, physical PDF p. 9, eq. (2.9); the oriented G_2 period is Candelas et al. 1991, physical PDF p. 16, eqs. (3.6)–(3.7); the source $\kappa_{\psi\psi\psi}$ and its square gauge weight are Candelas et al. 1991, physical PDF pp. 28–29, eqs. (4.4), (4.6). The affine negative prepotential and classical intersection are Candelas et al. 1991, physical PDF p. 32, eqs. (5.1)–(5.2), and the fixed $w^2 = 1$ transformation is Candelas et al. 1991, physical PDF pp. 37–38, eqs. (5.9),

(5.11)–(5.12) [GEO-E]. The chain rule, A^{-3} component conversion and finite coefficients are explicit [MATH].

Virtual invariants and covers. For the smooth quintic, the genus-zero hypersurface Euler-class identity, its bundle and rank are Hori, Katz, et al. 2003, physical PDF pp. 540–542, Theorem 26.1.1 [MATH]. The connected virtual invariants, limits of literal enumerativity and quintic generating function are Hori, Katz, et al. 2003, physical PDF pp. 579–584, secs. 29.1–29.2; the ambient formal Calabi–Yau transformation, class-P uniqueness and coordinate change are Hori, Katz, et al. 2003, physical PDF pp. 598–602, secs. 30.3–30.4 [MATH]. The original instanton organization, source low-degree values and its physical cover assumption are Candelas et al. 1991, physical PDF pp. 38–40, eq. (5.13) and Table 4 [GEO-E]. Divisor subtraction here is direct formal algebra, not an independent proof of the mirror premise or arbitrary-degree enumerativity.

Local curve. The ordered charges, field constraint and superpotential are Hori and Vafa 2000, physical PDF pp. 55–56, sec. 5 [GEO-E]. The local trilogarithm, dual noncompact period, cubic ambiguity and stated instanton derivative are Hori and Vafa 2000, physical PDF p. 60, eqs. (6.10)–(6.16) [GEO-E]. Elimination, Newton support, critical point and coordinate-sign checks are direct algebra in the declared torus chart [MATH]. The comparison with Chapter VII.4 concerns support, not equality of a physical NS5 polynomial and a Kasteleyn representative. E1–E4 are bounded answer submissions; E5 is written reasoning.

References

Candelas, P. et al. (1991). "A Pair of Calabi–Yau Manifolds as an Exactly Soluble Superconformal Theory". In: *Nuclear Physics B* 359, pp. 21–74. DOI: 10.1016/0550-3213(91)90292-6.

Hori, K., S. Katz, et al., eds. (2003). *Mirror Symmetry*. Vol. 1. Clay Mathematics Monographs. American Mathematical Society and Clay Mathematics Institute.

Hori, K. and C. Vafa (2000). *Mirror Symmetry*. arXiv: hep-th/0002222.

Chapter V.5

Holomorphic anomaly equations

V.5.1 Why a topological amplitude remembers both moduli

The B-model removes much of the metric dependence of a string amplitude, but it does not remove the integration over the shapes of the worldsheet. A handle can become a long tube, and a surface can split into two surfaces joined by a long tube. These regions are part of the amplitude. They are also precisely where the familiar argument that a BRST-exact insertion decouples needs care. An antiholomorphic deformation can be exact before integration and still leave a finite contribution after integration.

The useful question is therefore how the antiholomorphic dependence is organized. The holomorphic anomaly equation expresses it in terms of lower-genus amplitudes. A lost handle gives a second derivative of an amplitude at the preceding genus. A separating tube gives a product of first derivatives. This recursive structure makes the equation useful, but its integration leaves a holomorphic section. To determine an amplitude one also needs the geometry of the family, lower-genus input, a choice of frame, and independent information at its singular limits.

We work in the protected B-model sector of a compact Calabi–Yau threefold, on a regular local chart of its complex-structure moduli. Chapter 1 supplies the twisted Ward identity; Chapters 3 and 4 supply periods and the mirror computational setting. We first explain the worldsheet boundary mechanism, then define the covariant quantities that enter the equation. Local integrations and the first two recursion steps will make its information content explicit. At genus two the complete particular solution shows why a single primitive is insufficient. Finally a protected light-particle calculation supplies a conifold gap, and a finite linear system shows exactly what such additional information can fix.

The worldsheet factorization law, the special-geometry identities used in integrating it, and the isolated light spectrum are physical or geometric inputs with stated domains.

The local algebra below explains their consequences. It does not replace those inputs with a general proof.

V.5.2 Contact terms and the two nodal boundaries

Why does an exact antiholomorphic deformation survive the worldsheet integral? Let t^i be marginal complex-structure couplings and $F_g(t,\bar{t})$ the connected genus-g amplitude. In the twisted theory an antichiral deformation is a descendant obtained by two BRST contours. Writing the left and right charges as Q and $\widetilde{Q}$, its formal local structure is

$$\overline{\phi}_{\bar{i}}^{(2)} = \{Q, [\widetilde{Q}, \overline{\phi}_{\bar{i}}]\}. \tag{V.5.1}$$

Here the superscript denotes the integrated two-form descendant. Moving the contours through the antighost insertions that define the measure produces stress tensors. The stress tensors differentiate the complex structure of the worldsheet. Thus the apparent decoupling becomes a statement about an integral of a derivative on moduli space, rather than just a statement about a local operator.

For $g \geq 2$, let $\mathcal{M}_g^\epsilon$ denote the worldsheet moduli integral with small neighborhoods of degenerations removed. Collisions of insertions are regulated as well. Denote by $\eta_{\bar{i}}$ the moduli-space form produced by the contour manipulation. The structural step of the Ward identity is

$$\bar{\partial}_{\bar{i}} F_g = \lim_{\epsilon\to 0} \int_{\mathcal{M}_g^\epsilon} d\eta_{\bar{i}} = \lim_{\epsilon\to 0} \int_{\partial\mathcal{M}_g^\epsilon} \eta_{\bar{i}}. \tag{V.5.2}$$

This formula records a regulated degeneration calculation. A compactification adds nodal divisors; it does not justify discarding the limits around them as though the integrand were smooth everywhere. Already on a punctured sphere, moving one insertion into another produces a contact term. That collision mechanism is the first warning against setting an integrated exact descendant to zero.

To see how the limit works, take a local plumbing parameter q and write $q = \exp(-L + i\theta)$, where L is the tube length and θ its twist. The node is at $q = 0$, or $L \to \infty$. Propagation along the tube projects onto ground states in that limit. An insertion away from the tube gives no term growing with L, whereas its integral over the interior of the tube has a leading factor L. The normal derivative produced by the Ward identity can retain this factor:

$$\frac{\partial}{\partial L}\big[L\,\mathcal{A} + O(1)\big] \longrightarrow \mathcal{A}. \tag{V.5.3}$$

The expression assumes the long-tube factorization and measure of the protected sector. It explains why a finite boundary term can survive, without purporting to reconstruct the complete path integral.

Which tube states contribute? The twisted Calabi–Yau threefold has $\widehat{c} = 3$. For an external marginal insertion with left and right charges $(1,1)$, the Yukawa selection rule requires

$$q_j + q_k + 1 = 3, \qquad \widetilde{q}_j + \widetilde{q}_k + 1 = 3. \tag{V.5.4}$$

The charge-zero descendants vanish in this sector. The surviving endpoints consequently have

$$(q_j, \widetilde{q}_j) = (q_k, \widetilde{q}_k) = (1, 1). \tag{V.5.5}$$

They represent marginal deformations. Their integrated insertions act by covariant derivatives on the lower-genus amplitudes. This selection is a property of the stated sector; an arbitrary $\mathcal{N} = 2$ theory need not reduce to these endpoint states.

Figure V.5.1 distinguishes the two possible normalizations of a nodal surface, meaning the surfaces obtained by replacing the node by its two marked preimages. Removing a nonseparating node leaves one connected surface of genus $g-1$ with two marked points. Removing a separating node leaves two components of genera r and $g-r$, each with one marked point. Their moduli dimensions provide a useful geometric check:

$$\dim_{\mathbb{C}} \mathcal{M}_{g-1,2} = 3g-4, \qquad \dim_{\mathbb{C}}(\mathcal{M}_{r,1} \times \mathcal{M}_{g-r,1}) = 3g-4. \tag{V.5.6}$$

Both are divisors relative to $\dim_{\mathbb{C}} \mathcal{M}_g = 3g-3$. This check uses stable components in the range under discussion.

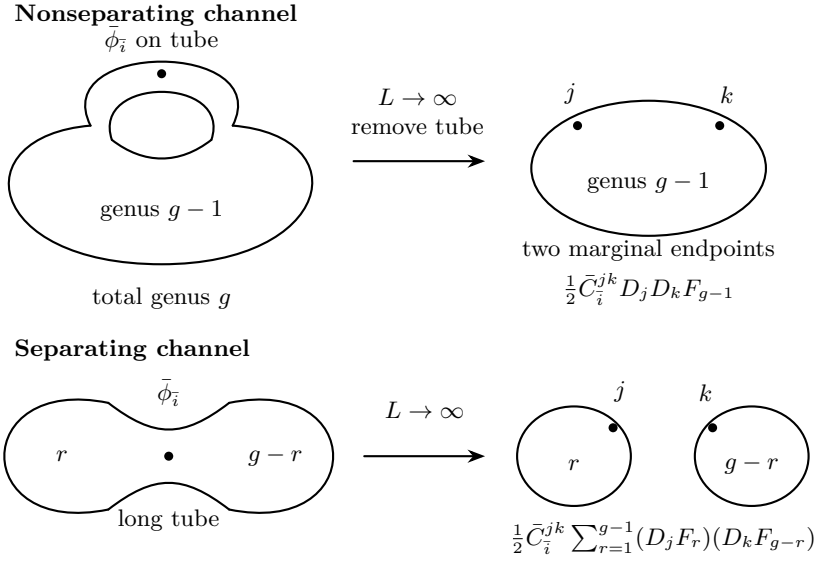


Figure V.5.1: The two nodal channels for a fixed total genus g. The upper row removes a nonseparating tube and retains one genus-$g-1$ component with marked endpoints j, k. The lower row removes a separating tube and retains genera r and $g-r$. The antichiral insertion lies in the long tube before the limit. The horizontal arrows mean removal of that tube, not motion in target space. Unordered endpoints in the upper row give a factor $1/2$. In the lower row an ordered sum over $r = 1, \ldots, g-1$ also requires $1/2$.

At genus two these channels have a particularly concrete description. The first gives a torus with two marked points, whose moduli dimension is two. The second gives two

once-marked tori, each of dimension one. Exchanging the two endpoints of the first channel describes the same node, so integrating over ordered endpoints requires division by two. For separating components, unequal genera occur twice in an ordered sum, and equal genera have an actual exchange symmetry. If $B_{r,g-r}$ denotes the symmetric contracted product of component amplitudes, the two ways of counting are

$$\frac{1}{2}\sum_{r=1}^{g-1} B_{r,g-r} = \sum_{r<g-r} B_{r,g-r} + \begin{cases} \frac{1}{2}B_{g/2,g/2}, & g \text{ even}, \\ 0, & g \text{ odd}. \end{cases} \tag{V.5.7}$$

For $g = 2$ the sole separating product has coefficient $1/2$; for $g = 3$ the two ordered products combine to coefficient one. These are the half factors that will reappear in the recursion.

Genus one supplies another recognizable degeneration. If τ is the torus modular parameter, $\operatorname{Im}\tau \to \infty$ pinches its nonseparating cycle. The resulting normalization is a sphere with two marked ends, understood with its torus degeneration measure. This cusp is a geometric example, not a derivation of every term in the separate genus-one anomaly equation. The connection to Chapter 1 is now precise: a local BRST relation must be used together with the integrated measure and its contact terms. The next step is to define what the endpoint derivatives mean on target-space moduli.

V.5.3 Frames and covariant derivatives

The amplitudes are compared at different complex structures. What must be held fixed to make a derivative meaningful? A holomorphic three-form Ω is defined only up to a nonzero holomorphic factor. It generates the Hodge line $\mathcal{L}$. On a regular chart choose the orientation for which $i\int_X \Omega\wedge\bar\Omega$ is positive and define

$$K = -\log\left(i\int_X \Omega\wedge\bar\Omega\right), \qquad G_{i\bar\jmath} = \partial_i\bar\partial_{\bar\jmath}K. \tag{V.5.8}$$

This is the period geometry of Chapter 3 in a chosen local frame. Under a holomorphic frame change with function $h(t)$,

$$\Omega' = e^h\Omega, \qquad K' = K - h - \bar h, \qquad F_g' = e^{w_g h}F_g, \qquad w_g = 2-2g. \tag{V.5.9}$$

The last law fixes our amplitude convention. In particular F_g is a local representative of a section of $\mathcal{L}^{2-2g}$, while F_1 has weight zero. Weight does not imply holomorphy of that representative.

If $T_{k_1\ldots k_n}$ has frame weight w and lower holomorphic tensor indices, define

$$D_iT_{k_1\ldots k_n} = \partial_iT_{k_1\ldots k_n} + wK_iT_{k_1\ldots k_n} - \sum_{a=1}^{n}\Gamma^{\ell}_{ik_a}T_{k_1\ldots\ell\ldots k_n}, \qquad K_i = \partial_iK. \tag{V.5.10}$$

The Christoffel connection here is explicitly

$$\Gamma^{\ell}_{ik} = G^{\ell\bar m}\partial_iG_{k\bar m}. \tag{V.5.11}$$

The line connection compensates changes of Ω; each tensor connection compensates changes of coordinates. These are different operations. For a scalar amplitude and its Hessian the rule gives

$$D_i F_g = (\partial_i + w_g K_i) F_g, \tag{V.5.12}$$

$$D_j D_k F_g = \partial_j (D_k F_g) + w_g K_j D_k F_g - \Gamma^{\ell}_{jk} D_\ell F_g. \tag{V.5.13}$$

Even at genus one the Hessian is not generally an ordinary second derivative, because its first derivative already has a lower index.

A nonconstant frame change tests the sign of the line connection. Direct substitution, with $h_i = \partial_i h$, gives

$$(\partial_i + w K'_i)(e^{wh} F) = e^{wh}\{\partial_i F + w h_i F + w(K_i - h_i) F\} = e^{wh} D_i F. \tag{V.5.14}$$

For a concrete local example take $g = 2$, $w = -2$, $h = t^2$, and a representative $F = 1 + t + b^2$, with b independent of t. After removing e^{-2t^2} the correct derivative is $1 - 2K_t F$. Using the opposite sign for the line term leaves, relative to its own putative transformation law, the extra term

$$2 w h_t F = -8t(1 + t + b^2). \tag{V.5.15}$$

A constant frame change would miss this error. This example tests the stated transformation law, without identifying the illustrative F with a physical amplitude.

A nonlinear coordinate change tests the tensor connection independently. Take a flat local metric $G_{t\bar{t}} = 1$ and the weight-zero scalar $F = t^3$. Set $t = u^2$ on a patch with $u \neq 0$, choosing one inverse branch. The transformed metric and connection are

$$G_{u\bar{u}} = 4u\bar{u}, \qquad \Gamma^{u}_{uu} = \frac{1}{4u\bar{u}} \partial_u (4u\bar{u}) = \frac{1}{u}. \tag{V.5.16}$$

Since $F = u^6$, its Hessian is

$$D_u D_u F = 30u^4 - \frac{1}{u}(6u^5) = 24u^4 = \left(\frac{dt}{du}\right)^2 \partial_t^2 (t^3). \tag{V.5.17}$$

Omitting the connection gives $30u^4$, with residual $6u^4$. A first derivative of a scalar transforms tensorially, but a second ordinary derivative differentiates the Jacobian as well. The subtraction removes that extra differentiation.

Let C_{ijk} be the holomorphic genus-zero Yukawa tensor in this amplitude frame, of line weight $+2$. Define its raised conjugate by

$$\bar{C}^{jk}_{\bar{i}} = e^{2K} \bar{C}_{\bar{i}\bar{m}\bar{n}} G^{j\bar{m}} G^{k\bar{n}}. \tag{V.5.18}$$

The factors e^{2K} and $\bar{C}$ transform respectively by $e^{-2h-2\bar{h}}$ and $e^{2\bar{h}}$, while G is invariant. Thus

$$(\bar{C}^{jk}_{\bar{i}})' = e^{-2h} \bar{C}^{jk}_{\bar{i}}. \tag{V.5.19}$$

The index placement and the full exponential are essential. The two source structures have the required weight because

$$-2 + w_{g-1} = w_g, \qquad -2 + w_r + w_{g-r} = w_g. \tag{V.5.20}$$

These checks fix the dictionary used in the next sections. Chapter 4's coordinate and period normalizations must be translated into this frame before inserting a Yukawa series. A chosen holomorphic limit of F_g also requires an antiholomorphic base point and a frame; taking that limit is an additional operation on the full $F_g(t,\bar{t})$.

V.5.4 The separate genus-one equation

What initializes the higher-genus calculation? Genus one has a torus measure and a mixed anomaly of its own. Let $\mathcal{F}$ be a torus fundamental domain, $q_\tau = e^{2\pi i\tau}$, and H_L, H_R the left and right Hamiltonians with the vacuum shifts appropriate to the trace. Write $\mathsf{F}_L, \mathsf{F}_R$ for the left and right fermion-number insertions, and F for the parity in the trace. The torus normalization used here is

$$F_1 = \frac{1}{2}\int_{\mathcal{F}} \frac{d^2\tau}{\tau_2}\,\mathrm{Tr}\big[(-1)^{\mathsf{F}}\mathsf{F}_L\mathsf{F}_R q_\tau^{H_L}\bar{q}_\tau^{H_R}\big]\,. \tag{V.5.21}$$

The factor $1/2$ is the torus reflection factor in this normalization. It must be preserved when comparing the anomaly with a differently normalized torus amplitude.

Let $\mathcal{H}_{\mathrm{prim}}$ denote the protected chiral-primary ground-state space. Multiplication by a marginal chiral field acts on this space by a matrix C_i; its conjugate acts by $\bar{C}_{\bar{\jmath}}$, with the state-space metric understood. The genus-one mixed equation is

$$\partial_i\bar{\partial}_{\bar{\jmath}}F_1 = \frac{1}{2}\,\mathrm{Tr}_{\mathcal{H}_{\mathrm{prim}}}(C_i\bar{C}_{\bar{\jmath}}) - \frac{\chi(X)}{24}G_{i\bar{\jmath}}. \tag{V.5.22}$$

Here $i,\bar{\jmath}$ are external marginal directions and $\chi(X)$ is the Euler characteristic of the Calabi–Yau threefold. The trace sums over the internal ground-state space, including its charge sectors. The Euler contribution is a separate term. Neither the torus reflection factor nor a single scalar Yukawa component replaces it.

This distinction matters even with one modulus. Having a single external coordinate does not make $\mathcal{H}_{\mathrm{prim}}$ a single state. A reduction of the trace to metric and Yukawa contractions requires its own state-space identity and normalization. We retain the full trace in the physical equation. The following mixed equation is instead a local mathematical example chosen to teach integration.

Treat t and b as independent variables, with b representing an antiholomorphic coordinate. Work on a simply connected chart containing the origin with $1-t-b\neq 0$, and choose the logarithm branch with $\log 1 = 0$. Suppose

$$\partial_t\partial_b F_1^{\mathrm{loc}} = \frac{a}{(1-t-b)^2}, \qquad a=\frac{5}{2}. \tag{V.5.23}$$

The superscript distinguishes this illustrative function from the physical amplitude. Integrating in t first gives

$$\partial_b F_1^{\mathrm{loc}} = \frac{a}{1-t-b} + H(b). \tag{V.5.24}$$

The function H is independent of t. A second integration gives

$$F_1^{\mathrm{loc}} = -a\log(1-t-b) + A(t) + B(b), \qquad B'(b) = H(b). \tag{V.5.25}$$

Thus a mixed source leaves two single-variable functions, with a constant shared between them. In a physical local complex chart they are the holomorphic and antiholomorphic homogeneous pieces.

Use the two axis values

$$F_1^{\mathrm{loc}}(t,0) = -\frac{5}{2}\log(1-t) + t^2, \tag{V.5.26}$$

$$F_1^{\mathrm{loc}}(0,b) = -\frac{5}{2}\log(1-b) + 3b. \tag{V.5.27}$$

They agree at the origin. Subtracting the logarithm from the first axis fixes $A(t)+B(0) = t^2$; the second fixes $A(0)+B(b) = 3b$. The redundant constant can be assigned between A and B arbitrarily, but their sum is fixed. The resulting function is

$$F_1^{\mathrm{loc}} = -\frac{5}{2}\log(1-t-b) + t^2 + 3b. \tag{V.5.28}$$

Differentiation verifies both the sign and the coefficient:

$$\partial_b F_1^{\mathrm{loc}} = \frac{5}{2(1-t-b)} + 3, \qquad \partial_t\partial_b F_1^{\mathrm{loc}} = \frac{5}{2(1-t-b)^2}. \tag{V.5.29}$$

At $(t,b) = (1/4, 1/4)$, which lies away from the pole, the source is 10, while the value and first barred derivative are

$$F_1^{\mathrm{loc}} = \frac{5}{2}\log 2 + \frac{13}{16}, \qquad \partial_b F_1^{\mathrm{loc}} = 8. \tag{V.5.30}$$

The first axis alone would still allow any $B(b) - B(0)$. Multiplying the logarithm by two would double the mixed source, even if the axis polynomials were unchanged. The integration data and the source normalization therefore play distinct roles.

The physical equation provides the type of genus-one information needed by recursion, but this illustrative logarithm supplies no physical Yukawa, Euler characteristic or global amplitude. In particular it does not determine the separately stipulated covariant values used next. The connection to Chapter 3 is the distinction between a local coordinate solution and a section obeying period transitions across the moduli space.

V.5.5 The first two higher-genus sources

How do the two worldsheet channels become a calculation? With the derivatives and raised coupling already defined, the higher-genus equation is

$$\bar\partial_{\bar\imath} F_g = \frac{1}{2}\bar C_{\bar\imath}^{jk}\left[D_j D_k F_{g-1} + \sum_{r=1}^{g-1}(D_j F_r)(D_k F_{g-r})\right], \qquad g \geq 2. \tag{V.5.31}$$

It concerns the full nonholomorphic amplitude on the regular chart. The CY3 charge selection, regulated contact terms and long-tube factorization described above are its worldsheet premises. The first term records a lost handle; the second records a

separating node. The half factor uses the ordered convention of (V.5.7). The equation does not by itself give the genus-zero geometry or the genus-one amplitude.

For one modulus write $D = D_t$ and $\bar{C} = \bar{C}^{tt}_{\bar{t}}$. Expanding the equation at genus two gives just one separating split:

$$\bar{\partial}_{\bar{t}} F_2 = \frac{\bar{C}}{2}\big[D^2 F_1 + (DF_1)^2\big]. \tag{V.5.32}$$

At genus three the ordered sum has two terms:

$$\bar{\partial}_{\bar{t}} F_3 = \frac{\bar{C}}{2}\big[D^2 F_2 + (DF_1)(DF_2) + (DF_2)(DF_1)\big]. \tag{V.5.33}$$

Although the products commute in this scalar one-modulus example, their two appearances encode the two orders of the split.

One can perform the split sum as a polynomial convolution. Introduce a formal variable x that records genus, and coefficients $d_r = DF_r$ at the chosen point. For the first two known derivatives set

$$P(x) = d_1 x + d_2 x^2, \qquad P(x)^2 = d_1^2 x^2 + 2d_1 d_2 x^3 + d_2^2 x^4. \tag{V.5.34}$$

The coefficient of x^g is the ordered product sum when the needed lower-genus d_r are supplied. The x^4 coefficient here is only the $r = 2$ product, since d_3 was not included. A truncated polynomial cannot supply omitted lower-genus terms. For $g = 2, 3$ all required coefficients are present.

Take the following independent local covariant data:

$$\bar{C} = 6, \quad D^2 F_1 = 5, \quad DF_1 = 2, \quad D^2 F_2 = 11, \quad DF_2 = 7. \tag{V.5.35}$$

These numbers stipulate the quantities at the chosen point. They are not ordinary derivatives to be extracted from the logarithmic example. The common prefactor is $6/2 = 3$. At genus two the two components are

$$N_2 = 3 \cdot 5 = 15, \qquad B_2 = 3 \cdot (2 \cdot 2) = 12, \qquad N_2 + B_2 = 27. \tag{V.5.36}$$

Here N_g names the nonseparating contribution and B_g the separating contribution in this example. At genus three the polynomial is $P(x) = 2x + 7x^2$, so

$$P(x)^2 = 4x^2 + 28x^3 + 49x^4, \qquad [x^3]P(x)^2 = 14 + 14 = 28. \tag{V.5.37}$$

Consequently

$$N_3 = 3 \cdot 11 = 33, \qquad B_3 = 3 \cdot 28 = 84, \qquad N_3 + B_3 = 117. \tag{V.5.38}$$

Keeping only one ordered product would give 42 instead of 84 for the separating term. Dropping the common half factor would double both components. Checking the two components separately exposes both errors; a total alone can conceal compensating mistakes.

Figure V.5.2 places these calculations alongside the integration problem. Lower-genus covariant data determine a source. The source determines an antiholomorphic

variation. It still allows addition of a holomorphic section. The worldsheet degeneration boundary that produced the equation and the target-moduli boundary conditions used to fix that section are different boundaries.

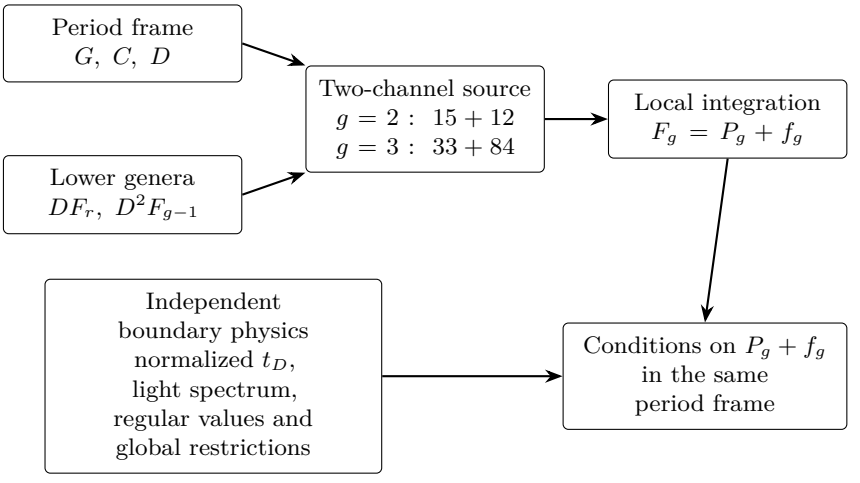


Figure V.5.2: What enters and what remains after a local recursion step. The upper route uses geometry and lower-genus covariant amplitudes to form the ordered $g = 2, 3$ sources. Local integration leaves $F_g = P_g + f_g$. The lower route supplies independent singular and regular boundary information in a specified period frame to constrain f_g. The arrows express dependence of information, not an identification of worldsheet degenerations with target-space singular limits.

The finite calculation establishes arithmetic conditional on the supplied inputs. It cannot determine the quantum measure or spectrum that made (V.5.31) applicable. Chapter XVIII.6 needs precisely this distinction when it assembles the full B-model calculation: periods, tensor connections, genus-one input and boundary physics all have to be present before a recursive source becomes an amplitude.

V.5.6 Integrating the genus-two equation

Can one integrate the raised Yukawa once and finish the calculation? The obstruction is that the other factors also depend on the antiholomorphic moduli. To expose it, define

$$A_{jk} = D_j \partial_k F_1 + (\partial_j F_1)(\partial_k F_1). \tag{V.5.39}$$

The genus-two equation is $\bar{\partial}_{\bar{i}} F_2 = \bar{C}_{\bar{i}}^{jk} A_{jk}/2$. The symmetry and covariant integrability of the Yukawa in special geometry permit a local propagator construction. In the

compatible local choice used here it begins with a section S of weight -2, satisfying

$$\bar{C}_{\bar{i}\bar{j}\bar{k}} = e^{-2K} D_{\bar{i}} D_{\bar{j}} \bar{\partial}_{\bar{k}} S. \tag{V.5.40}$$

Barred covariant derivatives use the conjugate tensor connections and the line structure appropriate to these components. The following definitions fix the related propagators without treating them as independent functions:

$$S_{\bar{i}} = \bar{\partial}_{\bar{i}} S, \quad S^j = G^{j\bar{i}} S_{\bar{i}}, \quad S_{\bar{i}}{}^j = \bar{\partial}_{\bar{i}} S^j, \quad S^{jk} = G^{j\bar{i}} S_{\bar{i}}{}^k. \tag{V.5.41}$$

All three S, S^i, S^{ij} have line weight -2. The construction gives the local identities

$$\bar{\partial}_{\bar{i}} S^{jk} = \bar{C}_{\bar{i}}^{jk}, \qquad \bar{\partial}_{\bar{i}} S^j = G_{k\bar{i}} S^{kj}, \qquad \bar{\partial}_{\bar{i}} S = G_{j\bar{i}} S^j. \tag{V.5.42}$$

The last two follow directly from the definitions; the first uses the special-geometry construction. Local integrability does not assert global existence of these propagators for an arbitrary family.

Apply the product rule before proposing a primitive. It gives

$$\bar{\partial}_{\bar{i}} \left(F_2 - \frac{1}{2} S^{jk} A_{jk} \right) = -\frac{1}{2} S^{jk} \bar{\partial}_{\bar{i}} A_{jk}. \tag{V.5.43}$$

The right-hand side need not vanish. An explicit scalar example makes the size and sign of the problem visible. Replace the barred derivative by d/db, take $S = b^2$ and $A = 1 + b$, and ask for a function with derivative $S'A/2$. The source and its actual primitive are

$$\frac{1}{2} S' A = b + b^2, \qquad F = \frac{1}{2} b^2 + \frac{1}{3} b^3 + H(t). \tag{V.5.44}$$

The proposed first primitive instead gives

$$\frac{1}{2} SA = \frac{1}{2} b^2 + \frac{1}{2} b^3, \qquad \frac{d}{db} \left(\frac{1}{2} SA \right) - (b + b^2) = \frac{1}{2} b^2. \tag{V.5.45}$$

For example the residual is $1/8$ at $b = 1/2$. A function of t cannot remove it. The example concerns the integration step; these S, A are not proposed as a Calabi–Yau realization.

In the tensor problem, $\bar{\partial} A$ is evaluated using the genus-one equation and the curvature of the moduli-space connection. The commutator is already nonzero for a weight-zero covector v_k:

$$[\bar{\partial}_{\bar{i}}, D_j] v_k = -(\bar{\partial}_{\bar{i}} \Gamma^{\ell}_{jk}) v_{\ell}. \tag{V.5.46}$$

For weight w one also has $w G_{j\bar{i}} v_k$. Special geometry expresses the connection curvature in metric and Yukawa contractions. These identities supply the further integrations by parts, introducing S^i and S as well as higher powers of S^{ij}. Their role is to integrate the remainder in (V.5.43), not to declare that remainder zero.

Define $C^{(1)}_i = D_i F_1$, $C^{(1)}_{ij} = D_i D_j F_1$, and $C_{ijkl} = D_i C_{jkl}$, the last tensor being symmetric in this special geometry. The complete particular solution in the selected

source frame is the following nine-term expression:

$$\begin{aligned} P_2 = {} & \frac{1}{2}S^{ij}C^{(1)}_{ij} + \frac{1}{2}C^{(1)}_i S^{ij} C^{(1)}_j - \frac{1}{8}S^{jk}S^{mn}C_{jkmn} \\ & - \frac{1}{2}S^{ij}C_{ijm}S^{mn}C^{(1)}_n + \frac{\chi}{24}S^i C^{(1)}_i \\ & + \frac{1}{8}S^{ij}C_{ijp}S^{pq}C_{qmn}S^{mn} + \frac{1}{12}S^{ij}S^{pq}S^{mn}C_{ipm}C_{jqn} \\ & - \frac{\chi}{48}S^i C_{ijk}S^{jk} + \frac{\chi}{24}\left(\frac{\chi}{24} - 1\right) S. \end{aligned} \tag{V.5.47}$$

The solution is $F_2 = P_2 + f_2$, where f_2 is locally holomorphic on a regular chart and may be meromorphic at the excluded divisors. Every term in P_2 has weight -2. For instance the cubic-propagator terms have weight $3(-2) + 2(+2) = -2$. The two cubic contractions are distinct with several moduli; they cannot generally be combined.

A one-modulus reduction lets the reader reconstruct the cancellation in manageable algebra. In this paragraph only write $s = S^{tt}$, $p = S^t$, $q = S$, $U = D_t F_1$, $V = D_t D_t F_1$, $C = C_{ttt}$, $C_4 = D_t C_{ttt}$, $B = \bar{C}^{tt}_{\bar{t}}$, $G = G_{t\bar{t}}$, $k = \chi/24$, and $\delta = \bar{\partial}_{\bar{t}}$. To specify the special-geometry premises of this reduction, use the normalized horizontal four-step chiral sector of a one-modulus CY3. The marginal multiplication map has transitions between charges $0, 1, 2, 3$. The two end transitions contribute G each to the trace, and the middle transition contributes BC. Consequently this restricted trace identity and the connection curvature are

$$\frac{1}{2}\operatorname{Tr}(C_t \bar{C}_{\bar{t}}) = G + \frac{1}{2}BC, \qquad \delta\Gamma^t_{tt} = 2G - BC. \tag{V.5.48}$$

These are supplied special-geometry identities in this sector and frame, not a scalar replacement for the general trace in (V.5.22). The propagator definitions, the genus-one equation, and covariant differentiation then give

$$\delta s = B, \quad \delta p = Gs, \quad \delta q = Gp, \quad \delta C = 0, \qquad \delta U = \frac{1}{2}BC + (1-k)G. \tag{V.5.49}$$

For clarity the two less immediate derivatives can be derived before using them. Since C has weight two and three lower indices, $C_4 = \partial_t C + 2K_t C - 3\Gamma^t_{tt} C$. Since $\delta C = 0$,

$$\delta C_4 = (2G - 3\delta\Gamma^t_{tt})C = -4GC + 3BC^2. \tag{V.5.50}$$

For $V = D_t U$, use (V.5.46). The compatible special-geometry derivative of the mixed source supplies $BC_4/2$; the covector commutator supplies the second term:

$$\delta V = \frac{1}{2}BC_4 - (2G - BC)U. \tag{V.5.51}$$

This last identity incorporates the sourced covariant derivative relations, rather than treating B and G as constant functions. It is one of the special-geometry inputs to the integration.

In one modulus the two cubic contractions in (V.5.47) combine, since $1/8 + 1/12 = 5/24$:

$$P = \frac{sV}{2} + \frac{sU^2}{2} - \frac{s^2 C_4}{8} - \frac{s^2 CU}{2} + kpU + \frac{5s^3C^2}{24} - \frac{kpCs}{2} + k(k-1)q. \tag{V.5.52}$$

Differentiate every product using the identities just stated. Two representative terms illustrate the operation:

$$\delta\left(\frac{sV}{2}\right) = \frac{BV}{2} + \frac{sBC_4}{4} - sGU + \frac{sBCU}{2}, \tag{V.5.53}$$

$$\delta\left(-\frac{kpCs}{2}\right) = -\frac{kGCs^2}{2} - \frac{kBCp}{2}. \tag{V.5.54}$$

Collecting the other six derivatives by their tensor monomials yields

$$\begin{aligned}\delta P - \tfrac{1}{2}B(V+U^2) = {} & sBC_4(\tfrac{1}{4}-\tfrac{1}{4}) + sBCU(\tfrac{1}{2}+\tfrac{1}{2}-1)\\ & + GsU[-1+(1-k)+k] + GCs^2[\tfrac{1}{2}-\tfrac{1}{2}(1-k)-\tfrac{k}{2}]\\ & + BC^2s^2[-\tfrac{3}{8}-\tfrac{1}{4}+\tfrac{5}{8}] + BCp[\tfrac{k}{2}-\tfrac{k}{2}]\\ & + Gp[k(1-k)+k(k-1)] = 0.\end{aligned} \tag{V.5.55}$$

The calculation makes the Euler terms visible in the cancellation. For a numerical specialization take $B=6$, $G=1$, $s=p=q=C=1$, $k=2$, $U=2$, $V=5$ and $C_4=3$. Then (V.5.52) gives $P=25/3$ and the derivative identities give $\delta P = 6(5+4)/2 = 27$. The value $25/3$ is a particular-solution value conditional on these algebraic inputs, not a physical genus-two free energy. If the term $-kpCs/2$ is omitted, the derivative has the additional residual

$$\frac{kC}{2}(Bp+Gs^2), \tag{V.5.56}$$

which is 7 at this specialization. Line weight alone would not detect that omission.

This explicit differentiation explains how the complete particular solution works under the sourced identities. It supplies neither a proof of general special geometry from finite values nor a global propagator construction. The adjacent connection is to Chapter 3: the same Hodge variation that gives periods also supplies the tensor curvature needed to integrate the higher-genus equation. The remaining holomorphic section is the next problem.

V.5.7 Local sections and compatible choices

What exactly is undetermined after antiholomorphic integration? On a regular simply connected chart, in a fixed holomorphic frame, two solutions with the same barred source differ by a holomorphic representative:

$$\bar\partial_{\bar i} F_g = \bar\partial_{\bar i}\widetilde F_g \quad\Longrightarrow\quad \widetilde F_g - F_g = f_g(t), \qquad \bar\partial f_g = 0. \tag{V.5.57}$$

The frame transition of f_g is still that of $\mathcal{L}^{2-2g}$. Locally calling it a function does not turn the global object into an unconstrained scalar. Its possible poles, growth and monodromy require information about the moduli space.

A first-order equation illustrates the kernel without the tensor machinery. Take independent t, b, exclude $b=1$, and impose

$$\partial_b F^{\mathrm{loc}} = \frac{7t}{3(1-b)^2}, \qquad F^{\mathrm{loc}}(t,0) = 2+3t. \tag{V.5.58}$$

Because $\partial_b(1-b)^{-1} = (1-b)^{-2}$, the general local antiholomorphic primitive is

$$F^{\mathrm{loc}} = \frac{7t}{3(1-b)} + H(t). \tag{V.5.59}$$

The axis condition fixes $7t/3 + H(t) = 2 + 3t$, hence

$$H(t) = 2 + \frac{2}{3}t, \qquad F^{\mathrm{loc}} = \frac{7t}{3(1-b)} + 2 + \frac{2}{3}t. \tag{V.5.60}$$

At $(t, b) = (1/2, 1/3)$ the value is $49/12$ and the source is $21/8$. Adding $11t^2$ preserves the source but changes the axis value by $11t^2$. Thus the axis condition supplies information that the differential equation cannot see. A local primitive already contains the correct dependence on b before the remaining information fixes H.

The same logic applies to a choice of propagators, with an essential compatibility condition. Consider a separate scalar example $S = b$, $A = 1 + b$, and set

$$P = \frac{1}{2}SA - \frac{1}{4}S^2 = \frac{1}{2}b + \frac{1}{4}b^2, \qquad \partial_b P = \frac{1}{2}A. \tag{V.5.61}$$

Let $h(t)$ be holomorphic and replace S by $S' = S + h(t)$ in *both* terms of this particular solution. Since $\partial_b S' = \partial_b S = \partial_b A = 1$, its derivative remains

$$\partial_b P' = \frac{1}{2}A + \frac{1}{2}S' - \frac{1}{2}S' = \frac{1}{2}A. \tag{V.5.62}$$

Expanding the full difference shows why it can be absorbed:

$$P' - P = \frac{1}{2}hA - \frac{1}{2}hS - \frac{1}{4}h^2 = \frac{1}{2}h - \frac{1}{4}h^2. \tag{V.5.63}$$

The same total solution $F = P + f$ therefore has

$$f' = f - \frac{1}{2}h + \frac{1}{4}h^2. \tag{V.5.64}$$

For $h = 2t$, the change in P is $t - t^2$ and the change in f is $-t + t^2$, so their sum is unchanged at every b.

Shifting only the first term would instead add $h(1+b)/2$, whose barred derivative is $h/2$. A holomorphic f cannot cancel that derivative. The complete example proves a local statement about two compatible particular solutions with the same source. In the BCOV construction the related S^{ij}, S^i, S must continue to obey all their differential identities; arbitrary independent shifts are not supplied by this scalar example.

This clarifies the meaning of ambiguity. It is a kernel of a local differential operator with prescribed section transitions, rather than permission to alter any intermediate expression freely. Chapter 4 teaches how a preferred period coordinate is selected; boundary conditions must be stated in that coordinate and frame to constrain the kernel. A finite meromorphic ansatz will require an additional global restriction before its number of coefficients can even be counted.

V.5.8 A protected conifold singularity

What independent physics can constrain the holomorphic remainder? Near an ordinary conifold, a vanishing three-cycle supplies a light charged particle in the four-dimensional type-IIB description. For the singular formula here the premise is precise: on the selected local $\mathcal{N} = 2$ branch there is exactly one light BPS hypermultiplet, with no additional light particles producing singular terms and no recombination changing the relevant protected spin trace. This premise is supplied by the physical conifold analysis. It is not inferred from the anomaly equation.

Choose an oriented vanishing cycle S^3 and a cycle A_D whose period is nonzero near the conifold, in the prescribed polarization. The normalized coordinate is

$$t_D = \frac{\int_{S^3} \Omega}{\int_{A_D} \Omega}. \tag{V.5.65}$$

In the coupling units used for the following F-terms, the source's holomorphic central-charge or mass parameter is t_D/λ. It is complex in general. An unsigned physical mass requires its modulus together with the physical unit and metric factors; inserting an absolute value into this holomorphic parameter would change the calculation.

The amplitudes organize protected couplings of two self-dual curvature insertions and graviphoton insertions. Denote them schematically by

$$\int d^4x\, R_+^2\, \mathcal{F}(\lambda, t_D), \qquad \mathcal{F}(\lambda, t_D) = \sum_g \lambda^{2g-2} F_g(t_D), \tag{V.5.66}$$

with the self-dual graviphoton absorbed into λ in this frame. The contributing BPS states have the universal Lorentz factor $[(\frac{1}{2}, 0) + 2(0, 0)]$ times a remaining spin representation. The two curvature insertions absorb that universal factor. For an isolated hypermultiplet the remaining spin representation is trivial. Its one-loop protected spin trace consequently gives the proper-time kernel

$$\mathcal{F}(\lambda, t_D)|_{\text{light}} \sim \int_\epsilon^\infty \frac{d\ell}{\ell} \frac{e^{-\ell t_D}}{4\sin^2(\ell\lambda/2)}. \tag{V.5.67}$$

Here ℓ is proper time, distinct from all moduli coordinates. We use this expression coefficientwise for $g \geq 2$. It is not a convergent unregulated real-axis expression for the complete function: the sine has poles, and the genus-zero and genus-one terms require separate treatment. The physical spin-trace argument supplies the kernel; the following expansion derives its higher-genus singular coefficients.

Use Bernoulli numbers defined by

$$\frac{x}{e^x - 1} = \sum_{n=0}^{\infty} B_n \frac{x^n}{n!}. \tag{V.5.68}$$

Expanding the cotangent and differentiating gives

$$\frac{1}{4\sin^2(x/2)} = -\frac{1}{2}\frac{d}{dx}\cot(x/2) = \frac{1}{x^2} + \sum_{g=1}^{\infty} \frac{(-1)^{g-1}(2g-1)B_{2g}}{(2g)!} x^{2g-2}. \tag{V.5.69}$$

In particular,

$$\frac{1}{4\sin^2(x/2)} = \frac{1}{x^2} + \frac{1}{12} + \frac{x^2}{240} + \frac{x^4}{6048} + \frac{x^6}{172800} + O(x^8). \tag{V.5.70}$$

For fixed $g \geq 2$, the term x^{2g-2} gives an integrable small-ℓ power ℓ^{2g-3} after the proper-time measure is included. Initially take $\operatorname{Re} t_D > 0$ so that the moment at large proper time converges. Substitution $y = \ell t_D$ gives

$$\int_0^\infty d\ell\, \ell^{2g-3} e^{-\ell t_D} = t_D^{2-2g} \int_0^\infty dy\, y^{2g-3} e^{-y} = (2g-3)!\, t_D^{2-2g}. \tag{V.5.71}$$

The coefficient is then continued on the selected local branch. The factorial cancels the denominator in the kernel coefficient:

$$A_g = \frac{(-1)^{g-1}(2g-1)B_{2g}}{(2g)!}(2g-3)! = \frac{(-1)^{g-1}B_{2g}}{2g(2g-2)}. \tag{V.5.72}$$

For the first three genera the intermediate factors are

$$A_2 = \frac{1!}{240} = \frac{1}{240}, \qquad A_3 = \frac{3!}{6048} = \frac{1}{1008}, \qquad A_4 = \frac{5!}{172800} = \frac{1}{1440}. \tag{V.5.73}$$

Each fixed-genus term in the one-scale light loop has only one negative power. Under the isolated-spectrum premise, other states remain massive and contribute regular terms near this point. Thus the singular part in the fixed period coordinate and amplitude frame has the gap form

$$F_g^{\mathrm{hol}}(t_D) = A_g t_D^{2-2g} + O(t_D^0), \qquad g \geq 2. \tag{V.5.74}$$

In particular the coefficients of $t_D^{-(2g-3)}, \ldots, t_D^{-1}$ vanish. The regular terms, contact choices and full amplitude remain undetermined. We have specified a holomorphic limit and polarization in this boundary formula, rather than identified it with an arbitrary representative of the full nonholomorphic F_g.

Two changes test the scope of the gap. First, hold the amplitude frame fixed and use a new coordinate s defined by $t_D = s + cs^2$ on an invertible patch near zero. At genus two,

$$\frac{A_2}{t_D^2} = \frac{A_2}{s^2}(1+cs)^{-2} = \frac{A_2}{s^2} - \frac{2cA_2}{s} + 3c^2A_2 + O(s). \tag{V.5.75}$$

For $c = 1$, the simple pole is $-1/(120s)$. It has appeared purely through a nonlinear coordinate replacement. Even $t_D = 2s$ changes the leading coefficient to $1/(960s^2)$. These are coordinate-only comparisons in a fixed amplitude frame. A simultaneous compatible period and section-frame transformation must transform all the objects and is not contradicted by this calculation.

Second, two independent identical light hypers with the same normalized central-charge parameter contribute two identical spin traces. Their genus-two singular coefficient is

$$2\frac{A_2}{t_D^2} = \frac{1}{120t_D^2}. \tag{V.5.76}$$

The coefficient counts a specified protected spectrum. If instead a second independent hyper has parameter $2s$ while the first has s, their summed genus-two coefficient in s is $A_2 + A_2/4 = 1/192$. Arbitrary extra particles cannot be replaced by a species count without their charges and spin traces. The source's shrinking lens-space example supplies a concrete setting where the single-hyper premise changes.

The connection to Chapter IV.5 and Chapter 3 is now operational. A vanishing cycle identifies a candidate light state, periods define its normalized coordinate, and protected spectrum information determines the spin trace. A discriminant zero alone supplies none of those normalizations. The conifold gap is valuable precisely because its singular coefficients come from physics independent of the recursive antiholomorphic equation.

V.5.9 Fixing a finite ambiguity with boundary data

How does independent boundary information finish a bounded integration problem? Before counting coefficients, specify the admissible function space. In this example alone let z be a dimensionless local variable, $s = 1 - z$, and restrict the unknown remainder to

$$f(z) = a_0 + \frac{a_1}{s} + \frac{a_2}{s^2}. \tag{V.5.77}$$

This three-term meromorphic ansatz is a hypothesis. It stipulates the maximum pole order and the allowed regular part. Neither the anomaly equation nor local holomorphy proves that a physical global ambiguity has this form. In particular the s in this section is not asserted to be the period t_D of the preceding section.

Suppose three independent conditions are supplied: leading pole coefficient 5, no simple pole, and value 9 at $z = 0$. Their exact meaning is

$$\lim_{s\to 0} s^2 f = 5, \qquad \lim_{s\to 0} s\left(f - \frac{5}{s^2}\right) = 0, \qquad f(0) = 9. \tag{V.5.78}$$

The first limit fixes $a_2 = 5$. After that substitution the second fixes $a_1 = 0$. Since $s = 1$ at $z = 0$, the third fixes $a_0 + a_1 + a_2 = 9$. In the ordered coefficient vector $(a_0, a_1, a_2)^{\mathsf{T}}$ these conditions become

$$\begin{pmatrix} 0 & 0 & 1 \\ 0 & 1 & 0 \\ 1 & 1 & 1 \end{pmatrix} \begin{pmatrix} a_0 \\ a_1 \\ a_2 \end{pmatrix} = \begin{pmatrix} 5 \\ 0 \\ 9 \end{pmatrix}. \tag{V.5.79}$$

The determinant is -1, so the rows are independent. Subtraction of the first two rows from the third isolates $a_0 = 4$:

$$(a_0, a_1, a_2) = (4, 0, 5), \qquad f(z) = 4 + \frac{5}{(1-z)^2}. \tag{V.5.80}$$

The values are distinct from the physical one-hyper coefficient $A_2 = 1/240$. The large-radius terminology for $z = 0$ only names the assigned boundary in this example; it does not identify z with a specific compact-family coordinate.

Withhold the no-simple-pole condition while retaining the other two. The reduced matrix and one null vector are

$$M_{\mathrm{red}} = \begin{pmatrix} 0 & 0 & 1 \\ 1 & 1 & 1 \end{pmatrix}, \qquad M_{\mathrm{red}} \begin{pmatrix} 1 \\ -1 \\ 0 \end{pmatrix} = 0. \tag{V.5.81}$$

It has rank two and nullity one. Writing $a_1 = \alpha$ gives the complete affine family

$$(a_0, a_1, a_2) = (4 - \alpha, \alpha, 5), \qquad f_\alpha = 4 - \alpha + \frac{\alpha}{s} + \frac{5}{s^2}. \tag{V.5.82}$$

The leading double pole and the value at $z = 0$ do not see motion along this null direction. For example $\alpha = -3$ gives

$$f_{-3} = 7 - \frac{3}{s} + \frac{5}{s^2}, \qquad f_{-3} - f_0 = 3 - \frac{3}{s}. \tag{V.5.83}$$

Both f_0 and f_{-3} have leading coefficient 5 and value 9 at $z = 0$. Only f_{-3} has a nonzero simple pole. At $z = 1/2$, $f_0(1/2) = 24$ and $f_{-3}(1/2) = 21$, so the surviving freedom changes ordinary values away from the singularity as well.

This is a concrete reasoning example for the written exercise. Suppose one has evaluated the local recursive source correctly and has fixed only the leading pole and the value at $z = 0$. Claiming uniqueness would fail because f_0 and f_{-3} satisfy all those conditions while giving different answers elsewhere. To exclude f_{-3} physically, one must first establish that the correct normalized period and frame are being used, that the isolated-hyper spectrum applies, and that the assumed global section space is appropriate. The rank computation cannot establish any of these premises. Conversely, a sourced gap cannot by itself prohibit additional regular functions outside the chosen finite ansatz.

Global restrictions can make a section space finite, but the allowed divisors, line-bundle transitions and growth conditions must be stated. In a genuine compact example the conditions are applied to the total $F_g^{\mathrm{hol}} = P_g^{\mathrm{hol}} + f_g$; known terms from P_g shift the right-hand side of the coefficient system. They are not automatically conditions on f_g alone. Chapters 3 and 4 provide the period and mirror-map information needed for that conversion. The future B-model construction in Chapter XVIII.6 adds global singularity data and physical boundary input to the local recursion. The three independent rows above demonstrate how this information can remove an ambiguity once the finite space has actually been specified.

V.5.10 Exercises

The four coefficient exercises use exactly the local conventions stated below. Written differentiation and interpretation remain part of each exercise even where a finite coefficient submission is available.

1. **FI-IV-5-E1. A first-order source.** Treat t, b as independent and solve $\partial_b F = (7/3)t/(1-b)^2$, with $F(t, 0) = 2 + 3t$, using $F = rt/(1-b) + c_0 + c_1 t$. Submit the ordered array (r, c_0, c_1) as rational strings in the field `coefficients`. Differentiate the answer and explain what freedom the axis value removes.

2. **FI-IV-5-E2. A mixed equation and two axes.** On a simply connected chart with $1 - t - b \neq 0$ and the chosen logarithm branch, solve $\partial_t \partial_b F_1 = (5/2)/(1 - t - b)^2$. Impose $F_1(t, 0) = -(5/2)\log(1 - t) + t^2$ and $F_1(0, b) = -(5/2)\log(1 - b) + 3b$. In $F_1 = q\log(1 - t - b) + pt^2 + rb$, submit q, p, r as rational strings in `log_coefficient`, `t2_coefficient`, and `b_coefficient`. Explain why a single axis does not determine the solution of the mixed equation.

3. **FI-IV-5-E3. Two channels at two genera.** Use the one-modulus source (V.5.31) with the full raised $\bar{C} = 6$, $D^2F_1 = 5$, $DF_1 = 2$, $D^2F_2 = 11$, and $DF_2 = 7$. These are supplied covariant values. Submit the nonseparating, separating and total contributions as integer arrays in the fields `nonseparating`, `separating`, and `total`, each ordered $[g = 2, g = 3]$. Write out both ordered genus-three products and relate their multiplicity to the two component genera.

4. **FI-IV-5-E4. Withholding a boundary condition.** Assume $f = a_0 + a_1/s + a_2/s^2$, $s = 1 - z$. Impose $a_2 = 5$, $a_1 = 0$ and $f(0) = 9$. Submit the integer array (a_0, a_1, a_2) in `coefficients`, together with the integer `remaining_dimension_without_gap` when the $a_1 = 0$ condition is withheld. In writing exhibit the null direction and a second function satisfying the retained conditions. This s has no assumed identification with a physical vanishing period.

5. **FI-IV-5-E5. What makes the result physical?** Give a written explanation of why a finite recursion evaluation cannot establish the worldsheet equation. Identify its BRST, measure, contact-term and degeneration premises. Explain which period normalization, line-bundle frame, global singularity restrictions and independent boundary physics would be needed to interpret a local no-simple-pole condition as a physical conifold gap. Distinguish the full $F_g(t, \bar{t})$ from a chosen holomorphic limit. Use either the compatible-propagator example or the withheld-condition family to explain why antiholomorphic integration leaves an unresolved section. This exercise calls for reasoning rather than a graded finite answer.

The public question file supplies the exact JSON structures and the chapter-local grading command. Rational fields use signed integer or numerator/positive-denominator strings; integer arrays use JSON numbers with mathematically integral values. The written explanations are not certified by acceptance of those finite submissions.

V.5.11 Take-home message

Antiholomorphic dependence survives because the integrated topological amplitude encounters contact terms and nodal worldsheet boundaries. The two nodal channels produce the covariant second derivative and the ordered product sum. Genus one has its own protected ground-state trace and Euler term. Integrating the higher-genus source requires compatible special-geometry identities and leaves a holomorphic section. Independent boundary physics, expressed in its actual period coordinate and frame, can then constrain that section.

After working through this chapter, the reader should be able to identify the two nodal channels and their half factors; transform a section-valued derivative under a

frame and coordinate change; integrate local first-order and mixed sources; evaluate the two first recursive sources and explain the full genus-two remainder; and use a protected singular input to solve a stated finite boundary problem. These are the ingredients needed for the later closed B-model construction. They do not determine global monodromy, a light spectrum or an all-genus physical amplitude from a differential equation alone.

Status and sources

Sections 5.1–5.2. The physical boundary mechanism and the torus degeneration use Bershadsky et al. (1993, physical PDF pp. 30–31, 35–37 and 42–47, eqs. (2.37), (2.43)–(2.44), (3.1)–(3.6)). The regulated measure, contact terms, CY3 $\widehat{c} = 3$ charge selection and long-tube factorization are sourced worldsheet inputs [WS-T]. The moduli dimensions and endpoint counting explain the geometry conditional on that input [MATH]. The chapter does not derive the general path-integral measure from the finite examples.

Sections 5.3–5.5. The Hodge frame and tensor connection use the stated restrictions on compact families and periods. The frame and nonlinear-coordinate examples are local transformation calculations [MATH]. The physical genus-one equation and the higher-genus recursion are Bershadsky et al. (1993, physical PDF pp. 47–48, eqs. (3.6), (3.10) and footnote 17) [WS-T]. The logarithmic mixed solution and supplied recursion components are conditional calculations [MATH]; their local inputs are not a computed CY amplitude.

There is an unresolved printed connection-sign discrepancy in the original v1: physical PDF p. 35, (2.41), prints $\partial_i - \Gamma_i - (2-2g)K_i$, whereas physical PDF p. 48 after (3.8) prints the scalar $\partial_i - (2g-2)K_i$. The explicit frame law (V.5.9) selects the latter scalar sign and the subtractive tensor connection. The early matrix-connection notation also uses its own curvature convention. We assert neither a published erratum nor a general conversion of all its operator-insertion conventions. The torus normalization is kept as in (2.37) and footnote 17; no alternative genus-one normalization is silently imported.

Sections 5.6–5.7. The propagator construction, repeated integration by parts and complete nine-term particular solution use Bershadsky et al. (1993, physical PDF pp. 98–101, eqs. (6.2)–(6.7)) [WS-T]. Special-geometry integrability and curvature identities remain sourced premises. The one-modulus differentiation uses the explicitly stated horizontal-sector trace and connection identities compatible with that integration; it does not prove a general tensor identity or reconcile all early printed conventions. The scalar residual, compatible full shift and local kernel are conditional algebra [MATH]. The ambiguity is a meromorphic $\mathcal{L}^{-2}$ section at genus two, not a universally global scalar.

Section 5.8. The conifold singular input is Huang et al. (2006, arXiv v1, physical PDF pp. 4, 10–12 and 24–25, eqs. (1.2), (2.24), (2.26)–(2.29), (3.78)–(3.79)) [BPS:1/2|short]. The reference algebra is local four-dimensional $\mathcal{N} = 2$. The protection mechanism is the isolated short hypermultiplet's graviphoton F-term spin trace, with exactly one light hyper and no additional singular light sector or relevant recombination.

Its power here is the fixed-period/frame singular coefficient and absent intervening poles for $g \geq 2$, not a full-function determination. The proper-time moments and coordinate/species consequences are conditional calculations [MATH]. Regular terms, contact choices, polarization and mass units remain additional information.

The HKQ v1 genus-one logarithm is printed with a plus sign at physical PDF p. 9, (2.21), and with a minus sign at physical PDF p. 24, (3.78), in its displayed $\hat{t}_D$ expression. This chapter imports neither coefficient and offers no invented erratum or demonstrated conversion. The proper-time display (2.29) contains lower-genus terms before subtraction, while its displayed series begins at $g = 2$; our use is explicitly coefficientwise at $g \geq 2$.

Sections 5.9–5.11. The finite ansatz, rank-three solution and rank-two withheld family are mathematical calculations [MATH]. They do not inherit a universal ambiguity dimension from the source's compact examples. The example-specific discussion of ambiguity in Bershadsky et al. (1993, physical PDF pp. 113–119, especially (7.5) and the parameter discussion on p. 119) is not a theorem for arbitrary families. Four finite submitted-answer tasks retain their separate written explanations, and E5 is written interpretation. General worldsheet factorization, special geometry, protected spectrum and global section restrictions are cited inputs rather than theorems proved by those tasks.

References

Bershadsky, M. et al. (1993). *Kodaira–Spencer Theory of Gravity and Exact Results for Quantum String Amplitudes*. Source edition: arXiv v1. arXiv: `hep-th/9309140`.

Huang, M.-x., A. Klemm, and S. Quackenbush (2006). *Topological String Theory on Compact Calabi–Yau: Modularity and Boundary Conditions*. arXiv v1 (13 December 2006); physical PDF pp. 4, 10–12, 24–25, eqs. (1.2), (2.24), (2.26)–(2.29), (3.78)–(3.79). arXiv: `hep-th/0612125`.

Chapter V.6

Open topological strings and branes

V.6.1 What an open string remembers

An open string can distinguish two branes that occupy the same point. Its endpoints carry Chan–Paton labels, and parallel transport acts on those labels even when the position is fixed. After a topological twist, we ask which boundary operators survive the scalar supercharge. Their answer depends on the support, the bundle and its connection, and the differential acting on the operators. Merely counting geometric intersections omits part of the problem.

The physical route into brane categories starts with this boundary problem. A compatible boundary gives a complex of open operators. Its cohomology retains protected states; resolutions make some such cohomology calculations finite. Products then remember how operators compose, and higher products retain information that the vector spaces alone forget. A categorical equivalence can transport these structures and their additive classes. To turn them into a physical spectrum still requires a background, a stability condition and a spacetime interpretation.

We will follow this route through six worked constructions. A real support and a complex support distinguish the elementary A and B boundaries. A flat bundle on a real torus removes some open cohomology through relative holonomy. A point resolution gives local Ext groups and a directed orbifold quiver. Chain maps fix a product sign. A surface McKay example transports a supported integral pairing. Finally, the degree-one open fields give ordinary or holomorphic Chern–Simons functionals under their respective geometric hypotheses.

The entry points are the twists of Chapter 1, bundles in Chapter III.5, cyclic actions in Chapter IV.3, and Lagrangian geometry in Chapter IV.6. The exit is practical: compute a protected open complex, recover its arrows and products, transport a supported Euler form, and identify the additional information needed for a physical interpretation. These operations supply the categorical refinement used in Chapter VI.5, the graded-quiver interface of Chapter VII.10, and the topological field theories of

V.6.2 A and B boundary conditions

Which boundary data let an open worldsheet preserve the selected scalar charge? The support answers where an endpoint may move; the Chan–Paton bundle answers what it carries. These are separate restrictions. We work at vanishing background B field and use the zero-central-charge sector of Chapter 1, with

$$Q_A = Q_- + \bar{Q}_+, \qquad Q_B = \bar{Q}_- + \bar{Q}_+, \qquad Q_A^2 = Q_B^2 = 0. \tag{V.6.1}$$

The boundary construction assumes that the background and its quantum anomaly conditions allow these scalar symmetries. It does not establish those conditions for every target.

Let $u\colon \Sigma \to X$ be the bosonic worldsheet map. A support $L \subset X$ imposes $u(\partial\Sigma) \subset L$. Tangent endpoint variations are allowed, while normal endpoint positions are fixed. For the elementary A boundary on a Kähler target of complex dimension n, L is Lagrangian:

$$\dim_{\mathbb{R}} L = n, \qquad \iota^* J = 0, \tag{V.6.2}$$

where ι is the inclusion and J is the Kähler two-form. The half-dimension condition is part of the definition. An isotropic curve in a six-real-dimensional space need not be Lagrangian.

We can check both conditions in coordinates without appealing to a brane picture. On $\mathbb{C}^3$ set $z^a = x^a + iy^a$ and choose the positive coefficient $g = 3/2$. The metric and Kähler form are

$$ds^2 = 2g \sum_{a=1}^{3} dz^a d\bar{z}^a = 3 \sum_{a=1}^{3} \big((dx^a)^2 + (dy^a)^2\big), \qquad J = ig \sum_{a=1}^{3} dz^a \wedge d\bar{z}^a. \tag{V.6.3}$$

Expanding one wedge gives $dz^a \wedge d\bar{z}^a = -2i\, dx^a \wedge dy^a$, so the real plane $y^1 = y^2 = y^3 = 0$ obeys

$$J = 3 \sum_a dx^a \wedge dy^a, \qquad \iota^* dy^a = 0, \qquad \iota^* J = 0, \qquad \dim_{\mathbb{R}} L = 3. \tag{V.6.4}$$

The nonunit metric coefficient survives in J but disappears from its vanishing pullback. By contrast, the complex line $z^2 = z^3 = 0$ has

$$J|_{\mathbb{C}} = 3\, dx^1 \wedge dy^1 \neq 0. \tag{V.6.5}$$

It is a local complex support, not a Lagrangian support. Figure V.6.1 shows the tangent directions responsible for the difference. A local complex support is only a geometry test here; the elementary B coupling below is the space-filling one.

The next condition comes from the boundary holonomy. Let a be a connection on the endpoint bundle E, $F_a = da + a \wedge a$, and let $H_{C;\tau}$ denote the holonomy around a boundary circle based at τ. Its traced variation has the curvature insertion

$$\delta \operatorname{Tr} H_C = \operatorname{Tr} \int_C \delta u^I \dot{u}^J (F_a)_{IJ}\, H_{C;\tau}\, d\tau. \tag{V.6.6}$$

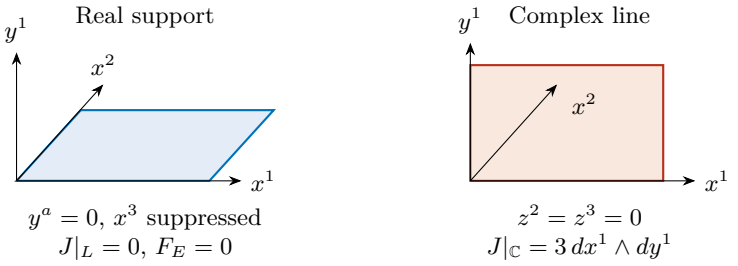


Figure V.6.1: Local supports in the same coordinate frame. The real plane has x^1, x^2, x^3 tangent and all y^a normal; x^3 is suppressed. The complex line has both x^1, y^1 tangent, so the Kähler two-form restricts nontrivially. Flatness of the A bundle is an additional connection condition, not a consequence of the drawing. The line is not the space-filling B boundary used to derive the elementary B coupling.

For the A transformation, the fermion replacing δu is tangent to L. Invariance for arbitrary boundary maps and allowed tangent fermions forces the curvature on L to vanish. For the elementary space-filling B boundary the anti-holomorphic fermion variation of the naive holonomy would also remove $(1,1)$ curvature. The B coupling must therefore be improved by a fermion-curvature term. Its cancellation of the mixed-curvature variation leaves precisely the holomorphic integrability condition:

$$\begin{aligned} &\text{A boundary:} && F_a|_L = 0, \\ &\text{improved B boundary:} && F_a^{0,2} = 0, \qquad \bar\partial_E^2 = F_a^{0,2}. \end{aligned} \tag{V.6.7}$$

The improved coupling is a sourced boundary construction. Imposing flatness on every B bundle would discard the distinction it was introduced to preserve. A holomorphic bundle can have nonzero $(1,1)$ curvature.

For a global elementary A example take the zero section $L = T^3 \subset T^*T^3$ with angular coordinates q^a. In cotangent coordinates p_a, the primitive $\theta = \sum_a p_a dq^a$ vanishes on L; thus $d\theta$ restricts to zero and the support has half the real dimension. A flat rank-two bundle on this torus is specified by commuting holonomies. One choice, used in the next section, is

$$U_1 = \begin{pmatrix} 1 & 0 \\ 0 & -1 \end{pmatrix}, \qquad U_2 = U_3 = I_2, \qquad [U_a, U_b] = 0. \tag{V.6.8}$$

Flatness does not require all the U_a to be the identity. For comparison a trivial holomorphic line bundle on a flat complex three-torus gives a space-filling B example with $a = 0$ and $F_a^{0,2} = 0$.

These examples answer a boundary symmetry question. They do not classify all A boundaries, nor do they establish stability of an untwisted physical brane. In particular, the Lagrangian condition alone is not the special-Lagrangian or stability condition discussed in Chapter IV.6. The next step is to let the permitted endpoint data act on open operators.

V.6.3 Open observables

How can a flat connection change protected open states if its curvature vanishes? An open string with both ends on E carries an element of $\mathrm{End}(E)$, the bundle of linear maps from each fiber to itself. Transport conjugates that element. Relative eigenvalues can therefore act nontrivially even when the connection is flat.

A cochain complex has spaces C^p, a degree-raising differential $D^p\colon C^p \to C^{p+1}$, and $D^{p+1}D^p = 0$. Its degree-p cohomology divides closed operators by exact operators:

$$H^p(C,D) = \frac{\ker(D^p)}{\mathrm{im}(D^{p-1})}, \qquad b_p = \dim C^p - \operatorname{rank} D^{p-1} - \operatorname{rank} D^p. \tag{V.6.9}$$

The second formula holds when the spaces are finite-dimensional, with zero differentials beyond the endpoints. Counting cochains alone counts states removed by the scalar charge.

The elementary open zero modes have a geometric realization. In the uncorrected sector their fermions behave as exterior generators, so the low-lying operator complexes are

$$\begin{aligned} &\text{A:} \quad (\Omega^\bullet(L, \mathrm{End}\, E), d_E), \qquad Q_A \;\propto\; d_E, \\ &\text{B:} \quad (\Omega^{0,\bullet}(X, \mathrm{End}\, E), \bar\partial_E), \quad Q_B \;\propto\; \bar\partial_E. \end{aligned} \tag{V.6.10}$$

These physical identifications come from the twisted boundary theory. Flatness or holomorphic integrability makes the corresponding differential square to zero. We use de Rham self-cohomology in the exact cotangent zero-section sector. Disk effects for a general A brane can change this description.

A local system is a flat vector bundle described by its monodromies. A product cell decomposition of T^3 has $\binom{3}{p}$ cells in degree p. With the holonomies in eq. (V.6.8), the full cellular local-system complex is

$$C^p = \mathrm{End}(\mathbb{C}^2) \otimes \Lambda^p \mathbb{C}^3, \qquad D = \lambda \sum_{a=1}^{3} e_a \wedge T_a, \qquad T_a = \mathrm{Ad}(U_a) - I, \quad \lambda = \frac{5}{3}. \tag{V.6.11}$$

Here e_a is an ordered degree-one basis for the circle directions, and $\mathrm{Ad}(U)M = UMU^{-1}$. This is a complete cellular complex for the local system, not a truncation of Fourier modes. A common nonzero scale λ changes representatives, not cohomology. At $\lambda = 0$ it would instead set the differential to zero.

Commuting holonomies give commuting T_a. Antisymmetry of the exterior generators then cancels each pair of terms:

$$D^2 = \lambda^2 \sum_{a<b} e_a \wedge e_b \wedge (T_a T_b - T_b T_a) = 0. \tag{V.6.12}$$

This checks that cohomology is defined; we must still find it. Let E_{ij} be the matrix with one nonzero entry in position (i,j). Conjugation acts as

$$\mathrm{Ad}(U_1)(E_{11}, E_{22}, E_{12}, E_{21}) = (E_{11}, E_{22}, -E_{12}, -E_{21}), \qquad T_2 = T_3 = 0. \tag{V.6.13}$$

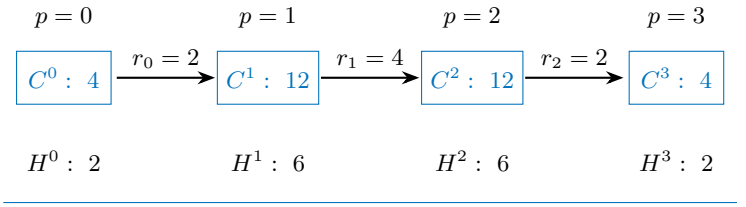


Figure V.6.2: The complete cellular $\mathrm{End}(E)$ complex for the selected torus holonomies. Numbers in the upper row are cochain dimensions; arrow labels are ranks, not maps equal to those integers. The lower row gives cohomology dimensions. The two off-diagonal characters have the explicit contraction shown below the row; the two diagonal characters have zero differential.

The diagonal subspace has $D = 0$. On each off-diagonal subspace $T_1 = -2$, hence $D = -\frac{10}{3}e_1\wedge$. Interior contraction ι_1 removes e_1 with the exterior sign and satisfies an anticommutator identity. It supplies the contracting homotopy

$$\iota_1(e_1 \wedge \alpha) + e_1 \wedge \iota_1\alpha = \alpha, \qquad h = -\frac{3}{10}\iota_1, \qquad Dh + hD = I. \tag{V.6.14}$$

For a closed α this gives $\alpha = D(h\alpha)$. Thus every closed off-diagonal cochain is exact, in every degree. The argument proves acyclicity of the complete summands.

The ranks can also be followed degree by degree. On one off-diagonal summand, $e_1\wedge$ maps the scalar to e_1, maps e_2, e_3 to e_{12}, e_{13}, and maps e_{23} to e_{123}. Its ranks are $(1, 2, 1)$. There are two such summands, while the two diagonal summands contribute no rank. Therefore

$$(\dim C^0, \dim C^1, \dim C^2, \dim C^3) = (4, 12, 12, 4), \qquad (r_0, r_1, r_2) = (2, 4, 2). \tag{V.6.15}$$

Substitution in eq. (V.6.9) yields

$$(b_0, b_1, b_2, b_3) = (4 - 2,\ 12 - 2 - 4,\ 12 - 4 - 2,\ 4 - 2) = (2, 6, 6, 2). \tag{V.6.16}$$

The surviving algebra of vector spaces is two copies of $\Lambda^\bullet\mathbb{C}^3$. Figure V.6.2 separates these summands from the contractible ones. With all holonomies trivial the ranks vanish and the cohomology dimensions become $(4, 12, 12, 4)$.

The conjugation inverse matters. Multiplying each holonomy by an arbitrary scalar $c_a \neq 0$ leaves its End action unchanged:

$$(c_aU_a)M(c_aU_a)^{-1} = U_aMU_a^{-1}. \tag{V.6.17}$$

For a line bundle this makes its self-End local system trivial, however nontrivial its own scalar holonomy. There is a useful sign-sensitive comparison. The involution $U_1 = \mathrm{diag}(1, -1)$ obeys $U_1^{-1} = U_1$, so it cannot distinguish UMU^{-1} from the incorrect expression UMU. Replace it by $\widehat{U}_1 = iU_1$. Its correct conjugation is unchanged, but

$$\widehat{U}_1M\widehat{U}_1^{-1} = U_1MU_1^{-1}, \qquad \widehat{U}_1M\widehat{U}_1 = -U_1MU_1. \tag{V.6.18}$$

In the incorrect expression the diagonal and off-diagonal characters exchange their roles. The total Betti numbers happen to stay the same for this example, while the actual differential and surviving matrix subspaces change. A dimension count with involutive holonomies alone misses that error; scalar cancellation tests the transport law itself.

The B example needs a different complete argument. For the trivial holomorphic line bundle on a flat complex three-torus, expand smooth periodic $(0,q)$ forms into lattice Fourier modes. On a mode labeled by a real lattice covector k, $\bar\partial$ acts by exterior multiplication by its associated $(0,1)$ covector ξ_k. A nonzero real k has $\xi_k \neq 0$. Choose v_k with $\xi_k(v_k) = 1$. Then

$$\bar\partial_k = \xi_k\wedge, \qquad (\xi_k\wedge)\iota_{v_k} + \iota_{v_k}(\xi_k\wedge) = I \quad (k \neq 0). \tag{V.6.19}$$

The contraction coefficients grow at most polynomially and can be chosen of size proportional to $1/|k|$, so they preserve the rapid Fourier decay of smooth forms. All nonzero modes are contractible. The zero mode has constant anti-holomorphic exterior generators and zero differential, giving

$$H^{0,q}(T^6,\mathcal{O}) = \Lambda^q\langle d\bar z^1, d\bar z^2, d\bar z^3\rangle, \qquad (h^{0,0},h^{0,1},h^{0,2},h^{0,3}) = (1,3,3,1). \tag{V.6.20}$$

Flatness, compactness and the trivial holomorphic bundle enter this argument. A finite collection of modes would not prove the result for the smooth complex. The next section keeps the same differential-first logic but replaces differential forms by a free resolution, making local support visible.

V.6.4 Ext groups as arrows

How do we calculate protected extension data for a brane localized at a point? A point does not carry the tangent forms of a space-filling brane, but the ambient directions still affect open extensions. A resolution retains these directions through equations defining the support.

Let $R = \mathbb{C}[x,y]$. An R-module is a vector space with compatible multiplication by polynomials. The point module $M = R/(x,y)$ has $x = y = 0$ on every element. A free resolution replaces it by free modules, with all nonzero-degree homology removed. With nonzero basis scales s_x, s_y, consider

$$\begin{gathered} 0 \longrightarrow P_2 = R \xrightarrow{d_2} P_1 = R^2 \xrightarrow{d_1} P_0 = R \longrightarrow M \longrightarrow 0, \\ d_1 = (s_x x, s_y y), \qquad d_2 = \begin{pmatrix} -s_y y \\ s_x x \end{pmatrix}. \end{gathered} \tag{V.6.21}$$

The chain degree decreases from P_2 to P_0. These scales rescale bases; they are not physical couplings. We first verify the complex identity

$$d_1 d_2 = -s_x s_y xy + s_x s_y yx = 0. \tag{V.6.22}$$

This identity alone does not give a resolution. Exactness requires every kernel to equal the preceding image.

In R, multiplication by x is injective, and multiplication by y remains injective modulo (x) because $R/(x) = \mathbb{C}[y]$. This is the regular-sequence property in this example. More explicitly, suppose (f, g) lies in $\ker d_1$. Coprimality of x and y forces x to divide g. Writing $g = s_x x h$ in the kernel equation gives

$$s_x x f + s_y y g = 0 \quad \Longrightarrow \quad g = s_x x h, \qquad f = -s_y y h, \qquad \begin{pmatrix} f \\ g \end{pmatrix} = d_2 h. \tag{V.6.23}$$

Thus $\ker d_1 = \operatorname{im} d_2$. The ring is a domain and both scales are nonzero, so $d_2 h = 0$ implies $h = 0$. Finally $\operatorname{im} d_1 = (x, y)$, whose quotient is M. This proves exactness at every term. Setting a scale to zero would change the ideal and invalidate this resolution.

For another module N, $\operatorname{Hom}_R(P_p, N)$ consists of R-linear maps. Precomposition with d raises its cochain degree. The Ext groups are defined by the resulting cohomology:

$$C_N^p = \operatorname{Hom}_R(P_p, N), \qquad \delta^p(f) = f \circ d_{p+1}, \qquad \operatorname{Ext}_R^p(M, N) = H^p(C_N, \delta). \tag{V.6.24}$$

A free resolution permits this definition to compute the derived Hom independently of the chosen free bases. For the point $N = R/(x - a, y - b)$, each copy of R maps to a one-dimensional fiber and polynomial multiplication evaluates at (a, b). Consequently

$$\mathbb{C} \xrightarrow{\delta^0} \mathbb{C}^2 \xrightarrow{\delta^1} \mathbb{C}, \qquad \delta^0 = \begin{pmatrix} s_x a \\ s_y b \end{pmatrix}, \qquad \delta^1 = (-s_y b, s_x a). \tag{V.6.25}$$

The composite is zero before or after evaluation. At coincidence $(a, b) = (0, 0)$, both maps vanish and the Ext dimensions are $(1, 2, 1)$.

For a separated point at least one entry of δ^0 is nonzero. Both differentials then have rank one. The kernel of δ^1 is the line spanned by $(s_x a, s_y b)$, exactly the image of δ^0. Hence

$$\dim \operatorname{Ext}_R^\bullet(M, N) = \begin{cases} (1, 2, 1), & (a, b) = (0, 0), \\ (0, 0, 0), & (a, b) \neq (0, 0). \end{cases} \tag{V.6.26}$$

The support change removes the local extensions in all degrees, not merely the degree-zero morphism. For $s_x = 2, s_y = 3$ and $(a, b) = (2, -1)$ the calculation is completely numerical:

$$\begin{gathered} \delta^0 = \begin{pmatrix} 4 \\ -3 \end{pmatrix}, \qquad \delta^1 = (3, 4), \qquad \delta^1 \delta^0 = 12 - 12 = 0, \\ (b_0, b_1, b_2) = (1 - 1, 2 - 1 - 1, 1 - 1) = (0, 0, 0). \end{gathered} \tag{V.6.27}$$

Checking only the coincident fiber would miss an incorrect sign in d_2, since every differential entry vanishes there. Exactness and the polynomial composition must be established before taking that fiber.

The mathematical Ext calculation is distinct from its physical realization. In the sourced large-radius, $B = 0$ calculation with smooth support $i\colon S \hookrightarrow X$ and honest bundle E, the demonstrated BRST construction is for identical Chan–Paton gauge fields at both ends. Its self-open strings involve $i_* E$. Define $K_S = \Lambda^{\dim_{\mathbb{C}} S} T^{*(1,0)} S$, the canonical line bundle of the support. In the source convention, the physical Chan–Paton object is written

$$E_{\text{phys}} = E \otimes \sqrt{K_S^\vee}, \qquad i_* E \text{ is the sheaf label.} \tag{V.6.28}$$

The square root here need not be an ordinary line bundle. The source uses the canonical Spin^c lift: its local square-root factors can have twisted transition functions, so E_{phys} need not be an honest bundle even when the sheaf-label bundle E is honest. For a complex support in the stated Calabi–Yau setting, the normal bundle has a Spin^c structure. An ordinary square root is available in the source's Spin case; a merely Spin^c normal bundle does not supply one. This is the anomaly-related meaning of the notation, not a claim that every canonical line bundle has a global square root. We use the source's canonical choice without an additional common line-bundle tensor. Its full anomaly argument is cited, and arbitrary new physical twists require rechecking the premises.

There is also a differential hidden by a naive normal-form count. The tangent-normal sequence and the associated self-Ext spectral sequence have the form

$$\begin{aligned} 0 \to TS \to TX|_S \to N_{S/X} \to 0, \\ E_2^{p,q} = H^p(S, \operatorname{End} E \otimes \Lambda^q N_{S/X}) \implies \operatorname{Ext}_X^{p+q}(i_*E, i_*E). \end{aligned} \tag{V.6.29}$$

A spectral sequence retains successive differentials between these intermediate groups; their direct sum is not generally the answer. For example, a holomorphic normal-valued section can be lifted smoothly to $TX|_S$. Its $\bar\partial$ is tangent-valued, representing the connecting map. The curvature-dependent boundary condition then contracts it to the next form:

$$H^0(S, \operatorname{End} E \otimes N_{S/X}) \xrightarrow{\alpha} H^1(S, \operatorname{End} E \otimes TS) \xrightarrow{\beta_{F_E}} H^2(S, \operatorname{End} E), \qquad d_2 = \beta_{F_E}\alpha. \tag{V.6.30}$$

Evaluating this map on a specified compact support requires its tangent-normal extension and bundle curvature. The source explains why the extra canonical square-root curvature in eq. (V.6.28) drops out of this d_2. Its explicit physical construction assumes the same endpoint gauge field: different fields can change fermion moding and zero modes. The point-module arithmetic above supplies no proof of that broader physical extension.

Equivariance now adds the endpoint labels missing from an ordinary support. A G-equivariant sheaf carries a compatible group action as well as its module structure. At the fixed point of $\mathbb{C}^n$, let $T = T_0\mathbb{C}^n$ be the tangent representation and $S_i = \mathcal{O}_0 \otimes R_i$. The point Koszul resolution generalizes the preceding regular-sequence construction. Dualizing its linear generators gives $\operatorname{Ext}^p(\mathcal{O}_0, \mathcal{O}_0) = \Lambda^p T$. For a finite group in characteristic zero, averaging over G makes taking invariants exact. Thus

$$\operatorname{Ext}_G^p(S_j, S_i) = \big(\operatorname{Hom}(R_j, R_i) \otimes \Lambda^p T\big)^G, \qquad T_{ij}^p = \dim \operatorname{Ext}_G^p(S_j, S_i). \tag{V.6.31}$$

The slots are intentional: the book arrow $i \to j$ counts T_{ij}^1. Here N_i is the multiplicity, or Chan–Paton rank, of the object at node i. Matrix fields on that arrow have size N_i by N_j. Linear coordinate functions transform contragrediently under pullback; they are not silently assigned the tangent weights in this formula.

For $G = \mathbb{Z}_3$ choose $\omega = e^{2\pi i/3}$, $R_i(g) = \omega^i$, and tangent weights $(1, 1, 1)$. A wedge of p distinct tangent directions has weight p, and $\operatorname{Hom}(R_j, R_i)$ has weight $i - j$. Invariance is the explicit condition

$$i - j + p = 0 \pmod 3, \qquad T_{ij}^p = \binom{3}{p} \delta_{j,i+p \pmod 3}. \tag{V.6.32}$$

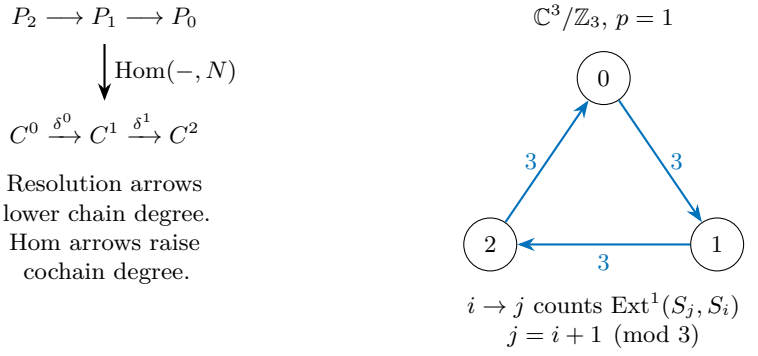


Figure V.6.3: Two uses of direction. On the left a homological resolution becomes a cohomological Hom complex by precomposition; the direction of the degree change reverses. On the right the $\mathbb{C}^3/\mathbb{Z}_3$ degree-one Ext table gives three book arrows on each directed link. The mathematical morphism in $\mathrm{Ext}^1(S_j, S_i)$ has reversed object slots relative to the displayed $i \to j$. Degree-two arrows, not drawn, reverse this cycle.

The binomial multiplicity counts which directions enter the wedge. With rows and columns ordered $0, 1, 2$, all four tables are

$$T^0 = T^3 = I_3, \qquad T^1 = \begin{pmatrix} 0 & 3 & 0 \\ 0 & 0 & 3 \\ 3 & 0 & 0 \end{pmatrix}, \qquad T^2 = \begin{pmatrix} 0 & 0 & 3 \\ 3 & 0 & 0 \\ 0 & 3 & 0 \end{pmatrix}. \tag{V.6.33}$$

The degree-one arrows form $0 \to 1 \to 2 \to 0$, with multiplicity three on each link. Degree two reverses them. Figure V.6.3 shows why this asymmetric example resolves an orientation ambiguity that a symmetric surface graph cannot detect.

Finally Ext degree and quiver grade serve different purposes. In the selected protected B-brane convention on a CY n-fold set $m = n - 2$. Only degrees $p = 1, \ldots, n - 1$ enter the matter-arrow grades. Under proper-support, Ext-finite CY Serre duality,

$$c = p - 1, \qquad \mathrm{Ext}^p(E, F) \simeq \mathrm{Ext}^{n-p}(F, E)^*, \qquad c_{\mathrm{partner}} = n - p - 1 = m - c. \tag{V.6.34}$$

The dual space is essential: this is a perfect pairing, not a canonical equality of vectors. For the threefold, $p = 1, 2$ gives $c = 0, 1$, while $p = 0, 3$ stays outside the matter-arrow range. This is the interface to Chapter VII.10. It is not a universal assignment of physical spacetime multiplets from an integer Ext degree. To learn interactions we must next compose actual representatives.

V.6.5 Products and interactions

Which information is missing from the Ext dimensions? A vector-space count says how many operators survive, but it does not say what happens when they meet. Yoneda multiplication composes extensions. Using a resolution, we can represent it by chain maps and calculate the signs rather than infer them from a proposed quiver interaction.

Return to the unscaled point resolution, $d_1 = (x, y)$ and $d_2 = (-y, x)^T$. Write its free exterior basis as $1, e_1, e_2, e_{12}$ with $e_{12} = e_1 \wedge e_2$ at chain level. A map I lowering the homological degree by one represents a cohomological degree-one endomorphism. Its closure condition is

$$\partial_{\mathrm{End}} I = dI - (-1)^{|I|} Id = dI + Id = 0, \qquad |I| = 1. \tag{V.6.35}$$

Maps differing by an endomorphism coboundary represent the same Ext class. This is the chain-map version of dividing closed operators by exact ones.

The two contractions have the explicit components

$$\begin{aligned} I_1|_{P_1} &= (1, 0), \quad I_1|_{P_2} = \begin{pmatrix} 0 \\ 1 \end{pmatrix}, \\ I_2|_{P_1} &= (0, 1), \quad I_2|_{P_2} = \begin{pmatrix} -1 \\ 0 \end{pmatrix}. \end{aligned} \tag{V.6.36}$$

For instance $I_1(e_{12}) = e_2$ while $I_2(e_{12}) = -e_1$. These signs use the ordered chain basis; changing the top basis requires changing its dual as well. The only nontrivial closure components are maps from P_2 to P_0:

$$d_1 I_1|_{P_2} + I_1|_{P_1} d_2 = y - y = 0, \qquad d_1 I_2|_{P_2} + I_2|_{P_1} d_2 = -x + x = 0. \tag{V.6.37}$$

Thus both contractions give closed endomorphisms before specializing x, y to the origin.

We use ordinary composition $I_1 I_2 = I_1 \circ I_2$ for the product of these representatives. On the top chain basis,

$$I_1 I_2(e_{12}) = -1, \qquad I_2 I_1(e_{12}) = 1, \qquad I_1^2 = I_2^2 = 0. \tag{V.6.38}$$

Let $\epsilon_{12} \colon P_2 \to M$ send the ordered top chain basis to 1. The augmentation $P_0 \to M$ therefore sends $I_1 I_2$ to $-\epsilon_{12}$. To identify the Yoneda algebra with an exterior algebra on its degree-one classes, the positive top Ext generator is

$$e_1^{\mathrm{Ext}} = [I_1], \qquad e_2^{\mathrm{Ext}} = [I_2], \qquad e_{12}^{\mathrm{Ext}} = -[\epsilon_{12}] = e_1^{\mathrm{Ext}} e_2^{\mathrm{Ext}}. \tag{V.6.39}$$

This states the top-generator sign explicitly. Below we suppress the superscript on the Ext generators. They are cohomology classes, not the free generators of the original resolution. The result is the exterior Yoneda algebra, with degree-zero unit and no groups above degree two.

Now rescale the cohomology basis, without changing the resolution,

$$(1, A, B, Z) = (1, 2e_1, 3e_2, 5e_{12}), \qquad AB = \frac{6}{5} Z, \quad BA = -\frac{6}{5} Z, \quad A^2 = B^2 = 0. \tag{V.6.40}$$

The coefficient $6/5$ is the product of the two degree-one scales divided by the top scale. It is not an interaction strength. To include all products, including the unit and zeros,

the table is

$\cdot$	1	A	B	Z
1	1	A	B	Z
A	A	0	$\frac{6}{5}Z$	0
B	B	$-\frac{6}{5}Z$	0	0
Z	Z	0	0	0

(V.6.41)

Rows multiply columns in the displayed algebra order. The vanishing top products follow either from repeated exterior generators or from degree exceeding two. For a collection of distinct branes, composition also requires matching endpoints; a symbol AB by itself does not specify a quiver path.

Binary multiplication still need not determine all open interactions. An A_∞ algebra has multilinear operations m_k of cohomological degree $2-k$, related by identities expressing coherent associativity. Before passing to cohomology m_1 is the differential. The arity-three identity relates the associator of m_2 to terms involving m_1 and m_3. In a minimal model $m_1 = 0$, those terms vanish, so m_2 is associative. Minimality leaves room for nonzero higher operations.

A reduced, nonunital example isolates this last point without asserting a brane realization. Take a graded vector space spanned by u in degree one and v in degree two, and define

$$m_1 = m_2 = 0, \qquad m_3(u,u,u) = \lambda v, \qquad \lambda = \frac{7}{3}, \qquad m_k = 0 \ (k \neq 3). \tag{V.6.42}$$

Set m_3 to zero whenever any argument is v. Its degree is consistent because

$$|m_3(u,u,u)| = |u| + |u| + |u| + (2-3) = 3 - 1 = 2 = |v|. \tag{V.6.43}$$

There is an all-input check of the identities, not just a sample of numerical arguments. A nonzero nested term would have to contain two m_3 operations, so it can only occur at arity five. The inner operation produces v, which kills the outer operation:

$$m_3\big(u^{\otimes r}, m_3(u,u,u), u^{\otimes(2-r)}\big) = 0, \qquad r = 0,1,2. \tag{V.6.44}$$

If an original argument was already v, either the inner or outer operation vanishes as well. Every other identity contains a zero operation. Thus the identities hold term by term, independently of their signs. The choice $\lambda = 0$ has the same underlying graded vector space and the same m_2, but different displayed higher data. This observation does not classify the algebras up to all possible changes of variables, nor distinguish every nonzero λ up to isomorphism.

Disk amplitudes are often written with suspended operations of degree $+1$. If s lowers degree by one, the degree translation is

$$r_k = s\, m_k\, (s^{-1})^{\otimes k}, \qquad |r_k| = -1 + (2-k) + k = 1. \tag{V.6.45}$$

This equation fixes degrees; applying it to individual tensor components also needs the Koszul signs of the tensor convention. One cannot copy an unsuspended component

into a suspended disk formula using its degree alone. A curved or weak structure may also have an m_0 term; the present example has none.

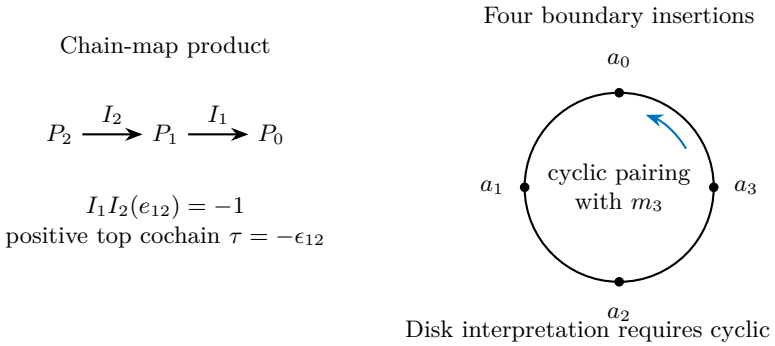


Figure V.6.4: The explicit binary computation and the additional data for a disk interpretation. On the left, composing I_2 then I_1 sends the ordered top chain generator to -1; the positive exterior top Ext generator is correspondingly $-\epsilon_{12}$. On the right, an oriented disk has a cyclic order of four boundary insertions, with a_0 paired against a three-input product. Turning such a product into an amplitude requires a compatible cyclic pairing and boundary sectors. These data are absent from the reduced u, v example.

Figure V.6.4 separates the product we computed from a disk amplitude. The latter needs cyclic pairing data as well as operations. Ext dimensions forget both multiplication and higher maps; the Yoneda table restores multiplication but does not automatically restore all higher maps. This is why the interaction discussion of Chapter VII.10 and the topological field theories of Volume XVIII need more than an adjacency matrix. The next construction asks which of these categorical structures can be transported between an orbifold and its selected resolution.

V.6.6 The fractional brane interface

Which part of a fractional-brane description survives a change of geometric presentation? Equivariant objects retain labels that the coarse quotient can lose. A suitable derived equivalence then transports Hom groups, shifts and additive classes. We will compute the transported Euler form, while keeping physical stability separate.

For $G = \mathbb{Z}_2$ acting on $\mathbb{C}^2$ by $(x, y) \mapsto (-x, -y)$, the two point modules have the same ordinary support and different actions on their generator α:

$$S_0 = \mathbb{C}\alpha, \quad g\alpha = \alpha, \qquad S_1 = \mathbb{C}\alpha, \quad g\alpha = -\alpha, \qquad x\alpha = y\alpha = 0. \tag{V.6.46}$$

An equivariant sheaf on $\mathbb{C}^2$ is equivalently a sheaf on the quotient stack $[\mathbb{C}^2/G]$; this retains the group action at the fixed point. Passing instead to the coarse quotient takes

invariant modules. In this example

$$(S_0)^G = \mathbb{C}\alpha, \qquad (S_1)^G = 0. \tag{V.6.47}$$

There are no nonzero $x\alpha$ or $y\alpha$ with which to form an invariant for S_1. A sheaf construction that keeps only the coarse quotient therefore loses the nontrivial fractional label.

To transport the objects, we need a theorem with specified geometry. A bounded derived category D^b consists of bounded complexes of coherent sheaves, with quasi-isomorphisms inverted. A quasi-isomorphism is a map inducing isomorphisms on every cohomology group. Morphisms to shifts recover Ext; an exact equivalence preserves these Hom spaces and the distinguished triangles encoding extensions.

Here is the sourced Bridgeland–King–Reid statement used in this chapter. Let M be a smooth quasiprojective complex variety of dimension n, and G a finite group of automorphisms. Assume that its canonical sheaf ω_M is locally trivial as a G-sheaf. Let Y be the component of $G\text{-Hilb}(M)$ containing the free orbits. The G-Hilbert scheme parametrizes G-invariant zero-dimensional subschemes whose functions carry the regular representation. With universal family $\mathcal{Z} \subset Y \times M$ and projections $p\colon \mathcal{Z} \to Y$, $q\colon \mathcal{Z} \to M$, the theorem states that

$$\dim\bigl(Y \times_{M/G} Y\bigr) \le n+1 \quad\Longrightarrow\quad Y \text{ is crepant}, \qquad \Phi = Rq_*p^*\colon D^b(Y) \xrightarrow{\sim} D^b_G(M). \tag{V.6.48}$$

The pullback p^* is already exact because the universal family is flat over Y. The source's low-dimensional theorem says that for $n \le 3$ the dimension condition holds, $G\text{-Hilb}(M)$ is irreducible and the crepant-resolution and equivalence conclusions follow. These are cited theorems, not consequences of the matrix calculations below. A determinant-one action in dimension four or five by itself supplies neither the missing dimension hypothesis nor a crepant resolution.

Our $M = \mathbb{C}^2$ example obeys these hypotheses: it is smooth and quasiprojective, and the action preserves the nowhere-zero two-form $dx \wedge dy$. Let $Y = G\text{-Hilb}(\mathbb{C}^2)$ and define

$$E_i = \Phi^{-1}(S_i), \qquad \operatorname{Hom}_{D^b(Y)}(E_i, E_j[p]) \simeq \operatorname{Hom}_{D^b_G(\mathbb{C}^2)}(S_i, S_j[p]). \tag{V.6.49}$$

We have specified these inverse images by the functor, not identified them with particular shifted line bundles. Making that identification would require an additional calculation with the chosen kernel.

The support condition now matters. Let $\mathcal{C}_{\mathrm{orb}}$ be the bounded equivariant category with cohomology supported at the origin, and set $\mathcal{C}_Y = \Phi^{-1}(\mathcal{C}_{\mathrm{orb}})$. Origin-supported coherent modules have finite length; their two simple objects are S_0, S_1. The inverse images are simple in the transported heart, the abelian category obtained by transporting those modules. They need not be simple coherent sheaves in every geometric heart. The group K_0 assigns an additive class to objects, with $[B] = [A] + [C]$ for a distinguished triangle $A \to B \to C \to A[1]$. Thus

$$K_0(\mathcal{C}_{\mathrm{orb}}) = \mathbb{Z}[S_0] \oplus \mathbb{Z}[S_1], \qquad K_0(\mathcal{C}_Y) = \mathbb{Z}[E_0] \oplus \mathbb{Z}[E_1], \qquad [E[1]] = -[E]. \tag{V.6.50}$$

Finite-length composition series establish the simple-class basis; the last relation follows from the triangle $E \to 0 \to E[1]$. This is the group of a category with a specified support

condition. We do not assert that it injects into unrestricted $K_0(Y)$. Even a point class on affine space can vanish after support is forgotten. Nor does this construction specify physical RR units.

We can compute the Euler form because the proper support makes the Ext groups finite. The tangent weights $(1,-1)$ reduce to $(1,1)$ modulo two. The invariant exterior powers give

$$T^0 = T^2 = I_2, \qquad T^1 = \begin{pmatrix} 0 & 2 \\ 2 & 0 \end{pmatrix}, \qquad \chi_{\text{old}} = T^0 - T^1 + T^2 = \begin{pmatrix} 2 & -2 \\ -2 & 2 \end{pmatrix}. \tag{V.6.51}$$

The two tangent directions both change the character, while their top wedge is invariant. Here the tables are symmetric, so the reversed slots used to draw book arrows do not change the Euler matrix with first argument in the row. They could not resolve the direction in the earlier chiral example. The general definition is

$$\chi(E,F) = \sum_p (-1)^p \dim \operatorname{Ext}^p(E,F), \qquad \chi(q,r) = q^T \chi_{\text{old}} r = 2(q_0 - q_1)(r_0 - r_1). \tag{V.6.52}$$

Additivity allows the form to descend to K_0. Exact equivalence preserves it because it preserves each Hom-to-shift space, not because rational Chern characters happen to agree.

Let $R = [E_0] + [E_1]$ denote the regular-representation class and $F = [E_1]$. The letter R in the remainder of this section denotes this class, not the polynomial ring. The new basis columns and coordinate rule are

$$B = \begin{pmatrix} 1 & 0 \\ 1 & 1 \end{pmatrix}, \qquad \det B = 1, \qquad q_{\text{old}} = B q_{\text{new}}. \tag{V.6.53}$$

Both arguments of a bilinear form change, so its matrix transforms by congruence:

$$\chi_{\text{new}} = B^T \chi_{\text{old}} B = \begin{pmatrix} 1 & 1 \\ 0 & 1 \end{pmatrix} \begin{pmatrix} 0 & -2 \\ 0 & 2 \end{pmatrix} = \begin{pmatrix} 0 & 0 \\ 0 & 2 \end{pmatrix}. \tag{V.6.54}$$

The null regular direction was already visible in the differences $q_0 - q_1$ in eq. (V.6.52). Figure V.6.5 locates it in the same integral group.

For a numerical check on both arguments take $n_{\text{new}} = (2,3)^T$ and $m_{\text{new}} = (1,-2)^T$. Their old coordinates and mixed pairing are

$$\begin{aligned} n_{\text{old}} &= \begin{pmatrix} 2 \\ 5 \end{pmatrix}, \qquad m_{\text{old}} = \begin{pmatrix} 1 \\ -1 \end{pmatrix}, \\ \chi(n,m) &= 2(2-5)(1+1) = -12 = (2,3) \begin{pmatrix} 0 & 0 \\ 0 & 2 \end{pmatrix} \begin{pmatrix} 1 \\ -2 \end{pmatrix}. \end{aligned} \tag{V.6.55}$$

The negative entry in m and the shift sign in eq. (V.6.50) are allowed additive operations. They establish no physical decay. An equivalence supplies no central charge, no choice of physical stability and no stability-preserving path through Kähler moduli. Chapter VI.5 can use the categorical refinement only with that distinction intact; Chapter III.5 supplies the complementary caution about integral charges versus rational characteristic classes.

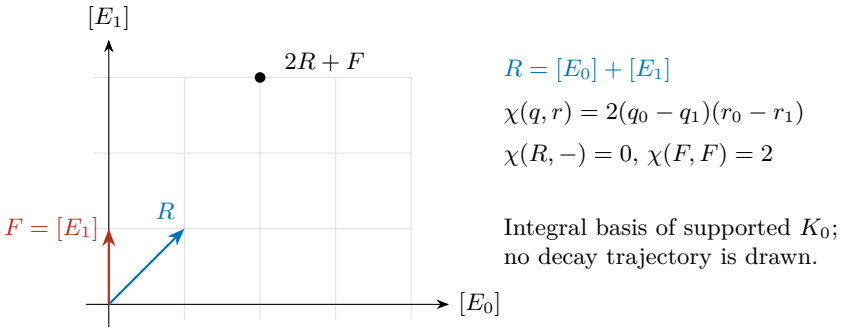


Figure V.6.5: A basis change within the transported origin-supported K_0. Horizontal and vertical axes give old coordinates in $[E_0], [E_1]$; the blue diagonal vector is the regular class $R = (1, 1)$, and the red vertical vector is F. The marked point $2R + F$ has old coordinates $(2, 3)$. The Euler form vanishes on the regular direction and is 2 on (F, F). The picture depicts additive categorical classes, with no claim that a basis vector is a stable physical brane at all moduli.

V.6.7 From open fields to actions

When does the protected open complex become a target-space gauge theory? Its degree-one field has the type of a connection, and its differential gives the linearized curvature. To identify a full functional we also need the product and an integration pairing. There is one particularly controlled A geometry in which disk instantons cannot change this route.

Take $X = T^*L$, with L compact and oriented of real dimension three. Choose the exact symplectic form $\omega = d\theta$, with $\theta|_L = 0$ on the zero section, and a compatible positive almost-complex structure I. Compatibility means that $g(v, w) = \omega(v, Iw)$ is a positive metric. For a smooth map of a compact unpunctured disk with $u(\partial D) \subset L$, Stokes gives

$$\int_D u^*\omega = \int_D d(u^*\theta) = \int_{\partial D} u^*\theta = 0. \tag{V.6.56}$$

Exactness of the ambient symplectic form and vanishing of its primitive on the boundary support are both used. Noncompactness of X by itself implies neither equality.

For an I-holomorphic map the area equals the positive energy, with the conventional energy normalization $E(u) = \frac{1}{2}\int_D |du|^2$. In oriented conformal coordinates (s, t), holomorphicity gives $u_t = Iu_s$, so

$$u^*\omega(\partial_s, \partial_t) = \omega(u_s, Iu_s) = |u_s|^2, \qquad \frac{1}{2}\big(|u_s|^2 + |u_t|^2\big) = |u_s|^2, \qquad E(u) = \int_D u^*\omega. \tag{V.6.57}$$

Equations (V.6.56) and (V.6.57) force $du = 0$. Every such holomorphic disk is constant. Smoothness and the absence of punctures remove additional boundary or asymptotic terms. This proof is geometric; the subsequent identification with a topological string action is a separate sourced physical construction.

In the exact cotangent sector, the degree-one A field is an $\mathrm{End}(E)$-valued one-form on L. The degree-one B field on a CY threefold X is an $\mathrm{End}(E)$-valued $(0,1)$ form. For B require an integrable reference bundle and a closed nowhere-zero holomorphic three-form Ω. Around these reference connections the field and curvature types are

$$\begin{aligned} &\text{A:} \quad A \in \Omega^1(L, \operatorname{End} E), \qquad F_A = dA + A \wedge A, \\ &\text{B:} \quad A \in \Omega^{0,1}(X, \operatorname{End} E), \quad F_A^{0,2} = \bar{\partial}_E A + A \wedge A. \end{aligned} \tag{V.6.58}$$

In the A row we use a flat reference and write its differential locally as d; globally it is the corresponding covariant differential. In the B row $D = \bar{\partial}_E$ satisfies $D^2 = 0$ before the perturbation A is added. The connection forms are complex matrix-valued forms in this calculation; no unmentioned Hermiticity convention is imposed.

The sourced classical topological open-string reductions yield Chern–Simons theory and holomorphic Chern–Simons theory respectively. Their common relative coefficients can be written as

$$\begin{aligned} S_A &= \kappa_A \int_L \operatorname{Tr}\left(\frac{1}{2} A \wedge dA + \frac{1}{3} A \wedge A \wedge A\right), \\ S_B &= \kappa_B \int_X \Omega \wedge \operatorname{Tr}\left(\frac{1}{2} A \wedge \bar{\partial}_E A + \frac{1}{3} A \wedge A \wedge A\right). \end{aligned} \tag{V.6.59}$$

The trace is the fundamental matrix trace. Topological metric independence and the absence of nonconstant disks control the cited A reduction in this sector. We do not derive the entire string-field construction from the cohomology dimensions. In B the scale of Ω is arbitrary nonzero holomorphic data; it is not a unit-comass normalization from a calibration problem.

To match the book's bare CS level, compare coefficients directly:

$$S_A = \frac{k}{4\pi} \int_L \operatorname{Tr}\left(A \wedge dA + \frac{2}{3} A \wedge A \wedge A\right), \qquad \kappa_A = \frac{k}{2\pi}. \tag{V.6.60}$$

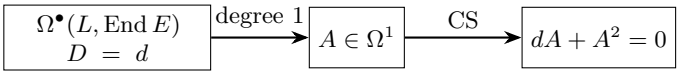
The source's displayed relative action has $\kappa_A = 1$ before an overall coupling. The hCS coefficient κ_B remains unspecified; this argument assigns it neither an integer level nor a relation to g_s. Global quantum CS level shifts, framing and gauge fixing belong to Volume XVIII.

We can nevertheless derive the classical variation completely. Let D denote the appropriate reference differential, let juxtaposition mean wedge product with matrix multiplication, and assume either a compact target without boundary or compactly supported variations that remove the integration-by-parts term. In B also use $d\Omega = 0$. The graded Leibniz rule for the quadratic term gives

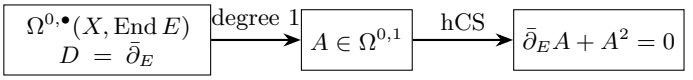
$$D(A\,\delta A) = (DA)\,\delta A - A\,D\delta A, \qquad \int \operatorname{Tr}(A\,D\delta A) = \int \operatorname{Tr}((DA)\,\delta A). \tag{V.6.61}$$

Here and in the next two equations the integral includes $\Omega\wedge$ in the B case. Moving the degree-two form DA past δA has sign $(-1)^{2\cdot 1} = +1$, so the two quadratic variations agree.

A model: exact cotangent zero section, $\dim_{\mathbb{R}} L = 3$



B model: CY threefold, $d\Omega = 0$, integrable reference bundle



Classical protected actions; further construction in Volume XVIII.

Figure V.6.6: The degree-one field in each open complex has the type of a connection. The product makes the nonlinear curvature, and the integration pairing produces CS or hCS. The upper row uses the exact cotangent zero-section sector with flat reference; the lower uses a CY threefold, a closed holomorphic volume form and an integrable reference bundle. The equations on the right are classical critical-point equations, not a full physical spectrum.

For the cubic term, graded cyclicity produces no sign on moving a degree-one factor past the other two. The three varied terms are equal:

$$\begin{aligned} \delta \operatorname{Tr}(A^3) &= \operatorname{Tr}(\delta A\, A^2 + A\, \delta A\, A + A^2 \delta A) \\ &= 3 \operatorname{Tr}(\delta A\, A^2). \end{aligned} \tag{V.6.62}$$

Combining the factors $1/2$ and $1/3$ with these multiplicities yields

$$\delta S = \kappa \int \operatorname{Tr}\big(\delta A (DA + A^2)\big), \qquad DA + A^2 = 0. \tag{V.6.63}$$

Thus CS gives a flat connection on L, while hCS gives a holomorphic structure on the reference smooth bundle. These are the nonlinear versions of the boundary conditions of Section V.6.2. Figure V.6.6 summarizes the types and assumptions in the two routes.

Constant components already show why the product is necessary. In a local complex threefold chart write $A = \sum_i A_i\, d\bar z^i$. With $i < j$ ordering, there is no extra $1/2$ in

$$F_A^{0,2} = \sum_{i<j} \big(\partial_{\bar i} A_j - \partial_{\bar j} A_i + [A_i, A_j]\big) d\bar z^i \wedge d\bar z^j. \tag{V.6.64}$$

If all A_i commute, constancy makes this zero. Choose instead the constant nonabelian matrices

$$A_1 = \begin{pmatrix} 0 & 2 \\ 0 & 0 \end{pmatrix}, \qquad A_2 = \begin{pmatrix} 0 & 0 \\ 3 & 0 \end{pmatrix}, \qquad A_3 = \begin{pmatrix} 5 & 0 \\ 0 & -5 \end{pmatrix}. \tag{V.6.65}$$

The derivative part vanishes, but the products do not. The elementary identity $E_{ij}E_{kl} = \delta_{jk}E_{il}$ gives

$$\begin{aligned} A_1A_2 &= 6E_{11}, & A_2A_1 &= 6E_{22}, \\ A_1A_3 &= -10E_{12}, & A_3A_1 &= 10E_{12}, \\ A_2A_3 &= 15E_{21}, & A_3A_2 &= -15E_{21}. \end{aligned} \tag{V.6.66}$$

All three independent curvature components therefore are

$$F_{12} = \begin{pmatrix} 6 & 0 \\ 0 & -6 \end{pmatrix}, \qquad F_{13} = \begin{pmatrix} 0 & -20 \\ 0 & 0 \end{pmatrix}, \qquad F_{23} = \begin{pmatrix} 0 & 0 \\ 30 & 0 \end{pmatrix}. \tag{V.6.67}$$

This field is off shell and does not define an integrable holomorphic structure. Constancy has removed derivatives, not nonabelian curvature.

The cubic term tests the same ordering. The coefficient of $d\bar{z}^1 \wedge d\bar{z}^2 \wedge d\bar{z}^3$ is the alternating sum of six matrix traces. Cyclicity groups three positive and three negative terms:

$$\begin{aligned} [\operatorname{Tr}(A^3)]_{123} &= 3\operatorname{Tr}(A_1A_2A_3 - A_1A_3A_2) \\ &= 3\operatorname{Tr}(A_1[A_2, A_3]) = 3\operatorname{Tr}(60E_{11}) = 180. \end{aligned} \tag{V.6.68}$$

Equivalently $\operatorname{Tr}(A_1A_2A_3) = 30$ and $\operatorname{Tr}(A_1A_3A_2) = -30$, giving $3(30 - (-30))$. For the constant cubic integrand its coefficient in S_B/κ_B is therefore 60, before the holomorphic volume factor and integration. No global off-shell action is assigned to an arbitrary local chart.

This calculation reaches the field-theory interface needed by Volume XVIII. It establishes the stated variation and local components; the topological string reduction remains a sourced physical input. A complete physical open-string theory, all-background open/closed decoupling and nonperturbative quantum hCS do not follow from it.

V.6.8 From categorical data to a physical spectrum

The worked examples leave a concrete interpretive question: what must be added before an Ext table becomes a physical BPS spectrum? First specify the background, support, bundles and anomaly conditions under which the protected boundary calculation applies. The smooth-support source used here demonstrates its corrected Ext spectral sequence for identical endpoint gauge fields at large radius and $B = 0$. Changing those conditions is a new physical problem, even if a mathematical Ext group can still be written.

Next select the heart and the stability or central-charge data appropriate to that background. In the McKay example the transported origin-supported heart makes E_0, E_1 simple, and their K_0 classes span a rank-two group. The calculation of -12 is an Euler pairing in that group. It does not decide which classes have stable representatives. For example, replacing a class by its negative can be achieved by a categorical shift, but a physical conclusion needs its grade and stability interpreted along a specified path. The BKR functor alone provides no such path in Kähler moduli.

Then supply the physical GSO projection and the relation between the protected degree and spacetime states. In our chiral example degree one gives grade zero in

a chosen quiver convention; this fact by itself does not identify a universal matter multiplet. Finally determine the interactions. The exterior table explicitly fixes the binary product, while the reduced u, v example demonstrates information in a higher product that the binary table omits. To extract physical disk amplitudes one also needs boundary sectors and the cyclic pairing.

There is a parallel route for deciding where A-model disks can return. In the cotangent example Stokes used a global primitive whose restriction to the support vanished, and positivity converted zero area into a constant map. For a general Lagrangian, being Lagrangian only annihilates the pullback of the two-form on the support. It does not set the integral of that two-form over a disk to zero. There may be no global primitive, or its restriction may have a nonzero boundary period; punctures or asymptotic ends also require their own boundary terms. Positive-area disks can then contribute to the open operations or obstruct an uncorrected cohomology description. The ordinary de Rham count must be reconsidered in that setting.

This gives a worked reasoning route for the written exercise below: start from the stated differential and its physical premises, locate the missing stability and spacetime data, and test precisely the geometric hypotheses that suppressed disks. The mathematical theorems quoted in this chapter transport categorical structures under their hypotheses. They do not supply the additional physical choices.

V.6.9 Exercises

The six numerical tasks below use the conventions and exact quantities worked in the chapter. The accompanying public questions specify the JSON submission structure; the numerical checks concern those quantities only. Explanations requested in each task, and the final written exercise, require written reasoning.

1. On $T^3 \subset T^*T^3$ use the flat rank-two bundle $U_1 = \mathrm{diag}(1, -1)$, $U_2 = U_3 = I$ and $D = \frac{5}{3}\sum_a e_a \wedge (\mathrm{Ad}(U_a) - I)$ on $C^p = \mathrm{End}(\mathbb{C}^2) \otimes \Lambda^p\mathbb{C}^3$. Find the ranks of D^0, D^1, D^2 and all four cohomology dimensions. Show the contracting homotopy on each nontrivial character. Explain separately why scalar line-bundle holonomy cancels in its own End system and why replacing an inverse by the original holonomy is not detected by involutions alone.

2. Resolve $\mathbb{C}[x, y]/(x, y)$ with $d_1 = (2x, 3y)$ and $d_2 = (-3y, 2x)^T$. Prove exactness before evaluating at a point. Apply Hom into the point $(a, b) = (2, -1)$ and give both differentials, the three separated-point Ext dimensions and the three coincident-point Ext dimensions. Explain why setting one generator scale to zero destroys the premise.

3. For $\mathbb{C}^3/\mathbb{Z}_3$ use tangent weights $(1, 1, 1)$, $\omega = e^{2\pi i/3}$ and $S_i = \mathcal{O}_0 \otimes R_i$, with $R_i(g) = \omega^i$. Compute every matrix $T^p_{ij} = \dim \mathrm{Ext}^p(S_j, S_i)$ for $p = 0, 1, 2, 3$ in label order $0, 1, 2$. Give the grades for Ext degrees one and two. Draw the degree-one arrows and explain which part of this calculation fixes their direction.

4. For the point Yoneda algebra use the ordered basis $1, A = 2e_1, B = 3e_2, Z = 5e_1e_2$. Give the coefficients of Z in AB, BA, A^2, B^2. Recover the top-generator sign

by composing the contraction chain maps. In the separate reduced algebra with $|u| = 1$, $|v| = 2$, $m_1 = m_2 = 0$ and $m_3(u,u,u) = \frac{7}{3}v$, give the output degree. Explain why its identities hold and why this alone supplies no physical superpotential.

5. For $\mathbb{C}^2/\mathbb{Z}_2$ with tangent weights $(1,-1)$, let $E_i = \Phi^{-1}(S_i)$ for the specified BKR equivalence. Work in the transported origin-supported K_0, with $R = [E_0] + [E_1]$, $F = [E_1]$. Find the old and new Euler matrices, the old coordinates of $n_{\text{new}} = (2,3)^T$, and its pairing with $m_{\text{new}} = (1,-2)^T$. Explain why a change of integral basis does not establish physical decay or stability, and why unrestricted $K_0(Y)$ is a different question.

6. For constant components $A_1 = 2E_{12}$, $A_2 = 3E_{21}$, $A_3 = \operatorname{diag}(5,-5)$, compute F_{12}, F_{13}, F_{23} and the coefficient of $d\bar{z}^1 \wedge d\bar{z}^2 \wedge d\bar{z}^3$ in $\operatorname{Tr}(A^3)$. Use $i < j$ curvature coefficients with no additional $1/2$. State in written work whether this field defines a holomorphic structure and which term prevents it.

7. Give a written route from categorical data to a proposed physical BPS spectrum. Identify the chosen heart, stability and central charge, background and anomaly conditions, GSO and spacetime interpretation, and interaction data. Contrast the BKR equivalence with an actual stability-preserving path in Kähler moduli. Reconstruct the exact cotangent Stokes and positive-energy argument and state which hypotheses fail for a general Lagrangian, allowing disks to re-enter. This is a written exercise with no automated scientific acceptance.

V.6.10 Take-home message

Take-home message of this chapter

Boundary conditions select an open complex; cohomology, products and higher operations retain progressively more of its protected information. Relative torus holonomy removes the off-diagonal cohomology through an explicit contraction. A point resolution gives Ext and fixes the directed cyclic quiver only after its object slots are declared. Chain maps determine the signed Yoneda product. The selected McKay theorem transports a supported integral Euler form, not physical stability. In the exact cotangent and CY threefold settings, degree-one fields give CS and hCS with the stated classical equations. Background, anomaly, stability and spacetime data remain necessary when this protected information is used to infer a physical spectrum.

Status and sources

All PDF locators below count physical pages from one. The exact source editions are Witten, hep-th/9207094v2; Katz–Sharpe, hep-th/0208104v4; Katz–Pantev–Sharpe, hep-th/0212218v3; Closset et al., 1811.07016v1; Herbst et al., hep-th/0402110v2; and Bridgeland–King–Reid, math/9908027v2. The last uses the 27-page arXiv original, not a repository cover version. Mathematical computations and cited mathematical

theorems carry [MATH]; the physical boundary and topological-string identifications carry [WS-T]. The metric, twists, orbifolds, calibration, quivers and Chern–Simons conventions are stated above. No untwisted universal spectrum, stability-preserving equivalence, new duality transfer or decoupling limit is inferred.

§V.6.2. The elementary Lagrangian support, flat A connection and improved holomorphic B connection are distinct worldsheet inputs [WS-T] from Witten (1995, PDF pp. 16, 18–19, secs. 3.1–3.2, eqs. (3.11)–(3.14)). The coordinate metric and pullback are direct [MATH] calculations in eqs. (V.6.3)–(V.6.5). Witten's elementary boundary choices do not classify all A/B boundaries. Their quantum consistency and the physical background are premises. Our $J = ig\,dz \wedge d\bar{z}$ is the book convention; the source's symplectic-form notation is not silently imported.

§V.6.3. The open de Rham and Dolbeault realizations are [WS-T] inputs from Witten (1995, PDF pp. 22–23, eqs. (3.20)–(3.24)). The complete cellular contraction and torus Betti numbers, and the smooth Fourier contraction for the trivial B line on a flat complex three-torus, are [MATH]. Their arguments are eqs. (V.6.11)–(V.6.20), not finite-mode proofs of a general bundle theorem. Source text extraction can lose overbars: the type $(0, q)$ and source field content specify $\bar{\partial}$. The A self-cohomology is used only in the uncorrected/exact sector. Scalar conjugation cancellation in eqs. (V.6.17)–(V.6.18) records a real limitation of involution-only controls: replacing U^{-1} by U survives those controls, whereas scalar invariance detects it. The admitted helper uses the inverse correctly. No exhaustive mutation claim is made.

§V.6.4. The physical Ext realization is [WS-T] with the large-radius, $B = 0$, smooth-support and honest-bundle hypotheses of Katz and Sharpe (2003, PDF pp. 7–11, secs. 2.1–2.2.2, and pp. 23–26, sec. 3.4.3). In particular pp. 24–26 restrict the demonstrated BRST spectral-sequence construction to identical Chan–Paton gauge fields at both ends. Pages 10–11, sec. 2.2.2, explain the anomaly and canonical Spin^c lift: the physical object $E \otimes \sqrt{K_S^\vee}$ can be twisted even though E is honest. The ordinary-root case requires the stronger Spin condition stated there. Page 26 fixes the dual in the square root and explains why its additional curvature drops out of d_2. The broader distinct-field realization is left to future work there. Katz, Pantev, et al. (2003, PDF p. 13) likewise states $E = F$ for its explicit realization and labels the wider statement a conjecture. These restrictions are retained in eqs. (V.6.28)–(V.6.30); our point calculation does not establish arbitrary intersecting-brane matter.

The exactness and separated-point calculation and finite cyclic invariant tables are [MATH]. The orbifold source examples are Katz, Pantev, et al. (2003, PDF pp. 14–17, secs. 3.2–3.3.2). The protected arrow slots and degree translation are [WS-T], using Closset et al. (2019, PDF pp. 18–19, eqs. (2.33)–(2.37), especially footnote 13). The proper-supported, Ext-finite CY Serre pairing and resulting $c \leftrightarrow m - c$ are [MATH], with the theorem cited rather than proved here. The source's PDF p. 6, eq. (1.11), writes a Serre relation without the explicit vector-space dual; eq. (V.6.34) includes that dual and the support conditions. Neither the abbreviated source notation nor equal dimensions define a canonical vector identification. Katz and Sharpe (2003, PDF p. 6) and Katz, Pantev, et al. (2003, PDF p. 16) explicitly warn that Ext degree need not universally determine low-energy matter type.

§V.6.5. The point Yoneda table and sparse reduced higher algebra are [MATH] calcula-

tions, including the chain representatives and positive top-generator sign in eqs. (V.6.36)–(V.6.39). The chain-map/Ext/minimal-model framework is sourced to Closset et al. (2019, PDF pp. 16–17, eqs. (2.26)–(2.31)). Its general sentence calling m_2 associative on PDF p. 16 is read together with the next-line minimality assumption. In a nonminimal A_∞ algebra m_2 is associative only up to the m_1, m_3 terms. Suspended degree-one operations, minimal versus weak structures and cyclic amplitudes follow Herbst et al. (2005, PDF pp. 28–30, eqs. (71)–(76) and surrounding discussion). The reduced nonunital example supplies no cyclic pairing, physical brane realization or superpotential. The degree translation alone does not import source tensor signs.

§V.6.6. The equivalence is the cited [MATH] result of Bridgeland et al. (2001, PDF pp. 3–4, theorems 1.1–1.2, p. 5 for shifts and derived Hom). The smooth quasiprojective, finite-action, locally G-trivial canonical-sheaf and fiber-product hypotheses appear adjacent to its use. The theorem is not proved by our arithmetic and is not extended to arbitrary higher-dimensional determinant-one quotients. The supported K_0, Euler form and integral change of basis are [MATH] under the specified equivalence and support condition. No injection into unrestricted $K_0(Y)$ or normalized RR lattice is asserted. The coarse-quotient loss of a fractional label is the example of Katz, Pantev, et al. (2003, PDF p. 14); the source's PDF p. 33 expressly disclaims a physical flow with Kähler moduli. The stability dependence of fractional collections is also explicit in Closset et al. (2019, PDF p. 16, footnote 11).

§V.6.7. Exact-disk constancy is [MATH], with Stokes and positive energy derived in eqs. (V.6.56)–(V.6.57); compare Witten (1995, PDF pp. 27–28, eqs. (4.3)–(4.7)). The classical perturbative topological A/CS and space-filling B/hCS identifications are [WS-T] inputs from the same source, PDF pp. 29–30, eqs. (4.8)–(4.9), and pp. 48–49, eqs. (4.51)–(4.52), respectively. Equation (4.52) leaves the overall coefficient undetermined. The fundamental trace and bare k are as defined above; no effective-level or g_s relation is supplied. The functional variation and all local nonabelian components and cubic coefficient are [MATH]. These computations require the stated integrable/flat reference and vanishing boundary terms.

§V.6.8 and exercises. The interpretation route retains the cited physical and theorem premises above. General A-target disk corrections are discussed by Witten (1995, PDF p. 48, eq. (4.50)). Exercises 1–6 ask for ranks, cohomology dimensions, differentials, degree tables, product coefficients, Euler and coordinate data, and curvature components. Exercise 7 asks for written reasoning. These calculations do not prove the BKR equivalence, Serre duality, general Dolbeault results or the physical premises. Mutation, n-ality and full topological field-theory constructions require additional input.

References

Bridgeland, T., A. King, and M. Reid (2001). "The McKay correspondence as an equivalence of derived categories". In: *J. Am. Math. Soc.* 14. Source edition math/9908027v2; chapter locators use 1-based physical PDF pages, pp. 535–554. DOI: 10.1090/S0894-0347-01-00368-X. arXiv: math/9908027.

Closset, C. et al. (2019). “Graded quivers and B-branes at Calabi-Yau singularities”. In: *JHEP* 03. Source edition 1811.07016v1; chapter locators use 1-based physical PDF pages, p. 053. DOI: 10.1007/JHEP03(2019)053. arXiv: 1811.07016 [hep-th].

Herbst, M., C.-I. Lazaroiu, and W. Lerche (2005). “Superpotentials, A(infinity) relations and WDVV equations for open topological strings”. In: *JHEP* 02. Source edition hep-th/0402110v2; chapter locators use 1-based physical PDF pages, p. 071. DOI: 10.1088/1126-6708/2005/02/071. arXiv: hep-th/0402110.

Katz, S. H., T. Pantev, and E. Sharpe (2003). “D branes, orbifolds, and ext groups”. In: *Nucl. Phys. B* 673. Source edition hep-th/0212218v3; chapter locators use 1-based physical PDF pages, pp. 263–300. DOI: 10.1016/j.nuclphysb.2003.09.022. arXiv: hep-th/0212218.

Katz, S. H. and E. Sharpe (2003). “D-branes, open string vertex operators, and Ext groups”. In: *Adv. Theor. Math. Phys.* 6. Source edition hep-th/0208104v4; chapter locators use 1-based physical PDF pages, pp. 979–1030. DOI: 10.4310/ATMP.2002.v6.n6.a1. arXiv: hep-th/0208104.

Witten, E. (1995). “Chern-Simons gauge theory as a string theory”. In: *Prog. Math.* 133. Source edition hep-th/9207094v2; chapter locators use 1-based physical PDF pages, pp. 637–678. arXiv: hep-th/9207094.

Chapter V.7

The topological vertex

V.7.1 A curve from two local patches

The resolved conifold has one compact curve, a $\mathbb{P}^1$, and two toric fixed points. Each fixed point has a neighborhood modeled on $\mathbb{C}^3$. This suggests a way to compute its topological string amplitudes: cut the geometry between the two fixed points, calculate a local contribution on each side, and sum over the data on the cut. The area of the curve should then appear only in the factor that joins the two sides. The question is what the cut remembers.

An open topological string boundary can wind more than once. Several boundaries can also carry the same winding. A partition organizes this information into a representation basis in which the joining operation is diagonal. The topological vertex assigns a function to three such boundary labels at a local toric junction. For the conifold, all four external labels are empty and only the internal partition is summed. A local rule therefore turns the compact curve problem into a sum over Young diagrams.

We will construct this sum in a fixed unrefined convention, compute its coefficients through curve degree four, and resum it using a symmetric-function identity. Taking its logarithm then extracts connected curves. Two mathematical statements enter at different points: a theorem about relative local vertices supplies the cut factors, while a closed local-curve theorem identifies the conifold series. Keeping these statements separate explains why a useful calculation needs less than a general physical interpretation of every three-leg amplitude.

The prerequisites are the integral toric diagrams of Chapter IV.4, the resolved conifold of Chapter IV.5, the curve weight and local Gromov–Witten problem of Chapter 2, and the open boundaries of Chapter 6. By the end, the reader should be able to translate an oriented web into a partition sum, evaluate its small Young-diagram contributions, propagate a framing change through a cut, and recover connected curve coefficients after removing a declared vacuum factor. These operations are the vertex interface needed for the engineering constructions of Chapters XI.7 and XIII.8.

V.7.2 Toric vertices and boundary partitions

What must two local patches share to reconstruct the compact curve? We first identify the geometric edge and then the boundary label placed on it. The resolved conifold is the total space

$$N = \mathrm{Tot}(\mathcal{O}_{\mathbb{P}^1}(-1) \oplus \mathcal{O}_{\mathbb{P}^1}(-1)) . \tag{V.7.1}$$

Its toric diagram can be drawn in the height-one lattice plane as the quadrilateral with vertices $(0,0), (1,0), (0,1), (-1,1)$. Choose the internal segment from $(0,0)$ to $(0,1)$. It separates two triangles of lattice area $1/2$. This triangulation is a smooth resolution phase; changing the triangulation is a geometric operation, not a relabeling of the same calculation.

The degeneration web is dual to these triangles. It is not the fan itself: a triangle becomes a trivalent vertex, and its common edge with another triangle becomes a web segment. For lattice vectors define $v \wedge w = v_1 w_2 - v_2 w_1$. Taking primitive outward normals to the left triangle in counterclockwise order, starting at the common edge, gives

$$(v_1, v_2, v_3) = \big((1,0), (0,1), (-1,-1)\big), \qquad v_1 + v_2 + v_3 = 0. \tag{V.7.2}$$

For the right triangle the corresponding order is

$$(v_1', v_2', v_3') = \big((-1,0), (0,-1), (1,1)\big), \qquad v_1' + v_2' + v_3' = 0. \tag{V.7.3}$$

Both triples have $v_i \wedge v_{i+1} = 1$, with indices understood cyclically. For example, $(0,1) \wedge (-1,-1) = 1$ and $(-1,-1) \wedge (1,0) = 1$. Thus each adjacent pair is an integral basis, rather than merely a pair of independent real vectors. The dual triangles have determinants 1 as well. Balance and unimodularity express the local smooth $\mathbb{C}^3$ geometry in this example.

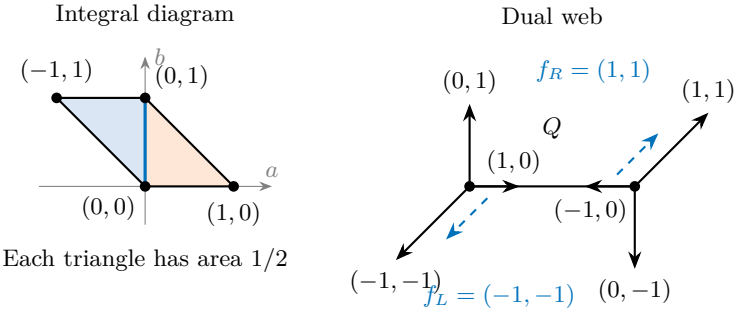


Figure V.7.1: The triangulated integral diagram and its dual degeneration web in the chosen conifold phase. The common vertical lattice edge is dual to the horizontal compact web segment. All local web vectors point out of their junctions; the two internal directions are opposite. Blue dashed arrows show the canonical internal frames $f_L = (-1,-1)$ and $f_R = (1,1)$, not additional geometric legs. The length in the drawing is schematic; the complexified curve weight is Q.

Figure V.7.1 fixes the orientation used below. The weight of the internal curve is inherited from Chapter 2. Write Q_{curve} at first and abbreviate it to Q throughout this chapter:

$$Q = Q_{\mathrm{curve}} = q_C = e^{2\pi i t_C} = e^{-T}, \qquad t_C = \frac{\int_C (B + iJ)}{4\pi^2 \alpha'}, \qquad T = -2\pi i t_C. \tag{V.7.4}$$

The equality involving T is understood modulo logarithm periods. The source variable T is not the book's t_C. Positive area suppresses the magnitude of Q at fixed B. The formal limit $Q = 0$ removes positive curve degree, rather than setting the area to zero.

A partition $\lambda = (\lambda_1 \geq \lambda_2 \geq \cdots > 0)$ is a finite decreasing list of positive integers. Its Young diagram has λ_i boxes in row i, with row index increasing downwards and column index increasing to the right. Define its size, transpose and two useful statistics by

$$|\lambda| = \sum_i \lambda_i, \qquad \lambda_j^t = \#\{i : \lambda_i \geq j\}, \qquad n(\lambda) = \sum_i (i-1)\lambda_i. \tag{V.7.5}$$

The empty partition $\varnothing$ has size zero. The content of a box (i, j) is $j - i$, and the quantity entering framing is

$$\kappa(\lambda) = \sum_i \lambda_i(\lambda_i - 2i + 1) = 2 \sum_{(i,j)\in\lambda} (j - i). \tag{V.7.6}$$

The second equality follows by summing $2j - 2i$ across each row. It lets us compute κ geometrically and will make the effect of transposition immediate.

To understand the label on the cut, let V be a boundary holonomy and let k_j count boundaries winding j times. Total winding and the number of boundaries are different:

$$d = \sum_{j\geq 1} j k_j, \qquad b = \sum_{j\geq 1} k_j, \qquad p_{\boldsymbol{k}}(V) = \prod_{j\geq 1} (\operatorname{Tr} V^j)^{k_j}, \qquad z_{\boldsymbol{k}} = \prod_{j\geq 1} j^{k_j} k_j!. \tag{V.7.7}$$

Only finitely many k_j are nonzero at fixed d. The same sequence describes a cycle type in the symmetric group S_d. If $\chi_\lambda(\boldsymbol{k})$ is its irreducible character, the Frobenius change of basis reads

$$s_\lambda(V) = \sum_{\boldsymbol{k}:\, \sum j k_j = d} \frac{\chi_\lambda(\boldsymbol{k})}{z_{\boldsymbol{k}}} p_{\boldsymbol{k}}(V), \qquad |\lambda| = d. \tag{V.7.8}$$

Here $s_\lambda(V)$ is the Schur character. This use of arbitrary partitions comes from the protected open A-model expansion with specified noncompact Lagrangian boundaries and its formal large-rank representation basis. It is not a statement about an arbitrary physical open-string spectrum.

At winding two, the two possible boundary cycle types are $k_1 = 2$ and $k_2 = 1$. Their boundary counts are two and one, respectively. The trivial and sign characters of S_2 give the explicit basis change

$$\begin{aligned} s_{(2)} &= \tfrac{1}{2}(p_1^2 + p_2), \qquad s_{(1,1)} = \tfrac{1}{2}(p_1^2 - p_2), \\ p_1^2 &= s_{(2)} + s_{(1,1)}, \qquad p_2 = s_{(2)} - s_{(1,1)}. \end{aligned} \tag{V.7.9}$$

Thus the row and the column are different boundary states of the same total winding. Their contents are $(0,1)$ and $(0,-1)$, giving $\kappa((2)) = 2$ and $\kappa((1,1)) = -2$. A single partition label does not specify a fixed number of boundary circles in the winding basis.

For later enumeration the complete lists up to degree four are

d	$\lambda \vdash d$
0	$\varnothing$
1	(1)
2	$(2),\ (1,1)$
3	$(3),\ (2,1),\ (1,1,1)$
4	$(4),\ (3,1),\ (2,2),\ (2,1,1),\ (1,1,1,1)$

(V.7.10)

The notation $\lambda \vdash d$ in this table means a partition of d. Opposite cut orientations will carry λ and λ^t. In particular, $(3,1)^t = (2,1,1)$, so transposition cannot be ignored merely because some small shapes are symmetric. An empty external label means that no external representation is prescribed; the external geometric leg still exists.

This identifies the boundary information required by the compact curve. The web fixes a smooth geometric decomposition, while the protected boundary expansion provides a basis for the joining sum. Neither the web nor a balance equation is a quiver or a derivation of QFT dynamics. The next task is to turn each boundary partition into an explicit rational weight.

V.7.3 Schur functions and specializations

How does a Young diagram become a local amplitude? We need a specialization of its Schur function, and its parameter must remain distinct from the curve weight. Use the local variables

$$q_v = r^2, \qquad u = q_v^{-1} = r^{-2}, \qquad \rho_i = -i + \tfrac{1}{2}, \qquad x_i = q_v^{\rho_i} = r^{1-2i} \quad (i \geq 1). \tag{V.7.11}$$

The coefficients of the curve series will be rational functions in r. We invert their denominators and exclude their poles, including the relevant roots of unity. For explicit numerical examples take real $r > 1$, so $0 < u < 1$. This is a convergent principal alphabet. A later continuation to a genus parameter is a separate operation; neither q_v nor r is the area variable Q.

The power sum $p_k(x) = \sum_i x_i^k$ is a geometric series. At real $r > 1$ it gives

$$p_k(x) = r^{-k} \sum_{j=0}^{\infty} r^{-2kj} = \frac{r^{-k}}{1 - r^{-2k}} = \frac{r^k}{r^{2k} - 1}. \tag{V.7.12}$$

The last rational expression also defines the formal specialization. To compute Schur functions without tableaux enumeration, define complete symmetric functions by

$$H(z) = \sum_{m \geq 0} h_m z^m = \prod_{i \geq 1} (1 - x_i z)^{-1} = \exp\left(\sum_{k \geq 1} \frac{p_k z^k}{k} \right), \qquad h_0 = 1. \tag{V.7.13}$$

Logarithmic differentiation compares the coefficient of z^{m-1} on each side and yields

$$mh_m = \sum_{k=1}^{m} p_k h_{m-k}, \qquad h_1 = p_1, \quad h_2 = \frac{p_1^2 + p_2}{2}, \quad h_3 = \frac{p_1^3 + 3p_1p_2 + 2p_3}{6}. \tag{V.7.14}$$

Each coefficient is finite algebra even though the alphabet is infinite. No truncation of the alphabet has been made.

For $\eta \subseteq \lambda$, the skew Schur function removes the boxes of η and is specified here by the Jacobi–Trudi identity

$$s_{\lambda/\eta}(x) = \det\bigl(h_{\lambda_i - \eta_j - i + j}(x)\bigr)_{1 \le i,j \le \ell}, \qquad h_m = 0 \ (m < 0). \tag{V.7.15}$$

Pad η by zero parts to the row count ℓ of λ. The function vanishes if η is not contained in λ, and $s_\lambda = s_{\lambda/\varnothing}$. These determinant and symmetric-function identities are used as mathematical identities; their general proofs are outside this chapter.

The first examples already distinguish transposes. Substituting (V.7.12) into (V.7.9) gives

$$s_{(1)} = \frac{r}{r^2 - 1}, \qquad s_{(2)} = \frac{r^4}{(r^2 - 1)(r^4 - 1)}, \qquad s_{(1,1)} = \frac{r^2}{(r^2 - 1)(r^4 - 1)}. \tag{V.7.16}$$

For a skew example, take $\lambda = (2, 1)$ and $\eta = (1)$. The removed corner leaves two boxes that impose no row or column ordering on one another. The determinant makes their independent contribution explicit:

$$s_{(2,1)/(1)} = \det \begin{pmatrix} h_1 & h_3 \\ 0 & h_1 \end{pmatrix} = h_1^2 = p_1^2. \tag{V.7.17}$$

At $r = 2$ the three ordinary values are $2/3, 16/45, 4/45$ and the skew value is $4/9$. At $r = 3/2$ they are $6/5, 324/325, 144/325$ and $36/25$. These examples use nonunit parameters, so a missing power of r remains visible.

For larger shapes a hook product is more efficient. The hook of a box consists of that box, the boxes to its right and those below it. Its length is

$$h_{ij} = \lambda_i - j + \lambda_j^t - i + 1, \qquad s_\lambda(x) = \frac{r^{-|\lambda| - 2n(\lambda)}}{\prod_{(i,j) \in \lambda} (1 - r^{-2h_{ij}})}. \tag{V.7.18}$$

This is the principal-specialization hook identity. Figure V.7.2 depicts a nonself-transpose pair. For $(3, 1)$, the four hooks are $4, 2, 1, 1$, $n = 1$ and $\kappa = 4$. For $(2, 1, 1)$ the hooks are the same, but $n = 3$ and $\kappa = -4$. The corresponding numerator powers in (V.7.18) are r^{-6} and r^{-10}. Thus their ratio is r^4.

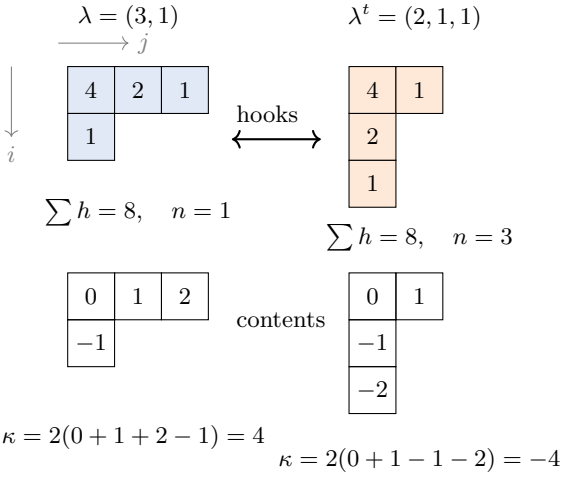


Figure V.7.2: A nonself-transpose pair with row index increasing downwards and column index increasing rightwards. The upper diagrams label each box by its hook length; the lower diagrams label its content $j - i$. Transposition preserves the multiset of hooks and reverses every content, so κ changes from 4 to -4. This is the pair needed in the degree-four conifold coefficient.

We will need an all-degree form of this cancellation, rather than just the example. Counting horizontal and vertical pairs of boxes gives

$$\sum_{(i,j)\in\lambda} h_{ij} = |\lambda| + n(\lambda) + n(\lambda^t), \qquad \kappa(\lambda) = 2\big(n(\lambda^t) - n(\lambda)\big). \tag{V.7.19}$$

Indeed, summing the arms counts $\sum_i \binom{\lambda_i}{2} = n(\lambda^t)$, and summing the legs counts $n(\lambda)$. Define $[m] = r^m - r^{-m}$. Replacing $1 - r^{-2h}$ by $r^{-h}[h]$ in the hook identity now yields

$$s_\lambda(x) = \frac{r^{\kappa(\lambda)/2}}{\prod_{\square\in\lambda}[h_\square]}, \qquad s_{\lambda^t}(x) = \frac{r^{-\kappa(\lambda)/2}}{\prod_{\square\in\lambda}[h_\square]}. \tag{V.7.20}$$

This also proves $s_\lambda(x) = q_v^{\kappa(\lambda)/2} s_{\lambda^t}(x)$ in the declared rational specialization. The sign of κ and the location of the transpose are therefore linked to the direction of the alphabet.

For three partitions λ, μ, ν, define the shifted alphabet $q_v^{\nu+\rho}$ to have entries $r^{2\nu_i - 2i + 1}$, with $\nu_i = 0$ past its last row; define $q_v^{\nu^t+\rho}$ in the same way using the transpose. In this convention the supplied normalized vertex is the Schur expression

$$C_{\lambda\mu\nu}(q_v) = r^{\kappa(\lambda)} s_\nu(x) \sum_\eta s_{\lambda^t/\eta}(q_v^{\nu+\rho}) s_{\mu/\eta}(q_v^{\nu^t+\rho}). \tag{V.7.21}$$

Only partitions η contained in both outer skew shapes contribute. The prefactor involves $\kappa(\lambda)$ in this convention. Moving it to another slot without converting the whole formula

changes the expression. The alternative prefactor $q_v^{\kappa(\lambda)/2+\kappa(\nu)/2}s_{\nu^t}(x)$ gives the same rule by (V.7.20).

Setting all labels empty or leaving only the third occupied immediately gives

$$C_{\varnothing\varnothing\varnothing}=1, \qquad C_{\varnothing\varnothing\lambda}=s_\lambda(x). \tag{V.7.22}$$

The one-leg relative quantity often written W_λ has the hook form $q_v^{\kappa(\lambda)/4}/\prod_\square[h_\square]$. Equation (V.7.20) identifies it with this same specialization. We will state its relative-theorem domain separately before identifying a closed invariant.

One occupied-three-leg example teaches how the shifted alphabet works. Put $\lambda=\mu=\nu=(1)$. The first alphabet entry changes from r^{-1} to r, so its first power sum is p_1+r-r^{-1}. There are exactly two intermediate partitions:

$$\eta=\varnothing:\ (p_1+r-r^{-1})^2, \qquad \eta=(1):\ 1, \qquad C_{(1)(1)(1)}=p_1\big((p_1+r-r^{-1})^2+1\big). \tag{V.7.23}$$

At $r=2$, $p_1+r-r^{-1}=13/6$, giving $C_{(1)(1)(1)}=205/54$. At $r=3/2$, the shifted sum is $61/30$ and the vertex is $4621/750$. Both terms in the η sum are necessary. This is an algebraic evaluation of the supplied formula, not a proof that a vertex with three occupied legs computes a general physical amplitude.

The calculation has converted open-boundary labels from Chapter 6 into explicit local functions. Its most common errors are to identify q_v with Q, reverse ρ while retaining the same hook numerator, or drop a transpose in (V.7.21). The conifold will use only the one-leg specialization, for which every needed factor is now explicit.

V.7.4 Gluing the conifold

Why should opposite boundaries carry transposed partitions? The gluing rule joins boundary orientations as well as representations. In the chosen source convention a reversed cut uses λ^t, and its sign combines with the curve-area weight into $(-Q)^{|\lambda|}$. Framing specifies the remaining local choice at infinity. Before summing anything, we must check that the two frames match.

A framing vector f_i on a leg v_i obeys $f_i\wedge v_i=1$. For a counterclockwise triple the canonical choice is $f_i=v_{i-1}$. The internal frames of (V.7.2) and (V.7.3) are therefore

$$f_L=v_3=(-1,-1), \qquad f_R=v_3'=(1,1)=-f_L, \qquad f_L\wedge v_1=f_R\wedge v_1'=1. \tag{V.7.24}$$

The edge mismatch integer in the source gluing rule is $n=f_R\wedge f_L=0$. There is no additional Casimir factor in this conifold phase. With cyclic slots chosen so that the internal label is the third, the reduced candidate series is

$$Z_{\mathrm{red}}(Q,r)=\sum_\lambda(-Q)^{|\lambda|}C_{\varnothing\varnothing\lambda}C_{\varnothing\varnothing\lambda^t}=\sum_\lambda(-Q)^{|\lambda|}s_\lambda(x)s_{\lambda^t}(x). \tag{V.7.25}$$

The vacuum is the empty partition and equals one. Figure V.7.3 shows where each factor belongs. We glue partition functions, which allow disconnected domains. Adding local connected free energies would not implement this sum over shared boundary states.

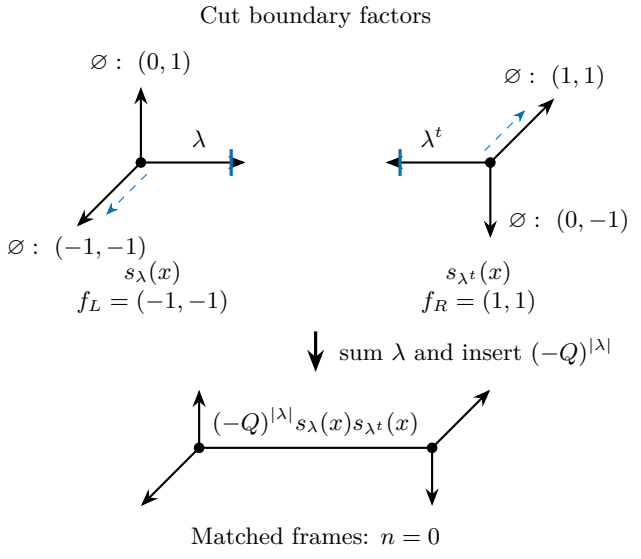


Figure V.7.3: Cutting and rejoining the same conifold web. The short blue transverse marks distinguish the cut boundaries; the local outgoing internal directions remain $(1, 0)$ and $(-1, 0)$. The left and right factors carry λ and λ^t, with opposite canonical frames. Rejoining sums the common partition and inserts $(-Q)^{|\lambda|}$. All four external representations are empty. The drawings specify the factorization; the closed-invariant identification uses the separate theorem in the following section.

The product of one-leg factors simplifies at every degree. From (V.7.20), transposition preserves the hooks and cancels the numerator:

$$s_\lambda(x) s_{\lambda^t}(x) = \frac{1}{\prod_{\square \in \lambda} [h_\square]^2}, \qquad c_d = [Q^d] Z_{\mathrm{red}} = (-1)^d \sum_{\lambda \vdash d} \prod_{\square \in \lambda} [h_\square]^{-2}. \tag{V.7.26}$$

Here and below $\lambda \vdash d$ means that λ partitions d. The following table lists all hook multisets needed through degree four, so that no coefficient requires an unstated enumeration:

Degree	Shapes	Hook multiset for each shape
1	(1)	1
2	$(2), (1, 1)$	$2, 1$
3	$(3), (1, 1, 1)$	$3, 2, 1$
	$(2, 1)$	$3, 1, 1$
4	$(4), (1, 1, 1, 1)$	$4, 3, 2, 1$
	$(3, 1), (2, 1, 1)$	$4, 2, 1, 1$
	$(2, 2)$	$3, 2, 2, 1$

For $d = 2$, both shapes have hooks $2, 1$. Their Schur numerator powers cancel within

each transposed pair, so

$$c_2 = s_{(2)}s_{(1,1)} + s_{(1,1)}s_{(2)} = \frac{2}{[1]^2[2]^2} = \frac{2r^6}{(r^2-1)^2(r^4-1)^2}. \tag{V.7.27}$$

For $d = 3$, the row and column give the same hook product but the middle shape has two hooks of length one. The sign of the propagator is negative at this degree:

$$c_3 = -2s_{(3)}s_{(1,1,1)} - s_{(2,1)}^2 = -\frac{2}{[1]^2[2]^2[3]^2} - \frac{1}{[1]^4[3]^2}. \tag{V.7.28}$$

This is a genuinely different contribution from simply counting three-box partitions. Their hook lengths determine different rational weights. The complete coefficients, including the vacuum and the five four-box shapes, are

$$\begin{aligned} c_0 &= 1, \qquad c_1 = -[1]^{-2}, \qquad c_2 = \frac{2}{[1]^2[2]^2}, \\ c_3 &= -\frac{2}{[1]^2[2]^2[3]^2} - \frac{1}{[1]^4[3]^2}, \\ c_4 &= \frac{2}{[1]^2[2]^2[3]^2[4]^2} + \frac{2}{[1]^4[2]^2[4]^2} + \frac{1}{[1]^2[2]^4[3]^2}. \end{aligned} \tag{V.7.29}$$

At $r = 2$, $[1] = 3/2$, $[2] = 15/4$, $[3] = 63/8$, so $c_1 = -4/9$ and $c_2 = 128/2025$. Directly evaluating (V.7.28) gives $-2(4096/8037225) - 1024/321489 = -33792/8037225$. This calculation illustrates how to reconstruct a coefficient from individual shapes before any resummation.

To sum all degrees, use the dual Cauchy identity for symmetric functions,

$$\sum_{\lambda} s_\lambda(a)s_{\lambda^t}(b) = \prod_{i,j}(1 + a_i b_j). \tag{V.7.30}$$

It holds as a formal graded identity in independent alphabets. It may be specialized when the resulting coefficient sums are defined. Here one can first use finite alphabets, replace b by $-Qx$, and take the convergent coefficientwise limit at real $r > 1$. Equivalently, the product below is defined u-adically, where only finitely many factors contribute at a fixed power of u. Homogeneity gives $s_{\lambda^t}(-Qx) = (-Q)^{|\lambda|}s_{\lambda^t}(x)$, hence

$$Z_{\mathrm{red}} = \prod_{i,j\geq 1}(1 - Qx_ix_j) = \prod_{i,j\geq 1}(1 - Qu^{i+j-1}) = \prod_{m\geq 1}(1 - Qu^m)^m. \tag{V.7.31}$$

There are m positive pairs (i, j) with $i + j - 1 = m$. That is the origin of the exponent m. It is not a degeneracy inferred from a brane spectrum. The product is first an element of $\mathbb{Q}[[u, Q]]$. Its fixed-Q coefficients have the rational continuations already obtained from hooks, so it also gives the series in $\mathbb{Q}(r)[[Q]]$.

A second coefficient route follows without enumerating partitions. Define $a_k = p_k(x)^2 = r^{2k}/(r^{2k} - 1)^2$. Differentiating the logarithm of the product gives

$$Q\frac{\partial_Q Z_{\mathrm{red}}}{Z_{\mathrm{red}}} = -\sum_{k\geq 1} a_k Q^k, \qquad nc_n = -\sum_{k=1}^{n} a_k c_{n-k}. \tag{V.7.32}$$

For instance $2c_2 = -a_1c_1 - a_2 = a_1^2 - a_2$ and $3c_3 = -a_1c_2 - a_2c_1 - a_3$. Iterating yields the compact independent formulae

$$\begin{aligned} c_1 &= -a_1, \qquad c_2 = \tfrac{1}{2}(a_1^2 - a_2), \\ c_3 &= \tfrac{1}{6}(-a_1^3 + 3a_1a_2 - 2a_3), \\ c_4 &= \tfrac{1}{24}(a_1^4 - 6a_1^2a_2 + 3a_2^2 + 8a_1a_3 - 6a_4). \end{aligned} \tag{V.7.33}$$

These expressions reproduce (V.7.29); agreement through four checks finite arithmetic, while the all-degree equality follows from the cited Cauchy identity and the justified specialization.

There is an informative wrong alternative. Omitting the transpose invokes ordinary Cauchy and gives $\prod_m (1 + Qu^m)^{-m}$. It has the same coefficient c_1, but its second coefficient is $(a_1^2 + a_2)/2$. At $r = 2$ this is $272/2025$, rather than $128/2025$. Thus the first curve coefficient cannot detect the orientation error. The explicit degree-two calculation does. Before passing this series to Chapter 8, we still owe the reader the precise theorem that makes it a closed curve invariant.

V.7.5 Relative and closed curve invariants

Which theorem identifies the cut factors, and which identifies the closed result? A formal relative vertex and an unmarked closed stable map have different domains. The symmetric-function calculation is useful because we can state both domains and translate the quantities explicitly, without assuming that erasing the relative boundaries preserves every hypothesis.

Li–Liu–Liu–Zhou construct relative invariants of formal toric Calabi–Yau threefolds. Their graph specifies integral positions, orientation and framing, together with an effective degree and relative partitions. The relative moduli carry an equivariant perfect obstruction theory, and localization uses projective fixed loci; the full moduli need not be proper. In the version used here, every connected domain component contains at least one relative marked point. These are marks with contact multiplicities, not arbitrary spectator insertions. Here v labels a univalent vertex, or external leg, and D_v is its component of the relative divisor. A relative stable morphism f maps a possibly disconnected nodal curve into the expanded relative target. Its marked points q_j^v meet D_v with positive contact orders μ_j^v; these orders form the partition μ^v, whose length $\ell(\mu^v)$ counts the marks there. Schematically the source domain includes

$$f^{-1}(D_v) = \sum_{j=1}^{\ell(\mu^v)} \mu_j^v q_j^v, \tag{V.7.34}$$

each connected component of the domain contains a q_j^v.

The effective data must also match at the graph's vertices. If e is the edge meeting the external vertex v, its nonnegative degree $d(e)$ equals $|\mu^v| = \sum_j \mu_j^v$. The two incident edges at a bivalent vertex have equal degrees. These conditions are part of the effective-class definition, not consequences of a later summation over arbitrary labels. The

invariant also specifies evaluation conditions: at every relative mark, the evaluation lies in the chosen divisor $L_v \subset D_v$. Equivalently, one inserts the pullback of its divisor class at that mark. These insertions reduce the virtual dimension to zero before equivariant localization; the source normalizes by the partition-automorphism factors. Thus both contact and evaluation data are needed to name the relative invariant.

The source's Theorem 7.5 concerns the effective-class gluing of the graph and its full smoothing and resolution. Its regular representation-basis form uses a graph without bivalent vertices. These formulations should not be interchanged with a graph after an unspecified partial operation. Also, the source's convention $p \wedge f = 1$ has the opposite order to our $f \wedge v = 1$; for the same oriented vector $p = v$, the comparison uses $f_{\text{relative}} = -f$. Our numerical edge has zero mismatch, so no additional framed cross-source identification is needed.

Their Corollary 8.8 identifies the formal relative vertex with the proposed vertex when at least one partition is empty, within the nonempty-triple domain of that statement. Each conifold cut vertex at positive internal degree has two empty external labels and one nonempty internal label. In our normalization its local factor is

$$W_{\lambda,\varnothing,\varnothing} = W_\lambda, \qquad W_\lambda = \frac{q_v^{\kappa(\lambda)/4}}{\prod_\square [h_\square]} = s_\lambda(x), \qquad |\lambda| > 0. \tag{V.7.35}$$

The hook conversion was derived in (V.7.19)–(V.7.20). The all-empty vacuum is normalized to one separately. Thus this relative theorem supplies exactly the occupied one-leg factors we use. It does not allow us to assert that a closed unmarked conifold map satisfies (V.7.34).

For the closed identification use Bryan–Pandharipande's local-curve theory, sections 2.1–2.2 and Corollary 7.3. Their domain permits disconnected stable maps but requires positive degree on every connected component; connected degree-zero components are removed. The base is a smooth projective curve. Their residue construction requires compact torus-fixed stable-map loci for a smooth quasiprojective threefold. In the present specialization,

$$\begin{aligned} X = \mathbb{P}^1, \quad g_{\text{base}} = 0, \quad (L_1, L_2) = (\mathcal{O}(-1), \mathcal{O}(-1)), \\ (k_1, k_2) = (-1, -1), \qquad (t_1, t_2) = (t, -t). \end{aligned} \tag{V.7.36}$$

The last pair specifies the anti-diagonal fiber action, with equivariant parameter t. It is unrelated to t_C. The genus of a connected worldsheet, the genus of the base, and the total arithmetic genus of a disconnected domain must not be identified.

For a nodal domain C with k connected components C_a of arithmetic genera h_a, additivity of the sheaf Euler characteristic gives

$$h(C) = 1 - \chi(\mathcal{O}_C) = 1 - k + \sum_{a=1}^{k} h_a, \qquad 2h(C) - 2 = \sum_{a=1}^{k} (2h_a - 2). \tag{V.7.37}$$

In particular $h(C)$ can be negative. With u_{BP} denoting the source genus variable, the reduced fixed-degree series is

$$Z'_d(N; u_{\text{BP}}) = \sum_{h \in \mathbb{Z}} u_{\text{BP}}^{2h-2} \, I^{\text{res}}_{h,d}(N), \qquad d > 0. \tag{V.7.38}$$

Here $I^{\mathrm{res}}_{h,d}$ is the equivariant residue invariant of maps of total degree d and arithmetic genus h, with positive degree on every connected component. It is the virtual integral over the compact fixed locus, weighted by the inverse equivariant Euler class of its virtual normal bundle. The prime removes connected degree-zero contributions. The exponent identity shows why weights of disconnected components multiply: two connected genus-zero components have $h=-1$ and weight u_{BP}^{-4}, the product of their two u_{BP}^{-2} weights. This is the genus bookkeeping needed when the logarithm later selects connected contributions. The localization construction itself is cited.

Properness is especially transparent for this negative bundle. A map to its total space is a map f to the base together with sections of f^*L_1 and f^*L_2. On any irreducible domain component of positive base degree e, either pulled-back line bundle has degree $-e<0$, hence has no nonzero section. On a contracted component a section is constant. Node matching forces this constant to vanish if it meets a component on which the section is zero. Every contracted component is connected by a chain to a positive-degree component, because the entire connected component has positive degree. Vanishing propagates along that chain. Thus both sections vanish everywhere:

$$\begin{gathered} H^0(C, f^*\mathcal{O}(-1)) = 0, \qquad f(C)\subset X, \\ \text{on each connected positive-degree domain.} \end{gathered} \tag{V.7.39}$$

At fixed genus and degree the reduced map moduli are consequently supported on the proper stable-map space of the projective base. The local obstruction theory still remembers the two normal bundles. In this geometry the residue definition agrees with the usual reduced local integral. The argument fails for an isolated connected degree-zero component, which could sit anywhere in the noncompact fiber. This is why the domain restriction cannot be dropped.

To translate the source parameters, retain the genus variable u_{BP} just defined and call its quantum variable Q_{BP}. Then

$$\begin{aligned} Q_{\mathrm{BP}} &= e^{iu_{\mathrm{BP}}} = q_v, \qquad d(2-0-1-1)=0, \\ \mathrm{GW}_d(g_{\mathrm{base}} \mid k_1,k_2) &= u_{\mathrm{BP}}^{d(2-2g_{\mathrm{base}}+k_1+k_2)} Z'_d(N). \end{aligned} \tag{V.7.40}$$

There is no hidden genus-parameter shift for our bundle. In particular, Q_{BP} is not our curve variable Q, and u_{BP} is not our product variable $u=r^{-2}$.

Let $D_\lambda = \dim_{Q_{\mathrm{BP}}} \lambda/d!$ denote the source quantum dimension divided by $d!$. Its exact factor places i outside the inverse:

$$D_\lambda = \prod_{\square\in\lambda} i\,[h_\square]^{-1}, \qquad i\big(e^{ihu_{\mathrm{BP}}/2}-e^{-ihu_{\mathrm{BP}}/2}\big)^{-1} = \frac{1}{2\sin(hu_{\mathrm{BP}}/2)}. \tag{V.7.41}$$

The two forms are consistent. In the balanced anti-diagonal case the cited Corollary 7.3, specialized to base genus zero, gives

$$Z'_d(N) = \sum_{\lambda\vdash d} D_\lambda^2 = (-1)^d \sum_{\lambda\vdash d} \frac{1}{\prod_\square [h_\square]^2} = [Q^d] Z_{\mathrm{red}}, \qquad d>0. \tag{V.7.42}$$

The last equality uses the all-degree hook cancellation, not a finite experiment. The empty disconnected vacuum is added as 1. The source theorem establishes the invariant; our calculation translates its coefficient into the same boundary sum.

For example, the degree-one quantum dimension is $i/[1]$, and its square gives $Z_1' = -[1]^{-2}$. At degree two the row and column both have $D_\lambda = i^2/([2][1]) = -1/([2][1])$. Squaring and adding gives $Z_2' = 2/([2]^2[1]^2)$. These are the coefficients computed before invoking the closed theorem, including their signs. At real $r > 1$ the negative first coefficient is a rational-function value, not a negative count of physical states.

This provides the closed local observable needed after the A-model construction in Chapter 2. The relative gluing theorem, the closed local-curve theorem, and the algebraic Cauchy resummation do different jobs. Their proofs are cited rather than supplied. In particular, the calculation with three occupied legs in the preceding Schur section has not acquired a general physical interpretation through this closed one-curve example.

V.7.6 Framing and orientation

Which frame changes merely re-express the cut, and which change the sum? A noncompact open boundary requires a framing choice. Its local transformation is part of the amplitude prescription. A closed geometry assembled from two boundaries must pair those choices consistently. We can see the distinction at the level of each partition.

For a leg v the integral solutions of $f \wedge v = 1$ differ by integer multiples of v. Write a shift as $f \mapsto f - nv$. In the selected convention a slot carrying λ acquires

$$F_n(\lambda) = (-1)^{n|\lambda|} q_v^{n\kappa(\lambda)/2} = (-1)^{n|\lambda|} r^{n\kappa(\lambda)}. \tag{V.7.43}$$

This sign and exponent belong together. Transposing the diagram sends each content $j - i$ to its negative, so (V.7.6) implies

$$|\lambda^t| = |\lambda|, \qquad \kappa(\lambda^t) = -\kappa(\lambda), \qquad F_n(\lambda) F_n(\lambda^t) = 1. \tag{V.7.44}$$

If the two cut frames are changed by the same relative integer, they remain opposite: since $v_1' = -v_1$ and $f_R = -f_L$, one has $f_R - nv_1' = -(f_L - nv_1)$. Thus the cancellation is a passive matched change, partition by partition. It does not require performing the entire sum.

For a nonzero edge mismatch n in the source rule, the changed slot carries λ^t. Its factor is therefore $(-1)^{n|\lambda|} r^{-n\kappa(\lambda)}$. Including the original propagator gives

$$Q^{|\lambda|} (-1)^{(n+1)|\lambda|} r^{-n\kappa(\lambda)}. \tag{V.7.45}$$

The minus sign in the Casimir exponent follows from the right-hand representation, not from an independent change in the definition of κ. Our matched conifold has $n = 0$.

To isolate a genuine change of prescription, hold the right boundary fixed and multiply only the left slot by $F_f(\lambda)$. Call the resulting function $Z^{[f]}$. This notation names a deliberate altered sum; it assigns no new geometry:

$$Z^{[f]} = \sum_\lambda (-Q)^{|\lambda|} (-1)^{f|\lambda|} r^{f\kappa(\lambda)} s_\lambda(x) s_{\lambda^t}(x). \tag{V.7.46}$$

Figure V.7.4 compares it with the passive operation. The vectors and starting representations are identical in both panels; only the declared frame operation differs.

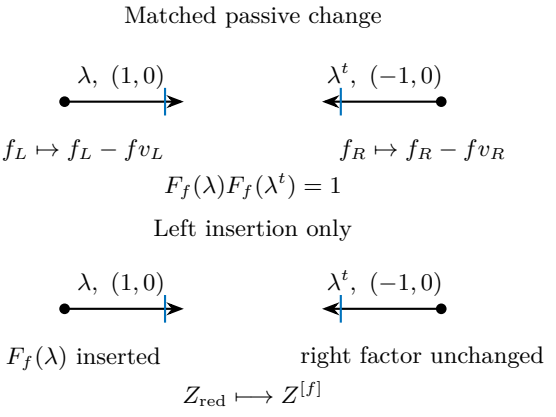


Figure V.7.4: The same cut labels under two operations. Above, a matched shift applies $F_f(\lambda)$ and $F_f(\lambda^t)$, whose product is one. Below, an insertion on the left alone changes the prescription to $Z^{[f]}$. Both start from $v_L = (1,0)$, $v_R = (-1,0)$ and the same opposite canonical frames. No identification with another toric geometry follows from the lower insertion without further web data.

The first three framing factors and curve coefficients can be derived directly from the small shapes:

$$\big(F_f((1)), F_f((2)), F_f((1,1))\big) = \big((-1)^f, r^{2f}, r^{-2f}\big), \tag{V.7.47}$$

$$c_0^{[f]} = 1, \qquad c_1^{[f]} = -(-1)^f p_1^2, \qquad c_2^{[f]} = s_{(2)}s_{(1,1)}(r^{2f} + r^{-2f}). \tag{V.7.48}$$

At degree one $\kappa = 0$, but the sign remains. At degree two both partitions have even size, so their signs are one; their opposite Casimirs produce the two powers of r. Omitting either power changes the answer even if degree one was correct.

For $r = 2$, $f = 1$ gives factors $(-1, 4, 1/4)$. The ordinary sum had $c_1 = -4/9$, $c_2 = 128/2025$; the changed one has

$$c_1^{[1]} = \frac{4}{9}, \qquad c_2^{[1]} = \frac{16}{45}\frac{4}{45}\left(4 + \frac{1}{4}\right) = \frac{272}{2025}. \tag{V.7.49}$$

The result $272/2025$ happened also to occur in the omitted-transpose example, but the first coefficients of those two altered prescriptions differ. A single coincident coefficient is not an identification of amplitudes. At $r = 3/2$ the same shift gives $c_1^{[1]} = 36/25$ and $c_2^{[1]} = (324/325)(144/325)(9/4 + 4/9) = 125712/105625$. A matched shift instead leaves $c_1 = -36/25$ and $c_2 = 93312/105625$ unchanged.

Framing therefore records a choice at infinity for an open factor, while the pairing of cut frames removes a passive ambiguity in the closed sum. This distinction is needed before combining many vertices in Section XIII.8.3. It does not supply a refined vertex: a second equivariant parameter and a preferred direction require additional input, rather than a renaming of the single q_v used here.

V.7.7 Connected curves and degree zero

How do we extract connected curve information without confusing it with a vacuum normalization? Two operations are needed. Dividing by the degree-zero term removes a declared curve-independent factor. Taking the formal logarithm then removes products of disconnected positive-degree contributions. They answer different questions, even though both simplify a partition function.

Suppose a completion has been declared as $Z_{\mathrm{declared}} = A(u)Z_{\mathrm{red}}$, where A is independent of Q and invertible in the chosen coefficient ring. Since $Z_{\mathrm{red}}(0) = 1$,

$$\begin{aligned} Z_{\mathrm{declared}}(0,u) = A(u), \qquad \frac{Z_{\mathrm{declared}}(Q,u)}{Z_{\mathrm{declared}}(0,u)} = Z_{\mathrm{red}}(Q,u), \\ F_{\mathrm{red}} = \log Z_{\mathrm{red}} \in Q\mathbb{Q}(r)[[Q]]. \end{aligned} \tag{V.7.50}$$

The logarithm uses its branch with $\log(1) = 0$. We do not need to define a logarithm of the arbitrary invertible factor A to perform the division. The resulting F_{red} has no constant curve term.

For comparison with the crystal description, let

$$M(u) = \prod_{m\geq 1}(1-u^m)^{-m} = 1 + u + 3u^2 + 6u^3 + 13u^4 + 24u^5 + 48u^6 + O(u^7). \tag{V.7.51}$$

This MacMahon function is the raw empty crystal vacuum. The normalized vertex instead has $C_{\varnothing\varnothing\varnothing} = 1$: the empty crystal contribution has been divided out. The raw and normalized quantities should not be inserted interchangeably into (V.7.25). In particular, assigning one raw M to each local vertex would give M^2 before any normalization, which is not an argument for a specific closed degree-zero factor.

An optional noncompact conifold completion can be declared using the constant-map convention $M(u)^{\chi/2}$ with $\chi = 2$, after the source's stated lower-genus polynomial subtractions:

$$Z_{\mathrm{declared}} = M(u)Z_{\mathrm{red}}, \qquad Z_{\mathrm{declared}}(Q,u)/Z_{\mathrm{declared}}(0,u) = Z_{\mathrm{red}}. \tag{V.7.52}$$

This is a choice of noncompact completion, not an unrestricted virtual integral over degree-zero maps in a nonproper target. Positive-degree properness in (V.7.39) does not fix it. The curve coefficients below need only the reduced normalization.

We can derive the connected answer directly from the product. In the formal u, Q expansion, or analytically at real $r > 1$ with $|Qu| < 1$, expand each logarithm and sum the geometric derivative:

$$\begin{aligned} F_{\mathrm{red}} &= \sum_{m\geq 1} m\log(1-Qu^m) = -\sum_{d\geq 1}\frac{Q^d}{d}\sum_{m\geq 1} mu^{md} \\ &= -\sum_{d\geq 1}\frac{Q^d}{d}\frac{u^d}{(1-u^d)^2} = -\sum_{d\geq 1}\frac{Q^d}{d}\frac{r^{2d}}{(r^{2d}-1)^2}. \end{aligned} \tag{V.7.53}$$

At fixed $r > 1$ the product itself converges normally for bounded Q, since $\sum_m m|Q|u^m$ converges. Its logarithmic Taylor expansion about $Q = 0$ has the additional radius

condition just stated. Continuing the fixed-degree rational functions is a third, separate operation.

It is useful to recover the same connected coefficients from the finite partition sum, independently of expanding the infinite product. Write $F_{\mathrm{red}} = \sum_{d\geq 1} f_d Q^d$ and $Z_{\mathrm{red}} = 1 + \sum_{d\geq 1} c_d Q^d$. Expanding $\log(1+y) = y - y^2/2 + y^3/3 - \cdots$ gives

$$f_1 = c_1, \qquad f_2 = c_2 - \tfrac{1}{2}c_1^2, \qquad f_3 = c_3 - c_1c_2 + \tfrac{1}{3}c_1^3. \tag{V.7.54}$$

At degree four the products have several decompositions, with multiplicities fixed by the powers of y:

$$f_4 = c_4 - c_1c_3 - \tfrac{1}{2}c_2^2 + c_1^2c_2 - \tfrac{1}{4}c_1^4. \tag{V.7.55}$$

The factors $1/2, 1/3, 1/4$ are the logarithm's combinatorial weights. Figure V.7.5 displays the inverse exponential decomposition at degree three. They remove disconnected combinations of curves of smaller degree, rather than removing the multiple covers already present in a connected contribution.

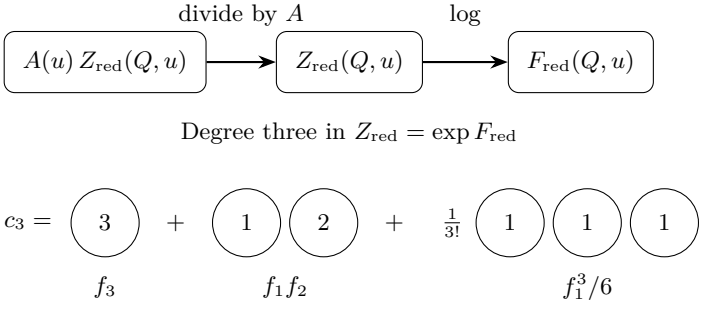


Figure V.7.5: Normalization and connected decomposition are separate. The upper row divides a Q-independent factor A from a declared partition function. The lower row depicts the exact degree-three coefficient of $\exp F$: one connected contribution of degree three, a pair of degrees one and two, and three degree-one components with factor $1/3!$. Circles indicate domain components and the numbers indicate curve degree, not genus or enumerative counts.

Substitute the a_k polynomials in (V.7.33). At degree two the a_1^2 terms cancel:

$$f_2 = \frac{a_1^2 - a_2}{2} - \frac{a_1^2}{2} = -\frac{a_2}{2}. \tag{V.7.56}$$

At degree three, use $c_1 = -a_1$ and $c_1c_2 = (-a_1^3 + a_1a_2)/2$ to obtain

$$f_3 = \frac{-a_1^3 + 3a_1a_2 - 2a_3}{6} + \frac{a_1^3 - a_1a_2}{2} - \frac{a_1^3}{3} = -\frac{a_3}{3}. \tag{V.7.57}$$

Both the disconnected three-single-cover term and the mixed one-plus-two term have disappeared. At degree four, substitution in (V.7.55) cancels $a_1^4, a_1^2a_2, a_2^2, a_1a_3$, leaving

$-a_4/4$. The general answer and its inverse reconstruction are

$$f_0 = 0, \qquad f_d = -\frac{a_d}{d} = -\frac{1}{d[d]^2}, \qquad nc_n = \sum_{k=1}^{n} k f_k c_{n-k}. \tag{V.7.58}$$

The last equation follows from $\partial_Q Z = (\partial_Q F)Z$ and recovers each original coefficient. It checks every degree independently, including the highest one retained.

For an exact numerical normalization example, choose $r = 2$ and a declared factor $A = 7/3$. Then $a_1 = 4/9$ and $a_2 = 16/225$. Through degree two the raw, normalized and connected lists are

$$\begin{aligned} [Q^{0,1,2}]Z_{\text{declared}} &= (7/3, -28/27, 896/6075), \\ [Q^{0,1,2}]Z_{\text{red}} &= (1, -4/9, 128/2025), \\ [Q^{0,1,2}]F_{\text{red}} &= (0, -4/9, -8/225). \end{aligned} \tag{V.7.59}$$

For instance $128/2025 - (4/9)^2/2 = 128/2025 - 200/2025 = -8/225$. Conversely $f_2 + f_1^2/2 = 128/2025$. Multiplication of the entire normalized list by $7/3$ restores the raw list, including its degree-zero entry. Nothing requires the declared factor to be one or positive; invertibility and independence of Q are the relevant conditions. This example does not evaluate $M(1/4)$.

A curve-dependent division changes the observable. Dividing by e^Q would give $\log(Z_{\text{red}}/e^Q) = F_{\text{red}} - Q$, shifting f_1 by -1. Even though its value at $Q = 0$ is one, this is not degree-zero normalization. The curve variable distinguishes the two operations immediately.

Finally we translate to the usual topological genus expansion. Introduce a topological parameter g_s by coefficientwise meromorphic continuation $q_v = e^{ig_s}$, or $r = e^{ig_s/2}$. This is not an identification with an unconverted ten-dimensional physical string coupling. Then

$$r^d - r^{-d} = 2i\sin(dg_s/2), \qquad f_d = \frac{1}{d\,[2\sin(dg_s/2)]^2}. \tag{V.7.60}$$

The rational coefficient was negative on the real branch $r > 1$, and the sine expression has a positive leading Laurent coefficient. The factor $i^2 = -1$ explains the change. The convention $q_v = e^g$ instead would produce a hyperbolic denominator with the original negative sign. Source symbols called g_s therefore require a conversion before comparison.

Expanding about $g_s = 0$ at fixed positive degree gives

$$\begin{aligned} f_d &= \frac{1}{d^3 g_s^2} + \frac{1}{12d} + \frac{dg_s^2}{240} + O(g_s^4), \\ F_{\text{red}} &= \frac{\mathrm{Li}_3(Q)}{g_s^2} - \frac{1}{12}\log(1-Q) + O(g_s^2). \end{aligned} \tag{V.7.61}$$

The leading degree-d term agrees with the $1/d^3$ local genus-zero cover coefficient of Chapter 2 for the isolated $(-1,-1)$ curve. The genus-zero and genus-one functions above concern positive curve degree only. Lower-genus polynomial terms and noncompact degree-zero choices remain separate.

At a fixed degree, poles occur where $r^{2d} = 1$, equivalently where the sine denominator vanishes. In particular $r = 1$ is a pole, not a numerical limit in the convergent crystal regime. The small-g_s expression is a formal Laurent expansion and does not assert convergence of the genus sum or evaluation at roots of unity. The resulting free-energy interface is precisely what Chapter 8 needs before discussing Gopakumar–Vafa invariants. A BPS spectrum, its integrality and the physical F-term identification in Chapter 10 require their own physical input; they do not follow from the sign of a rational coefficient or a finite partition calculation.

V.7.8 Exercises

The first four exercises accept exact numerical submissions in the companion. Choose any rational $1 < r \leq 4$. Supply r and every scientific answer as rational strings such as `"3/2"`; integer parameters such as `order` and `framing` are JSON numbers. Arrays are ordered by increasing curve degree, including degree zero where specified. The companion's public question file gives the full schemas and resource bounds. Submit through `benchmark/PROTOCOL.md`; acceptance concerns only the submitted bounded calculation.

1. **Schur and vertex weights.** Task `IV07-E1`. Compute $s_{(1)}, s_{(2)}, s_{(1,1)}$ from the power sums, the determinant for $s_{(2,1)/(1)}$, and the two intermediate-partition terms of $C_{(1)(1)(1)}$. Submit exactly the fields `r`, `schur`, `skew`, `vertex`, with the three ordinary Schur values in the stated order. Explain in your working why the row and column differ. The three occupied legs here are an algebraic exercise in the supplied rule.

2. **A compact curve through degree four.** Task `IV07-E2`. Choose an integer `order` from 1 to 4. Evaluate every coefficient of the matched conifold sum through that order using the hook table, and independently reproduce them by (V.7.32). Submit exactly `r`, `order`, `coefficients`, the last an array of length `order`+1. Use empty external labels, the transposed right internal label, no additional framing and vacuum one. In your working, identify the first degree that detects omission of the transpose.

3. **Change only one slot.** Task `IV07-E3`. Choose an integer `framing` f between -2 and 2. Insert $F_f(\lambda)$ on the left only. Submit exactly `r`, `framing`, `factors`, `coefficients`. The factor array has the three entries for $(1), (2), (1,1)$; the coefficient array contains degrees $0, 1, 2$ of $Z^{[f]}$. Derive the two-box result by summing both shapes. State in your working why this changed prescription is different from a matched passive shift.

4. **Remove a vacuum and extract connected curves.** Task `IV07-E4`. Choose integer `order` from 1 to 4 and a nonzero rational `degree_zero` A with $|A| \leq 100$. Form AZ_{red}, divide by its constant curve term, and take the logarithm of the result. Submit exactly `r`, `order`, `degree_zero`, `raw`, `normalized`, `connected`; each array has length `order`+1. Include the zero connected constant term. Verify

the exponential reconstruction at every retained degree. This task uses a declared rational factor; it does not ask for a rational evaluation of MacMahon's infinite product.

5. **Which theorem and which normalization?** Written task `IV07-E5`. Explain the distinction between the raw crystal vacuum $M(u)$ and $C_{\varnothing\varnothing\varnothing} = 1$. For a declared $M(u)Z_{\mathrm{red}}$, justify division by its value at $Q = 0$ and explain the different effect of dividing by e^Q. Distinguish a passive frame shift from the one-slot insertion and identify the extra information required for refinement. State the graph, effective-class, obstruction and fixed-locus hypotheses of the relative gluing theorem and the nonempty one-leg scope of its identification theorem, including the marked-component condition. Then explain why the unmarked closed conifold instead uses the separate closed local-curve theorem with base genus zero, levels $(-1,-1)$, anti-diagonal weights, positive degree on each connected component and zero genus shift. Track the source quantum-dimension factor with i outside the inverse. Separate these cited results from the finite degree-four computation and from a physical BPS or general-vertex interpretation. This reasoning exercise requires written assessment; the numerical companion does not grade it.

V.7.9 Take-home message

A cut toric curve carries a partition label. Its local normalized one-leg factors are Schur specializations; opposite orientation transposes the second label, and the matched propagator carries the signed area weight. For the resolved conifold this produces a sum whose hook factors, Cauchy product and connected logarithm can all be computed explicitly. Matched framing changes cancel before summation, while a one-sided insertion defines a different expression.

The mathematical interpretation has two parts. Relative one-leg invariants identify the cut factors under their relative hypotheses. A separate closed local-curve theorem identifies the reduced conifold coefficients, and the hook calculation translates between its quantum dimensions and the vertex sum at all degrees. Vacuum normalization is a declared degree-zero choice. The next physical step, in Chapter 8, is to organize connected curve information as a protected BPS expansion; Chapter 10 addresses its relation to spacetime couplings. The ordinary vertex here supplies neither that physical argument nor the additional parameter and preferred direction of refinement.

Status and sources

§7.1–7.2: boundary and geometric input. The winding/representation expansion is protected open A-model input with specified noncompact Lagrangian boundaries and formal large-rank labels, [WS-T]. The local primitive balanced web and the two unimodular triangles are geometric statements [MATH]. Source anchors are Aganagic et al. (2005), v3, physical pp. 4 and 16–19, and Iqbal and Kashani-Poor (2006), v2, physical pp. 6–7. Chapter IV.4 supplies the integral toric frame, Chapter IV.5 the geometry, and Chapter 2 the curve weight. Chapters XI.7 and XIII.8 use this construction.

§7.3: local algebra. Equations (V.7.11)–(V.7.23) use the alphabet and principal specialization stated above. The supplied normalized Schur rule and its bounded algebraic examples are [MATH]. The exact frame is Iqbal and Kashani-Poor (2006), physical p. 7, (7), and pp. 24–25, (63)–(67). The equivalent normalization is Okounkov et al. (2006), v2, physical p. 14, (3.15); the one-leg expression is Li et al. (2009), v3, physical pp. 4–5, (2.2), (2.6)–(2.7). The principal hook and Jacobi–Trudi identities are cited mathematical tools, not proved here in full generality. The occupied-three-leg calculation uses only the algebra of the supplied expression.

§7.4: joining and resummation. The conifold product and connected coefficients are mathematical consequences [MATH] of the specified gluing and the cited dual Cauchy identity. The source gluing is Iqbal and Kashani-Poor (2006), physical p. 8, (10)–(12), with the conifold product on physical p. 17, (41). Equation (V.7.31) also matches the unrefined expression in Iqbal, Kozcaz, et al. (2009), v2, physical p. 23, (63), after its variable conversion. The displayed hook table supplies every partition through degree four. These finite comparisons do not prove an all-degree identity; the latter uses dual Cauchy under its formal or convergent specialization hypotheses.

§7.5: two different theorem domains. The relative and closed constructions use distinct mathematical theorems [MATH]. For the relative construction use Li et al. (2009), v3, physical pp. 14–16, Definitions 4.1–4.4, pp. 19–21, Definition 4.6/Theorem 4.8, pp. 54–55, Proposition 7.4/Theorem 7.5, and p. 57, Corollary 8.8. The effective graph/class, relative obstruction theory, projective fixed loci and a relative mark on each connected component remain essential. The representation formula uses a regular graph; the gluing theorem uses full smoothing/resolution. Corollary 8.8 is used only for a nonempty triple with an empty partition. It is not applied directly to the closed unmarked domain.

For that closed domain use Bryan and Pandharipande (2008), arXiv v3, physical pp. 7–9, sections 2.1–2.2, and pp. 33–34, section 7/Corollary 7.3. The assumptions are the smooth projective base $\mathbb{P}^1$, bundle $\mathcal{O}(-1) \oplus \mathcal{O}(-1)$, anti-diagonal weights, compact fixed loci and nonconstant maps on every connected domain component. Equations (V.7.39)–(V.7.42) give the negative-bundle properness argument, zero shift and all-degree hook translation of the squared quantum dimension. The unsquared source factor is $i[h]^{-1}$. The vacuum is separately added as one. General virtual localization and both theorem proofs are cited rather than reproduced.

§7.6–7.7: frame, vacuum and connected curves. The framing, vacuum and connected-curve formulas have the mathematical scope stated above [MATH]. Framing uses Iqbal and Kashani-Poor (2006), (9)–(10), and Aganagic et al. (2005), physical p. 19, (3.6)–(3.7). MacMahon versus normalized vacuum uses Okounkov et al. (2006), physical p. 19, (3.20)–(3.23); its optional constant-map completion uses physical p. 4, section 2.1, with the stated lower-genus subtractions. No unrestricted noncompact degree-zero integral is inferred. The logarithm and sine conversion use Iqbal and Kashani-Poor (2006), physical pp. 14 and 17, (29), (41); its $q = e^{ig_s}$ differs from the $q = e^{g_s}$ source choice in Aganagic et al. (2005), physical p. 47, (7.1). Here g_s is a topological genus parameter; a physical dilaton identification requires another dictionary.

Scope. The finite examples compare hook, determinant and one-leg formulas through size four, conifold and connected coefficients through Q^4, and the product modulo

u^9. They also illustrate vacuum and occupied-one-box algebra, re-exponentiation, and nonunit framing and normalization. The refined vertex uses an additional parameter and a preferred direction, as described in Iqbal, Kozcaz, et al. (2009), physical pp. 1 and 6. The general physical identification of occupied-three-leg amplitudes requires additional input. No new duality primitive, general BPS spectrum, integrality theorem or QFT construction is inferred. The historical theorem status printed in a source edition is not asserted to be the current status of the general subject.

References

Aganagic, M. et al. (2005). "The Topological vertex". In: *Commun. Math. Phys.* 254. Source edition: arXiv v3, 12 June 2003, pp. 425–478. DOI: 10.1007/s00220-004-1162-z. arXiv: hep-th/0305132.

Bryan, J. and R. Pandharipande (2008). "The Local Gromov-Witten theory of curves". In: *J. Am. Math. Soc.* 21, pp. 101–136. DOI: 10.1090/S0894-0347-06-00545-5. arXiv: math/0411037.

Iqbal, A. and A.-K. Kashani-Poor (2006). "The Vertex on a strip". In: *Adv. Theor. Math. Phys.* 10.3. Source edition: arXiv v2, 11 July 2006, pp. 317–343. DOI: 10.4310/ATMP.2006.v10.n3.a2. arXiv: hep-th/0410174.

Iqbal, A., C. Kozcaz, and C. Vafa (2009). "The Refined topological vertex". In: *JHEP* 10. Source edition: arXiv v2, 12 March 2009; only boundary distinction and unrefined equation (63) used, p. 069. DOI: 10.1088/1126-6708/2009/10/069. arXiv: hep-th/0701156.

Li, J. et al. (2009). "A Mathematical theory of the topological vertex". In: *Geom. Topol.* 13.1. Source edition: arXiv v3, 9 October 2007; theorem subclass and normalization explicitly stated, pp. 527–621. DOI: 10.2140/gt.2009.13.527. arXiv: math/0408426.

Okounkov, A., N. Reshetikhin, and C. Vafa (2006). "Quantum Calabi-Yau and classical crystals". In: *Prog. Math.* 244. Source edition: arXiv v2, 11 November 2003, p. 597. DOI: 10.1007/0-8176-4467-9_16. arXiv: hep-th/0309208.

Chapter V.8

Gopakumar–Vafa invariants and BPS state counting

V.8.1 One curve and many rational numbers

A membrane wrapped on a compact curve looks like a particle to an observer who cannot resolve the curve. A string worldsheet can wrap the same curve more than once. These two descriptions suggest different kinds of numbers: multiplicities of particles and coefficients of a sum over maps. The distinction already matters for the smallest local Calabi–Yau example, a rigid sphere with normal bundle $\mathcal{O}(-1)\oplus\mathcal{O}(-1)$. Its degree-two genus-zero Gromov–Witten contribution is $1/8$. The fraction does not mean that the geometry contains one eighth of a particle.

Chapter 2 explained why a virtual count of maps can be rational. Here we ask a further question: can the connected map amplitudes be organized by a protected particle observable with integer coefficients? The Gopakumar–Vafa organization answers this question through a circle reduction. A fixed five-dimensional particle contributes a tower of circle momenta. Rewriting that tower as worldline windings gives a universal sine factor and a winding measure. Together they turn simple protected inputs into rational amplitudes at many genera and degrees.

The particle interpretation needs a supersymmetric compactification and actual normalizable short-particle sectors. We will state that input before computing its consequence. The mathematical route starts instead with virtual Gromov–Witten invariants and asks whether the transformed coefficients are integral and finite in genus. Theorems answer that question under their own hypotheses. Their conclusions and the physical interpretation meet in the same formula, but their premises are different.

Our route keeps one example visible throughout. We first isolate the short representation and the signed trace, then derive the winding measure and expand the local sphere contribution. We invert a mixed rational table without rounding, compute a larger spin example, and finish by testing the domains of the integrality and finiteness theorems. In particular, the genus label of a protected coefficient will not be a positive particle multiplicity.

Reader contract

The prerequisites are the connected positive-degree GW series of Chapter 2 and the conditional IIA/M-theory circle dictionary of Volume II, Chapter 9. By the end of this chapter the reader should be able to distinguish reduced from full short representations; derive the $1/k$ winding measure; expand, invert and reconstruct a finite GW/GV table in a specified coupling frame; compute a signed spin character separately from its ordinary dimension; and state where local, closed-target and physical conclusions apply. Chapter 7 supplies another computation of local amplitudes, while Chapter 10 develops their physical F-term role.

V.8.2 The M-theory particle interpretation

What observable of a wrapped particle can survive in a topological amplitude? Begin with M-theory on a supersymmetric Calabi–Yau threefold X, giving a five-dimensional theory with eight real supercharges. In modern terminology this is five-dimensional $\mathcal{N} = 1$; the original GV papers call it $\mathcal{N} = 2$. Fix a nonzero effective curve charge β of positive area and assume that its sector contains discrete, normalizable one-particle BPS states. A curve class by itself does not establish those states. Nor does a numerical integer extracted from amplitudes establish their normalizability.

At zero center-of-mass momentum the massive spatial little group is

$$\mathrm{Spin}(4) = SU(2)_L \times SU(2)_R, \qquad (j_L, j_R) \in \tfrac{1}{2}\mathbb{Z}_{\geq 0} \times \tfrac{1}{2}\mathbb{Z}_{\geq 0}. \tag{V.8.1}$$

Both factors describe spatial spin. The R subscript on j_R does not denote the supersymmetry R-symmetry, which rotates the supercharges and is a different group. The double cover Spin(4) is needed because the states can have half-integral spins. The labels are not left- and right-moving worldsheet sectors either.

Choose the BPS orientation for which the universal short factor carries left spin. The finite internal spin representation of a fixed-charge short sector is written

$$\mathcal{H}_\beta = \big([\tfrac{1}{2}, 0] + 2[0, 0]\big) \otimes \mathcal{H}_\beta^{\mathrm{red}}, \qquad \mathcal{H}_\beta^{\mathrm{red}} = \sum_{j_L, j_R} N_\beta(j_L, j_R)[j_L, j_R]. \tag{V.8.2}$$

The translational continuum has been removed by working at fixed center-of-mass momentum. The superscript "red" means that the universal short factor has also been stripped, exactly once. The integers $N_\beta(j_L, j_R)$ in an actual finite short sector are nonnegative multiplicities. They are not the GV integers that we are about to define.

The short factor can be understood from the two active fermionic creation operators of a left doublet. Their zero-, one- and two-occupation sectors transform as

$$\Lambda^0[\tfrac{1}{2}] \oplus \Lambda^1[\tfrac{1}{2}] \oplus \Lambda^2[\tfrac{1}{2}] = [0] \oplus [\tfrac{1}{2}] \oplus [0] \equiv I_1. \tag{V.8.3}$$

The two singlets have even grading and the doublet has odd grading. This describes the universal representation factor after shortening has been assumed; it does not infer

shortening from a curve count. Ordinary dimensions ignore that grading. Thus

$$\begin{aligned} \dim I_1 &= 1+2+1=4, \qquad \dim \mathcal{H}_\beta = 4D_\beta, \\ D_\beta &= \sum_{j_L,j_R} N_\beta(j_L,j_R)(2j_L+1)(2j_R+1). \end{aligned} \tag{V.8.4}$$

All three dimensions refer to the chosen fixed-charge sector. An opposite-charge sector is not automatically added. For a single reduced $[0,0]$, $D_\beta = 1$ and the full short sector has four internal states. Confusing the reduced singlet with a full one-state particle would miss the factor four.

The protected trace keeps left spin resolved and sums over right spin with a sign. For a right irrep, every magnetic weight has the same parity $(-1)^{2j_R}$. Consequently its signed dimension is

$$\mathrm{Tr}_{[j_R]}(-1)^{2J_R^3} = \sum_{m_R=-j_R}^{j_R} (-1)^{2m_R} = (-1)^{2j_R}(2j_R+1). \tag{V.8.5}$$

A right singlet contributes 1, while a right doublet contributes -2. Taking this trace on the reduced sector leaves a virtual left representation,

$$\sum_{j_L,j_R} (-1)^{2j_R}(2j_R+1)N_\beta(j_L,j_R)[j_L] = \sum_{h\geq 0} n_\beta^h I_h, \qquad I_h = I_1^{\otimes h}, \quad I_0 = [0]. \tag{V.8.6}$$

This is a representation-ring equality. Negative coefficients are allowed on its right-hand side even though the original multiplicities were nonnegative. Tensor powers of I_1 form a useful integral basis for finite left representations: the highest spin in I_h is $h/2$ with multiplicity one, so the top spin can be removed successively with integer coefficients. Section V.8.5 will perform this change of basis explicitly.

To convert the representation to a function introduce the formal left-spin fugacity $y = e^{i\lambda}$. With $l = 2j_L$ and $r = 2j_R$, the left magnetic weights give

$$\chi_l(y) = \sum_{m=-l,-l+2,\dots,l} y^m, \qquad \mathrm{Tr}_{[l/2]}(-1)^{2J_L^3} y^{2J_L^3} = (-1)^l \chi_l(y). \tag{V.8.7}$$

The sign $(-1)^l$ follows because m and l have the same parity. It is independent of the right sign just derived. Combining the two operations produces

$$P_\beta(y) = \sum_{l,r} N_\beta(l/2, r/2)(-1)^{l+r}(r+1)\chi_l(y). \tag{V.8.8}$$

This formula determines every sign in the later finite spin examples. In particular, evaluating P_β at $y = 1$ still gives a signed index, not D_β.

The character of the universal left factor is especially useful. The two singlets contribute 2 and the doublet contributes $-(y + y^{-1})$, so

$$\mathrm{sch}\, I_1 = 2 - y - y^{-1} \equiv z = 4\sin^2(\lambda/2), \qquad \mathrm{sch}\, I_h = z^h. \tag{V.8.9}$$

The sine follows from $y + y^{-1} = 2\cos\lambda$, not from an additional sign choice. Applying the character to (V.8.6) therefore gives

$$P_\beta(y) = \sum_{h\geq 0} n_\beta^h z^h. \tag{V.8.10}$$

The I_1 stripped in (V.8.2) must not be inserted again into this reduced numerator. Its effect is already included in the sourced particle-loop amplitude. The extra oscillator factor in that amplitude will lower the sine power from $2h$ to $2h-2$.

Figure V.8.1 separates the three operations. Removing a universal tensor factor, tracing right spin, and evaluating a left character are different maps. Only the first has the simple ordinary dimension ratio four.

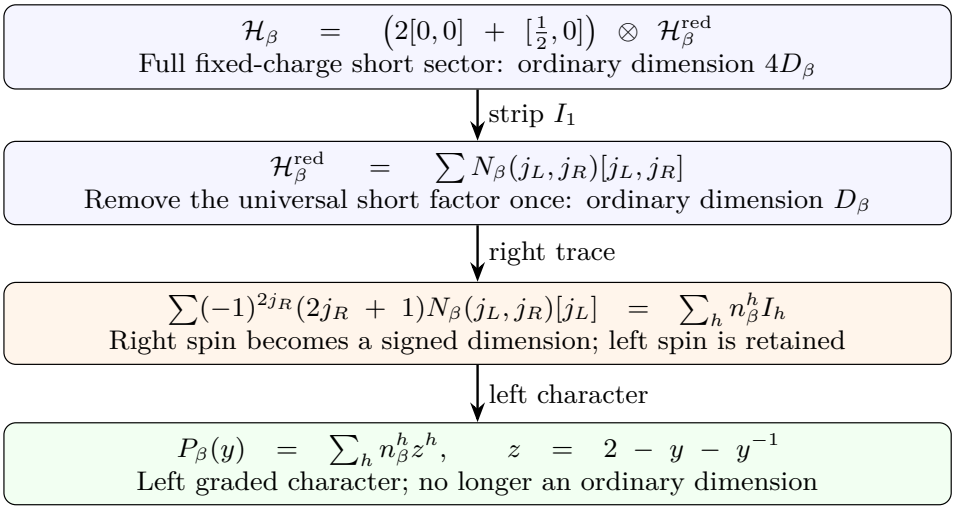


Figure V.8.1: Reduction of a fixed-charge short sector. The universal factor has ordinary dimension four and is stripped once. Right spin is replaced by $(-1)^{2j_R}(2j_R+1)$, while left spin survives until its graded character is taken. The bottom polynomial is expressed in $z = 2 - y - y^{-1}$; it cannot be interpreted as an ordinary dimension.

There is a representation-level reason to expect protection. The right short factor that occurs in a long representation has signed dimension

$$\mathrm{sdim}\big(2[0]_R + [\tfrac{1}{2}]_R\big) = 2 - 2 = 0. \tag{V.8.11}$$

A tensor factor with this trace removes the long representation from the resolved-left trace. The physical assertion is stronger than this finite equality: one needs a well-defined discrete trace in which long-multiplet recombination and deformations introduce no uncancelled continuum or boundary contribution. We use that protected-trace assertion as a physical input. The finite spin identities explain the cancellation once the relevant representations and trace exist.

For the simplest reduced singlet the representation and character give

$$\mathcal{H}_\beta^{\mathrm{red}} = [0,0] \quad \Longrightarrow \quad P_\beta(y) = 1, \qquad n_\beta^0 = 1, \quad n_\beta^{h>0} = 0. \tag{V.8.12}$$

This is the input representation for an isolated spherical wrapped particle in the original physical discussion. A positive integer here specifies a protected contribution conditional on the particle interpretation. The separate local curve theorem will establish the same transform coefficient from enumerative geometry without deriving a physical Hilbert space.

Finally, we must connect the curve weight to the conventions of Chapter 2. Write

$$t_\beta = \frac{1}{4\pi^2\alpha'}\int_\beta (B + iJ), \qquad Q_\beta = e^{2\pi i t_\beta}, \qquad Q_\beta\big|_{B=0} = e^{-2\pi \operatorname{Im} t_\beta}. \tag{V.8.13}$$

If A is the dimensionless area variable in the GV source, its weight $e^{-2\pi A}$ agrees with this expression at $A = \operatorname{Im} t_\beta$ and $B = 0$. This is an action-weight translation, not an absolute particle-mass formula in book units. The IIA D2/D0 interpretation uses the inherited M-theory circle premise from Volume II, Chapter 9. The formal topological parameter λ includes the graviphoton normalization and is not identified with bare ten-dimensional g_s. These distinctions are needed before the circle-momentum sum can be interpreted correctly.

V.8.3 The multicover organization

How can one particle produce contributions at many degrees? Compactify the five-dimensional particle theory on a circle. A fixed charged particle now has integer KK momentum m. Its protected one-loop contribution can be expressed using a proper-time integral. Reorganizing the sum over m into windings changes the representation of the same contribution. It does not supply an independent elementary particle for every winding number.

First fix the coupling frame, because the hyperbolic and trigonometric kernels have different Taylor signs. Before continuation the source uses a hyperbolic proper-time expression. Its simultaneous coupling and proper-time continuation can be written formally as

$$s_{\mathrm{hyp}} = is, \qquad \lambda_{\mathrm{hyp}} = i\lambda, \qquad \frac{s_{\mathrm{hyp}}}{\lambda_{\mathrm{hyp}}} = \frac{s}{\lambda}, \qquad \frac{ds_{\mathrm{hyp}}}{s_{\mathrm{hyp}}} = \frac{ds}{s}. \tag{V.8.14}$$

Thus the charge exponential retains its ratio of proper time to coupling. The even integer power in the kernel satisfies

$$\left(2i\sinh\frac{is}{2}\right)^{2h-2} = \left(-2\sin\frac{s}{2}\right)^{2h-2} = \left(2\sin\frac{s}{2}\right)^{2h-2}. \tag{V.8.15}$$

This is the sine frame used below. We use the source's formal continued expression coefficientwise. We do not assert that this substitution alone deforms an integration contour without residues or specifies a nonperturbative completion.

For a fixed class and a basis contribution n_β^h, the continued KK expression has the structure

$$n_\beta^h \sum_{m\in\mathbb{Z}} \int_{s>0} \frac{ds}{s} \left(2\sin\frac{s}{2}\right)^{2h-2} \exp\left[-\frac{2\pi s}{\lambda}(A+im)\right]. \tag{V.8.16}$$

Here $A>0$, and the ultraviolet endpoint requires separate treatment. The numerator z^h of the reduced character and the universal denominator z of the sourced loop combine to give the exponent $h-1$. Formula (V.8.16), including that oscillator denominator and its protected-coupling interpretation, is physical input; the next step is the explicit winding calculation.

The momentum-dependent exponential is a Fourier series. In the distributional identity with unit-spaced modes,

$$\sum_{m\in\mathbb{Z}} e^{-2\pi i m s/\lambda} = \sum_{k\in\mathbb{Z}} \delta(s/\lambda - k), \qquad \delta(s/\lambda - k) = \lambda\,\delta(s-k\lambda) \quad (\lambda>0). \tag{V.8.17}$$

The second equality is the delta-function Jacobian. For $k>0$, its integral with the proper-time measure is

$$\int_{s>0} \frac{ds}{s} \lambda\delta(s-k\lambda) f(s) = \frac{\lambda}{k\lambda} f(k\lambda) = \frac{1}{k} f(k\lambda). \tag{V.8.18}$$

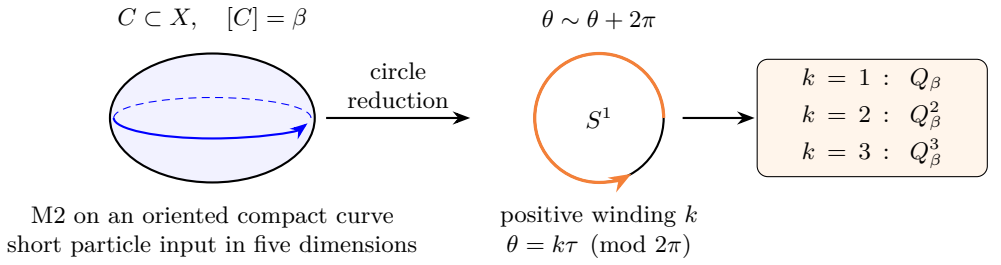
The $1/k$ does not come from guessing an automorphism factor after the answer is known. It follows from the combination of the Fourier delta function and ds/s. Omitting the Jacobian would introduce an erroneous coupling dependence.

Negative k do not lie in the chosen positive proper-time domain. The $k=0$ term sits at the ultraviolet endpoint and is excluded from this winding calculation. That exclusion is different from restricting to nonzero curve classes: a nonzero β also has a zero-winding term in the Poisson representation. The associated ultraviolet/local terms and their regularization are not computed here. Restoring the B-field phase through Q_β gives the connected positive-degree formula

$$F_+(\lambda, Q) = \sum_{\beta\neq 0} \sum_{h\geq 0} \sum_{k\geq 1} \frac{n_\beta^h}{k} \left(2\sin\frac{k\lambda}{2}\right)^{2h-2} Q_\beta^k. \tag{V.8.19}$$

The class sum is over the effective positive-area sector appropriate to the expansion. The disconnected function would be $\exp(F_+)$ after its degree-zero normalization is specified. Our coefficients and inversions concern F_+ itself.

Figure V.8.2 depicts the map $\theta = k\tau$ around the compactification circle. The degree of the monomial is multiplied by k, while the particle charge entering the starting sector remains β. A genuine one-particle sector of charge 2β would be an additional input to the class sum, distinct from the $k=2$ winding of charge β.



The fixed particle charge is β. Winding k changes the instanton monomial to $Q_{k\beta}$ and contributes the measure $1/k$.

Figure V.8.2: A wrapped M2 particle and its circle winding. The oriented compact curve represents β; the arrow on S^1 chooses positive winding. With τ of period 2π, $\theta = k\tau$ gives $Q_\beta^k = Q_{k\beta}$ and measure $1/k$. The particle input is fixed while k varies. The diagram does not assert the existence of an additional charge-$k\beta$ one-particle sector.

To read off genus, expand the kernel rather than retaining only its leading pole. Define the rational coefficients

$$\left(2\sin\frac{x}{2}\right)^{2h-2} = \sum_{g\geq h} C_{h,g} x^{2g-2}, \qquad C_{h,h} = 1. \tag{V.8.20}$$

The first power is x^{2h-2} because $2\sin(x/2) = x + O(x^3)$. Hence a reduced basis label h starts at worldsheet genus $g = h$ but generally contributes at higher g. For the pole at $h = 0$, start with

$$\left(2\sin\frac{x}{2}\right)^{2} = 2(1-\cos x) = x^2\left(1 - \frac{x^2}{12} + \frac{x^4}{360} - \frac{x^6}{20160} + O(x^8)\right). \tag{V.8.21}$$

Inverting the parenthesis yields

$$\left(2\sin\frac{x}{2}\right)^{-2} = \frac{1}{x^2} + \frac{1}{12} + \frac{x^2}{240} + \frac{x^4}{6048} + O(x^6). \tag{V.8.22}$$

For example, the coefficient of x^4 inside the reciprocal parenthesis is $1/144 - 1/360 = 1/240$. This makes the first nontrivial mixing from $h = 0$ to $g = 2$ explicit. The other needed kernels follow from powers of the same sine square,

$$\begin{gathered}\left(2\sin\frac{x}{2}\right)^{0} = 1, \qquad \left(2\sin\frac{x}{2}\right)^{2} = x^2 - \frac{x^4}{12} + O(x^6), \\ \left(2\sin\frac{x}{2}\right)^{4} = x^4 + O(x^6).\end{gathered} \tag{V.8.23}$$

In particular $h = 1$ contributes only to $g = 1$, and the $h = 2$ contribution to $g = 3$ has a minus sign. These facts prevent a genus-by-genus divisor inversion from treating each row independently.

$h\backslash g$	0	1	2	3
0	1	1/12	1/240	1/6048
1	0	1	0	0
2	0	0	1	−1/12
3	0	0	0	1

Table V.8.1: The sine coefficients $C_{h,g}$ through genus three. Columns are worldsheet genera and rows are reduced representation-basis labels. Entries with $g < h$ vanish by the lowest sine power; the further zeros in the $h = 1$ row follow from its constant kernel. The negative entry is fixed by the sine frame.

For finite arithmetic choose one free primitive charge ray, $\beta = b\beta_0$ with $b > 0$, and put $Q = Q_{\beta_0}$. This specialization does not assert that every integral homology group is torsion-free. Define the coefficient table in the formal frame $\lambda = au$, $a > 0$, by

$$F_+(au, Q) = \sum_{g\geq 0}\sum_{d\geq 1} N_{g,d}(a)u^{2g-2}Q^d, \qquad N_{g,d}(1) = N_{g,d}. \tag{V.8.24}$$

A single (b, h, k) term of (V.8.19) has $d = kb$. Substitution of (V.8.20) gives its genus-g coefficient as

$$\frac{n_b^h}{k}C_{h,g}(ka)^{2g-2} = a^{2g-2}C_{h,g}k^{2g-3}n_b^h. \tag{V.8.25}$$

Summing all possibilities for the same monomial proves the full ray relation,

$$N_{g,d}(a) = a^{2g-2}\sum_{k|d} k^{2g-3}\sum_{h=0}^{g} C_{h,g}n_{d/k}^h. \tag{V.8.26}$$

At $g = 0$ the scaling factor is a^{-2}, not one. At $g = 1$ it is one, and at $g = 2$ it is a^2. The rational coefficients depend on the declared formal parameter even though the protected inventory does not.

We can now use the local rigid sphere as a complete example. The relevant local theorem concerns an elementary cluster: the normal operator splits into two identical line operators, their pullbacks to nontrivial covers are injective, and all nonconstant maps in the chosen neighborhood are covers of the core. For the rational core with normal bundle $\mathcal{O}(-1)\oplus\mathcal{O}(-1)$, the local connected series under this obstruction theory has $n_1^0 = 1$ and all other $n_b^h = 0$. This is a cited local theorem; the following expansion illustrates its consequence. It does not apply the closed-target theorem to an arbitrary noncompact target.

The degree-d piece in the nonunit frame $\lambda = 2u$ is

$$[Q^d]F_+(2u, Q) = \frac{1}{4d^3u^2} + \frac{1}{12d} + \frac{d}{60}u^2 + \frac{d^3}{378}u^4 + O(u^6). \tag{V.8.27}$$

The genus-zero d^{-3} combines the winding d^{-1} and the leading sine pole d^{-2}. The genus-two coefficient instead grows as d, because the x^2 term of the same sine pole is multiplied by $1/d$. The complete finite table is

$g\backslash d$	1	2	3	4
0	1/4	1/32	1/108	1/256
1	1/12	1/24	1/36	1/48
2	1/60	1/30	1/20	1/15
3	1/378	4/189	1/14	32/189

Table V.8.2: All sixteen coefficients $N_{g,d}(2)$ for the local sphere through $d = 4$, $g = 3$. The variable is u with $\lambda = 2u$. The nonunit scale changes genus zero as well as the positive powers of the coupling.

For instance at degree two, $1/[2(2\sin 2u)^2]$ gives $u^{-2}/32 + 1/24 + u^2/30 + 4u^4/189 + O(u^6)$. In the unit frame its genus-zero coefficient is $1/8$, the fraction that opened the chapter. The single protected input therefore populates four distinct genus rows here. Replacing $1/k$ with $1/k^2$ would already change the genus-zero degree-two result to $1/16$ in that unit frame.

The sphere is a local contribution at positive area. Taking the area to zero can invalidate integrating out a massive particle. Degree-zero and classical amplitudes, unrestricted noncompact integrals, and a prescription across massless thresholds are outside this computation. Within the declared positive-degree series, however, (V.8.26) is a concrete linear transformation that the reader can invert. That is the next step beyond the rational GW organization of Chapter 2.

V.8.4 Recovering integer data

Which part of a rational GW table remains after covers and lower-genus contributions are removed? The forward map mixes both degree and genus, so its inverse must account for both. We continue on the fixed free ray and assume exact rational input through $1 \le d \le D$ and $0 \le g \le G$. No integrality constraint is imposed. In particular, calling n_d^h a primitive contribution below distinguishes it from a winding contribution; it does not require the charge $d\beta_0$ itself to be primitive in the homology lattice.

Remove the known scale before subtracting covers. At a given degree d, define the residual

$$R_{g,d} = a^{2-2g} N_{g,d}(a) - \sum_{\substack{k|d \\ k>1}} k^{2g-3} \sum_{h=0}^{g} C_{h,g} n_{d/k}^h. \tag{V.8.28}$$

Every d/k in the second term is smaller than d. If the complete lower-degree columns have been recovered, this is a known rational number. The remaining $k = 1$ term is still mixed in genus,

$$R_{g,d} = \sum_{h=0}^{g} C_{h,g} n_d^h = n_d^g + \sum_{h=0}^{g-1} C_{h,g} n_d^h. \tag{V.8.29}$$

Thus the actual inverse is

$$n_d^g = R_{g,d} - \sum_{h=0}^{g-1} C_{h,g} n_d^h. \tag{V.8.30}$$

Order the unknowns first by increasing degree, and within each degree by increasing genus. The forward map is lower triangular in that order, with diagonal $a^{2g-2}C_{g,g} = a^{2g-2} \neq 0$. This proves uniqueness of the finite rational inverse. The absence of higher h terms follows from the lowest sine power, so no information beyond genus G is needed to recover the table through genus G.

The first four genus rows show what is being subtracted. In the unit frame,

$$N_{0,d} = \sum_{k|d} \frac{n^0_{d/k}}{k^3}. \tag{V.8.31}$$

Genus zero has only degree mixing, reproducing the multiple-cover structure familiar from Chapter 2. At genus one there is already a second source,

$$N_{1,d} = \sum_{k|d} \frac{1}{k} \left(\frac{n^0_{d/k}}{12} + n^1_{d/k} \right). \tag{V.8.32}$$

The $h = 0$ correction must be removed even if all the desired $h = 1$ coefficients happen to be integers. The next rows are

$$N_{2,d} = \sum_{k|d} k \left(\frac{n^0_{d/k}}{240} + n^2_{d/k} \right), \tag{V.8.33}$$

$$N_{3,d} = \sum_{k|d} k^3 \left(\frac{n^0_{d/k}}{6048} - \frac{n^2_{d/k}}{12} + n^3_{d/k} \right). \tag{V.8.34}$$

The zero $h = 1$ contributions in the last two rows and the minus sign in the fourth row come from the sine coefficients. They cannot be inferred from a genus-zero divisor formula alone.

Figure V.8.3 resolves the dependencies of one component. At degree four, the possible input degrees are one, two and four. At genus two, only the $h = 0, 2$ terms survive. Read backwards, first divide the coefficient by a^2, then remove the degree-one and degree-two covers and the already known genus-zero term at degree four.

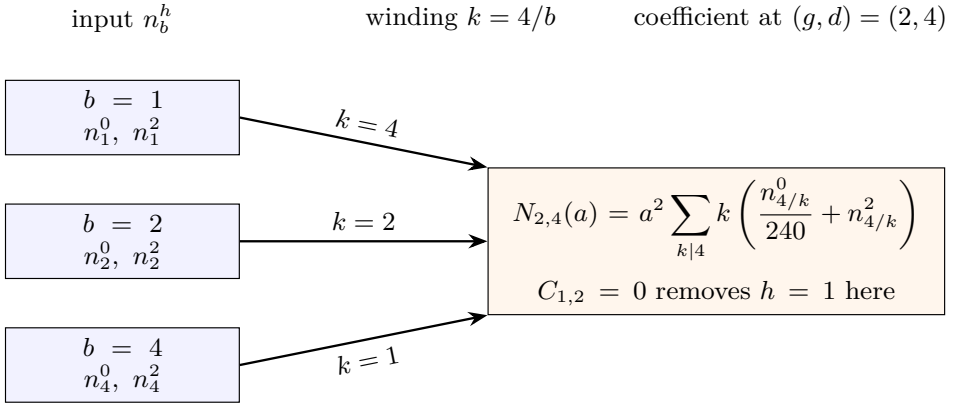


Figure V.8.3: The actual contributions to $N_{2,4}(a)$. The divisor condition is $kb = 4$; the three arrows have $k = 4, 2, 1$. Each carries $a^2 k(n_b^0/240 + n_b^2)$, while $C_{1,2} = 0$ removes n_b^1. After normalizing to $a^{-2}N_{2,4}(a)$, degree-first and genus-second subtraction isolates n_4^2 without rounding.

Consider the following mixed input in the unit frame. It is an algebraic example, with no asserted Calabi–Yau realization.

$g\backslash d$	1	2	3	4
0	2	$-11/4$	$2/27$	$149/32$
1	$7/6$	$1/3$	$-29/18$	$7/12$
2	$1/120$	$481/240$	$1/40$	$967/240$
3	$1/3024$	$-995/6048$	$1/112$	$-7955/6048$

Table V.8.3: Rational GW input for the inverse example and Exercise E2. All entries are coefficients of $u^{2g-2}Q^d$ with $\lambda = u$. The negative entries are retained exactly.

At degree one there are no lower-degree covers. The first two subtractions give

$$\begin{aligned} n_1^0 &= 2, \qquad n_1^1 = \frac{7}{6} - \frac{2}{12} = 1, \\ n_1^2 &= \frac{1}{120} - \frac{2}{240} = 0, \qquad n_1^3 = \frac{1}{3024} - \frac{2}{6048} = 0. \end{aligned} \tag{V.8.35}$$

At degree two the genus-zero cover is $n_1^0/8 = 1/4$. Therefore

$$n_2^0 = -\frac{11}{4} - \frac{2}{8} = -3. \tag{V.8.36}$$

To recover genus one, first remove the $k = 2$ term, which includes both lower-degree

genus labels, and then remove the $h = 0$ term at degree two,

$$n_2^1 = \frac{1}{3} - \frac{1}{2}\left(\frac{2}{12} + 1\right) - \frac{-3}{12} = \frac{4}{12} - \frac{7}{12} + \frac{3}{12} = 0. \tag{V.8.37}$$

The cover subtraction alone would give $-1/4$, not the desired coefficient. The second subtraction is equally necessary.

The higher-genus components test that the whole lower triangle is being used. At degree two, genus two gives

$$n_2^2 = \frac{481}{240} - 2\left(\frac{2}{240} + 0\right) - \frac{-3}{240} = \frac{481 - 4 + 3}{240} = 2. \tag{V.8.38}$$

At genus three the cover and the within-degree subtraction involve different factors,

$$\begin{aligned} n_2^3 &= \frac{-995}{6048} - 8\left(\frac{2}{6048}\right) - \left(\frac{-3}{6048} - \frac{2}{12}\right) \\ &= \frac{-995 - 16 + 3 + 1008}{6048} = 0. \end{aligned} \tag{V.8.39}$$

A sign error in $C_{2,3}$ would remain invisible in the genus-zero row but fail this cancellation.

At degree three the only proper divisor contribution has $k = 3$, and at degree four both $k = 2$ and $k = 4$ contribute. For the genus-zero row the remaining entries are

$$n_3^0 = \frac{2}{27} - \frac{2}{27} = 0, \qquad n_4^0 = \frac{149}{32} - \frac{-3}{8} - \frac{2}{64} = 5. \tag{V.8.40}$$

The same two subtractions in every row yield the complete result

$h\backslash d$	1	2	3	4
0	2	−3	0	5
1	1	0	−2	0
2	0	2	0	0
3	0	0	0	0

Table V.8.4: All sixteen rational candidates obtained from Table V.8.3. They happen to be integers. No positivity, integrality or existence condition was imposed while solving the triangular system.

Forward reconstruction checks a different operation from merely repeating the inverse. For example, the degree-four genus-two component receives a primitive contribution and two covers,

$$N_{2,4} = \frac{5}{240} + 2\left(\frac{-3}{240} + 2\right) + 4\left(\frac{2}{240}\right) = \frac{5 + 954 + 8}{240} = \frac{967}{240}. \tag{V.8.41}$$

At genus three the same classes give

$$N_{3,4} = \frac{5}{6048} + 8\left(\frac{-3}{6048} - \frac{2}{12}\right) + 64\left(\frac{2}{6048}\right) = \frac{5 - 8088 + 128}{6048} = -\frac{7955}{6048}. \tag{V.8.42}$$

The large negative cover contribution comes from n_2^2, even though all n_d^3 vanish. A nonzero genus-three GW row therefore does not imply a nonzero genus-three GV row. Conversely, reconstructing only the leading pole would leave most of the input table untested.

A second example changes the coupling as well as the inventory. Take the supplied rows $n^0 = (3, -1, 2, 0)$, $n^1 = (-2, 4, 0, 1)$, $n^2 = (1, 0, -3, 0)$ and $n^3 = (0, 0, 0, 2)$. These are again finite algebraic data. At $\lambda = (3/2)u$, the first entry must include the inverse scale square,

$$N_{0,1}(3/2) = \left(\frac{3}{2}\right)^{-2} 3 = \frac{4}{3}, \qquad N_{0,2}(3/2) = \frac{4}{9}\left(-1 + \frac{3}{8}\right) = -\frac{5}{18}. \tag{V.8.43}$$

Keeping the lower-h terms at positive genus gives, for example,

$$\begin{aligned} N_{2,1}(3/2) &= \frac{9}{4}\left(\frac{3}{240} + 1\right) = \frac{729}{320}, \\ N_{3,1}(3/2) &= \frac{81}{16}\left(\frac{3}{6048} - \frac{1}{12}\right) = -\frac{1503}{3584}. \end{aligned} \tag{V.8.44}$$

Exercise E3 asks for all sixteen entries. This example makes the frame visible at both the pole and the higher powers. No redefinition of the integer inventory is needed when only the formal expansion variable changes.

Integrality does not follow from this triangular algebra. As a minimal counterexample, choose rational input $N_{0,1} = 1/2$ in the unit frame. The first diagonal equation forces

$$N_{0,1} = \frac{1}{2} \quad \Longrightarrow \quad n_1^0 = \frac{1}{2}. \tag{V.8.45}$$

No higher-degree or higher-genus subtraction can change it. Rounding to one or zero would fail forward reconstruction. An empty inventory similarly gives a zero amplitude table, but the absence of a protected index contribution need not mean the absence of a nonempty underlying state space, as Section V.8.5 will show.

We have established a unique rational inverse through any complete finite rectangle in degree and genus on the chosen ray. The special property that geometric GW data produce integers requires a theorem or a physical protected-state construction with its premises. Finite agreement with an integer table neither extends that claim to all orders nor constructs a new geometry. What the calculation supplies for later geometric engineering and instanton applications is a reliable separation of degree covers from genus mixing, with an exact reconstruction in the same frame.

V.8.5 Spin and genus

What does the GV genus label measure if it is not a positive particle multiplicity? It labels the tensor-power basis I_h of the reduced left-spin representation after a right-spin trace. The worldsheet genus g labels a power of the topological coupling. The two are related by the sine kernel, rather than identified term by term. We now compute

a complete spin inventory so that this distinction can be seen without assuming a geometric realization.

First make the basis change explicit. Since $I_1 = [\frac{1}{2}] + 2[0]$ and $I_0 = [0]$, the smallest half-integral irrep obeys

$$[\tfrac{1}{2}] = I_1 - 2I_0. \tag{V.8.46}$$

The negative coefficient expresses a change of basis in the representation ring; there are still two ordinary states in $[\frac{1}{2}]$. To obtain the spin-one irrep, use the Clebsch–Gordan product $[\frac{1}{2}] \otimes [\frac{1}{2}] = [1] + [0]$,

$$I_1^{\otimes 2} = ([\tfrac{1}{2}] + 2[0])^{\otimes 2} = [1] + 4[\tfrac{1}{2}] + 5[0], \qquad [1] = I_2 - 4I_1 + 3I_0. \tag{V.8.47}$$

Thus even a single positive spin-one irrep has both positive and negative coefficients in this basis. Ordinary dimensions check the equality independently: $3 = 16 - 4 \cdot 4 + 3$.

The corresponding graded characters follow by applying the already fixed left sign. They are

$$\mathrm{sch}[\tfrac{1}{2}] = -(y + y^{-1}) = z - 2, \qquad \mathrm{sch}[1] = y^2 + 1 + y^{-2} = z^2 - 4z + 3. \tag{V.8.48}$$

For the second equality, set $y + y^{-1} = 2 - z$ and square it, subtracting one. This is an explicit dictionary between a positive ordinary irrep and a signed polynomial basis. It is also why omitting the left sign in the trace would alter the genus coefficients even when the right trace were correct.

Take the reduced fixed-charge inventory of Exercise E4. It consists of five $(0,0)$ multiplets, two $(\frac{1}{2},0)$ multiplets, one $(0,\frac{1}{2})$ multiplet and one $(1,0)$ multiplet. Here and below a multiplet means a reduced little-group representation; the universal short factor has already been removed. Table V.8.5 shows both operations on each summand.

(j_L, j_R)	multiplicity	right factor	contribution to $P(y)$	ordinary dimension
$(0,0)$	5	1	5	5
$(\frac{1}{2},0)$	2	1	$-2(y+y^{-1})$	4
$(0,\frac{1}{2})$	1	-2	-2	2
$(1,0)$	1	1	y^2+1+y^{-2}	3

Table V.8.5: Complete reduced spin data for E4. The right factor is $(-1)^{2j_R}(2j_R+1)$; the left sign is included in the character column. The last column uses unsigned dimensions and includes the stated multiplicities. The word "nonnegative" in the public coefficient-array name refers to powers of y, not to signs of coefficients.

Add the magnetic weights before changing basis. The full Laurent polynomial is

$$\begin{aligned} P(y) &= 5 - 2(y + y^{-1}) - 2 + (y^2 + 1 + y^{-2}) \\ &= 4 - 2(y + y^{-1}) + (y^2 + y^{-2}). \end{aligned} \tag{V.8.49}$$

The nonnegative-power coefficients in order y^0, y^1, y^2 are therefore $(4, -2, 1)$. Symmetry supplies the y^{-1}, y^{-2} coefficients. This records the entire polynomial, rather than only its value at one fugacity.

For an independent change of basis, use

$$z^2 = (2 - y - y^{-1})^2 = 6 - 4(y + y^{-1}) + (y^2 + y^{-2}). \tag{V.8.50}$$

Subtracting the $y^{\pm 2}$ term first, then the $y^{\pm 1}$ term, gives

$$P(y) = 2 - 2z + z^2, \qquad (n^0, n^1, n^2) = (2, -2, 1). \tag{V.8.51}$$

The same result follows directly at the representation level,

$$5[0] + 2[\tfrac{1}{2}] - 2[0] + [1] = 3I_0 + 2(I_1 - 2I_0) + (I_2 - 4I_1 + 3I_0) = 2I_0 - 2I_1 + I_2. \tag{V.8.52}$$

This second route checks both the right signed dimension and the left basis conversion. It does not interpret $n^1 = -2$ as a negative number of particles.

The ordinary reduced dimension is a different sum,

$$D = 5 \cdot 1 + 2 \cdot 2 + 1 \cdot 2 + 1 \cdot 3 = 14, \qquad \dim \mathcal{H} = 4D = 56. \tag{V.8.53}$$

By contrast, $P(1) = 4 - 4 + 2 = 2$, equal to n^0 because $z = 0$ at $y = 1$. There is no reason for 2, 14 and 56 to agree: they respectively measure the signed trace, the reduced ordinary dimension and the full short ordinary dimension.

Inserting the same supplied inventory at a single charge into the sine organization makes the difference between h and g visible. Its $k = 1$ contribution is

$$2\left(2\sin\frac{\lambda}{2}\right)^{-2} - 2 + \left(2\sin\frac{\lambda}{2}\right)^{2} = \frac{2}{\lambda^2} - \frac{11}{6} + \frac{121}{120}\lambda^2 - \frac{251}{3024}\lambda^4 + O(\lambda^6). \tag{V.8.54}$$

For example the λ^4 coefficient is $2/6048 - 1/12 = -251/3024$. The polynomial basis stops at $h = 2$ but this amplitude has higher-genus terms. Worldline oscillators and winding produce those terms; they do not require extra reduced spin representations at every genus.

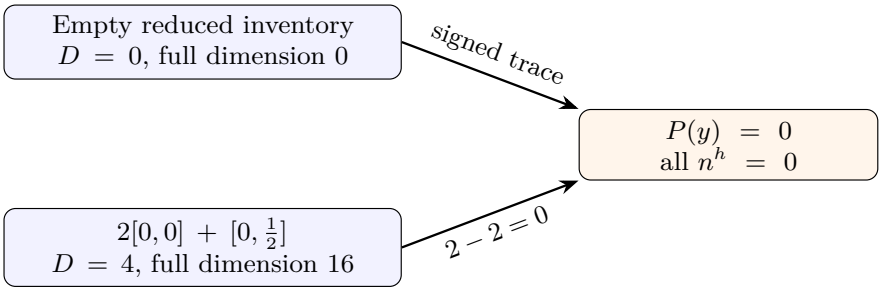
The converse failure is just as useful. Consider the E5 inventory $2[0, 0] + [0, \frac{1}{2}]$. The right trace cancels identically at every left fugacity,

$$P(y) = 2 \cdot 1 + 1 \cdot (-2) = 0, \qquad n^h = 0 \quad \text{for every } h. \tag{V.8.55}$$

Its ordinary dimensions remain

$$D = 2 \cdot 1 + 1 \cdot 2 = 4, \qquad \dim \mathcal{H} = 4 \cdot 4 = 16. \tag{V.8.56}$$

No CPT-conjugate sector has been added. Figure V.8.4 compares this nonempty finite representation with the empty one. Both map to exactly the same polynomial, so even an all-orders knowledge of this trace could not distinguish them.



These supplied finite representations have identical protected characters and different ordinary dimensions. No inverse of this trace recovers both inventories.

Figure V.8.4: Noninjectivity of the signed trace for supplied fixed-charge representations. The upper input has no states; the lower input has reduced dimension four and full short dimension sixteen. Both give $P(y) = 0$ and hence identical GV basis coefficients. This is a finite representation calculation, not a proposed wall-crossing event in a specific Calabi–Yau compactification.

The information loss occurs before the GW/GV transform. The rational transform is invertible on complete finite tables in its declared frame; the right-spin trace is not invertible on representation inventories. Adding the E5 inventory to any supplied reduced inventory preserves its protected character while increasing its ordinary reduced dimension by four. Recovering exact GV coefficients therefore recovers a protected organization, not the multiplicities $N_\beta(j_L, j_R)$.

The physical protected trace can remain unchanged when short states combine into long representations under deformations, as in the sourced GV construction. The finite E5 example illustrates a mathematical obstruction to reconstruction; it neither prescribes which states appear along a physical deformation nor supplies a four-dimensional stability-chamber formula. Those require physical state and stability information beyond this unrefined trace. The distinction will matter when Chapter 10 uses protected couplings rather than a full particle census.

V.8.6 Scope of integrality

When does the rational inverse actually produce integers, and what does genus finiteness mean? The answer depends on the input object. A finite rational table, a local curve contribution and a closed-target GW theory have different hypotheses. We begin with the closed case to identify the theorem's domain, then return to two local elementary clusters whose behavior differs already at degree two.

Let (X, ω) be a closed symplectic real six-manifold with $c_1(X) = 0$. For unmarked connected stable maps in a nonzero class A, the real virtual dimension is

$$\operatorname{vdim}_{\mathbb{R}} \overline{\mathcal{M}}_{g,0}(X, A) = 2\langle c_1(X), A\rangle + (6-6)(1-g) = 0. \tag{V.8.57}$$

Pairing the virtual class with 1 therefore defines rational numbers,

$$\mathrm{GW}_{A,g}(X) = \left\langle [\overline{\mathcal{M}}_{g,0}(X,A)]^{\mathrm{vir}}, 1 \right\rangle \in \mathbb{Q}. \tag{V.8.58}$$

This is a connected nonzero-class invariant with the virtual GW definition. The generating series is interpreted in the Novikov completion: below fixed energy and genus bounds the sums used in the structural decomposition are finite. Degree-zero terms are excluded. These conditions are part of the input, not optional choices of normalization for an unrestricted sum.

In this domain the Ionel–Parker integrality theorem states that the unique coefficients in

$$\sum_{A\neq 0, g\geq 0} \mathrm{GW}_{A,g}\, \lambda^{2g-2} Q_A = \sum_{B\neq 0, h\geq 0} \sum_{k\geq 1} \frac{n_B^h}{k} \left(2\sin\frac{k\lambda}{2}\right)^{2h-2} Q_{kB}, \qquad n_B^h \in \mathbb{Z}. \tag{V.8.59}$$

The class sums mean the positive-area part of the stated completed series. The analytic and geometric proof of this theorem is cited, not reproduced here. Unlike a fit to several rows, it is a statement about the transformed geometric series in its whole domain.

General divisibility is a relation in integral homology, $kB = A$. Coefficient extraction is consequently

$$\mathrm{GW}_{A,g} = \sum_{\substack{k\geq 1,\ B\neq 0 \\ kB=A}} k^{2g-3} \sum_{h=0}^{g} C_{h,g} n_B^h. \tag{V.8.60}$$

There can be more than the simple free-ray divisor indexing used for our tables. The finite ray calculation is a declared specialization, not a replacement for the theorem when homology has torsion or several independent generators. In particular, nothing here restricts B to primitive lattice classes.

Finiteness in genus is an additional conclusion. The Doan–Ionel–Walpuski theorem applies to a closed symplectic real six-manifold and each nonzero class A satisfying $\langle c_1(X), A\rangle = 0$, with BPS coefficients defined by its GW transform on those classes. It yields

$$\text{for each such } A \text{ there exists } g_A \text{ such that } n_A^h = 0 \quad \text{for every } h \geq g_A. \tag{V.8.61}$$

This is classwise finiteness. It is not a supplied effective value of g_A, nor a uniform bound valid for all positive classes at once. The earlier integrality paper explicitly did not establish this genus-finiteness conclusion. We cite the later theorem for it rather than infer it from a finite list of zero coefficients. The classwise condition $c_1(A) = 0$ in this theorem is also weaker than requiring $c_1(X) = 0$ globally.

A smooth projective quintic threefold illustrates how to check the closed CY hypotheses without asserting any new numerical inventory. If H is the hyperplane class on $\mathbb{P}^4$ and X is cut out by a degree-five equation, the normal bundle is $\mathcal{O}_X(5)$. Adjunction gives

$$K_X = (K_{\mathbb{P}^4} \otimes \mathcal{O}_{\mathbb{P}^4}(5))\big|_X = \mathcal{O}_{\mathbb{P}^4}(-5+5)\big|_X = \mathcal{O}_X, \qquad c_1(X) = 0. \tag{V.8.62}$$

Smoothness makes it a manifold; projectivity makes it compact and supplies a Kähler, hence symplectic, form. Its complex dimension is $4-1=3$, so its real dimension is six. For every nonzero effective class, the stated integrality and classwise finiteness theorems apply to the connected virtual counts. This checks the hypotheses but computes no quintic GW or GV number and constructs no physical BPS state.

Now consider the resolved-conifold local geometry $Y=\mathrm{Tot}(\mathcal{O}(-1)\oplus\mathcal{O}(-1)\to\mathbb{P}^1)$. The canonical bundle calculation is

$$K_Y=\pi^*\left(K_{\mathbb{P}^1}\otimes\det(\mathcal{O}(-1)\oplus\mathcal{O}(-1))^{-1}\right)=\pi^*\mathcal{O}(-2+2)=\mathcal{O}_Y. \tag{V.8.63}$$

It is Calabi–Yau but noncompact: the vector-bundle fibers are noncompact. Thus this calculation does not place Y in the closed-target theorem. Its compact-core contribution uses the separate local obstruction theory already stated in Section V.8.3. More precisely, an elementary cluster has a core curve C, a sufficiently small neighborhood, and an almost complex structure for which the normal operator splits as $D_0\oplus D_0$, the pullback of D_0 is injective on every nontrivial cover, and the nonconstant maps in that neighborhood are covers of C. These conditions let the local contribution be defined and computed. They are not consequences of the word "noncompact."

For the rational elementary cluster, the local result is

$$F_{+,\mathrm{sphere}}(\lambda,Q)=\sum_{k\ge1}\frac{Q^k}{k(2\sin(k\lambda/2))^2},\qquad n_1^0=1,\quad n_b^h=0\text{ otherwise.} \tag{V.8.64}$$

The exact local theorem establishes this series; our sixteen-entry expansion is an illustration. The same local framework also contains a genus-one elementary cluster, with its balanced and super-rigid normal-operator hypotheses. This is a distinct model, not the rational curve with its genus-one amplitude selected.

For that genus-one cluster the cited local disconnected series is the partition generating function. Calling it Z_1^{elem}, its connected logarithm is

$$Z_1^{\mathrm{elem}}(Q)=\prod_{b\ge1}(1-Q^b)^{-1},\qquad F_1^{\mathrm{elem}}=\log Z_1^{\mathrm{elem}}=\sum_{b\ge1}\sum_{k\ge1}\frac{Q^{kb}}{k}. \tag{V.8.65}$$

The sine exponent for $h=1$ is zero. Comparison with the transform gives $n_b^1=1$ for every $b>0$, with the other n_b^h vanishing. In particular there is an imprimitive input at degree two as well as a winding of the degree-one input.

The degree-two connected coefficient can be checked in two independent ways. In the double sum there are exactly the pairs $(b,k)=(2,1)$ and $(1,2)$, so

$$[Q^2]F_1^{\mathrm{elem}}=1+\frac{1}{2}=\frac{3}{2}. \tag{V.8.66}$$

Alternatively $Z_1^{\mathrm{elem}}=1+Q+2Q^2+O(Q^3)$ because the two degree-two partitions are 2 and $1+1$. Taking its logarithm yields

$$\log(1+Q+2Q^2+O(Q^3))=Q+\left(2-\frac{1}{2}\right)Q^2+O(Q^3)=Q+\frac{3}{2}Q^2+O(Q^3). \tag{V.8.67}$$

Keeping only the primitive lattice class would give $1/2$ instead of $3/2$. This concrete local example explains why "primitive contribution" cannot mean that every imprimitive one-particle or transformed input has been discarded. It also illustrates classwise finiteness without finiteness of the number of nonzero degree classes: each b has only $h = 1$, while infinitely many b occur.

Figure V.8.5 keeps the two theorem branches separate. The compact quintic lies in the closed branch. The local sphere and genus-one cluster lie in the elementary-cluster branch with their specified obstruction hypotheses. An arbitrary rational table lies in neither merely because its first extracted entries happen to be integral.

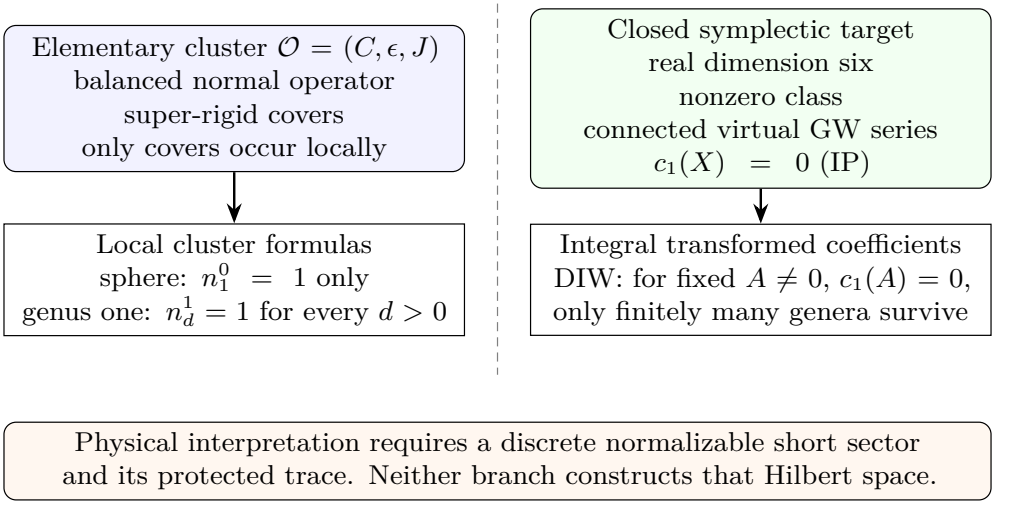


Figure V.8.5: Two mathematical domains and the additional physical input. The left branch concerns elementary-cluster contributions with balanced normal operators and super-rigid covers. Here C is the core, ϵ the neighborhood radius and J the almost complex structure. The right branch uses a closed symplectic target and the connected virtual nonzero-class series. The stated IP theorem assumes $c_1(X) = 0$; the DIW finiteness conclusion is classwise for $A \neq 0$, $c_1(A) = 0$. Neither branch alone identifies a physical particle Hilbert space.

The common misconception is that an integral invariant is a positive number of all BPS particles in any compactification or chamber. The examples separate three failures of that inference. The rational inverse can return $1/2$ on arbitrary input. Positive reduced representations can have negative I_h coefficients. A nonempty representation can have identically zero protected character. Even where a mathematical theorem establishes integrality and finiteness, the physical interpretation still needs actual normalizable discrete short sectors, the supersymmetric compactification and the protected one-loop coupling.

A generic four-dimensional D-brane stability-chamber count is a further object. We have not computed its stability conditions or its wall crossing. Nor does this chapter construct the three-dimensional M2 probe theories of Volume VIII. Chapter 5's

conifold singularity and fixed-frame gap concern a separately specified light-particle limit; sending a positive-area curve to zero inside the present expansion does not establish that limit. Chapter 10 takes up the protected F-term dictionary, while the resolved-conifold and instanton applications in Volume XVIII and the planned treatment of instanton partition functions require their own physical constructions. What can travel to those chapters without a new spectrum assertion is the explicit sine transform, its rational inverse, and the distinction between an index and an ordinary count.

V.8.7 Exercises

Exercises E1–E5 have bounded numerical submissions; each accompanying explanation is written work. E6 is entirely written. In all matrix submissions the rows are g or $h = 0, 1, 2, 3$ and the columns are $d = 1, 2, 3, 4$. Entries are exact rational strings such as `"-11/4"`, not rounded decimals. Unlisted inputs through the stated order vanish. The supplied finite inventories are algebraic examples unless a local theorem is explicitly assumed.

E1. Assume the positive-degree local $(-1,-1)$ contribution $n_1^0 = 1$ and no other inputs. At $\lambda = 2u$, compute all sixteen coefficients of $u^{2g-2}Q^d$ in the connected free energy. Submit `{"gw":table}`. In the written calculation derive the delta-function Jacobian and explain how the winding measure combines with the leading sine pole into k^{-3}. Distinguish zero winding from zero curve degree.

E2. At $\lambda = u$, use the rational GW input of Table V.8.3. Recover all sixteen n_d^h by subtracting covers and lower-h terms. Submit `{"primitive":table}`. Do not impose integrality. In the written calculation explain why degree-two genus one needs both subtractions and reconstruct at least one genus-three coefficient.

E3. Start with the four input rows $n^0 = (3,-1,2,0)$, $n^1 = (-2,4,0,1)$, $n^2 = (1,0,-3,0)$ and $n^3 = (0,0,0,2)$. At $\lambda = (3/2)u$, reconstruct all sixteen rational GW coefficients. Submit `{"gw":table}`. In the written work explain why $h = 0$ contributes above genus zero and how the nonunit scale acts on the pole.

E4. The universal four-state factor is already stripped. The reduced inventory $(2j_L, 2j_R, \text{multiplicity})$ is $(0,0,5)$, $(1,0,2)$, $(0,1,1)$, $(2,0,1)$. Compute the entire Laurent character and its expansion in $z = 2 - y - y^{-1}$. Submit integer arrays `n` $= (n^0, n^1, n^2)$ and `character_nonnegative` containing the coefficients of y^0, y^1, y^2, together with integer `reduced_dimension`, in one object with exactly those three fields. Negative powers follow by symmetry. Explain in writing why a negative n^h is consistent with nonnegative multiplicities.

E5. For the reduced inventory $2[0,0] + [0,\frac{1}{2}]$, submit the integers `signed_index`, `reduced_dimension` and `full_short_dimension` as three fields of one object. Use the fixed-charge sector without an extra opposite-charge copy. Explain why a vanishing result for the first field does not force either dimension to vanish and why this finite example is not a physical wall-crossing prescription.

E6. A rational GW table produces integer candidates through $d = 4$, $g = 3$. Explain separately what the finite extraction establishes, what the closed symplectic integrality theorem establishes, what classwise genus finiteness adds, and what the physical M2 interpretation requires. Compare a compact CY threefold, the local $(-1, -1)$ cluster with its specified obstruction theory, and a chamber-dependent four-dimensional D-brane count. Use the genus-one elementary cluster to explain why excluding every imprimitive input loses the degree-two value 3/2. Explain why neither integer arithmetic nor a signed trace proves supersymmetry or state existence.

The public question inventory gives the exact JSON schemas; submit through `benchmark/PROTOCOL.md`. Rational table tasks use strings for every entry, including integers and zeros. The spin tasks use JSON integer values. Numerical acceptance concerns the stated fields only; the written interpretations are not machine-certified.

V.8.8 Take-home message

Take-home message

A wrapped short particle supplies a protected spin observable after a universal factor is stripped and right spin is traced with a sign. Circle momenta reorganize into positive windings with measure $1/k$, while the continued sine kernel mixes a reduced label h into worldsheet genera $g \geq h$. The resulting GW/GV map has a unique rational inverse in a fixed frame. Integrality and classwise genus finiteness are special theorems for geometric input under stated hypotheses, with separate local cluster formulas for the noncompact examples. The protected trace loses information before the invertible transform begins: it cannot recover ordinary state multiplicities. Rational amplitudes, signed protected integers and full particle counts are three different quantities.

Status and sources

§V.8.1–V.8.2. The wrapped-M2 compactification setup follows Gopakumar and Vafa (1998a, physical PDF pp. 6–8, especially (3.3) on p. 8) and Gopakumar and Vafa (1998b, physical PDF pp. 8–9, index and (3.1)). Normalizable discrete short sectors, the supersymmetric CY3 compactification and the nonperturbative IIA/M lift are physical premises, independent of the representation arithmetic. The short-factor and right-trace protection assertion is [BPS:1/2|idx] conditional on the sourced protected trace. Equations (V.8.3)–(V.8.10) are representation arithmetic [MATH] once the sector is supplied. The action-weight translation is [MATH], using the stated curve weights and physical IIA/M circle units. It fixes neither an absolute source mass in book units nor $\lambda = g_s$.

§V.8.3. The protected amplitude organization and its continuation are [BPS:1/2|idx], sourced from Gopakumar and Vafa (1998b, physical PDF pp. 9–10, (3.2)–(3.3)). The Poisson/Jacobian derivation is conditional formal algebra; it supplies no integration

contour or ultraviolet completion. The local sphere formula is a cited [MATH] result from Ionel and Parker (2018, Definition 3.1, physical PDF p. 9, Proposition 3.4(c) and proof, physical PDF p. 12), under elementary-cluster obstruction hypotheses. The scalar coefficients and ray transform are [MATH]; the independent finite comparisons cover $0 \le h, g \le 5$ and degrees through six, at scales $1, 2, 3/2$. The local table illustrates the theorem rather than proving it.

§V.8.4. The finite inverse and reconstruction are [MATH] under the declared free-ray and exact rational truncation assumptions. Their lower-triangular origin is also explained in Gopakumar and Vafa (1998b, physical PDF p. 10, (3.3)). The local calculations compare every returned component through degree six and genus five at scales $1, 2, 3/2$, alongside zero and nonintegral inputs. Graded E1–E3 consume all sixteen submitted coefficients per task, including scientific mutations of higher components. These bounded comparisons establish neither geometric realization nor an all-orders physical identity. The fractional-input example marks the difference from the cited closed-target theorem.

§V.8.5. The supplied character and dimension results, including E4's reduced dimension fourteen and E5's full fixed-charge dimension sixteen, are [MATH]. The right-spin protected interpretation and its information-loss boundary are [BPS:1/2|idx], following Gopakumar and Vafa (1998b, physical PDF pp. 8–9); finite representation noninjectivity does not supply a wall-crossing rule. The universal four-state factor, its single removal and the left/right signs are defined above.

§V.8.6. Closed-target integrality is the cited [MATH] Structure Theorem and transform in Ionel and Parker (2018, physical PDF pp. 1–4 and p. 33, (0.1), (8.9)). The exact hypotheses are closed symplectic real dimension six, $c_1(X) = 0$, the connected nonzero-class virtual GW series and its Novikov completion. Classwise finiteness is a cited [MATH] result from Doan et al. (2025, v2, physical PDF pp. 1–2, (1.1), Conjecture 1.2 and Theorem 1.7), for $A \neq 0$, $c_1(A) = 0$ in a closed symplectic six-manifold. No effective uniform genus cutoff or physical Hilbert-space construction follows. The separate genus-one elementary-cluster formula and its hypotheses use Ionel and Parker (2018, Definition 3.1 and Proposition 3.4(d), physical PDF pp. 9, 12). Adjunction and the displayed degree-two logarithm are elementary consequences, not numerical quintic claims. Chapter 5 discusses the separate conifold-gap dictionary. Chapters XI.7 and XVIII.4 and the discussion of Nekrasov partition functions and the Omega background use these results.

Source conventions. Two differences in the exact source editions affect transcription. In GV-II physical PDF p. 7 the general character is printed as $(-4)^r \sinh^{2r}(s/2)$, while its $r = 1$ example is printed as $2 - e^{-2s} - e^{2s}$; at the same s the general expression instead gives $2 - e^{-s} - e^{s}$. Our signs use the independently displayed representation identity (3.1), its direct character calculation and the continued sine formula (3.2). In IP v6 physical PDF p. 33, (8.8) names the transformed coefficients $e_{A,h}$, while (8.9) calls them $n_{A,h}$ and expresses them through the elementary-cluster coefficients and the structural virtual counts also named $e_{B,g}$. We use the Structure Theorem, (0.1) and (8.9), keeping the two roles distinct. These are statements about the printed editions,

not assertions of published errata. In IP and DIW the source variable t is our formal λ, not the book's Kähler coordinate t_β.

Exercises and scope. Exercises E1–E5 are bounded calculations. E6 asks for written interpretation. These finite calculations do not establish the physical premises.

References

Doan, A., E.-N. Ionel, and T. Walpuski (2025). *The Gopakumar–Vafa finiteness conjecture*. Read edition: arXiv v2, 29 November 2025. arXiv: 2103.08221 [math.SG].

Gopakumar, R. and C. Vafa (1998a). *M-Theory and Topological Strings–I*. Source edition: arXiv v1, 25 September 1998. arXiv: hep-th/9809187 [hep-th].

Gopakumar, R. and C. Vafa (1998b). *M-Theory and Topological Strings–II*. Source edition: arXiv v1, 15 December 1998. arXiv: hep-th/9812127 [hep-th].

Ionel, E.-N. and T. H. Parker (2018). "The Gopakumar–Vafa formula for symplectic manifolds". In: *Annals of Mathematics* 187.1. Read edition: arXiv v6, 8 October 2017; physical PDF has 45 pages, distinct from journal pagination, pp. 1–64. DOI: 10.4007/annals.2018.187.1.1. arXiv: 1306.1516 [math.SG].

Chapter V.9

Matrix models and topological recursion

A Gaussian matrix already contains surfaces. Contract four entries in a cyclic trace and the two index lines of each propagator distinguish a sphere from a torus. The same contractions also compute moments of an eigenvalue distribution. Summing those moments produces a function with a cut, and resolving that cut produces a Riemann surface. This is the route from a matrix integral to a spectral curve.

The useful question is how much of the original problem survives on that curve. We shall derive its planar resolvent from an expectation-value identity, specify the sheets and periods, and then compute the first stable correlators by branch-point residues. A nonunit Gaussian example will run through the entire construction; a quartic example will show which parts depend on the potential. The last step is to identify what a formal series leaves undetermined about contours and physical couplings. Chapters 3–5 supply the period and topological-amplitude background, while Chapter 10 returns to the physical F-term interface.

V.9.1 A matrix integral as an expansion

Why should a finite collection of integration variables know about genus? The answer is the cyclic order supplied by an ordinary matrix trace. Let M be an $N \times N$ Hermitian matrix. Take dM to be flat Lebesgue measure on its independent real components, up to an overall constant: it is the product of dM_{ii} and $d\operatorname{Re} M_{ij}\, d\operatorname{Im} M_{ij}$ for $i < j$. This measure is both translation invariant and unitarily invariant; unitary invariance alone would not suffice. For a convergent contour we define normalized expectations by

$$Z = \int dM\, e^{-\operatorname{Tr} V(M)/\hbar_{\mathrm{m}}}, \qquad \langle \mathcal{O} \rangle = \frac{1}{Z} \int dM\, \mathcal{O}(M) e^{-\operatorname{Tr} V(M)/\hbar_{\mathrm{m}}}, \qquad t_{\mathrm{m}} = N\hbar_{\mathrm{m}}. \tag{V.9.1}$$

The trace here is the ordinary trace on matrix indices. Multiplying dM by a constant changes Z but leaves every normalized expectation unchanged. We keep this distinc-

tion because the correlators below will not determine an absolute partition-function normalization. The parameter $\hbar_{\mathrm{m}}$ belongs to this matrix problem. Identifying it with a physical string coupling g_s requires a further physical dictionary.

For $V(M) = mM^2/2$, with $m, \hbar_{\mathrm{m}} > 0$, completing the square in a matrix source J gives

$$\frac{Z[J]}{Z[0]} = \left\langle e^{\mathrm{Tr}\, JM} \right\rangle = \exp\left[\frac{\hbar_{\mathrm{m}}}{2m}\,\mathrm{Tr}\, J^2\right]. \tag{V.9.2}$$

Differentiating twice with respect to J_{ji} and J_{lk} produces the covariance

$$\langle M_{ij} M_{kl}\rangle = \frac{\hbar_{\mathrm{m}}}{m}\delta_{il}\delta_{jk}. \tag{V.9.3}$$

Thus a contraction joins the first index of one entry to the second index of the other. Drawing both index lines turns an edge into a ribbon. The ordering in $\mathrm{Tr}\, M^k$ tells us how these ribbons attach around a vertex; it cannot be discarded as it could for k identical scalar variables.

Consider the first example that distinguishes the topologies. Write $\mathrm{Tr}\, M^4 = M_{ij}M_{jk}M_{kl}M_{li}$ and label its four factors cyclically. The three Wick pairings give

$$\begin{aligned} &(12)(34): \quad (\hbar_{\mathrm{m}}/m)^2 N^3, \\ &(14)(23): \quad (\hbar_{\mathrm{m}}/m)^2 N^3, \\ &(13)(24): \quad (\hbar_{\mathrm{m}}/m)^2 N. \end{aligned} \tag{V.9.4}$$

For example, pairing the first and third factors gives $\delta_{il}\delta_{jk}$, and pairing the second and fourth gives $\delta_{ji}\delta_{kl}$. All four indices coincide. Pairing adjacent factors instead leaves three independent indices. Each free index sums to N, so the different powers have a direct origin in the integral. Dividing by N and using $c = t_{\mathrm{m}}/m$ gives the exact answer

$$\frac{1}{N}\langle \mathrm{Tr}\, M^4\rangle = 2c^2 + \frac{c^2}{N^2}. \tag{V.9.5}$$

The third pairing is suppressed by N^{-2}, although its covariance and its four factors are identical to those of the first two. Figure V.9.1 displays the cyclic attachment data.

To extend the count, expand polynomial interactions about the Gaussian. Every interaction vertex contributes $\hbar_{\mathrm{m}}^{-1}$, every edge contributes $\hbar_{\mathrm{m}}$, and every closed index face contributes N. If a connected vacuum graph has V interaction vertices, E edges and F faces, then

$$V - E + F = 2 - 2g, \qquad \hbar_{\mathrm{m}}^{E-V} N^F = \hbar_{\mathrm{m}}^{2g-2} t_{\mathrm{m}}^F. \tag{V.9.6}$$

Masses, interaction coefficients and graph symmetry factors multiply this expression. They do not change its genus exponent. The cyclic ribbons are orientable because of the two Kronecker deltas in (V.9.3).

An inserted trace has the same cyclic index structure as a vertex but no factor $\hbar_{\mathrm{m}}^{-1}$. With n such insertions the closed surface obtained by filling all faces instead obeys

$$V + n - E + F = 2 - 2g, \qquad \hbar_{\mathrm{m}}^{E-V} N^F = \hbar_{\mathrm{m}}^{2g+n-2} t_{\mathrm{m}}^F. \tag{V.9.7}$$

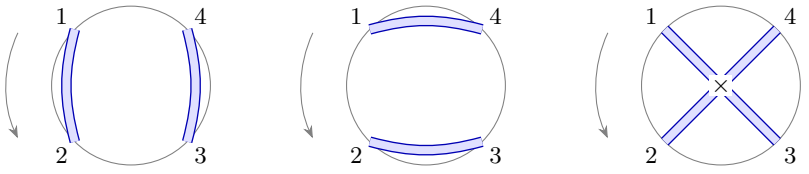


Figure V.9.1: Three contractions of the same cyclic trace. Thick bands join paired half-edges, whose cyclic order is fixed counterclockwise. The number F counts closed matrix-index lines after the ribbons are attached to the trace vertex and the faces are filled. Crossing in the last planar drawing represents a genus-one ribbon surface; it is not an interaction vertex. Every edge has covariance $\hbar_{\mathrm{m}}/m$.

Equivalently the inserted traces mark n boundaries before they are capped. Connected expectations select connected ribbon graphs. This explains the powers used later in stable recursion, but says nothing by itself about convergence after summing all graphs.

We now turn from individual pairings to their generating function. Define the random trace r, the scaled expectation R, and its planar coefficient R_0 by

$$r(x) = \operatorname{Tr} \frac{1}{x - M}, \qquad R(x) = \hbar_{\mathrm{m}} \langle r(x) \rangle, \qquad w_0(x) = \frac{R_0(x)}{t_{\mathrm{m}}}. \tag{V.9.8}$$

The formal large-x expansion follows by expanding each inverse:

$$w_0(x) = \sum_{k \geq 0} \frac{\mu_k}{x^{k+1}}, \qquad \mu_k = \lim_{N \to \infty} \frac{1}{N} \langle \operatorname{Tr} M^k \rangle, \qquad \mu_0 = 1. \tag{V.9.9}$$

Here the planar limit holds t_{m} fixed. It is also meaningful as extraction of the genus-zero ribbon coefficient in a formal series. Those are distinct ways to supply the expansion; an arbitrary convergent integral is not automatically accompanied by such an asymptotic expansion.

There is a short combinatorial derivation of the Gaussian answer. In a planar pairing of $2k$ cyclic factors, contract the first factor. The remaining factors on its two sides must pair within their own intervals, otherwise the ribbons cross. Summing over the length of the first interval gives

$$\mu_{2k} = c \sum_{j=0}^{k-1} \mu_{2j} \mu_{2(k-1-j)}, \qquad \mu_{2k+1} = 0, \qquad \mu_0 = 1. \tag{V.9.10}$$

The factor c combines the edge covariance with its planar index sum. Odd moments vanish under $M \mapsto -M$. Multiplying this recurrence by x^{-2k-1} and summing gives a

quadratic for the generating function:

$$cw_0(x)^2 - xw_0(x) + 1 = 0, \qquad w_0(x) = \frac{x - \sqrt{x^2 - 4c}}{2c}. \tag{V.9.11}$$

The square root is asymptotic to x at the chosen infinity. The other root grows as x/c and cannot generate moments with $\mu_0 = 1$. The recurrence or the binomial expansion gives the entire planar moment sequence,

$$\mu_{2k} = \frac{1}{k+1}\binom{2k}{k}c^k, \qquad w_0 = \frac{1}{x} + \frac{c}{x^3} + \frac{2c^2}{x^5} + \frac{5c^3}{x^7} + \frac{14c^4}{x^9} + \cdots. \tag{V.9.12}$$

The coefficient $2c^2$ is exactly the two planar pairings in (V.9.5).

For the real positive Gaussian the cut has a spectral meaning. The unit-mass planar density ρ is defined by $w_0(x) = \int \rho(\lambda)d\lambda/(x-\lambda)$. Let w_+ and w_- denote its upper and lower boundary values. On the upper lip of $[-2\sqrt{c}, 2\sqrt{c}]$ the selected square root is $+i\sqrt{4c - \lambda^2}$, so

$$\rho(\lambda) = \frac{w_-(\lambda) - w_+(\lambda)}{2\pi i} = \frac{\sqrt{4c - \lambda^2}}{2\pi c}, \qquad |\lambda| < 2\sqrt{c}. \tag{V.9.13}$$

It is zero outside this interval. This jump convention is essential: R_0 instead of w_0 would give a density of total mass t_{m}. The unit mass can be checked without the generating function. Substitute $\lambda = 2\sqrt{c}\,u$ and use the beta integral:

$$\int \lambda^{2k}\rho(\lambda)d\lambda = \frac{2(4c)^k}{\pi}B\left(k + \frac{1}{2}, \frac{3}{2}\right) = \frac{1}{k+1}\binom{2k}{k}c^k. \tag{V.9.14}$$

In particular $B(1/2, 3/2) = \pi/2$ gives normalization one. The density integral and the planar contraction recurrence therefore answer the same moment problem by different calculations.

We will keep $m = 3/2$ and $t_{\mathrm{m}} = 6$ as the running example. They give $c = 4$, so

$$\rho(\lambda) = \frac{\sqrt{16 - \lambda^2}}{8\pi}, \quad \operatorname{supp}\rho = [-4, 4], \quad (\mu_0, \ldots, \mu_8) = (1, 0, 4, 0, 32, 0, 320, 0, 3584). \tag{V.9.15}$$

For example $\mu_6 = 5(4)^3 = 320$; it is not the unit-variance value five. The cut shrinks when $t_{\mathrm{m}} \to 0$ at fixed m, eventually collapsing to a point. The limiting measure is well defined, but the collapsed curve will not be regular recursion data. Similarly $m = 0$ does not define this confining Gaussian reference.

The matrix integral has now produced both a topological count and a planar spectrum. To change the potential efficiently we need an identity that does not enumerate pairings individually. The next section derives that identity at the level of expectations. This will also separate it from an equation for a stationary eigenvalue configuration, a distinction needed before using matrix curves in Chapter 10 or in the local-CY constructions of Volume XVIII.

V.9.2 Loop equations

What fixes the curve when the matrix weight is no longer Gaussian? For the flat measure fixed above, unitary diagonalization converts the matrix integral into an eigenvalue integral, up to a normalization independent of the eigenvalues:

$$Z \;\propto\; \int \prod_{i=1}^{N} d\lambda_i \, \Delta(\lambda)^2 \exp\left[-\frac{1}{\hbar_{\mathrm{m}}} \sum_i V(\lambda_i)\right], \qquad \Delta = \prod_{i<j} (\lambda_i - \lambda_j). \tag{V.9.16}$$

The exponent two is the $\beta = 2$ Hermitian ensemble. The logarithm of Δ^2 makes coincident eigenvalues unfavorable, so an ensemble with a quadratic potential has a spread of eigenvalues even though its classical potential has a single minimum. This is the mechanism behind the semicircle.

Assume that integration by parts has no boundary term on the chosen contour. For a formal Gaussian expansion, Gaussian integration by parts supplies the corresponding algebraic statement order by order. Apply it to $(x - \lambda_i)^{-1}$ times the weight, summing over i:

$$0 = \left\langle \sum_i \frac{1}{(x-\lambda_i)^2} + 2 \sum_{i \neq j} \frac{1}{(x-\lambda_i)(\lambda_i - \lambda_j)} - \frac{1}{\hbar_{\mathrm{m}}} \sum_i \frac{V'(\lambda_i)}{x - \lambda_i} \right\rangle. \tag{V.9.17}$$

The first sign is positive because we differentiate with respect to λ_i, not x. The pair sum can be symmetrized before taking an expectation. Its contribution from a pair $i < j$ is

$$\frac{2}{\lambda_i - \lambda_j} \left(\frac{1}{x - \lambda_i} - \frac{1}{x - \lambda_j} \right) = \frac{2}{(x-\lambda_i)(x-\lambda_j)}. \tag{V.9.18}$$

Consequently the first two terms of (V.9.17) combine into $r(x)^2$ exactly. There is no remaining diagonal derivative term in this expectation identity.

To express the last term, subtract and add $V'(x)$. Define

$$\begin{aligned} P(x) &= \hbar_{\mathrm{m}} \left\langle \operatorname{Tr} \frac{V'(x) - V'(M)}{x - M} \right\rangle, \\ C_2(x,x') &= \langle r(x) r(x') \rangle - \langle r(x) \rangle \langle r(x') \rangle. \end{aligned} \tag{V.9.19}$$

For polynomial V', the divided difference in P is a polynomial; there is no singularity at an eigenvalue. Multiplying the identity by $\hbar_{\mathrm{m}}^2$ now gives

$$R(x)^2 + \hbar_{\mathrm{m}}^2 C_2(x,x) - V'(x) R(x) + P(x) = 0. \tag{V.9.20}$$

The connected term is part of the exact expectation equation. Dropping it is a planar approximation, justified by the formal genus count or by an independently supplied large-N expansion.

It is useful to see precisely why a saddle equation differs. A stationary configuration of the effective eigenvalue action obeys

$$V'(\lambda_i) = 2\hbar_{\mathrm{m}} \sum_{j \neq i} \frac{1}{\lambda_i - \lambda_j}. \tag{V.9.21}$$

Multiply this by $\hbar_{\mathrm{m}}/(x-\lambda_i)$ and sum, but do not perform integration by parts. With $\widehat{R}=\hbar_{\mathrm{m}}r$ and the analogous unevaluated polynomial $\widehat{P}$ one obtains

$$\widehat{R}^2+\hbar_{\mathrm{m}}\partial_x\widehat{R}-V'\widehat{R}+\widehat{P}=0. \tag{V.9.22}$$

Indeed $\partial_x r=-\sum_i(x-\lambda_i)^{-2}$ restores the diagonal term that was absent from the pair sum alone. Equation (V.9.22) concerns a stationary configuration; (V.9.20) concerns a normalized expectation. Replacing the connected fluctuation by this derivative would change the finite-N problem. Both equations can have the same leading planar curve.

Suppose now that $R=R_0+\hbar_{\mathrm{m}}^2R_1+\cdots$ and that the corresponding expansion exists for P and C_2. At leading order (V.9.20) becomes an algebraic equation. The half-force variable is defined by

$$R_0^2-V'R_0+P_0=0, \qquad y=\frac{V'}{2}-R_0, \qquad y^2=\frac{V'^2}{4}-P_0. \tag{V.9.23}$$

For the Gaussian, $P=mt_{\mathrm{m}}$ is exact, and this recovers (V.9.11). For a higher potential, coefficients of P_0 include moments not fixed until a filling sector and a physical branch have been chosen. The curve equation is therefore the start of a solution, rather than a contour prescription.

We work out an even quartic example in a regime with a regular positive one-cut solution:

$$V(x)=\frac{m}{2}x^2+\frac{g}{4}x^4, \qquad m,t_{\mathrm{m}}>0, \quad g\geq 0. \tag{V.9.24}$$

Assume the cut is $[-\sqrt{s},\sqrt{s}]$, with $s>0$. Evenness and the large-x degree suggest the ansatz

$$2y=(gx^2+b)\sqrt{x^2-s}, \qquad R_0=\frac{1}{2}\left(mx+gx^3-(gx^2+b)\sqrt{x^2-s}\right). \tag{V.9.25}$$

The square root again approaches x on the physical sheet. Expand it before fixing b and s:

$$(gx^2+b)\sqrt{x^2-s}=gx^3+\left(b-\frac{gs}{2}\right)x-\left(\frac{bs}{2}+\frac{gs^2}{8}\right)x^{-1}+O(x^{-3}). \tag{V.9.26}$$

The unwanted x term in R_0 vanishes when $b=m+gs/2$. Its x^{-1} term must be t_{m}, giving

$$b=m+\frac{gs}{2}, \qquad \frac{ms}{4}+\frac{3gs^2}{16}=t_{\mathrm{m}}, \qquad s=\frac{8t_{\mathrm{m}}}{m+\sqrt{m^2+12gt_{\mathrm{m}}}}. \tag{V.9.27}$$

Rationalizing the positive quadratic root gives the last expression. Unlike a formula with g in the denominator, it displays the Gaussian limit $s\to 4t_{\mathrm{m}}/m$ without cancellation of two nearly equal terms. The other algebraic root cannot describe a positive real cut in this regime.

The jump of this resolvent gives the normalized density

$$\rho(\lambda)=\frac{g\lambda^2+b}{2\pi t_{\mathrm{m}}}\sqrt{s-\lambda^2}, \qquad -\sqrt{s}<\lambda<\sqrt{s}. \tag{V.9.28}$$

It is nonnegative because $b > 0$. Its integral is one by (V.9.27). To check that assertion directly, the two required integrals are

$$\int_{-\sqrt{s}}^{\sqrt{s}} \sqrt{s-\lambda^2}\, d\lambda = \frac{\pi s}{2}, \qquad \int_{-\sqrt{s}}^{\sqrt{s}} \lambda^2 \sqrt{s-\lambda^2}\, d\lambda = \frac{\pi s^2}{8}. \tag{V.9.29}$$

They give $bs/(4t_{\mathrm{m}}) + gs^2/(16t_{\mathrm{m}}) = 1$ after substituting b. The same beta integrals generate higher moments. This is one way to verify the large-x conditions by real spectral data rather than by another expansion of the same square root.

The polynomial in the Ward equation has an independent expression. For $V' = mx + gx^3$, the divided difference is $m + g(x^2 + xM + M^2)$. The odd expectation vanishes, so if M_2 denotes the coefficient of x^{-3} in R_0, then

$$P_0(x) = mt_{\mathrm{m}} + gM_2 + gt_{\mathrm{m}}x^2, \qquad M_2 = \frac{ms^2 + gs^3}{16}. \tag{V.9.30}$$

The second formula follows either from the x^{-3} term of the ansatz or from $t_{\mathrm{m}} \int \lambda^2 \rho\, d\lambda$. It closes the constant coefficient of P_0 without guessing it.

Take $m = 2$, $g = 1$, $t_{\mathrm{m}} = 5$. The endpoint equation is $s/2 + 3s^2/16 = 5$, whose positive root is $s = 4$, and $b = 4$. Thus $M_2 = (2 \cdot 16 + 64)/16 = 6$ and

$$P_0 = 5x^2 + 16, \qquad (x^3 + 2x)^2 - 4(5x^2 + 16) = (x^2 + 4)^2(x^2 - 4). \tag{V.9.31}$$

To recover several moments without a long binomial expansion, insert $R_0 = \sum M_k x^{-k-1}$ into its quadratic. The constant term fixes $M_2 = 6$; the next three even powers give

$$\begin{aligned} M_4 &= M_0^2 - 2M_2 = 25 - 12 = 13, \\ M_6 &= 2M_0M_2 - 2M_4 = 60 - 26 = 34, \\ M_8 &= 2M_0M_4 + M_2^2 - 2M_6 = 130 + 36 - 68 = 98. \end{aligned} \tag{V.9.32}$$

Here $M_0 = 5$ and every odd M_k vanishes. In particular this resolvent is $5/x + 6/x^3 + 13/x^5 + 34/x^7 + 98/x^9 + \cdots$, not a unit-mass resolvent. Its normalized density has moments $M_k/5$.

The factor $(x^2 + 4)^2$ in (V.9.31) is a warning about geometry. Its double zeros are not additional simple branch points of the normalized double cover. In this one-cut solution we may use $x = z + 1/z$ and $2y = (x^2 + 4)(z - 1/z)$ on a sphere. The only ramification points of x are still $z = \pm 1$. The plane equation alone has concealed this smooth normalization, the infinity sheet, and the contour defining the total filling. These are the extra data we now supply. They are related to the period vocabulary of Chapter 3, but are not fixed by that vocabulary.

V.9.3 Branch points and local data

A residue is computed in a local coordinate on a smooth curve. Which curve and coordinate does the matrix solution provide? Return to the Gaussian and set $a =$

$\sqrt{t_{\rm m}/m} > 0$. Its normalized compact curve is a sphere $\Sigma = \mathbb{P}^1$, carrying meromorphic functions

$$x(z) = a(z + z^{-1}), \qquad y(z) = \frac{ma}{2}(z - z^{-1}), \qquad \bar{z} = z^{-1}. \tag{V.9.33}$$

They obey $y^2 = m^2(x^2 - 4a^2)/4$ and satisfy $x(\bar{z}) = x(z)$, $y(\bar{z}) = -y(z)$. The two points over a generic x are z and $1/z$. The infinity $z \to \infty$ is physical because

$$R_0(z) = \frac{mx(z)}{2} - y(z) = \frac{ma}{z} \sim \frac{t_{\rm m}}{x(z)}. \tag{V.9.34}$$

At $z = 0$ the same expression diverges. That point is the other infinity on the compact curve, rather than a finite eigenvalue.

The projection loses a local inverse when dx vanishes. Differentiating (V.9.33) gives

$$dx = a(1 - z^{-2})dz, \qquad dy = \frac{ma}{2}(1 + z^{-2})dz, \qquad d\bar{z} = -\frac{dz}{z^2}. \tag{V.9.35}$$

For $e = \pm 1$ we have

$$x(e) = 2ae, \qquad x'(e) = 0, \qquad x''(e) = 2ae, \qquad y'(e) = ma. \tag{V.9.36}$$

A point e of Σ is a ramification point; $x(e)$ is its branch value in the base plane. Locally $u = z - e$ satisfies

$$x(z) - 2ae = ae\,u^2 + O(u^3), \qquad y(z) = ma\,u + O(u^2), \qquad \bar{z} = e - u + O(u^2). \tag{V.9.37}$$

The two local inverse branches meet here. The conditions that dx have a simple zero and that dy be nonzero at that zero are the regularity conditions used below. They hold for both Gaussian endpoints when $m, t_{\rm m} > 0$.

Figure V.9.2 distinguishes these points from their images. For the running example $a = 2$, so the branch values are $-4, 4$ and the prefactor in y is $ma/2 = 3/2$. The radius of the cut has changed with $t_{\rm m}/m$, while the ramification preimages remain $-1, 1$. At $t_{\rm m} = 0$ the map loses this regular structure. It is not permissible simply to insert $a = 0$ into a recursion requiring simple ramification.

The next object is a symmetric bidifferential $B(p, q)$ on Σ. It has a unit double pole on the diagonal, no residue and no other poles; on higher-genus curves we also choose its vanishing compact A periods. We use the ordinary normalized choice, conventionally called $\kappa = 0$. On the sphere there are no compact handle periods to impose, and the answer is

$$B(p, q) = \frac{dp\,dq}{(p - q)^2}. \tag{V.9.38}$$

It is regular at an infinity in either variable away from the diagonal. For example $p = 1/v$ turns it into $-dv\,dq/(1 - qv)^2$. The unit coefficient is fixed, not another adjustable matrix coupling. In the residue calculation one evaluates both arguments at functions of the same point. The result is a quadratic differential:

$$B(q, \bar{q}) = \frac{dq\,d(1/q)}{(q - 1/q)^2} = -\frac{dq^2}{q^2(q - 1/q)^2} = -\frac{dq^2}{(q^2 - 1)^2}. \tag{V.9.39}$$

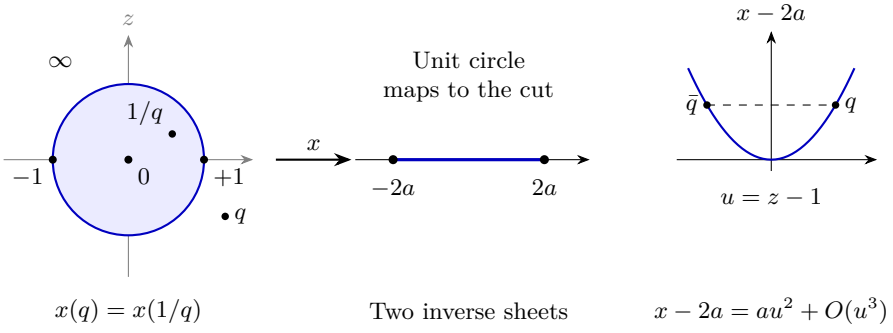


Figure V.9.2: The normalized Gaussian cover. Points z and $1/z$ on the sphere have the same base coordinate x. Its unit circle maps to the cut; $|z| > 1$ contains the physical infinity and $|z| < 1$ the other infinity. Ramification points $z = \pm 1$ map to the endpoints $x = \pm 2a$. The right panel shows the local quadratic projection near $z = 1$; the two inverse branches are exchanged, not identified as points of the smooth curve.

Treating $\bar{q}$ as an independent variable after this substitution would lose the negative derivative. The sign will enter both of our stable examples.

A curve also needs its filling data. Let A_{ccw} enclose the whole cut counterclockwise in the physical x sheet. Its upper lip goes from the right endpoint to the left endpoint. Shrinking the contour onto the cut gives

$$\begin{aligned} \frac{1}{2\pi i}\oint_{A_{\mathrm{ccw}}} R_0\,dx &= \frac{1}{2\pi i}\int_{-2a}^{2a}(R_{0,-} - R_{0,+})\,d\lambda \\ &= t_{\mathrm{m}}\int_{-2a}^{2a}\rho(\lambda)d\lambda = t_{\mathrm{m}}. \end{aligned} \tag{V.9.40}$$

This is a full contour, including both lips. The polynomial $V'/2$ has zero contour integral, so

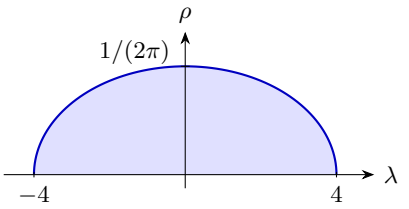
$$t_{\mathrm{m}} = -\frac{1}{2\pi i}\oint_{A_{\mathrm{ccw}}} y\,dx. \tag{V.9.41}$$

A convention with a positive period of this half-force y uses the reversed contour. A source using twice this y also changes the factor. Both choices must be translated before comparing period formulas.

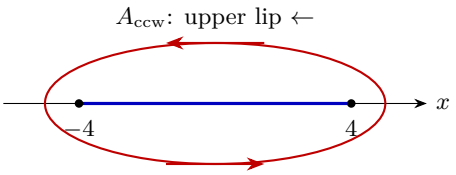
There is an independent coordinate calculation of the same period. Using (V.9.34) and (V.9.35) gives

$$R_0\,dx = t_{\mathrm{m}}(z^{-1} - z^{-3})dz, \qquad \frac{1}{2\pi i}\oint_{|z|=r>1} R_0\,dx = t_{\mathrm{m}}. \tag{V.9.42}$$

The large circle is oriented positively and deforms toward the unit circle on the physical sheet. The residue of the expression at zero is t_{m}; its residue at the other infinity is the negative of that value, as required on a compact sphere. One cannot contract the contour freely when poles and punctures are retained. Nevertheless it is not a



Unit-mass density, $c = 4$



Physical infinity sheet

Figure V.9.3: Actual Gaussian density for $m = 3/2$, $t_{\mathrm{m}} = 6$, together with the full physical-sheet contour. The density has unit area and height $1/(2\pi)$ at the origin. The cut endpoints are $-4, 4$. The upper lip of the counterclockwise contour runs right to left; the lower lip runs left to right, giving $R_{0,-} - R_{0,+}$ in the filling integral. The diagram uses the physical infinity sheet throughout.

compact handle cycle: $H_1(\mathbb{P}^1) = 0$. This distinction prevents importing an independent symplectic handle pair from the compact-period discussion of Chapter 3.

For several regular cuts the corresponding convention is

$$t_i = \frac{1}{2\pi i} \oint_{A_{i,\mathrm{ccw}}} R_0\, dx, \qquad \sum_i t_i = t_{\mathrm{m}}, \qquad t_i = \hbar_{\mathrm{m}} N_i \quad \text{in a fixed-occupation sector.} \tag{V.9.43}$$

The contour choice supplies information not contained in the polynomial Ward equation. The integers N_i describe occupations at finite matrix size; fixed fillings in a large-N expansion mean fixed scaled parameters or occupation ratios as N varies, not holding all these integers and N separately constant.

The data for recursion are now explicit: the smooth curve, the two meromorphic functions, their local conjugation, the normalized bidifferential and the filling sector. Figure V.9.3 explains the orientation behind the positive filling six in our example. None of these operations fixes a Calabi–Yau holomorphic 3-form or its noncompact-period regulator. Chapter 4 treats those normalizations in the mirror setting. Here they perform the more limited job of making the next branch residues unambiguous.

V.9.4 Topological recursion

How do local branch neighborhoods recover higher-topology matrix correlators? The recursion answers this question for a specified set of curve data. Its general relation to formal matrix integrals is a cited theorem, with hypotheses stated below. We first make its operation visible by computing two complete Gaussian examples and comparing them with the Ward identity and finite Wick contractions.

We write $W_n^{(g)}$ for a meromorphic n-form on Σ^n. The stable range is $2g - 2 + n > 0$. We use the source convention

$$W_1^{(0)} = 0, \qquad W_2^{(0)}(p_1, p_2) = B(p_1, p_2), \qquad 2g - 2 + n > 0 \text{ for stable correlators.} \tag{V.9.44}$$

The zero here is a recursion initial value. The physical disc $R_0\,dx$ is supplied separately and is nonzero. Inserting $y\,dx$ in place of the zero in the recursive sum would define a different formula unless all unstable terms were correspondingly removed. In the formal matrix sector the relation to connected trace expectations has the genus powers derived in (V.9.7):

$$\begin{aligned}\langle r(x_1)\cdots r(x_n)\rangle_c = \delta_{n,1}\frac{R_0(x_1)}{\hbar_{\mathrm m}} - \frac{\delta_{n,2}}{(x_1-x_2)^2} \\ + \sum_{g\ge 0}\hbar_{\mathrm m}^{2g+n-2}\frac{W_n^{(g)}(p_1,\dots,p_n)}{\prod_{i=1}^n dx(p_i)}, \qquad x_i = x(p_i).\end{aligned} \tag{V.9.45}$$

The second term is present only for $n=2$. The disc term and that Cauchy subtraction are exceptional; stable forms use the displayed genus power directly. Dividing a form by the product of differentials here means taking its scalar coefficient in the chosen x_i charts.

For q near a ramification point, let $\bar q$ be its other local preimage at the same x. Define the kernel by a short local integral with the direction shown:

$$K(p,q) = \frac{\frac12\displaystyle\int_q^{\bar q} B(p,\xi)}{(y(q)-y(\bar q))dx(q)}. \tag{V.9.46}$$

It is a one-form in p divided by a one-form in q. The integral stays inside the branch neighborhood. Its direction fixes a sign; reversing it while leaving the denominator unchanged reverses the computed residues.

Let $I=\{p_1,\dots,p_n\}$. With an ordered splitting of its labeled arguments the recursion is

$$\begin{aligned}W_{n+1}^{(g)}(p,I) = \sum_e \operatorname*{Res}_{q=e} K(p,q)\Bigg[W_{n+2}^{(g-1)}(q,\bar q,I) \\ + \sum_{h=0}^{g}{}'\sum_{J\subseteq I} W_{|J|+1}^{(h)}(q,J)W_{n-|J|+1}^{(g-h)}(\bar q, I\setminus J)\Bigg].\end{aligned} \tag{V.9.47}$$

The first term is absent when $g=0$. The prime removes factors $W_1^{(0)}$; equivalently they vanish under (V.9.44). Both J and its complement occur when distinct ordered terms survive. The first term reduces the genus by one and supplies two local arguments. The second term splits the other arguments and the genus between two correlators. Products in square brackets are quadratic differentials in q after pullback, so multiplication by K leaves a one-form in the variable whose residue is taken.

The sphere Gaussian data make the local integral elementary. Since $B(p,\xi) = dp\,d\xi/(p-\xi)^2$, its antiderivative is $dp/(p-\xi)$. Also $(y(q)-y(1/q))dx(q) = t_{\mathrm m}(q-1/q)(1-q^{-2})dq$. Therefore

$$K(p,q) = \frac{\dfrac{1}{p-1/q} - \dfrac{1}{p-q}}{2t_{\mathrm m}(q-1/q)(1-q^{-2})}\frac{dp}{dq}. \tag{V.9.48}$$

The combination $ma^2 = t_{\rm m}$ explains why m has disappeared in this uniformizer. It will reappear when we return to the x coordinate.

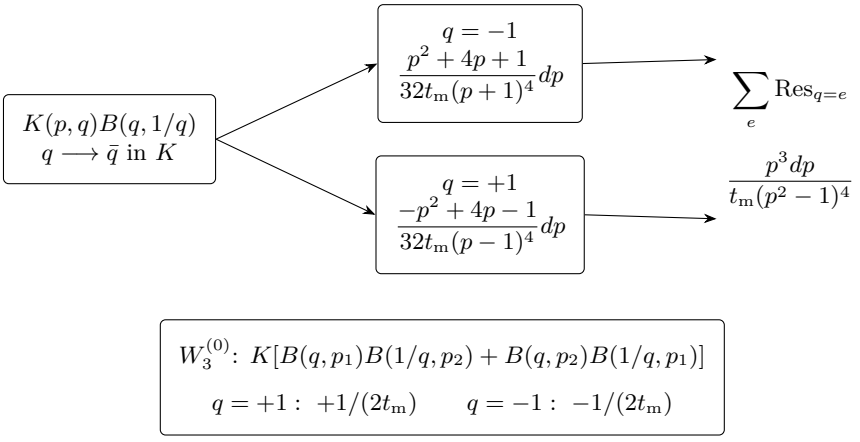


Figure V.9.4: The first stable residue mechanisms with the fixed Gaussian data. For $W_1^{(1)}$ the kernel multiplies the pulled-back $B(q,1/q)$ and the two branch residues add. For $W_3^{(0)}$ there are two ordered products, related by exchange of the external arguments. The displayed weights are the actual coefficients of $\prod_i (p_i - e)^{-2} dp_1 dp_2 dp_3$, with $e = +1, -1$. The kernel integral runs from q to $\bar{q}$ in both cases.

Start with the genus-one one-form. Only the nonseparating term remains in (V.9.47):

$$W_1^{(1)}(p) = \sum_{e=\pm 1} \operatorname*{Res}_{q=e} K(p,q)B(q,1/q). \tag{V.9.49}$$

The negative sign in (V.9.39) and the difference of the two fractions in the kernel both matter. Simplifying their product before expanding gives

$$K(p,q)B(q,1/q) = \frac{q^3\,dp\,dq}{2t_{\rm m}(q^2-1)^3(pq-1)(p-q)}. \tag{V.9.50}$$

There is a third-order pole at each branch point for generic external p. Its residue cannot be found from the leading singular term alone.

To carry out the local calculation, remove that pole at $e = \pm 1$:

$$H_e(q) = \frac{q^3}{2t_{\rm m}(q+e)^3(pq-1)(p-q)}, \qquad \operatorname*{Res}_{q=e} KB = \frac{1}{2}H_e''(e)\,dp. \tag{V.9.51}$$

This is simply the coefficient of $(q-e)^2$ in the Taylor expansion of H_e. A convenient way to take the two derivatives is to use $L_e = H_e'/H_e$. Direct differentiation gives

$$\begin{aligned} H_e(e) &= \frac{1}{16t_{\rm m}e(p-e)^2}, \qquad & L_e(e) &= \frac{e}{2}, \\ L_e'(e) &= -\frac{9}{4} + \frac{p^2+1}{(p-e)^2}, \qquad & \frac{1}{2}H_e''(e) &= \frac{H_e(e)}{2}\left[-2 + \frac{p^2+1}{(p-e)^2}\right]. \end{aligned} \tag{V.9.52}$$

For example $L_e(q) = 3/q - 3/(q+e) - p/(pq-1) + 1/(p-q)$, so every term in these evaluations follows from a rational derivative. Substitution of $e = -1$ and $e = +1$ yields the two distinct answers

$$\begin{aligned} \operatorname*{Res}_{q=-1} KB &= \frac{p^2+4p+1}{32t_{\mathrm{m}}(p+1)^4}\,dp, \\ \operatorname*{Res}_{q=+1} KB &= \frac{-p^2+4p-1}{32t_{\mathrm{m}}(p-1)^4}\,dp. \end{aligned} \tag{V.9.53}$$

Putting them over a common denominator gives the numerator identity

$$\begin{aligned} &(p^2+4p+1)(p-1)^4 \\ &\qquad + (-p^2+4p-1)(p+1)^4 = 32p^3. \end{aligned} \tag{V.9.54}$$

Thus the complete form is

$$W_1^{(1)}(p) = \frac{p^3}{t_{\mathrm{m}}(p^2-1)^4}\,dp. \tag{V.9.55}$$

It has poles only at the branch points and decays at physical infinity. Figure V.9.4 keeps the two contributions separate; omitting either one would spoil this full rational function.

We can test it by a route that never evaluates a recursion residue. The planar connected two-resolvent uses the Cauchy subtraction

$$C_2^{(0)}(x,x')\,dx\,dx' = B(p,p') - \frac{dx\,dx'}{(x-x')^2}, \qquad x = x(p), \quad x' = x(p'). \tag{V.9.56}$$

The subtraction cancels the diagonal double pole when viewed as a matrix connected expectation. It is the reason that $W_2^{(0)} = B$ is not itself the scalar two-resolvent. Substituting the Gaussian uniformization and simplifying gives

$$C_2^{(0)}(x,x') = \frac{1}{2(x-x')^2}\left[\frac{xx'-4c}{\sqrt{x^2-4c}\sqrt{x'^2-4c}} - 1\right], \qquad C_2^{(0)}(x,x) = \frac{c}{(x^2-4c)^2}. \tag{V.9.57}$$

For the diagonal limit set $x' = x + \delta$. The expression inside square brackets starts as $2c\delta^2/(x^2-4c)^2$; both its constant and linear terms vanish. This makes the coincident value finite away from the endpoints.

For the Gaussian $P = mt_{\mathrm{m}}$ has no genus-one coefficient. The $\hbar_{\mathrm{m}}^2$ term of the exact Ward identity is therefore

$$(2R_0 - mx)R_1 + C_2^{(0)}(x,x) = 0, \qquad R_1(x) = \frac{t_{\mathrm{m}}}{m^2(x^2-4c)^{5/2}}. \tag{V.9.58}$$

Here $2y = m\sqrt{x^2-4c}$, so this also says $2yR_1 = C_2^{(0)}$. On the physical branch $\sqrt{x^2-4c} = a(p-1/p)$. Multiplying the last expression by $dx = a(1-p^{-2})dp$ gives

$$R_1(x(p))dx(p) = \frac{t_{\mathrm{m}}}{m^2a^4}\frac{p^3}{(p^2-1)^4}dp = W_1^{(1)}(p). \tag{V.9.59}$$

This verifies the entire one-form, not only its first asymptotic coefficient. It also identifies the matrix observable computed by the residue.

For a finite comparison with entrywise contractions, expand the answer at infinity:

$$R_1(x) = \frac{t_{\mathrm{m}}}{m^2 x^5}\left[1 + \frac{10c}{x^2} + \frac{70c^2}{x^4} + \frac{420c^3}{x^6} + O(x^{-8})\right]. \tag{V.9.60}$$

For a single trace of $2k$ factors, a genus-one pairing has $E = k$, $V = 1$ and $F = k - 1$. After multiplying the trace expectation by $\hbar_{\mathrm{m}}$ its coefficient of $\hbar_{\mathrm{m}}^2$ is t_{m}^{k-1}/m^k times the number of such pairings. The finite numbers for lengths $4, 6, 8, 10$ are respectively $1, 10, 70, 420$, exactly the numbers in (V.9.60). The length-four result was already obtained explicitly in (V.9.4).

For clarity, those counts can be reconstructed by a permutation calculation. Label all factors and let γ advance once around each trace. A pairing is a fixed-point-free involution α; its index faces are the cycles of $\gamma\alpha$. Count these cycles and apply $V - E + F = 2 - 2g$, retaining only pairings connecting all trace vertices for a cumulant. This gives the following finite census:

Trace length	Total pairings	Genus zero	Genus one
4	3	2	1
6	15	5	10
8	105	14	70
10	945	42	420

Higher genera account for the remaining length-eight and length-ten pairings. This is a finite check of the displayed coefficients, rather than a proof of the recursion for arbitrary length or genus. At our nonunit parameters the coefficients of $x^{-1}, \dots, x^{-11}$ in R_1 are

$$(0, 0, 0, 0, 8/3, 0, 320/3, 0, 8960/3, 0, 71680). \tag{V.9.61}$$

For instance the x^{-9} coefficient is $70t_{\mathrm{m}}^3/m^4 = 70 \cdot 216 \cdot 16/81 = 8960/3$. It belongs to a genus-one correction to R, whereas the corresponding planar coefficient in w_0 was 3584. Mixing these two moment normalizations would obscure the comparison.

The other first stable object is $W_3^{(0)}$. Only the two ordered splitting terms survive:

$$W_3^{(0)}(p_0, p_1, p_2) = \sum_{e=\pm 1} \operatorname*{Res}_{q=e} K(p_0, q)\big[B(q, p_1)B(1/q, p_2) + B(q, p_2)B(1/q, p_1)\big]. \tag{V.9.62}$$

To compute their residues, take $q = e + u$. Equations (V.9.37) and (V.9.48) give

$$\begin{aligned} K(p_0, q) &= -\frac{1}{4t_{\mathrm{m}} e\, u(p_0 - e)^2}\frac{dp_0}{dq} + O(1)\frac{dp_0}{dq}, \\ B(q, p_1)B(1/q, p_2) &= -\frac{dq^2\, dp_1 dp_2}{(p_1 - e)^2(p_2 - e)^2} + O(u)dq^2 dp_1 dp_2. \end{aligned} \tag{V.9.63}$$

The negative pullback sign cancels the kernel sign. The ordered sum supplies a factor

two. Therefore the residue at e is $dp_0dp_1dp_2/[2t_{\rm m}e\prod_{i=0}^{2}(p_i-e)^2]$, and the full result is

$$W_3^{(0)}(p_0,p_1,p_2)=\frac{dp_0dp_1dp_2}{2t_{\rm m}}\left[\frac{1}{\prod_{i=0}^{2}(p_i-1)^2}-\frac{1}{\prod_{i=0}^{2}(p_i+1)^2}\right]. \tag{V.9.64}$$

The answer is symmetric in all three external points even though the kernel singled out p_0. Equivalently one obtains the same weights by taking residues of $\prod_i B(q,p_i)/(dx(q)dy(q))$: $x''(e)y'(e)=2t_{\rm m}e$. This is a check of the ordered sum and its factor, not an additional physical correspondence.

A direct connected Wick comparison tests a different observable from R_1. For three traces of length two there are eight connected pairings. Each trace must send one factor to each of the other two traces, so choosing which labeled factor follows one specified edge at each vertex gives $2^3=8$. Every such pairing has $E=3$, $V=3$, $F=2$ and $g=0$. Consequently

$$\left\langle(\operatorname{Tr}M^2)^3\right\rangle_c=\hbar_{\rm m}\frac{8t_{\rm m}^2}{m^3}\quad\text{at its planar connected order.} \tag{V.9.65}$$

One can extract precisely this coefficient from (V.9.64). On physical infinity set $u=1/x$. Solving the quadratic map gives $p^{-1}=au+a^3u^3+O(u^5)$, whence

$$\frac{dp/dx}{(p-e)^2}=\frac{a}{x^2}+\frac{2ea^2}{x^3}+O(x^{-4}),\qquad [x_0^{-3}x_1^{-3}x_2^{-3}]\frac{W_3^{(0)}}{dx_0dx_1dx_2}=\frac{8a^6}{t_{\rm m}}=\frac{8t_{\rm m}^2}{m^3}. \tag{V.9.66}$$

The first sign in the expansion is positive because both dp/dx and $(p-e)^2$ are positive on large positive real p. The difference of the two branch products cancels terms of odd total matrix degree and retains this even-degree coefficient. At $m=3/2, t_{\rm m}=6$ its value is $256/3$. Other finite comparisons give $2t_{\rm m}/m^2$ for lengths $(2,1,1)$ and $12t_{\rm m}^2/m^3$ for $(3,2,1)$.

We can now state the precise boundary of the all-orders statement. For polynomial formal one-matrix sectors, the cited formal matrix-model theorem identifies the fixed-filling coefficients with the $\kappa=0$ curve invariants, with the source's separate definitions for the exceptional free energies. Its Gaussian-block construction expands about chosen occupied critical points X_i, with

$$V'(X_i)=0,\qquad V''(X_i)\neq 0\quad(N_i>0),\qquad \hbar_{\rm m}=T/N,\qquad t_i=T\frac{N_i}{N}. \tag{V.9.67}$$

The nonzero Hessian gives an invertible reference covariance. The expansion is formal in T, organized into genus coefficients at the specified fillings. Separately, the finite-filling spectral curve used in the regular residue formula must have simple zeros of dx and nonzero dy there. We use this polynomial theorem as a sourced mathematical result. The general all-orders proof is not supplied by the finite calculations above, and no extension to arbitrary convergent integrals or critical double-scaling limits is assumed.

The distinction between the two regularity requirements has a concrete example. For the pure quartic $V=x^4/4$ the real integral converges, but its occupied classical critical point at zero has $V''(0)=0$. Its finite-$t_{\rm m}>0$ one-cut curve nevertheless has

$$s=4\sqrt{t_{\rm m}/3},\qquad b=s/2,\qquad 2y=(x^2+s/2)\sqrt{x^2-s}. \tag{V.9.68}$$

Parameterize $x = \sqrt{s}\,(z + z^{-1})/2$. At $z = \pm 1$, $x^2 = s$ and $y'(z) = 3s^{3/2}/4 \neq 0$. Thus the branch neighborhoods are regular, although this is not the nondegenerate Gaussian reference required by (V.9.67). A theorem about that reference cannot be justified solely by seeing a regular finite-t_{m} curve. Degenerate references need their own construction.

Finally, $W_1^{(1)}$ is a one-form correlator, not the genus-one free energy F_1. A variation with respect to a potential can relate correlators to free-energy derivatives, but integration requires normalization information. Genus zero and genus one have their own exceptional free-energy definitions; the stable residue formula alone does not fix them. Chapter 5's nonholomorphic BCOV amplitudes also carry different geometric and boundary data. A similar splitting of surfaces does not identify those amplitudes with the meromorphic objects calculated here. We have a worked tool for the formal matrix sector and applications in Volume XVIII, with its limits visible.

V.9.5 Which partition function?

The recursion has produced numbers and meromorphic forms, but which partition function do they describe? Four objects enter at different stages. A formal fixed-filling matrix expansion starts from a reference covariance and occupations. Recursion starts from (Σ, x, y, B) and its branch and cycle choices. A convergent matrix integral additionally specifies an integration chain and measure. A protected physical coupling additionally needs a string embedding and an identification of observables. We work through the missing information rather than identifying these four objects by their use of the word partition function.

First consider absolute normalization. If the convention for formal logarithmic coefficients is

$$\log Z = \sum_{g \geq 0} \hbar_{\mathrm{m}}^{2g-2} F_g^{\log}, \qquad F = -\log Z \quad \text{in the cited curve convention,} \tag{V.9.69}$$

then the coefficients called F_g in those two conventions have opposite signs in a common measure and parameter frame. Moreover, a multiplicative factor independent of the potential changes the free energy without changing the normalized trace expectations:

$$\widetilde{Z} = C(\hbar_{\mathrm{m}}, N) Z, \qquad \langle \mathcal{O} \rangle_{\widetilde{Z}} = \langle \mathcal{O} \rangle_Z, \qquad \log \widetilde{Z} = \log Z + \log C. \tag{V.9.70}$$

The resolvent cannot determine C. Gaussian volume factors, division by a group volume, and exceptional low-genus definitions therefore matter when making a partition-function comparison. They were not needed for the normalized calculations of the preceding sections.

Second, a formal expansion about one sector does not select a convergent chain. A generalized scalar chain has the form $\gamma = \sum_i c_i \gamma_i$ with complex coefficients and convergent ends. Its integral is defined linearly. For eigenvalues the corresponding

expansion separates occupation components:

$$\begin{aligned} Z_\gamma &= \frac{1}{N!}\int_{\gamma^N}\prod_j d\lambda_j\,\Delta(\lambda)^2 e^{-\sum_j V(\lambda_j)/\hbar_{\mathrm{m}}} \\ &= \sum_{\sum_i N_i=N}\left(\prod_i c_i^{N_i}\right) Z_{N_1,\dots,N_d}. \end{aligned} \tag{V.9.71}$$

Here $Z_{N_1,\dots,N_d}$ uses the product chain with N_i eigenvalues on γ_i and includes $1/\prod_i N_i!$. For a complex chain this is an oriented holomorphic integral, not a positive probability measure. Each component satisfies the same integration-by-parts equations when the boundary terms vanish. Those equations do not fix the coefficients c_i. In applying a large-N genus expansion to convergent components one must supply a separate topological-expansion hypothesis; convergence itself is not that hypothesis.

A scalar example isolates what perturbation theory misses. Assume two nondegenerate critical points x_0, x_1 of a polynomial V and independently specified convergent steepest-descent chains $\mathcal{J}_0, \mathcal{J}_1$ in a non-Stokes coupling sector. Let $V_j = V(x_j)$ and suppose

$$V'(x_j) = 0, \qquad V''(x_j) \neq 0, \qquad \operatorname{Re}\frac{V_1 - V_0}{\hbar_{\mathrm{m}}} > 0. \tag{V.9.72}$$

We assume these chains exist with the stated descent and dominance properties. This is a conditional example, not a construction of global chains for every matrix potential. Near x_j the Taylor expansion is

$$V(x_j + \xi) = V_j + \frac{1}{2}V''(x_j)\xi^2 + O(\xi^3). \tag{V.9.73}$$

Rescale ξ by $\sqrt{\hbar_{\mathrm{m}}}$ along the chosen descent direction. Its Gaussian integral gives

$$I_j = \int_{\mathcal{J}_j} e^{-V(x)/\hbar_{\mathrm{m}}}dx \sim e^{-V_j/\hbar_{\mathrm{m}}}\sqrt{\frac{2\pi\hbar_{\mathrm{m}}}{V''(x_j)}}\,(A_j + O(\hbar_{\mathrm{m}}))\,. \tag{V.9.74}$$

The nonzero A_j includes the oriented chain phase and the square-root choice. Odd local Gaussian moments vanish, so the expansion after the leading square root proceeds in integer powers under these saddle assumptions. The chain sum has a relative correction

$$\frac{I_1}{I_0} \sim \frac{A_1}{A_0}\sqrt{\frac{V''(x_0)}{V''(x_1)}}\,e^{-(V_1-V_0)/\hbar_{\mathrm{m}}}\,(1 + O(\hbar_{\mathrm{m}}))\,. \tag{V.9.75}$$

Thus $\Gamma = \mathcal{J}_0$ and $\Gamma' = \mathcal{J}_0 + \mathcal{J}_1$ have the same formal power series in their dominant sector and different exact integrals. Along a fixed ray with positive real action gap, the correction is smaller than every power of the small coupling. For example, if the ray parameter is $\epsilon > 0$ and the real gap is $3/(2\epsilon)$, then

$$\lim_{\epsilon\to 0^+}\epsilon^{-k}e^{-3/(2\epsilon)} = 0 \quad \text{for every fixed } k, \qquad e^{-3/(2\cdot 0.1)} = e^{-15} \simeq 3.06\times 10^{-7}. \tag{V.9.76}$$

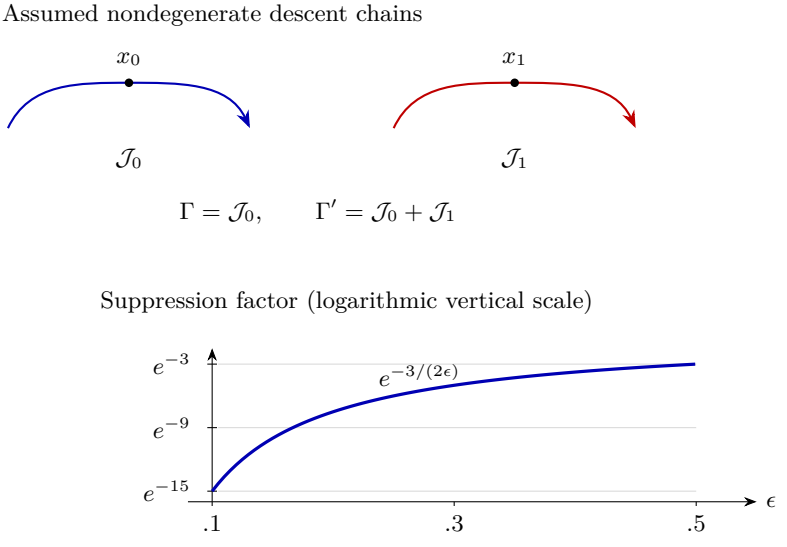


Figure V.9.5: A conditional two-saddle comparison. The upper panel states the assumed chains through x_0, x_1 and the two choices $\Gamma = \mathcal{J}_0$ and $\Gamma' = \mathcal{J}_0 + \mathcal{J}_1$. It does not specify a global polynomial or assert chain existence. The lower panel plots the actual suppression function $e^{-3/(2\epsilon)}$ on a logarithmic vertical scale. Both choices share the dominant formal sector; their difference survives in an exponential sector invisible to its power-series coefficients.

The limit follows by taking the logarithm, $-3/(2\epsilon) - k\log\epsilon \to -\infty$. This numerical value illustrates an action-gap suppression only; no particular polynomial or global contour with this value has been inferred.

Figure V.9.5 separates the assumed chain geometry from the actual suppression function. On a Stokes ray, descent chains can change their decomposition and the coefficients representing a fixed contour can change with them. This is a change of representation of an analytically continued exact integral, not a discontinuity of that same integral. A complete matrix transseries, its coefficients and its global continuation are further problems. Neither the scalar example nor the branch recursion proves their general existence.

Third, even the planar curve comparison at the physical interface requires explicit translations. In the Dijkgraaf–Vafa matrix notation, write ω_{DV} for their resolvent and y_{mat} for their matrix curve variable. With their matrix parameter mapped to $\hbar_{\mathrm{m}}$ we have

$$\omega_{\mathrm{DV}} = -\frac{R_0}{t_{\mathrm{m}}}, \qquad y_{\mathrm{mat}} = V' + 2t_{\mathrm{m}}\omega_{\mathrm{DV}} = 2y, \qquad f_{\mathrm{mat}} = 4P_0. \tag{V.9.77}$$

These are translations of matrix definitions. They do not yet identify their parameter with the physical string coupling g_s. The normalized density and the full-contour filling following from these definitions are

$$\begin{aligned} \rho(\lambda) &= \frac{y_{\mathrm{mat},+} - y_{\mathrm{mat},-}}{4\pi i t_{\mathrm{m}}}, \\ t_i &= -\frac{1}{4\pi i}\oint_{A_i,\mathrm{ccw}} y_{\mathrm{mat}}\,dx, \qquad \Delta t_i = \hbar_{\mathrm{m}}\Delta N_i \quad (\hbar_{\mathrm{m}} \text{ fixed}). \end{aligned} \tag{V.9.78}$$

For our Gaussian example the upper jump is $2im\sqrt{16-\lambda^2}$. Dividing it by $4\pi i \cdot 6$ gives the unit-mass density in (V.9.15). The same full contour gives $\oint y_{\mathrm{mat}}dx/(2\pi i) = -12$, rather than six. The sign and factor two are fixed by the contour already drawn, not by a name assigned to its period.

The source's geometric variable has a further phase. Its geometric curve and its matrix curve are written respectively as

$$y_{\mathrm{geo}}^2 + V'^2 + f_{\mathrm{geo}} = 0, \qquad y_{\mathrm{mat}}^2 - V'^2 + f_{\mathrm{mat}} = 0. \tag{V.9.79}$$

An algebraic translation is $y_{\mathrm{geo}} = iy_{\mathrm{mat}}$ and $f_{\mathrm{geo}} = -f_{\mathrm{mat}}$. It follows that the differentials also change phase, $y_{\mathrm{geo}}dx = i\,y_{\mathrm{mat}}dx$. A holomorphic 3-form normalization and the reduction over its fiber must be specified before using this as a physical period dictionary. A plane equation alone does not supply them. Noncompact conjugate periods also need a regulator, as in Chapters 3 and 4.

The historical physical proposal is that a specified local-CY B-model sector and its type-IIB brane/flux embedding relate these fixed-filling matrix quantities to protected physical F-terms. The local geometry, normalization of the holomorphic form, relation between flux and ranks, choice of periods and their regulator, and identification of the protected observable are additional physical inputs. The curve and its period rewriting share those same inputs; they are not two independent physical tests of the proposal.

We have derived matrix quantities and displayed the necessary translations. We use this as a historical physical proposal with the stated local-CY and protected-sector assumptions. Chapter 8 discusses the restrictions on protected spacetime couplings, and Chapter 10 develops the F-term mechanisms. Chapters XVIII.7 and XVIII.8 are the downstream construction targets for the matrix tools, not results established by this chapter.

A common misconception

A formal genus series is not a complete definition of a nonperturbative integral. The chain coefficients in (V.9.71) and the exponentially small distinction in (V.9.75) survive the same boundary-free loop equations. A physical interpretation needs its own coupling and observable dictionary. In particular the meromorphic curve invariants here are not identified with the full nonholomorphic BCOV amplitudes of Chapter 5.

V.9.6 Exercises

The first four exercises have bounded exact-answer checks. Use the same conventions as the derivations, including the ordinary trace, physical infinity, half-force y and full counterclockwise contour. In the public companion each submission has fields `task` and `answer`. Rational answer entries are strings, including zeros; only the sheet sign is an integer. Arrays include every zero coefficient and use ascending degree order where polynomial coefficients are requested. The companion's public question records specify the exact JSON structure. Written explanations accompany the calculations but are not certified by the numerical checks.

1. **Gaussian spectrum (IV09-E1).** Take $m = 3/2$, $t_{\mathrm{m}} = 6$ and a unit-mass density. Use the ansatz $w_0 = 2[x - \sigma\sqrt{x^2 - D}]/D$, with the square root asymptotic to x. Derive D, choose $\sigma = \pm 1$, and give all nine moments $\mu_0, \ldots, \mu_8$. Explain the physical-sheet choice and check the total density mass by integration. Submit `discriminant`, `sheet_sign` and `moments` in `answer`; the last field has nine entries.

2. **A quartic cut (IV09-E2).** For $V = x^2 + x^4/4$, $t_{\mathrm{m}} = 5$, take $2y = (x^2 + b)\sqrt{x^2 - A^2}$ with $A^2, b > 0$. Derive the expectation-value Ward equation, then its planar quadratic. Determine A^2, b, all three ascending coefficients of P_0, and all nine coefficients $M_0, \ldots, M_8$ of R_0. Explain why M_0 is not one and why the double zeros of the plane polynomial are not new simple branch points. Submit `A2`, `b`, `P` (length three) and `moments` (length nine).

3. **The normalized cover (IV09-E3).** For $m = 3/2$, $t_{\mathrm{m}} = 6$, write $x = 2(z + 1/z)$ and $y = Y(z - 1/z)$. Find the two ramification preimages in increasing real order, their x images in the same order, the coefficient Y, and the coefficient C in $B = C\, dz_1 dz_2/(z_1 - z_2)^2$. Evaluate $(2\pi i)^{-1} \oint_{A_{\mathrm{ccw}}} R_0 dx$. Explain why the upper lip is traversed right to left and why this contour is not a compact handle cycle. Submit `branch_z`, `branch_x`, `y_prefactor`, `bergman_coefficient` and `filling`; each branch array has length two.

4. **The first stable residues (IV09-E4).** Use (V.9.48) with $t_{\mathrm{m}} = 6$ and $B(q, 1/q) = -dq^2/[q^2(q-1/q)^2]$. Evaluate both residues as $N_-(p)dp/(p+1)^4$ and $N_+(p)dp/(p-1)^4$. Give the three ascending coefficients of each numerator, including zeros. Sum them as $N(p)dp/[(p-1)^4(p+1)^4]$ and give all five coefficients of N. Compute the two ordered terms for $W_3^{(0)}$ and give its weights $[\alpha, \beta]$ multiplying respectively $\prod_i (p_i - 1)^{-2}$ and $\prod_i (p_i + 1)^{-2}$. Finally transform $W_1^{(1)} = R_1 dx$ with $x = 2(p + 1/p)$ and give all 11 coefficients of $x^{-1}, \ldots, x^{-11}$ in R_1. Submit `branch_minus_num`, `branch_plus_num`, `W11_num`, `W03_weights` and `R1_moments`, with lengths $3, 3, 5, 2, 11$. Explain the pullback sign and why this does not determine F_1.

5. **Two conditional contours (IV09-E5, written).** Assume two nondegenerate critical points, independently specified convergent descent chains, and a non-Stokes sector with positive real action gap as in (V.9.72). At scalar $N = 1$, compare $\mathcal{J}_0$ and $\mathcal{J}_0 + \mathcal{J}_1$. Explain the shared dominant formal power series and the differing exponential sector, the change of chain representation on a Stokes ray, and why vanishing-boundary loop equations do not select one contour. Separate what follows from the assumed chains from a global chain-existence assertion.

6. **The physical interface (IV09-E6, written).** Separate a formal fixed-filling expansion, normalized recursion data, a convergent contour integral with measure, and the protected local-CY physical proposal. Name the normalization, regulator, flux/rank and observable inputs needed at each interface. Explain why the Gaussian checks and the formal theorem do not establish a universal nonperturbative physical partition function. State what further dictionary would be needed to compare the curve invariants with the BCOV amplitudes or a chosen holomorphic limit in Chapter 5.

V.9.7 Take-home message

The matrix trace fixes a cyclic ordering, its index contractions give ribbon topology, and the exact expectation Ward equation gives the planar curve after a filling sector is chosen. The normalized curve, local conjugation and bidifferential then let branch residues compute stable correlators. In the Gaussian example both branch contributions are essential for $W_1^{(1)}$; the pullback sign and ordered splitting are essential for $W_3^{(0)}$. The complete one-form agrees with a separate Ward calculation, and the retained coefficients agree with finite connected Wick counts. The all-orders formal theorem is cited under its own hypotheses. Contours, absolute normalization and the protected physical dictionary remain further information.

After working through the chapter the reader should be able to derive a Gaussian resolvent and its sheet, solve the regular quartic one-cut example, specify branch and filling data on the normalized curve, evaluate the first stable residues with their pullbacks, and separate a formal expansion from a convergent integral or physical F-term identification.

Status and sources

§V.9.1. The covariance, index-loop Euler count, Gaussian generating function, positive-sheet resolvent and normalized density are conditional mathematical derivations [MATH]. The matrix-sector definitions use ordinary traces and the local $\hbar_{\mathrm{m}}, t_{\mathrm{m}}, R, w_0, y$ frame. General formal matrix expansion and the trace interpretation are discussed by Eynard and Orantin (2007, v4, physical PDF pp. 47–49, Definition 10.1 and (10-7)–(10-14)); the matrix formulation also appears in Dijkgraaf and Vafa (2002, v2, physical PDF pp. 11–13, secs. 3.1–3.2). The Gaussian density moments are derived here for all nonnegative integer degrees. The finite nonplanar counts in the text have only the stated finite scope.

§V.9.2. The boundary-free $\beta = 2$ expectation identity and the quartic one-cut solution are mathematical consequences of the stated ensemble and planar-expansion premises [MATH]. The expectation equation is Eynard and Orantin (2007, v4, physical PDF p. 48, (10-9)). The equation obtained from stationary eigenvalues in Dijkgraaf and Vafa (2002, v2, physical PDF p. 13, (3.3)) is a different finite-N object. The explicit cancellation in (V.9.18) is the reason no stationary resolvent derivative remains in the expectation identity. The quartic example is restricted to $m, t_{\mathrm{m}} > 0, g \geq 0$ and the displayed regular real one-cut branch.

§V.9.3. Normalization, simple branch data and the sphere bidifferential are used in the sense of Eynard and Orantin (2007, v4, sec. 3, physical PDF pp. 9–13, sec. 4.1, p. 20). The Gaussian uniformization, pullback and full cut-period evaluations are mathematical calculations [MATH]. The cycle is a puncture/cut contour, not a compact handle generator. Chapter 3's period frame and Chapter 4's holomorphic-form conventions are not redefined.

§V.9.4. The recursion initial values and the q-to-$\bar{q}$ integral are source definitions, specifically Eynard and Orantin (2007, v4, physical PDF pp. 20–21, Definition 4.2 and (4-3), (4-7)–(4-9)). The symmetric three-point residue formula is its Theorem 4.1, physical PDF p. 23, (4-20). The full $W_1^{(1)}$ and $W_3^{(0)}$ calculations and their stated finite Wick comparisons are conditional mathematics [MATH]; they do not determine F_1 or prove an all-orders statement. The general identification is the cited polynomial formal matrix-model theorem [MATH], Eynard and Orantin (2007, v4, physical PDF pp. 47–49, Definition 10.1 and Theorem 10.1). We retain the nondegenerate occupied Gaussian reference, fixed fillings, $\kappa = 0$, and separately regular simple-ramification curve; rational-potential extensions, degenerate references and critical/double-scaling limits are excluded here. The source's exceptional definitions of $F^{(0)}, F^{(1)}$ are on physical PDF pp. 22–23. Its $-\log Z$ convention is explicit on physical PDF p. 48, (10-6), whereas (V.9.69) labels the log-Z coefficients separately.

§V.9.5. Convergent generalized paths, occupation components and common boundary-free loop equations follow Eynard (2009, v1, physical PDF pp. 4–6, (1.5)–(1.20)). Its sec. 1.1.3 separately assumes the component topological expansion; no general asymptotic existence theorem is imported here. The conditional two-saddle estimate follows from the supplied nondegenerate descent-chain and positive-action-gap premises [MATH]. It is not a matrix transseries construction.

The local-CY and protected physical proposal is historically attributed to Dijkgraaf and Vafa (2002, v2, physical PDF pp. 1–8 and 11–16). The physical equality is a proposal. Curve rewriting and its period reformulation do not supply independent physical tests. In particular neither a physical coupling identification, a flux/rank dictionary, higher-genus physical matching nor a nonperturbative completion has been established by the finite matrix calculations. The Chapter 5 BCOV amplitudes retain their own Hodge, anomaly and boundary conditions.

There are literal normalization inconsistencies in this exact DV v2 source. Physical PDF p. 14 (printed p. 13), (3.9), prints $\mu/(\pi i)$ times the upper-minus-lower jump of its matrix y; its preceding definitions instead imply the coefficient $1/(4\pi i\mu)$ in our translated frame. Physical PDF p. 15 (printed p. 14) prints $\Delta S_i = \Delta N_i/g_s$, although $S_i = g_s N_i$ gives $\Delta S_i = g_s \Delta N_i$ at fixed g_s. These are inconsistencies in the displayed source formulas; no published erratum is asserted. Its (3.10) on that page writes a positive $(2\pi i)^{-1} \oint y_{\mathrm{mat}} dx$. Our explicitly full A_{ccw} contour gives $-2t_i$ for that integral. Equation (V.9.78) states our derived full-contour convention and does not silently replace the source by an unspecified half-contour. Its geometric (2.7) on physical PDF p. 6 and matrix (3.7) on physical PDF p. 13 also require the phase and sign translation in (V.9.79).

Exact originals of EO v4, DV v2 and Eynard v1 are available for these anchors, including original-page images of the kernel direction and the two DV discrepancies. Earlier limited source access is not a restriction on the present exposition. Physical page numbers count the DV cover as page one; its body printed page numbers are one less. The source versions stated here govern the formulas, independently of the publication metadata in the bibliography.

References

Dijkgraaf, R. and C. Vafa (2002). "Matrix Models, Topological Strings, and Supersymmetric Gauge Theories". In: *Nucl. Phys. B* 644. Version 2, 11 August 2002, pp. 3–20. DOI: 10.1016/S0550-3213(02)00766-6. arXiv: hep-th/0206255.

Eynard, B. (2009). "Large N expansion of convergent matrix integrals, holomorphic anomalies, and background independence". In: *JHEP* 03. Inspected arXiv version 1, 13 February 2008; contour definitions only, no general asymptotic theorem imported, p. 003. DOI: 10.1088/1126-6708/2009/03/003. arXiv: 0802.1788 [math-ph].

Eynard, B. and N. Orantin (2007). *Invariants of algebraic curves and topological expansion*. Version 4, 7 May 2007. arXiv: math-ph/0702045.

Chapter V.10

Topological amplitudes as physical F-terms

V.10.1 A physical use for a topological amplitude

A gravitational coupling can retain information that a generic scattering process loses. In a type-II Calabi–Yau compactification, select two gravitons and an even number of graviphotons, the vector particles in the supergravity multiplet. For particular external components their string amplitude reduces to an internal topological amplitude. The selection is essential. The result concerns a family of curvature couplings in an effective action, with specified tensor contractions and field conventions.

This gives a physical destination for the computations of this volume. Twisting made an internal worldsheet theory tractable. Periods and mirror symmetry supplied coordinates and genus-zero information. The holomorphic anomaly described how higher-genus amplitudes acquire dependence on both moduli and their complex conjugates. We now ask which experiment can use those answers. The mechanism starts with physical vertex operators: their internal charges supply the twist, their spacetime factors absorb zero modes, and their pictures determine the superghost insertions. Superspace then organizes the resulting interactions.

The setting of the closed-string argument is smooth compact Calabi–Yau threefold compactification, without flux or orientifold projection, at a regular moduli patch with four-dimensional $\mathcal{N} = 2$ supersymmetry. A local gauge theory requires a further limit. An $\mathcal{N} = 1$ superpotential from branes and flux requires further physical identifications. These steps have different hypotheses, so we will perform them separately. In particular, a compact gravitational coupling does not become a gauge observable solely because its coefficient was calculated topologically.

By the end of the chapter the reader should be able to count the selected external insertions, reconstruct both curvature contractions and their factorials, translate homogeneous weights into canonical mass dimensions, test what a gravitational limit holds fixed, and identify the additional input in an open-string or flux extraction. The spin-structure sum, nonrenormalization argument and brane/flux correspondence

are sourced physical results. We derive their stated algebraic consequences and their limitations, rather than supply new proofs of those physical results.

V.10.2 The selected amplitude and its zero modes

Why can a physical amplitude contain the twisted theory of Chapter 1? The relevant compactification has an internal $(2,2)$ superconformal theory of central charge $c = 9$. Its spectral flow relates Neveu–Schwarz and Ramond states. The graviphoton is a Ramond–Ramond state with a distinguished internal spectral-flow factor. A generic gauge boson does not have that factor, even when its spacetime quantum numbers look similar. The graviton has a zero-picture vertex, while a graviphoton may be represented in picture $-1/2$ in each chiral half of the worldsheet theory.

Let ϕ denote the bosonized superghost, S a spacetime spin field and Σ the internal Ramond factor. Suppressing momentum and polarization indices only in the following schematic factorization, the selected vertex contains

$$V_T^{(-1/2,-1/2)} \;\sim\; e^{-\phi/2} S\, e^{-\widetilde{\phi}/2} \widetilde{S}\, \Sigma, \qquad |q_L(\Sigma)| = |q_R(\Sigma)| = \frac{3}{2}. \tag{V.10.1}$$

For the type-IIA choice the internal charges have opposite signs between left and right movers; for type IIB they have the same sign. In either case we choose the sector that produces the appropriate internal twist. The spacetime components below follow the anti-self-dual convention of the explicit physical calculation.

Take stable genus $g \geq 2$. A picture-changing insertion raises the picture by one. The required total picture in each chiral half is $2g - 2$. If the number of graviphotons is $2g - 2$, their combined picture is $-(g - 1)$, and hence the number n_{pc} must satisfy

$$-\frac{1}{2}(2g-2) + n_{\mathrm{pc}} = 2g - 2, \qquad n_{\mathrm{pc}} = 3g - 3. \tag{V.10.2}$$

The gravitons are in picture zero and add nothing to the left side. In the chiral half in which Σ has charge $+3/2$, the internal charge sum selects $3g - 3$ factors of the supercurrent G^-,

$$(2g-2)\frac{3}{2} - (3g-3) = 0. \tag{V.10.3}$$

The other chiral half uses its corresponding twist. This is the same number of supercurrent insertions that occurs in the topological measure. The charge equality explains why these insertions are possible; it is not by itself an evaluation of their correlation function.

More explicitly, write μ_a for the Beltrami differentials representing complex-structure deformations of the worldsheet. At stable genus the number of moduli and of b-ghost zero modes is

$$\dim_{\mathbb{C}} \mathcal{M}_g = 3g - 3, \qquad a = 1, \ldots, 3g - 3. \tag{V.10.4}$$

In the twisted description the superghost zero modes can be paired with this same basis. The physical calculation, after the spin-structure sum and the cancellation of the

appropriate determinants, leaves the internal measure with insertions of the form

$$\prod_{a=1}^{3g-3} G^{-}(\mu_a) \prod_{a=1}^{3g-3} \widetilde{G}^{\mathrm{tw}}(\overline{\mu}_a). \tag{V.10.5}$$

The tilde denotes the right-moving current appropriate to the chosen A- or B-twist. Boundary terms in the twisting, the flat bundle of the twisted fields and the sum over physical spin structures matter in this reduction. The intuitive account of inserting spectral flow is useful for the count; the explicit bosonization calculation supplies these additional steps. We use that physical reduction as an input.

The spacetime zero modes explain why the answer contains two curvatures. After twisting, let ψ^i have spin one and χ_i have spin zero, with $i = 1, 2$ labelling the two complex spacetime species. For each species and each chiral half, the zero modes are counted by holomorphic one-forms and constant functions on the genus-g surface Σ_g,

$$n(\psi^i) = h^0(\Sigma_g, K_{\Sigma_g}) = g, \qquad n(\chi_i) = h^0(\Sigma_g, \mathcal{O}) = 1. \tag{V.10.6}$$

The selected graviton pair supplies the factors that absorb the χ_i zero mode and one ψ^i zero mode. The remainder is therefore

$$n_{\mathrm{remaining}}(\psi^i) = g - 1, \qquad n_{\mathrm{remaining}}(\chi_i) = 0. \tag{V.10.7}$$

One must absorb these modes using operators that still define physical untwisted vertices. The cited construction does this at $g - 1$ of the spectral-flow insertion points, converting the chosen spacetime component there. The resulting external multiplicities are

$$(n_R, n_T, n_{\text{component each}}, n_{\text{remaining } \psi \text{ each}}) = (2, 2g - 2, g - 1, g - 1). \tag{V.10.8}$$

Thus $g - 1$ graviphotons carry one selected component and $g - 1$ the other. The component labels will be made explicit in the next section.

For example, at genus two there are two ψ^i modes and one χ_i mode per species. The two gravitons leave one ψ^i mode. Two Ramond–Ramond insertions, split one and one between components, and three picture changes give

$$g = 2: \quad (n_R, n_T, n_{\text{component each}}, n_{\text{remaining } \psi \text{ each}}) = (2, 2, 1, 1), \qquad n_{\mathrm{pc}} = 3. \tag{V.10.9}$$

At genus four the same subtraction is $4 - 1 = 3$ for each species. The six graviphotons have total picture -3, so nine picture changes yield the required total picture 6,

$$g = 4: \quad (2, 6, 3, 3), \qquad -3 + 9 = 6. \tag{V.10.10}$$

Figure V.10.1 displays this example. It separates mode saturation from the independent charge and picture equalities.

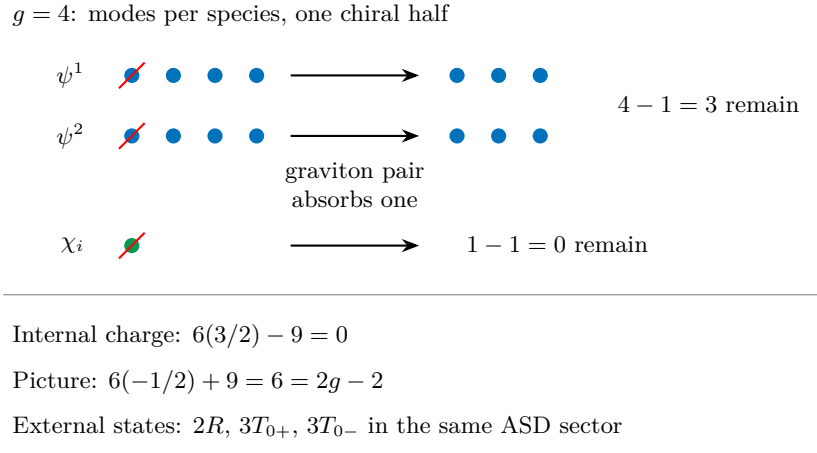


Figure V.10.1: Genus four, with one row for each spacetime species in one chiral half. Four one-form modes become three after the selected graviton pair; the scalar mode is completely absorbed. The second chiral half has the corresponding count. Six spectral-flow insertions supply internal charge magnitude nine and picture -3 per chiral half; nine selected picture changes supply the compensating charge and total picture six. The diagram records counts, while the physical spin-structure sum is an additional ingredient.

An extra graviphoton pair at fixed genus changes these equalities. Its picture contribution is -1, requiring another picture change, but its internal charge contribution is $+3$ in the displayed chiral half. With the same G^- prescription the net extra charge is $+2$, rather than zero. This attempted extension is not the same selected amplitude. Extra insertions cannot be added to a protected answer without checking the selection rule again.

Genus one needs its own treatment. The external-state interpretation is a two-graviton R^2 coupling without background graviphotons, so the spacetime count is $(2, 0, 0, 0)$. The torus has a complex modulus and conformal Killing zero modes; setting $3g-3 = 0$ in the stable-genus prescription would lose the measure. In the conventions of Chapter 5, the separate internal torus trace includes the left and right fermion-number insertions,

$$F_1 = \frac{1}{2}\int_{\mathcal{F}} \frac{d^2\tau}{\tau_2}\, \mathrm{Tr}_{RR}\Big[(-1)^F F_L F_R q^{L_0 - c/24}\bar{q}^{\bar{L}_0 - c/24}\Big], \qquad q = e^{2\pi i\tau}. \tag{V.10.11}$$

Here F_L, F_R are worldsheet fermion-number operators, not spacetime field strengths, and $\mathcal{F}$ is a modular fundamental domain. Infrared regularization and the genus-one anomaly retain the qualifications of Chapter 5. Equation (V.10.11) is the cited torus definition, not a consequence of the preceding stable-genus ghost count.

There is also a distinction between selection and protection. For a fixed coupling with Weyl-multiplet power $2n$, the physical charge analysis excludes contributions at genus smaller than n. The higher-genus argument invokes more physics. The type-II

dilaton belongs to a hypermultiplet, whereas the selected local chiral coupling belongs to the vector/gravity sector. A higher-genus correction would introduce additional dilaton dependence; the $\mathcal{N}=2$ no-mixing argument excludes that dependence in this sector. The original calculation presents this as an additional indication of genus exclusivity; the later protected-amplitude formulation states the restricted result more strongly. Neither is a nonrenormalization statement for arbitrary hypermultiplet couplings or nonlocal amplitudes.

Chapter 1 supplied the scalar-charge language of the internal twist, and Volume II, Chapter 4 supplied the physical RNS and GSO ingredients. Here they meet only for the specified vertices. The next question is which spacetime interaction has precisely their component amplitudes.

V.10.3 Tensor contractions and chiral couplings

Does the label R^2T^{2g-2} specify an interaction? It specifies field content but leaves tensor contractions open. Let R and T in this section denote the source anti-self-dual curvature and graviphoton strength. Their tensor and field normalizations are those of the selected physical amplitude, and its coefficient will be called f_g. Define the invariant contractions

$$\begin{aligned} R^2 &= R_{\mu\nu\rho\sigma}R^{\mu\nu\rho\sigma}, \qquad T^2 = T_{\mu\nu}T^{\mu\nu}, \\ (RT)^2 &= (R_{\mu\nu\rho\sigma}T^{\rho\sigma})(R^{\mu\nu}{}_{\alpha\beta}T^{\alpha\beta}). \end{aligned} \tag{V.10.12}$$

The contraction with one curvature between two strengths is $TRT = T^{\mu\nu}R_{\mu\nu\rho\sigma}T^{\rho\sigma}$. For $g \geq 3$, its square times $(T^2)^{g-3}$ has the same field content as the other two candidates. Dimension counting alone cannot exclude it.

The two-curvature part obtained in the source calculation is, for $g \geq 2$,

$$\mathcal{I}_g = g f_g \left[R^2 (T^2)^{g-1} + 2(g-1)(RT)^2 (T^2)^{g-2} \right]. \tag{V.10.13}$$

Its two coefficients, and the coefficient of the third candidate when it exists, are

$$(c_1, c_2, c_3) = \big(g f_g,\, 2g(g-1) f_g,\, 0 \big), \qquad g \geq 3. \tag{V.10.14}$$

The vanishing third coefficient follows from a worldsheet amplitude and the Riemann vanishing argument in the source. It is not implied by the tuple of insertion counts. At genus one the corresponding term is separately $f_1 R^2$. We do not evaluate a zero prefactor multiplying a negative power of T^2 to define that case.

A useful way to test both nonzero contractions is to resolve two component amplitudes. In the source convention

$$T_{0+} = T_{01} + iT_{02}, \qquad T_{0-} = T_{01} - iT_{02}. \tag{V.10.15}$$

These are components *within one anti-self-dual field*. The plus and minus subscripts do not denote the two Hodge eigenspaces. The corresponding curvature component labels are defined in the same complex basis. The source component expansion gives the coefficients of two monomials,

$$\begin{aligned} R_{0+0+}R_{0-0-}(T_{0+}T_{0-})^{g-1} &: \quad g^2 f_g, \\ R_{0-0-}R_{0303}(T_{0+})^{g}(T_{0-})^{g-2} &: \quad -g(g-1) f_g. \end{aligned} \tag{V.10.16}$$

The first receives contributions from both terms of (V.10.13); the second only from the second term. We use these component projections as sourced tensor algebra rather than claim a new expansion of the whole conformal-supergravity action.

The passage from a coefficient to an amplitude still has factorials. Differentiating a monomial $x^r y^s$ once for every identical external x and y gives $r!s!$. The two curvature components here are distinct, so the factors required by the two rows are respectively $((g-1)!)^2$ and $g!(g-2)!$. Thus

$$\mathcal{A}_g^{(1)} = g^2 f_g \left((g-1)!\right)^2 = (g!)^2 f_g, \tag{V.10.17}$$

while

$$\mathcal{A}_g^{(2)} = -g(g-1) f_g \, g!(g-2)! = -(g!)^2 f_g. \tag{V.10.18}$$

The relative minus sign is already present in the source component projection. In its vertex description the T_{0+} and T_{0-} spin-field terms have opposite relative signs; the supersymmetry contour operation relating the two amplitudes retains that sign. A factorial is positive and cannot create or remove it. This gives a check on the second contraction that a single schematic curvature monomial would miss.

Work through genus three at the supplied regular value $f_3 = 5/7$. The invariant itself is

$$\mathcal{I}_3 = \frac{15}{7} R^2 (T^2)^2 + \frac{60}{7} (RT)^2 T^2, \qquad c_3 = 0. \tag{V.10.19}$$

The two projected coefficients are $9(5/7) = 45/7$ and $-3 \cdot 2(5/7) = -30/7$. Their identical-vertex factors are different,

$$\mathcal{A}_3^{(1)} = \frac{45}{7}(2!)^2 = \frac{180}{7}, \qquad \mathcal{A}_3^{(2)} = -\frac{30}{7}(3!)(1!) = -\frac{180}{7}. \tag{V.10.20}$$

Equal magnitudes emerge after the factorials, rather than at the level of the raw component coefficients. These are source-normalized amplitudes; an absolute canonical graviphoton normalization has not yet entered.

The supersymmetric organization explains why these interactions occur as a family. Denote the $\mathcal{N} = 2$ Weyl multiplet by W_{Weyl}. Its lowest tensor component is a graviphoton-related tensor T_W, and its higher components contain the curvature. Let X^I be reduced chiral multiplets of Weyl weight one, with compensator X^0 and physical ratios $Z^A = X^A/X^0$. A local chiral coefficient has the homogeneity property

$$F_g(aX) = a^{2-2g} F_g(X), \qquad F_g(X) = (X^0)^{2-2g} F_g^{\mathrm{hol}}(Z). \tag{V.10.21}$$

The superscript on F_g^{hol} specifies a chosen local holomorphic coefficient. It distinguishes this coefficient from the full amplitude of Chapter 5. Since W_{Weyl} has Weyl weight one, the conformal F-density has the required weight,

$$\left[F_g(X)(W_{\mathrm{Weyl}}^2)^g\right]_F, \qquad (2-2g) + 2g = 2. \tag{V.10.22}$$

Extracting its highest component produces two curvatures and $2g-2$ lowest tensor components, together with the other terms of its supersymmetric completion. Equation (V.10.22) is a compact organization of the sourced invariant; it does not fix all physical field normalizations.

The same powers appear in the formal connected topological free energy,

$$\mathcal{F}_{\rm top}(\lambda_{\rm top}) = \sum_{g\geq 0} \lambda_{\rm top}^{2g-2} F_g. \tag{V.10.23}$$

For $g \geq 1$ the exponent counts the background graviphoton powers in this family. It does not count all external legs, which also include two gravitons. The power match does not identify the formal parameter $\lambda_{\rm top}$ with a bare physical string coupling g_s. The physical calculation suppresses some genus-independent constants and factors that can be absorbed into field normalization.

There is one more convention issue before restoring units. The explicit component calculation calls its tensors anti-self-dual. The heuristic zero-mode discussion elsewhere describes its converted vertex as having opposite self-duality; we follow the explicit same-sector component calculation for (V.10.16). Another common formulation uses Euclidean self-dual tensors. Reversing a Euclidean orientation changes the Hodge label according to

$$*_{\rm new} = -*_{\rm old}, \qquad *_{\rm old} T = T \implies *_{\rm new} T = -T. \tag{V.10.24}$$

This is a possible translation of labels, not a determination of the relative orientations of two sources. It neither conjugates one invariant at fixed orientation nor fixes the signed continuation to canonical Lorentzian fields. Chapters 3 and 5 supplied the homogeneous and Hodge-line language. The next section translates it into a stipulated local frame where mass dimensions can be checked explicitly.

V.10.4 Canonical fields and gravitational limits

What is actually small when a gravitational scale becomes large? A curvature density evaluated on a background and a vertex with canonical external gravitons have different answers. We first restore units without claiming an absolute compactification normalization. Choose a fixed regular Hodge frame and reference point, set the compensator to a mass scale M, and parametrize a chosen graviphoton polarization by

$$X^0 = M, \qquad T_W = \eta \frac{F_{\rm can}}{M}, \qquad [M] = 1, \quad [F_{\rm can}] = 2, \quad [\eta] = 0. \tag{V.10.25}$$

Here brackets denote mass dimension, $F_{\rm can}$ is a canonically normalized Maxwell strength and $\eta \neq 0$ is an unfixed constant in this local parametrization. It is not a full moduli-dependent on-shell identification of the physical graviphoton. In particular the conformal gauge involving the Kähler potential is not globally replaced by a constant over moduli space.

Substitute (V.10.25) and (V.10.21) into a two-curvature term. Both tensor contractions acquire the same dimensional prefactor,

$$M^{2-2g} F_g^{\rm hol} \left(\eta \frac{F_{\rm can}}{M}\right)^{2g-2} R^2 = F_g^{\rm hol} \eta^{2g-2} M^{4-4g} R^2 F_{\rm can}^{2g-2}. \tag{V.10.26}$$

Only tensor and genus-dependent combinatorial constants are suppressed in this dimensional formula. Using $[R] = 2$, the operator and its coefficient in a four-dimensional

density have dimensions

$$[R^2 F_{\rm can}^{2g-2}] = 4 + 2(2g-2) = 4g, \qquad [C_g] = 4 - 4g. \tag{V.10.27}$$

These are different from the homogeneous Weyl weight $2-2g$ of $F_g(X)$. The difference is the $2g-2$ additional powers of M^{-1} in the tensor map. Assigning Weyl weight one directly to a canonical Maxwell strength would erase those powers.

For genus two the operator has dimension eight, the coefficient has dimension minus four and $F_2(X)$ has Weyl weight minus two. At genus three the corresponding numbers are twelve, minus eight and minus four. Normalization can change the numerical coefficient even after these powers are fixed. Under a positive field redefinition $F_{\rm new} = \rho F_{\rm old}$, equality of the same coupling requires

$$C_{g,{\rm old}} R^2 F_{\rm old}^{2g-2} = C_{g,{\rm old}} \rho^{2-2g} R^2 F_{\rm new}^{2g-2}, \qquad C_{g,{\rm new}} = \rho^{2-2g} C_{g,{\rm old}}. \tag{V.10.28}$$

At the nonunit choice $\rho = 3/2$ this gives

$$\frac{C_{2,{\rm new}}}{C_{2,{\rm old}}} = \left(\frac{2}{3}\right)^2 = \frac{4}{9}, \qquad \frac{C_{3,{\rm new}}}{C_{3,{\rm old}}} = \left(\frac{2}{3}\right)^4 = \frac{16}{81}. \tag{V.10.29}$$

A numerical coefficient without its field convention is insufficient to compare physical responses.

Now introduce a dimensionless parameter $\widehat{\epsilon} > 0$ and a fixed mass unit $\mu > 0$. The following is a supplied limit model, not a claim that every Calabi–Yau compactification realizes it:

$$M = \frac{3\mu}{\widehat{\epsilon}}, \qquad F_{\rm can} = 5\mu^2 \widehat{\epsilon}^{\,b}, \qquad F_g^{\rm hol} = f_0 \widehat{\epsilon}^{\,p}. \tag{V.10.30}$$

We hold η, f_0, μ, the tensor polarization and canonical momenta fixed. For a density at fixed geometric curvature, substitution into (V.10.26) gives the complete scale dependence

$$\mathcal{L}_g \;\propto\; f_0 \eta^{2g-2} 5^{2g-2} 3^{4-4g} \widehat{\epsilon}^{\,d} R^2, \qquad d = p + (2g-2)(2+b). \tag{V.10.31}$$

The mass-unit powers cancel: $(4-4g) + 2(2g-2) = 0$. Thus the coefficient of R^2 after the background substitution is dimensionless, as a four-dimensional density requires. For example, with $g = 2$, $b = p = 0$, $\widehat{\epsilon} = 1/10$ and $\eta = f_0 = 1$, it is $1/32400$, independent of the chosen mass unit μ. The power $2(2g-2)$ in d comes from M^{4-4g}; the remaining $b(2g-2)$ comes from the canonical field. The dimensionless background combination in these conventions is

$$\eta \frac{F_{\rm can}}{M^2} = \frac{5\eta}{9} \widehat{\epsilon}^{\,b+2}. \tag{V.10.32}$$

Thus a fixed canonical field, $b = 0$, and a fixed value of this combination, $b = -2$, are different limiting experiments.

For canonical gravitons write the metric as $g_{\mu\nu} = \eta_{\mu\nu}^{\rm flat} + 2h_{\mu\nu}/M$. The flat metric $\eta_{\mu\nu}^{\rm flat}$ is unrelated to the scalar normalization η in (V.10.25). The linearized curvature is proportional to $\partial^2 h/M$. Consequently a formal vertex with two canonical gravitons and the same graviphoton background has the scaling

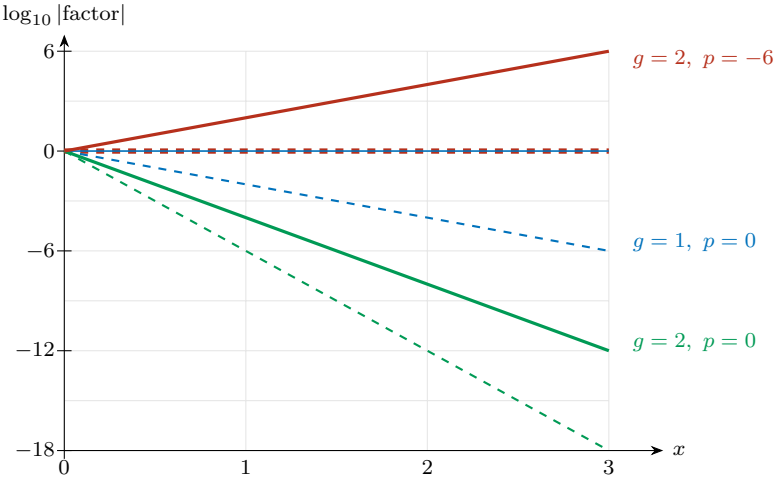
$$R^2\big|_{h^2} \;\propto\; M^{-2} (\partial^2 h)^2, \qquad V_{hh,g} \;\propto\; \widehat{\epsilon}^{\,d+2}. \tag{V.10.33}$$

This is a coefficient and field-normalization diagnostic at fixed momenta. A nonzero formal vertex does not guarantee a nonzero on-shell S-matrix element. Total derivatives, kinematics, cancellations among terms and the completion of the selected operator still matter.

At fixed canonical field and bounded coefficient, $b = p = 0$, genus one has $d = 0$ and genus two has $d = 4$. Their density and formal two-graviton powers are respectively

$$g = 1 : \ (d, d+2) = (0, 2), \qquad g = 2 : \ (d, d+2) = (4, 6). \tag{V.10.34}$$

The genus-one term can therefore give an unsuppressed response to fixed external curvature while its canonical two-graviton vertex carries M^{-2}. Calling both quantities a gravitational amplitude would obscure the distinction. Figure V.10.2 plots these powers along with a singular-coefficient case.



$x = -\log_{10} \widehat{\epsilon}$, $b = 0$; solid: density; dashed: formal hh vertex

Blue density and red dashed vertex coincide at zero.

Figure V.10.2: Powers in the supplied limit model at fixed canonical field. The horizontal coordinate is $x = -\log_{10} \widehat{\epsilon}$, and the vertical coordinate is the logarithm of the absolute scaling factor after dividing out all fixed prefactors. Solid curves are fixed-curvature densities; dashed curves include the extra inverse-M^2 from two canonical gravitons. The singular genus-two coefficient with $p = -6$ makes the density grow and its formal vertex remain constant. The solid and dashed slopes are $-d$ and $-(d+2)$, respectively; these encode the stated exponents, not predictions of a particular compactification.

Two counterexamples diagnose overstrong decoupling arguments. First, letting a genus-two coefficient grow as $F_2^{\mathrm{hol}} = f_0 \widehat{\epsilon}^{-6}$ gives

$$g = 2, \ p = -6, \ b = 0 : \qquad d = -2, \qquad d + 2 = 0. \tag{V.10.35}$$

The density grows and the formal vertex is unsuppressed. This violates the bounded-coefficient premise, so inverse powers of M alone cannot settle the limit. Second, at genus three with a growing canonical field,

$$g = 3,\ p = 0,\ b = -2: \qquad d = 0, \qquad d + 2 = 2, \qquad F_{\text{can}} = 5\mu^2\widehat{\epsilon}^{-2}. \tag{V.10.36}$$

Now the dimensionless combination (V.10.32) remains fixed. Such a sequence is not the fixed-field experiment of (V.10.34). The effective-field-theory regime and backreaction must be checked separately before assigning either sequence a physical interpretation.

Chapters 4 and 5 already required coordinate, frame and light-species information when extracting local coefficients. Those requirements persist in a limit: a singular coefficient cannot be replaced by a bounded one, and a change of units cannot be hidden in a change of notation. The next section gives an actual geometric setting for a correlated gauge-theory limit, rather than infer a gauge theory from these formal exponents.

V.10.5 A local gauge theory from a shrinking fibre

Which geometric limit can keep a gauge scale while removing bulk gravity? In the cited pure-$SU(2)$ type-IIA construction, start with an A_1 singularity resolved by a fibre $\mathbb{P}^1$. D2 branes wrapped on that sphere in opposite orientations produce the W^+ and W^- states. Fibering this geometry over a base $\mathbb{P}^1$ gives the local Calabi–Yau threefold setting for four-dimensional $\mathcal{N} = 2$ engineering. For the simplest ruled surface the base and fibre form $\mathbb{P}^1 \times \mathbb{P}^1$. Figure V.10.3 shows which two areas play different roles.

Let t_f be the dimensionless fibre parameter in string units and t_b the base parameter in the source convention. The physical identifications used in the construction have the proportionalities

$$t_f \ \propto\ \frac{M_W}{M_{\text{string}}}, \qquad t_b \ \propto\ \frac{1}{g^2_{\text{source}}}. \tag{V.10.37}$$

The wrapped-brane spectrum and these relations are physical inputs, not consequences of a ratio of power series. Keeping M_W finite while the string scale increases requires $t_f \to 0$. Asymptotic freedom makes the bare source coupling weak at that increasing scale, so $t_b \to \infty$. They must be correlated to preserve a field-theory scale.

Write $q_b = e^{-t_b}$ in the source real scaling slice, let Λ be the gauge-theory mass scale and let $a \neq 0$ denote a Cartan expectation value on the chosen regular Coulomb patch. Retain nonzero dimensionless constants C_b, C_f. The specified scaling is

$$q_b = C_b(\epsilon\Lambda)^4, \qquad t_f = C_f\epsilon a, \qquad [\epsilon] = -1. \tag{V.10.38}$$

Here $[a] = [\Lambda] = 1$. Unlike $\widehat{\epsilon}$ in the previous section, ϵ is dimensionful. Its products with a and Λ are dimensionless, as the geometric parameters require. The fourth power is the one in the pure-$SU(2)$ engineering limit; it is not derived from the gravitational exponent $4 - 4g$.

Dividing the two equations in (V.10.38) eliminates the small parameter while retaining all constants,

$$\frac{q_b}{t_f^4} = \frac{C_b\epsilon^4\Lambda^4}{C_f^4\epsilon^4 a^4} = \frac{C_b\Lambda^4}{C_f^4 a^4}. \tag{V.10.39}$$

The quotient is finite on the nonzero-a patch. Taking logarithms on the positive real slice also makes the base growth explicit,

$$t_b = -\log C_b - 4\log(\epsilon\Lambda) = -4\log t_f + \log\left(\frac{C_f^4 a^4}{C_b\Lambda^4}\right). \tag{V.10.40}$$

Thus the base grows logarithmically as the fibre shrinks. The finite constant term retains the mass and normalization choices, rather than silently setting Λ or the proportionality constants to one.

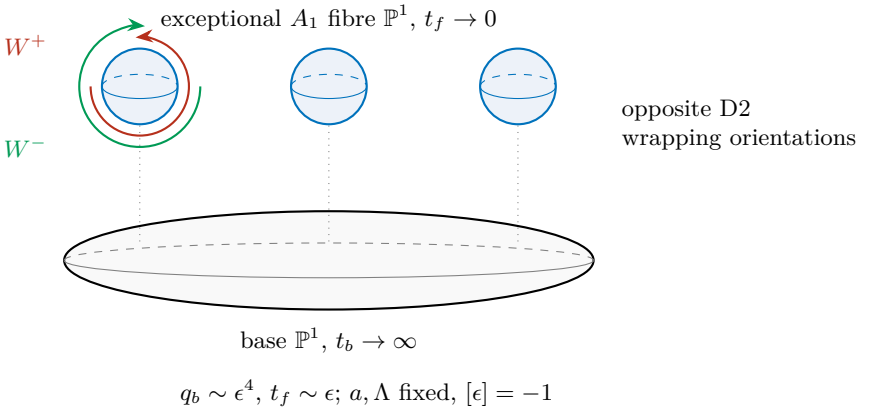


Figure V.10.3: The two geometric roles in the local A_1 construction. An exceptional fibre sphere sits above each point of the base sphere; only three sample fibres are drawn. Opposite orientations of a wrapped D2 brane give the charged W states. The arrows label the correlated limit in string units, $t_f \to 0$ and $t_b \to \infty$, while a and Λ remain fixed. This sketch depicts the fibration and its scales, not a metric embedding of the Calabi–Yau threefold.

For a numerical example keep the nonunit choices $C_b = 7/3$, $C_f = 5/2$, $\Lambda = 2\mu$ and $a = 3\mu$. At $\epsilon = 1/(10\mu)$ the two geometric parameters are

$$q_b = \frac{7}{3}\left(\frac{1}{5}\right)^4 = \frac{7}{1875}, \qquad t_f = \frac{5}{2}\frac{3}{10} = \frac{3}{4}. \tag{V.10.41}$$

Their fourth-power quotient is

$$\frac{q_b}{t_f^4} = \frac{7}{1875}\frac{256}{81} = \frac{1792}{151875}. \tag{V.10.42}$$

To approach the local limit more closely, reduce ϵ by a factor of one hundred to $1/(1000\mu)$. Then

$$q_b = \frac{7}{3}\left(\frac{1}{500}\right)^4 = \frac{7}{187500000000}, \qquad t_f = \frac{3}{400}, \qquad \frac{q_b}{t_f^4} = \frac{1792}{151875}. \tag{V.10.43}$$

The first point illustrates exact cancellation and need not already lie in an accurate small-fibre regime. The second has much smaller fibre parameter. Neither finite arithmetic evaluation proves that all string or bulk interactions have decoupled. It verifies which combination is held fixed by the specified scaling.

At $a = 0$ the division in (V.10.39) is unavailable and the wrapped states become singular in the physical description. That point requires its own light-field treatment. It is not a counterexample to the regular-patch algebra. Similarly, the source's expression involving $\exp(-1/g^2_{\text{source}})$ is kept in its source convention; translating it to a normalized instanton action requires the gauge-coupling dictionary. A power match alone cannot fix factors of 2π or the global form of the gauge group.

The example gives a concrete reason for carrying local-limit data along with a topological answer. The geometry identifies which masses and couplings survive; mirror methods from Chapters 3 and 4 then compute selected quantities in that limit. The ratio here does not determine a metric, the full BPS spectrum or an all-genus gauge partition function. XI develops the construction and those additional identifications. For this chapter the useful conclusion is narrower: a finite gauge combination arises from a correlated base/fibre limit, with its physical premises stated before taking that limit.

V.10.6 Boundaries and a flux superpotential

When can open topological amplitudes enter a physical $\mathcal{N} = 1$ chiral coupling? Boundary conditions and the physical embedding must be specified. We begin with the restricted compactified open-superstring example in which an internal $c = 9$ theory gives four-dimensional $\mathcal{N} = 1$ Yang–Mills coupled to supergravity. Denote the gauge field-strength superfield by W_α. It is distinct from the $\mathcal{N} = 2$ Weyl multiplet W_{Weyl} and from a scalar superpotential W_{eff}.

Consider only the orientable worldsheet contribution with no handles and $h \geq 2$ boundaries. Represent it as a cylinder with $h-2$ interior slits. Each slit adds a boundary and has two endpoints carrying the curvature singularities used for spectral flow. Their physical insertions are gauginos Ψ. Before absorbing spacetime zero modes, the count for each species is $h - 1$ modes of ψ^i and one of χ_i. Two gauge-field vertices absorb the scalar modes and one one-form mode per species, leaving

$$n_{\text{remaining}}(\psi^i) = (h-1) - 1 = h - 2, \qquad n_{\text{remaining}}(\chi_i) = 0. \tag{V.10.44}$$

Converting one endpoint component on each slit supplies the required remaining modes. There are $h - 2$ insertions of each selected gaugino component and two gauge insertions in total,

$$n_F = 2, \qquad n_{\Psi,+} = n_{\Psi,-} = h - 2, \qquad n_\Psi = 2(h-2). \tag{V.10.45}$$

These endpoint labels describe the selected source components; they do not supply a universal helicity prescription for every brane system.

The boundary traces contain information that the insertion number alone does not retain. In this example both gauge insertions sit on the chosen outer boundary

and a gaugino pair sits on each slit boundary. If F_h^0 denotes the corresponding open topological coefficient, the component structure is

$$F_h^0 \ \mathrm{Tr}\, F^2 \left[\mathrm{Tr}\, \Psi^2\right]^{h-2} . \tag{V.10.46}$$

Here F denotes the gauge strength of the open sector, not the closed-string canonical graviphoton used earlier. Combining all fields into one trace would change the color contraction. The source expresses the selected interaction as an $\mathcal{N} = 1$ chiral term with powers schematically organized by

$$\int d^2\theta \, F_h^0 (W_\alpha W^\alpha)^{h-1}, \qquad h \geq 2, \tag{V.10.47}$$

with its boundary color structure retained as in (V.10.46). This expression is not a rule for assigning an arbitrary disk amplitude to a scalar superpotential.

For $h = 2$ there are no slits or gaugino pairs and the selected term is a gauge kinetic chiral coupling. For $h = 4$ there are two slits and four gauginos,

$$h = 4 : \qquad n_F = 2, \quad n_\Psi = 4, \quad F_4^0 \, \mathrm{Tr}\, F^2 (\mathrm{Tr}\, \Psi^2)^2. \tag{V.10.48}$$

Figure V.10.4 makes both endpoint pairs and the periodic cylinder direction visible. Substituting $h = 1$ into the slit count would give a negative number; the disk requires a separate argument. Moreover, the parent compactified open string needs its unoriented and global consistency conditions. The source states that the nonorientable worldsheets do not contribute to this selected amplitude by its zero-mode structure, which does not authorize discarding them from the consistent parent theory. Anomalies, tadpoles and boundary choices are still physical constraints on that theory.

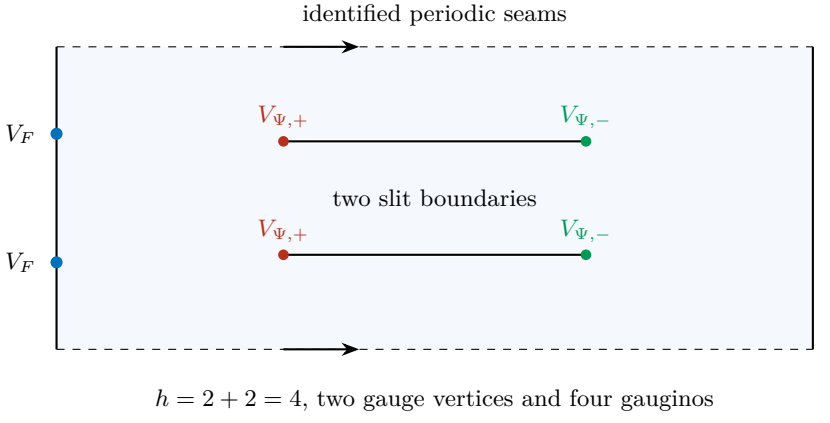


Figure V.10.4: An orientable $g = 0$, $h = 4$ surface drawn as a cylinder cut along its periodic direction. The upper and lower dashed edges are identified with the indicated same direction, while the left and right edges are its two original boundaries. Each interior slit supplies one additional boundary and a pair of gaugino insertions. The two gauge vertices on the left boundary give $\mathrm{Tr}\, F^2$; the two slit boundaries give $(\mathrm{Tr}\, \Psi^2)^2$. The drawing fixes insertion and trace placement, rather than depicting the unoriented completion.

There is a second, distinct route to a scalar superpotential. The Dijkgraaf–Vafa local proposal starts with type IIB D5 branes on resolved rational curves and a specified geometric transition. To describe its geometry without confusing several superpotentials, write $W_{\mathrm{tree}}(x)$ for the chosen tree polynomial of degree $n+1$. Take the generic case in which W'_{tree} has n distinct simple roots x_i, indexed by $i = 1, \ldots, n$. Let u, v, x, y be local complex coordinates. The resolved curves occur at those critical points in the singular geometry

$$uv + y^2 + W'_{\mathrm{tree}}(x)^2 = 0, \qquad W'_{\mathrm{tree}}(x_i) = 0. \tag{V.10.49}$$

The proposal relates a distribution of wrapped D5 branes to a deformed geometry with compact three-cycles,

$$uv + y^2 + W'_{\mathrm{tree}}(x)^2 + P_{n-1}(x) = 0. \tag{V.10.50}$$

The degree-$n-1$ deformation polynomial P_{n-1} is fixed by the local period data. Its letter distinguishes it from the numerical f_g and the supplied test polynomial below. The physical transition, the identification of ranks with fluxes and the gauge-dynamical interpretation are additional premises of this specified construction.

Choose the holomorphic three-form Ω with a fixed normalization. Let A_i be the compact three-cycles and B_i their noncompact duals. In these local period conventions the genus-zero function is specified by

$$S_i = \int_{A_i} \Omega, \qquad \frac{\partial F_0}{\partial S_i} = \int_{B_i}^{\text{regulated}} \Omega. \tag{V.10.51}$$

The noncompact periods require a regulator and a prescription for polynomial terms. They cannot be inferred solely from the compact periods without that information. After integrating over the two-sphere fibres, the periods can be represented by integrals of $y\,dx$ on the curve $y^2 + W'_{\mathrm{tree}}(x)^2 + P_{n-1}(x) = 0$. Figure V.10.5 shows the cut and regulator geometry of this representation.

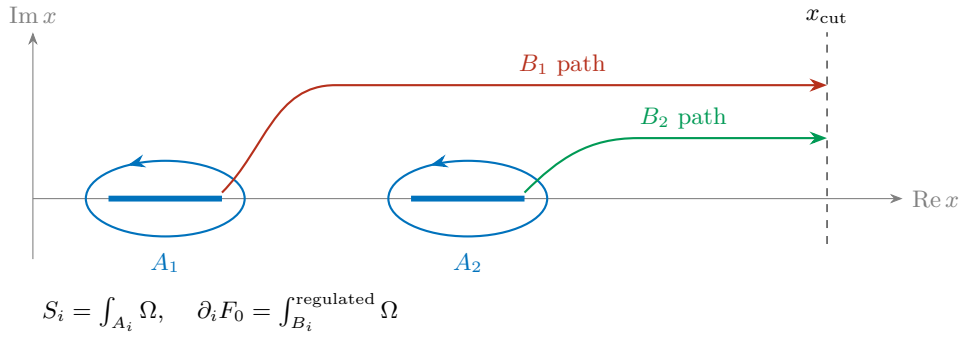


Figure V.10.5: The two-cut version of the local period construction, shown on the x plane. Oriented loops around the cuts represent the compact period contours after fibre integration. Dual paths run from the cuts toward a common large cutoff x_{cut}, with small vertical offsets to distinguish their projections. The full cycles live in the local threefold. Fixing the three-form normalization and regulating the dual periods are part of specifying F_0, before the flux functional is used.

For integral fluxes or brane multiplicities N_i and a specified coefficient α, the cited local proposal gives

$$W_{\mathrm{eff}} = \sum_i \left(N_i \frac{\partial F_0}{\partial S_i} + \alpha S_i \right). \tag{V.10.52}$$

This is separate from (V.10.47). It uses a geometric transition and flux/period dictionary rather than just the slit zero-mode calculation. Chapter 6 supplied boundary vocabulary, and Chapter 9 supplies matrix-model methods. Neither vocabulary nor a recursion formula by itself establishes the physical premise behind (V.10.52). Volume XVIII, Chapter 7 develops that correspondence in its own local setting.

We can work out how the functional operates without asserting a new Calabi–Yau realization. Supply a mass unit μ and coordinates s_i by $S_i = \mu^3 s_i$, and set $F_0 = \mu^6 f(s_1, s_2)$. Then

$$\frac{\partial F_0}{\partial S_i} = \mu^3 \frac{\partial f}{\partial s_i}, \qquad W_{\mathrm{eff}} = \mu^3 w, \qquad [F_0] = 6, \quad [W_{\mathrm{eff}}] = 3. \tag{V.10.53}$$

These local units for S_i, F_0 differ from compact homogeneous special-geometry weights. The derivative removes three powers of mass, as required for a scalar $\mathcal{N} = 1$ superpotential.

For an algebraic example choose

$$f = \frac{5}{4} s_1^2 - \frac{2}{3} s_1 s_2 + \frac{7}{8} s_2^2, \qquad N = (2, 3), \quad \alpha = \frac{1}{5}. \tag{V.10.54}$$

Its first derivatives and Hessian are

$$\partial_1 f = \frac{5}{2} s_1 - \frac{2}{3} s_2, \qquad \partial_2 f = -\frac{2}{3} s_1 + \frac{7}{4} s_2, \qquad H = \begin{pmatrix} 5/2 & -2/3 \\ -2/3 & 7/4 \end{pmatrix}. \tag{V.10.55}$$

The Hessian is symmetric, with unequal entries. This matters when computing both gradient components; exchanging the diagonal entries would change the answer. Substitution into (V.10.52) yields

$$\begin{aligned} w &= 2\left(\frac{5}{2}s_1 - \frac{2}{3}s_2\right) + 3\left(-\frac{2}{3}s_1 + \frac{7}{4}s_2\right) + \frac{1}{5}(s_1 + s_2) \\ &= \frac{16}{5}s_1 + \frac{247}{60}s_2. \end{aligned} \tag{V.10.56}$$

For example, the second coefficient is $-4/3+21/4+1/5 = (-80+315+12)/60 = 247/60$, rather than the first coefficient copied into a second slot. Hence

$$\nabla w = HN + \frac{1}{5}\begin{pmatrix}1\\1\end{pmatrix} = \begin{pmatrix}16/5\\247/60\end{pmatrix}. \tag{V.10.57}$$

At $(s_1, s_2) = (2/3, -4/5)$, the value is

$$w = \frac{16}{5}\frac{2}{3} + \frac{247}{60}\left(-\frac{4}{5}\right) = \frac{32}{15} - \frac{247}{75} = -\frac{29}{25}. \tag{V.10.58}$$

The quadratic f is a supplied test function, not a computed set of Calabi–Yau periods. Its linear w illustrates differentiation and units; it is not a physical vacuum or stability calculation. The distinction between a sourced physical functional and a chosen function on which it acts prevents an algebraic exercise from being mistaken for a new brane construction.

V.10.7 Local coefficients and missing dynamics

What remains to be supplied even after a protected amplitude is known? The first issue already arose in Chapter 5. A full topological amplitude $F_g(t, \bar{t})$ generally depends on both vector moduli and their conjugates. A coefficient in a local chiral superspace term must be chiral. If one substitutes a genuinely nonholomorphic function of chiral superfields X and antichiral superfields $\bar{X}$, its derivative is

$$\overline{D}\, F_g(X, \bar{X}) = \sum_{\bar{i}} \frac{\partial F_g}{\partial \bar{X}^{\bar{i}}} \overline{D}\bar{X}^{\bar{i}}, \tag{V.10.59}$$

which need not vanish. The naive local F-density would therefore fail the chirality condition. The physical amplitude contains contributions from propagation of massless particles; these can be nonlocal in the effective action and account for the nonholomorphic dependence. The anomaly is physical information, rather than a reason to discard that dependence from the full answer.

A chosen local holomorphic coefficient F_g^{hol} instead requires a holomorphic frame, a base point or limit, and a local subtraction prescription. In the base-point description, one holds the antichiral expectation value fixed while expanding in chiral fluctuations. In canonical coordinates at that point the sourced expansion has the form

$$F_g(t_0 + x, \bar{t}_0) = \sum_{n \geq 0} \frac{x^{i_1} \cdots x^{i_n}}{n!} D_{i_1} \cdots D_{i_n} F_g(t_0, \bar{t}_0). \tag{V.10.60}$$

The x^i are chiral variables. The fixed $\bar{t}_0$ are parameters of the expansion, not antichiral superfields inserted into a local invariant. This distinction preserves chirality without asserting that the full amplitude is globally holomorphic.

Frame choices also persist. With the Hodge-frame convention of Chapter 5,

$$\Omega \longmapsto e^{h(t)}\Omega, \qquad K \longmapsto K - h - \bar{h}, \qquad F_g \longmapsto e^{(2-2g)h(t)}F_g. \tag{V.10.61}$$

The last transformation expresses the line weight, rather than the canonical mass dimension calculated earlier. For instance a constant frame change $e^h = 2$ at genus two multiplies the coefficient by $1/4$. Comparing that number to a differently framed result without translating the frame would create a spurious discrepancy.

Solving an anomaly equation still leaves holomorphic information. If $F_g^{\text{particular}}$ is a chosen particular solution, then at fixed lower-genus data and connection the local general form includes

$$F_g = F_g^{\text{particular}} + f_g^{\text{ambiguity}}(t), \qquad \bar{\partial} f_g^{\text{ambiguity}} = 0. \tag{V.10.62}$$

Boundary behavior and regularization fix this remaining term when enough information is available. Near a conifold, even a universal-looking singular formula requires the specified isolated light species, its central-charge coordinate and the chosen units. An additional light multiplet or a change of coordinate/frame can change what one should compare. The statements in Chapter 5 about an isolated light $\mathcal{N} = 2$ hypermultiplet do not become species-independent here.

A second issue is the information carried by holomorphic data. An explicit $\mathcal{N} = 1$ example shows why knowing a scalar superpotential alone cannot generally determine the kinetic metric. Take a single chiral scalar Z with

$$K = cZ\bar{Z}, \qquad W = \frac{m}{2}Z^2, \qquad c > 0. \tag{V.10.63}$$

The coefficient c is dimensionless, $[Z] = 1$ and $[m] = 1$. Let A_{aux} denote its complex auxiliary field, distinct from holomorphic derivatives sometimes used for the F-flat equations. The auxiliary part of the stipulated action is

$$\mathcal{L}_{\text{aux}} = cA_{\text{aux}}\overline{A}_{\text{aux}} + mZA_{\text{aux}} + \bar{m}\bar{Z}\overline{A}_{\text{aux}}. \tag{V.10.64}$$

Treat A_{aux} and its conjugate as independent in the variation. Their equations give

$$c\overline{A}_{\text{aux}} + mZ = 0, \qquad cA_{\text{aux}} + \bar{m}\bar{Z} = 0, \qquad A_{\text{aux}} = -\frac{\bar{m}\bar{Z}}{c}. \tag{V.10.65}$$

Substituting into all three terms, rather than just the quadratic term, yields

$$\mathcal{L}_{\text{aux,on}} = \frac{|mZ|^2}{c} - \frac{|mZ|^2}{c} - \frac{|mZ|^2}{c} = -\frac{|mZ|^2}{c}, \qquad V = \frac{|mZ|^2}{c}. \tag{V.10.66}$$

The kinetic term has coefficient c. With $Z_{\text{can}} = \sqrt{c}\,Z$, its normalization and the mass follow as

$$c|\partial Z|^2 = |\partial Z_{\text{can}}|^2, \qquad V = \frac{|m|^2}{c^2}|Z_{\text{can}}|^2, \qquad m_{\text{can}} = \frac{|m|}{c}. \tag{V.10.67}$$

The same function of the original coordinate, $W = mZ^2/2$, therefore allows different normalized masses when the kinetic coefficient changes. In canonical coordinates the superpotential itself reads $W = mZ_{\mathrm{can}}^2/(2c)$, so the result is also visible directly in the fermion mass of the chiral multiplet.

Using a fixed mass unit, take the numerical value of real m to be $7/3$. First set $c = 1$, then $c = 5/2$. The coefficients of $|Z|^2$ in the potential and the canonical mass squares, in that unit squared, are

c	$V/\lvert Z\rvert^2$	m_{can}^2
1	49/9	49/9
5/2	98/45	196/225

. (V.10.68)

For the second row, $|m|^2/c = (49/9)(2/5) = 98/45$, followed by one more division by c for the canonical mass square. Thus the comparison changes a physical normalized observable while leaving the coordinate superpotential fixed. It is an elementary field-theory example, with no assertion that the two metrics arise from the same Calabi–Yau model.

This example does not negate $\mathcal{N} = 2$ special geometry. A complete $\mathcal{N} = 2$ vector-multiplet model, with its additional special-Kähler hypotheses and period data, relates its metric to a prepotential. The example above has only $\mathcal{N} = 1$ and supplies K independently. Selected higher F_g data do not by themselves specify all D-terms, hypermultiplet metrics or scattering. Even where the genus-zero prepotential determines a vector metric, those additional sectors require their own physical input.

The same distinction guides later applications. XI supplies local geometric engineering and its mass dictionary. Volume XVIII supplies the specified topological-string and gauge-theory constructions. An Omega-background interpretation additionally requires the actual supersymmetric background, its deformation parameters, their units and the dictionary to the selected physical observable. Matching the power of λ_{top} to a graviphoton power establishes none of those identifications by itself. Protected amplitudes give exact access to selected interactions once that physical dictionary is present.

V.10.8 Exercises

The first five exercises have bounded exact-answer versions in the companion, with identifiers IV10-E1 through IV10-E5. Rational entries are submitted as exact fraction strings; integer counts and exponents are integers. The sixth is a written interpretation task.

1. For the compact flux-free type-IIA setting, give the four insertion counts in (V.10.8) for $g = 1, 2, 4$, in that order. State the numbers of gravitons, total graviphotons, insertions of each chosen spacetime component and remaining ψ modes per species and chiral half. Explain in writing why the genus-one torus measure cannot be obtained from the stable-genus count. Use the separate genus-one R^2 interpretation for its row.

2. At $g = 3$ and $f_3 = 5/7$, calculate all three coefficients in (V.10.14). Then compute both component amplitudes using the distinct identical-vertex factors in (V.10.17) and (V.10.18). Explain the origin of the relative sign and why it is not a change of Hodge chirality. These are source-normalized numbers.

3. With $T_W = \eta F_{\text{can}}/M$ and $X^0 = M$, give for $g = 2, 3$ the operator dimension, its coefficient dimension, the homogeneous weight of $F_g(X)$ and the coefficient rescaling under $F_{\text{new}} = (3/2)F_{\text{old}}$. Keep η unfixed. Explain which inverse powers of M account for the difference between weight and canonical dimension.

4. Use $C_b = 7/3$, $C_f = 5/2$, $\Lambda = 2\mu$ and $a = 3\mu$ to compute q_b/t_f^4 in the KKV limit. Independently, in the gravitational limit model set $b = 0$ and give the fixed-curvature density and canonical two-graviton exponents for $(g, p) = (1, 0), (2, 0), (2, -6)$, in that order. Discuss the bounded-coefficient assumption and distinguish dimensionful ϵ from dimensionless $\widehat{\epsilon}$.

5. Apply the stipulated flux functional with $N = (2, 3)$, $\alpha = 1/5$ and the supplied f in (V.10.54). Calculate both components of ∇w, the value at $(2/3, -4/5)$ and the mass dimensions of F_0 and W_{eff} in the local units of (V.10.53). State why this computation establishes neither a Calabi–Yau period solution nor a physical vacuum.

6. Explain the difference between a full $F_g(t, \bar{t})$, a chosen local holomorphic coefficient and a normalized physical amplitude. Use the $K = cZ\bar{Z}$ example to name one observable that requires metric information. Identify boundary and regularization information needed even for protected coefficients, and explain why an arbitrary open amplitude is not automatically a scalar superpotential. Include the genus-one fixed-curvature example and state what additional physical input an Omega-background dictionary would need. This is a written argument, without a numerical certificate.

V.10.9 Take-home message

Take-home message

The bridge from a topological string to a physical coupling is a selected amplitude. Its Ramond–Ramond charges, picture changes and spacetime zero modes lead to two gravitons and $2g - 2$ graviphotons at stable genus. The physical calculation fixes two tensor contractions; supersymmetry organizes them in a Weyl-multiplet chiral invariant. Canonical dimensions, field normalization and local-limit assumptions must then be restored. The KKV base/fibre limit and the specified D5/flux proposal supply additional physical routes to selected gauge-theory quantities. A full nonholomorphic amplitude, a local holomorphic coefficient and a physical normalized measurement carry different information.

Status and sources

Sections 10.1–10.2. The compact type-II setting, internal charges and selected physical vertices follow Antoniadis et al. (1993, arXiv v1, physical PDF pp. 3–9, secs. 2–3). The physical-to-topological amplitude reduction is its sec. 4, physical PDF p. 18, eq. (4.12) and the following comparison with F_g. The zero-mode explanation is Bershadsky et al. (1993, arXiv v1, physical PDF pp. 125–128, sec. 8.1, eqs. (8.1)–(8.5)); that source explicitly describes its account as heuristic and points to the detailed physical spin-structure calculation. The stable picture arithmetic, mode subtraction and genus examples are conditional algebra. The torus trace is the separate genus-one definition from Chapter 5 and Bershadsky et al. (1993, physical PDF pp. 30–31, sec. 2.3); the R^2 interpretation is in Antoniadis et al. (1993, physical PDF p. 3). The direct lower-genus selection and the additional higher-genus dilaton/no-mixing indication are distinguished in Antoniadis et al. (1993, physical PDF p. 23, sec. 6). Gopakumar and Vafa (1998, arXiv v1, physical PDF p. 3, sec. 2) states the stronger protected result in its selected vector/gravity sector; it is not used here as a general nonrenormalization theorem.

Section 10.3. Both contractions, their relative coefficient and the absent third structure are those of Antoniadis et al. (1993, physical PDF pp. 12–13, eq. (3.22)). The component projections and vertex signs are in its Appendix, physical PDF pp. 24–26, eqs. (A.1)–(A.5). The factorial reduction and the $g = 3$ evaluation are algebraic consequences. Homogeneity and the conformal chiral invariant follow its physical PDF pp. 19–21, eqs. (5.1)–(5.7). The normalization caveat is already present in its physical PDF p. 8, footnote 2, and p. 19, eq. (5.2). The self-duality wording in Bershadsky et al. (1993, physical PDF p. 127) is retained as distinct from the explicit same-anti-self-dual component analysis. Gopakumar and Vafa (1998, physical PDF p. 3 and footnote 4) uses Euclidean self-dual notation. Orientation reversal alone supplies no signed Lorentzian or canonical-field conversion.

Sections 10.4–10.5. The fixed-frame tensor map, η, ρ, μ and $\widehat{\epsilon}$ use the local definitions above and the Hodge and ambiguity restrictions of Chapter 5. Dimensions, rescalings and limit exponents are conditional calculations, not universal decoupling statements or guarantees of a nonzero on-shell amplitude. The A_1 fibre, wrapped W states and pure-$SU(2)$ correlated limit follow Katz et al. (1996, arXiv v2, physical PDF pp. 3–5, sec. 2, eq. (2.1)). The nonunit finite quotient checks only the supplied scaling, without proving the spectrum, metric, global gauge group or all-genus transfer. Its source coupling exponent has not been equated to the house instanton normalization.

Section 10.6. The $g = 0$, $h \geq 2$ orientable example, its boundary traces, chiral interpretation and unoriented consistency qualifications follow Bershadsky et al. (1993, physical PDF pp. 129–131, sec. 8.2, eq. (8.7)). The specified local D5 construction, three-form and regulated periods follow Dijkgraaf and Vafa (2002, arXiv v1, physical PDF pp. 3–7, secs. 2.1–2.2); the flux functional is its physical PDF p. 17, eq. (3.12). This version is the source used here, independently of Chapter 9's version choice. The physical transition and flux/rank identification are cited premises. The symmetric-Hessian polynomial and its units are supplied algebraic examples, not realized periods or vacuum data.

Section 10.7 and exercises. The local/nonlocal distinction follows Antoniadis et al. (1993, physical PDF pp. 20–21, eqs. (5.5)–(5.7)) and Bershadsky et al. (1993, physical PDF pp. 128–129). The frame and light-species qualifications are as in Chapter 5. The off-shell $\mathcal{N} = 1$ grammar is the prerequisite of Volume I, Chapter 2. Auxiliary elimination and canonical mass here are derived for the explicitly supplied action, with $c > 0$; this is not a counterexample to complete $\mathcal{N} = 2$ special geometry. Five bounded exercises test the displayed conditional calculations; the sixth requires written scientific interpretation.

Scope of the physical inputs. The physical compactification, spin-structure reduction, protected-sector argument, open-string embedding and local flux correspondence are sourced physical inputs. The arithmetic identities hold under their stated premises. Generic decoupling, full QFT equivalence and a universal physical normalization do not follow. The open chiral interpretation, the Dijkgraaf–Vafa correspondence and the local/nonlocal distinction retain their stated domains.

References

Antoniadis, I. et al. (1993). *Topological Amplitudes in String Theory*. Source edition: arXiv v1, 26 July 1993, 30 physical PDF pages. arXiv: `hep-th/9307158`.

Bershadsky, M. et al. (1993). *Kodaira–Spencer Theory of Gravity and Exact Results for Quantum String Amplitudes*. Source edition: arXiv v1, physical pages 125–131. arXiv: `hep-th/9309140`.

Dijkgraaf, R. and C. Vafa (2002). *Matrix Models, Topological Strings, and Supersymmetric Gauge Theories*. Source edition: arXiv v1, 28 June 2002, physical PDF pages 3–7 and 17. arXiv: `hep-th/0206255`.

Gopakumar, R. and C. Vafa (1998). *M-Theory and Topological Strings–I*. Source edition: arXiv v1, 25 September 1998, physical PDF page 3. arXiv: `hep-th/9809187`.

Katz, S., A. Klemm, and C. Vafa (1996). *Geometric Engineering of Quantum Field Theories*. Source edition: arXiv v2, 8 October 1996, physical PDF pages 3–5. arXiv: `hep-th/9609239`.